RAPID EVALUATION OF OPTIONS FOR THE PRIMARY RECOVERY OF ANTIBODY FRAGMENTS EXPRESSED IN HIGH CELL DENSITY CULTURES

A thesis submitted to the University of London
for the degree of Doctor of Philosophy

by

Heidi Salte

August 2006

The Advanced Centre for Biochemical Engineering
Department of Biochemical Engineering
University College London
Torrington Place
London WC1E 7JE

ProQuest LLC
789 East Eisenhower Parkway
P.O. Box 1346
Ann Arbor, MI 48106-1346

Abstract

This thesis investigates methods for the rapid determination of suitable operating conditions for the primary recovery of antibody fragments from high cell density fermentation broths by two alternative processes: centrifugation and expanded bed adsorption. The methodologies applied involve the use of predictive tools, such as scale-down techniques and simulations, in order to ensure rapid prediction of large-scale process performance. This is followed by the visualisation of suitable processing conditions for recovery of the high cell density cultures investigated using Windows of Operation.

Challenges related to protein recovery from high cell density expression systems were identified and addressed. Existing USD clarification approaches lead to an over-prediction of separation performance when tested with high cell density cultures of *E. coli* whole cells and periplasmically lysed *E. coli* cells. This was attributed to aggregation effects occurring in the low shear environment of a laboratory centrifuge, which would not be apparent in the settling region of a continuous-flow industrial centrifuge. A modified USD clarification methodology was developed, which resulted in accurate predictions of large-scale performance. This novel USD clarification method was applied to *E. coli* homogenates and *P. pastoris* cultures of varying solids concentrations. For these feedstocks, a laboratory-based protocol for the determination of centrifugal dewatering was developed and applied. Windows of Operation were generated, visualising the available operating conditions for a number of industrial centrifuges, when the process was constrained by pre-defined performance and operating criteria.

The main challenge identified upon processing of *E. coli* homogenate by expanded bed adsorption relate to cell-cell and/or cell-adsorbent interactions. These interactions were more prominent in the 1.9 mm ID scale-down column than in the 25 mm ID column, probably as a result of the high particle to column diameter ratio in the scale-down bed. As a consequence, the behaviour of the beds differed in terms

of level of expansion, breakthrough profiles, binding capacity and yield. Industrial-scale EBA process performance was investigated using the general rate model to predict the output. This formed the basis for the generation of a series of Windows of Operation, displaying the most suitable combinations of load volume and flow rate for the processing of *E. coli* homogenates of a range of solids concentrations by EBA.

A comparative study was performed based on the identification of suitable operating conditions from the Windows of Operation generated for *E. coli* homogenate, and suggested that EBA provides higher yields, shorter processing times and greater throughput relative to a more conventional processing route, comprising centrifugation, filtration and packed bed chromatography.

Acknowledgements

First and foremost I would like to thank my supervisor Prof. Nigel Titchener-Hooker for his guidance and support over the last four years. His optimism and encouragement has been invaluable to me throughout this project.

Moreover, I would like to thank Prof. Mike Hoare for expert advice regarding my centrifugation work. The help and support from fellow researchers, especially from Dr. Nik Willoughby, Andrew Tustian, Samir Ujam, Dr. Josh King and Dr. Helen Baldascini, is also greatly appreciated.

I would like to thank Dr. Arild Johannessen and his colleagues at Biosentrum and Rogaland Research for giving me the opportunity to go to London and carry out this PhD.

Finally, a special thank you to my family, friends and Samir for their continued encouragement and support.

Table of contents

List of figures

List of tables

Nomenclature

Symbols

A	Absorbance	-
a	Langmuir parameter ($=bC_p^{max}$)	-
b	Binding constant (Langmuir parameter)	mL mg^{-1}
C	Clarification	%
C	Equilibrium concentration of product in the liquid	mg mL^{-1}
C_0	Initial product concentration	mg mL^{-1}
C_f (t)	Feed concentration profile of product	mg mL^{-1}
C_L	Bulk phase concentration of product	mg mL^{-1}
C_p	Product concentration in stagnant fluid inside the pore	mg mL^{-1}
C_p^{max}	Max concentration of product on the adsorbent particles	mg mL^{-1}
C_p^*	Concentration of product on the adsorbent particles	mg mL^{-1}
c	Fractional level of clarification	-
c	Σ correction factor to account for non-ideality	-
D	Dewatering	%
D_{ax}	Axial dispersion coefficient	$m^2 s^{-1}$
D_c	Column diameter	m
D_m	Molecular diffusivity	$m^2 s^{-1}$
D_p	Intra-particle diffusivity	$m^2 s^{-1}$
DW_{sed}	Weight of dried sediment	g
d	Fractional level of dewatering	-
d_p	Particle diameter	m
dw_r	Ratio of cell dry weight to cell wet weight	-
F	Fractional recovery of solids	-
f_l	Correction factor for spacer caulks	-
g	Acceleration due to gravity	m s^{-2}
H	Expanded bed height	m
H_0	Settled bed height	m
k	Consistency index (viscosity determination)	$mPa.s^n$
k_f	Film mass transfer coefficient	m s^{-1}

L	Length of bowl chamber	m
MW	Molecular weight	Da
N	Rotational speed	rpm
N_{AD}	Number of active discs in a disc-stack	-
N_D	Dimensionless dispersion number	-
N_T	Number of theoretical plates	-
n	Flow behaviour index (viscosity determination)	-
n	Richardson-Zaki parameter	-
OD	Optical density	-
Pe	Peclet number (=UH/D_{ax})	-
Q	Flow rate	$L\ h^{-1}$
R	Radial coordinate of particle	m
R_p	Particle radius	m
r	Radial position of particle in centrifugal field	m
r_1	Inner disc radius	m
r_2	Outer disc radius	m
r_e	Effective radius	m
r_i	Inner radius	m
r_o	Outer radius	m
RCF	Relative centrifugal force	-
Re	Reynolds number (=$Ud_p\rho/\mu$)	-
Re_t	Reynolds number under terminal free-fall conditions (=$U_t d_p\rho/\mu$)	-
s_e	Effective settling distance	m
Sc	Schmidt number (= $\mu/\rho D_m$)	-
Sh	Sherwood number (= $2k_fR_p/D_m$)	-
t	Time	min
$t_{comp.}$	Time for solids compaction	min
t_{down}	Downtime of centrifuge	min
$t_{proc.}$	Processing time	min
t_r	Mean residence time in column	min
U	Liquid velocity	$m\ s^{-1}$
U_{mf}	Minimum fluidisation velocity	$m\ s^{-1}$

U_t	Particle free-fall velocity	$m\ s^{-1}$
V	Volume	L
V_S	Solids holding capacity	L
V_{sg}	Centrifugal settling velocity	$m\ s^{-1}$
V_{sg}^*	Hindered centrifugal settling velocity	$m\ s^{-1}$
v	Interstitial velocity	$m\ s^{-1}$
W_f	Weight of the feed	g
W_s	Weight of supernatant	g
WW_{sed}	Weight of wet sediment	g
x	Fraction of overall centrifugation time for acceleration	-
Y	Yield	%
y	Fraction of overall centrifugation time for deceleration	-
Z	Axial coordinate	m

Greek letters

α	Experimentally determined coefficient	-
ε	Bed voidage	-
ε_0	Settled bed voidage	-
ε_p	Particle porosity	-
ϕ	Solids fraction	-
γ	Shear rate	s^{-1}
λ	The ratio of the molecular diameter of the product to the pore diameter of the adsorbent.	-
μ	Viscosity	mPa.s
μ_a	Apparent viscosity ($= \gamma^{n-1}k'$)	mPa.s
μ^*	Viscosity at high solids density	mPa.s
θ	Half disc angle	rad
ρ	Liquid density	$kg\ m^{-3}$
ρ_p	Particle density	$kg\ m^{-3}$
σ	Particle geometric factor	-
σ	Variance of the tracer output signal (RTD curve)	-

σ_{θ}^{2}	Dimensionless variance ($=\sigma^2/t_r^2$)	-
τ	Shear stress	mPa
τ_{tor}	Particle tortuosity factor	-
ω	Angular velocity around the centre of rotation	rad s^{-1}
Σ	Sigma factor	m^2

1 Introduction

1.1 Project significance

Antibodies and antibody derivatives constitute 20-30% of biopharmaceutical products currently in development (Glennie and Johnson, 2000; Roque *et al.*, 2004). Approximately 200 antibodies and antibody fragments are now in clinical trials - this represents a significant increase from 25 years ago, when only two monoclonal antibodies were the subject of clinical trials (Roque *et al.*, 2004). 13 antibody-based therapeutics have already reached the market (Roque *et al.*, 2004), and it is expected that this number will continue to increase in the following years.

Antibody fragments have a number of potential applications; as human therapeutics, in diagnosis, as research tools and in consumer applications to mention some. For many of the applications, large amounts of protein are required. In order to meet the market's demands, efficient production strategies are necessary. Recent advances in cell culture have resulted in expression systems capable of growing to high cell densities – allowing for the production of recombinant antibody fragments in high titres. However, as cell density increases, the challenges rise on the downstream side of the process. A significant percentage - 50-80% - of the total manufacturing cost of a therapeutic antibody is incurred during downstream processing (Roque *et al.*, 2004), hence efficient development and operation of processes for recovery of the antibody fragments are required. A key part of any downstream process relates to the initial stages of cell removal prior to high resolution purification. The development of methods for the rapid assessment of these initial steps provided the motivation for this doctoral study.

The following section (section 1.2) provides general theory about antibodies and antibody fragments, including a description of antibody structure and potential applications. This is followed by a discussion of strategies for the production of antibody fragments in *E. coli* and *P. pastoris* (section 1.3). Section 1.4 considers the recovery of antibody fragments from fermentation broths and discusses alternative

methods for biomass separation and for the release of intracellular product. Section 1.5 focuses on the application of scale-down techniques for the prediction of large-scale centrifugation and EBA performance, whereas section 1.6 introduces the concept of Windows of Operation for the visualisation of available operating conditions. The main thesis goals and aims are presented in section 1.7, and the introduction concludes with an overview over the thesis layout (section 1.8).

1.2 Antibodies and antibody fragments

1.2.1 Antibody structure

Antibodies are Y-shaped molecules consisting of two identical heavy (H) chains and two identical light (L) chains. The H and L chains are kept together by disulfide bridges and non-covalent bonds (Madigan *et al.*, 2000). The chains can be divided in variable (V) and constant (C) domains. The variable domains of the heavy and light chain, referred to as V_H and V_L, respectively, are located at the N-terminal part of the antibody molecule. V_H and V_L are extremely variable in amino acid sequence and together these domains form the unique antigen-recognition site of each antibody. In addition to the variable regions, each L chain contains one constant region, (C_L), and each H chain has three constant regions (C_H1, C_H2 and C_H3). The amino acid sequences of these remaining C-terminal domains are much less variable than in V_H and V_L.

Figure 1.1 shows the structure of an immunoglobulin class G (IgG) molecule, which is the most abundant type of antibodies.

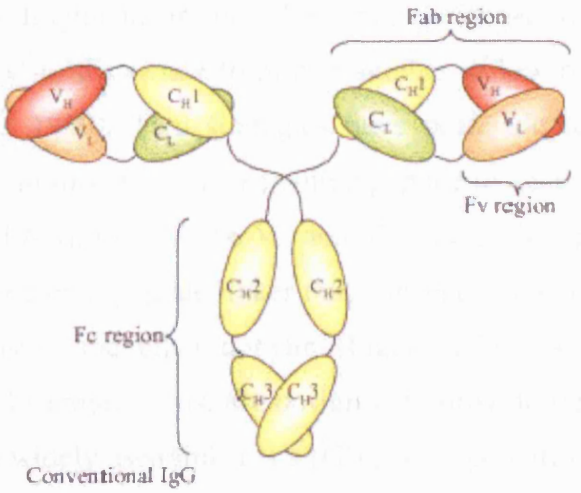

Figure 1.1. Illustration of a typical structure of an IgG antibody molecule. (From Joosten *et al.*, 2003)

1.2.2 Antibody fragments

When an IgG molecule is treated with proteolytic enzymes, it breaks into several fragments. One fragment is called Fc, for fragment crystallisable. Fc consists of the C-terminal half of both the H chains, C_H2 and C_H3, joined by a disulfide bond. Fc contains the site at which the antibody can bind to a receptor on a target cell, but has no effect on antigen recognition or antigen binding.

Several functional antigen-binding antibody fragments can also be engineered by proteolysis of whole antibodies. One type of fragment released when antibodies are digested contains the complete L chain plus the N-terminal half of the H chain (V_H and C_H1), linked by a disulfide bond. These fragments combine with antigen; hence they are called Fab fragments, for fragment of antigen binding. Fab can be further cleaved by enzymatic approaches, yielding the Fv fragment. This fragment, consisting of V_H and V_L only, is the smallest antibody fragment that still retains the entire antigen binding activity of the molecule (Brinkmannn *et al.*, 1997; Joosten *et al.*, 2003; Verma *et al.*, 1998). The amino acid sequence of this portion of the antibody varies considerably from one molecule to another. The Fc, Fab and Fv regions of the IgG molecule are indicated in Figure 1.1.

Normally, native Fv fragments are unstable since the non-covalently associated V_L and V_H domains tend to dissociate from one another at low protein concentrations (Glockshuber *et al.*, 1990). Two strategies have been adopted to overcome this problem. The first is to link the domains with a peptide to generate a single-chain Fv (scFv) (Bird *et al.*, 1988). In scFv the V_H and V_L antigen binding domains are held together and stabilised by a peptide linker that connects the C-terminus of V_H or V_L with the N-terminus of the other domain (Figure 1.2). Various linkers, usually consisting of about 15 amino acids, are designed to provide flexibility and enhance solubility. The most widely used linker is a $(Gly_4\text{-}Ser)_3$ peptide (Joosten *et al.*, 2003).

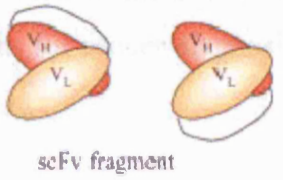

Figure 1.2. Illustration of scFv fragments formed by linking V_H and V_L with a polypeptide linker.
(From Joosten *et al.*, 2003)

The second strategy used to stabilise Fv fragments is to introduce cysteines at the interface between the V_H and V_L domains, forming a disulphide bridge that holds the domains together, this construct is referred to as disulphide stabilized Fv (dsFv) (Glockshuber *et al.*, 1992).

1.2.3 Applications of antibody fragments

Antibody genes are easily accessible to manipulations since the various functions of an antibody molecule are confined to separate domains. This allows for their properties to be altered and novel molecules can be engineered, which are then attractive to research, biotechnology and medicine (Glockshuber *et al.*, 1992).

Most applications of recombinant antibody fragments are related to diagnosis and therapy in human medicine (Joosten *et al.*, 2003). Due to their reduced size

compared to their parental whole antibodies, antibody fragments are potentially more effective than whole antibodies for the diagnosis or therapy of many diseases. The reduced size of Fab and scFv fragments permits them to penetrate tissues and solid tumours more readily than whole antibodies, and to be cleared more rapidly from the blood. These properties make antibody fragments well suited for *in vivo* applications such as the treatment of drug overdoses, medical imaging and tumor targeting (Eldin *et al.*, 1997; Roque *et al.*, 2004).

A relatively new application of antibody fragments is in bi-functional molecules, endowed with new properties by fusion with other molecules. In medicine, this approach is referred to as "Magic Bullet" and aims to deliver a protein drug, which is only active where it is required (Joosten *et al.*, 2003). This approach not only limits the dose of the drug, but also results in fewer side effects of the drug towards healthy tissue. Such fusion proteins are ideal immuno-agents for cancer diagnosis and cancer therapeutics.

Antibody fragments are also considered as components of a variety of consumer goods; for instance, antibody fragments can be used in shampoos to prevent formation of dandruff, or in toothpaste to protect against caries (Frenken *et al.*, 1998). Also suggested applications are the use in biosensors, treatment of wastewater and in the food-industry (Joosten *et al.*, 2003).

1.3 Production of antibody fragments

In order to use antibody fragments in large-scale applications, a suitable expression system has to be chosen. Antibody fragments can be manufactured microbially, rather than with the mammalian cell culture technique required for monoclonal antibody production. Several expression systems are available, both from prokaryotic and eukaryotic origins.

1.3.1 Expression systems for antibody fragments

1.3.1.1 Antibody fragment expression in *E. coli*

Much work on antibody fragment production has been focused on *E. coli* as an expression system. Amongst the advantages of this system is the ability to grow rapidly and to high density on inexpensive substrates, producing proteins in relatively large amounts. Besides that, *E. coli* is well characterised and is easily accessible for genetic modifications, and can easily be scaled-up for production of proteins of interest. One drawback of the *E. coli* expression system is that it is unable to carry out eukaryotic post-translational modifications and is therefore not suitable when glycosylation of antibody fragments is required (Joosten *et al.*, 2003).

Several expression strategies are available for *E. coli* antibody fragment production, such as direct cytoplasmic expression, periplasmic expression and secretion of fusion proteins to either the periplasm or the extracellular environment.

High-level expression of antibody fragments in the cytoplasm is associated with formation of aggregates and inclusion bodies. Although inclusion bodies in some cases can greatly simplify purification, there is no guarantee that the laborious *in-vitro* refolding process will yield sufficiently large amounts of biologically active product.

Proteins associated with a fusion "partner", such as maltose binding protein, thioredoxin and glutathione S-transferase, are less likely to accumulate as inclusion bodies in the cell cytoplasm (Baneyx, 1999). Drawbacks of this mechanism are related to the release of target protein, which requires use of very expensive proteases. Moreover, cleavage is often not complete, leading to reduction in yields.

A more favourable expression strategy appears to be periplasmic expression, first reported by Skerra and Pluckthun (1988). One major advantage of this method is that the antibody fragments are produced in an assembled, functional form. This is due to the oxidising environment of the periplasm, which allows for the transformation of

cysteine thiols into disulfides. Inclusion bodies are not formed to such a great extent as in the cytoplasm, and hence complex renaturation and refolding processes *in vitro* are not required. Moreover, there are less proteases present in the periplasm compared to the cytoplasm, and so proteolytic degradation is less of a problem compared to cytoplasmic expression.

However, there are also problems related to periplasmic expression, such as leakage of periplasmic proteins to the culture (Harrison *et al.*, 1997). Another possible issue is lysis of *E. coli* cells after long periods of antibody production (Sommerville *et al.*, 1994). The host strain, plasmid and growth conditions seems to have an effect on the extent of this phenomena to a greater extent than the type of antibody fragment being expressed and choice of signal sequence.

Alternative prokaryotic expression systems available for antibody fragment production are *Lactobacillus*, *Bacillus* and *Streptomyces* strains (Joosten *et al.*, 2003).

1.3.1.2 Antibody fragment expression in *P. pastoris*

P. pastoris represents attractive possibilities for the cost-effective large-scale production of antibody fragments. As a yeast based protein-expression system it is efficient and economical compared with bacterial and mammalian sources (Fisher *et al.*, 1999) and it typically yields higher quantities of secreted functional proteins than baculovirus and mammalian cells (Pennel and Eldin, 1998). Many of the advantages of this yeast system over other expression systems are related to the fact that yeasts are both microorganisms and eukaryotes (Verma *et al.*, 1998). As a single-celled microorganism it is easy to genetically manipulate and culture. Large-scale fermentation of these organisms is a well-established technology already used for production of several other recombinant proteins and also, extensive knowledge is available on downstream processes.

A major advantage of *P. pastoris* over bacterial expression systems is its ability to perform many of the post-translational modifications performed by higher eukaryotic cells, such as proteolytic processing, folding, disulfide bond formation and

glycosylation. The ability to express correctly folded secreted proteins provides a distinct advantage over bacterial systems that often require laborious and inefficient procedures to denature and refold proteins expressed as insoluble inclusion bodies.

Proteins can be produced in *P. pastoris* under fully validated conditions (Fisher *et al.*, 1999), which is essential for the production of vaccines or therapeutics. The acceptance of the *P. pastoris* expression system is illustrated by the fact that a number of proteins synthesized in *P. pastoris* are being tested for use as human pharmaceuticals in clinical trials (Cereghino and Cregg, 2000).

Heterologous proteins can be expressed either intracellularly or, when linked to the appropriate signal sequences, secreted. Secreted proteins are easily and efficiently purified from the supernatant, as *P. pastoris* secretes only low levels of endogenous proteins. The low level of host proteins in the growth medium facilitates purification of the final secreted product. In the case of a target protein that is not secreted in its native system, intracellular expression is often the best alternative, as exposing the protein to the secretory pathway may result in the product being altered by glycosylation or to lack other essential post-translational modifications. However, the purification of an intracellular protein is generally more difficult than for secreted proteins, as the target product often represents less than 1% of the total intracellular proteins (Daly and Hearn, 2005).

Reported levels of scFv production in *P. pastoris* in shake-flasks range from 10 to 250 $\mu g\ mL^{-1}$ (Eldin *et al.*, 1997). Scaled up to fermentation, *P. pastoris* can grow to cell densities of 500-600 OD_{600} units. Product expression levels in the range of $g\ L^{-1}$ can be expected, ranking the *P. pastoris* expression system as one of the most productive eukaryotic expression systems available (Cregg *et al.*, 2000). Growth to high cell density is especially important for secreted proteins, as the concentration of product in the medium is approximately proportional to the concentration of cells in the culture.

Potential problems related to the *P. pastoris* expression system includes inefficient secretion of some larger proteins (>30 kDa), proteolysis of secreted proteins during

high-cell-density fermentations, inappropriate glycosylation of glycoproteins, toxicity of some proteins leading to low expression levels and low transformation frequencies (Fisher *et al.*, 1999).

Other yeast expression systems for antibody fragments include *Candidia boidinii*, *Hansenuela polymorpha*, *Saccharomyces cerevisiae* and *Pichia methanolica*.

1.3.1.3 Alternative hosts for antibody fragment production

There are also several eukaryotic systems available for production of antibody fragments, like mammalian cells, insect cells, plants, transgenic animals and lower eukaryotes (Verma *et al.*, 1998). Methods for production of therapeutic whole antibodies in mammalian cells are well established, however, large-scale production is expensive and time-consuming. Plants show several advantages as large-scale antibody production systems, for instance plants are easy to grow, at low costs. Drawbacks of this system are related to the time-consuming process of generating transgenic plants that express the antibody. In addition, the downstream processing to isolate the expressed antibodies from the plant is relatively expensive and laborious (Joosten *et al.*, 2003).

1.3.2 Fermentation strategies

1.3.2.1 *E. coli* fermentation strategies

The large-scale production of heterologous proteins from *E. coli* is affected by a number of factors, such as choice of strain and expression vector, mode of cultivation (batch/fed-batch), fermentation temperature, medium composition and time and duration of induction.

Both continuous and fed-batch cultures have been investigated for expression of antibody fragments by *E. coli*. *E. coli* fed-batch fermentations have proven to generate a higher biomass concentration, and hence are associated with higher product titres, than batch fermentations. Expression levels reported (Carter *et al.*,

1992) shows a 4-5 fold increase in antibody fragment titres by applying fed-batch relative to batch cultivation. Regardless of whether a batch or a fed-batch protocol is applied, it is essential to design the process so as to optimise level of product expression and minimise problems related to substrate inhibition, limited oxygen transfer capacity and the formation of growth inhibitory by-products (Bowering, 2000). One such by-product is acetate, which is produced in the presence of excess glucose. A high acetate concentration may reduce growth rate and cell density, and hence product yield. In order to avoid excess levels of acetate, the specific growth rate can be controlled by limiting essential nutrients (for example carbon and nitrogen) (Korz *et al.*, 1995). Another alternative is to utilise a different carbon source, such as glycerol, which is not associated with acetate formation. It has also been shown that the specific growth rate can be controlled by lowering the temperature of the culture (Bowering, 2000).

Media composition is known to influence the product yield, as well as its location. Defined media is usually used when it is important to control the concentration of the various nutrients during the fermentation in order to maximise cell growth. Complex medium are often associated with higher growth rates than defined medium, however as the complex media can vary in both composition and quality, the fermentations based on this type of media are often less reproducible.

Product expression in *E. coli* is most commonly controlled by a *lac* promoter (Donovan *et al.*, 1996), or a derivative of it. *lac*UV5 is a close relative to the *lac* promoter, other related promoters are the stronger *tac* and *trc*, which are hybrids of the tryptophan and *lac* promoters. Protein expression from these promoters is induced by lactose or isopropyl β-D-thiogalactopyranoside (IPTG). An advantage of IPTG over lactose is that the former is not involved in cell metabolism, making it easier to assess the effect of inducer concentration on the expression levels achieved. A drawback of this inducer is its high cost, which especially affects large-scale fermentation processes. However for the expression of high-value-products, the cost of the inducer is less of a problem. IPTG can be toxic to humans and may therefore not be a good choice in productions of therapeutic proteins.

In addition to the type of inducer, its concentration, the induction temperature, point of induction and duration of induction are factors that affect the production of heterologous proteins. A reduced inducer concentration may improve the yield of functional protein; this is achieved by reducing the rate at which the protein is formed, which is essential in order to avoid overwhelming the export pathway of the host. A reduction in temperature during induction appears to improve protein expression by the same mechanism. Short induction times are favourable when product is located in the periplasm, as leakage into supernatant and the ratio of product found in insoluble fractions increases with induction time (Verma *et al.*, 1998).

1.3.2.2 *P. pastoris* fermentation strategies

Pichia pastoris is well suited for fermentative growth, as it reaches very high cell densities during the course of the fermentation. Various fed-batch and continuous culture protocols are available for high cell density fermentations of *P. pastoris*, all based on the following fundamental steps:

- Initial growth on glycerol in defined media. At this stage growth is rapid, but heterologous gene expression is fully repressed.
- Upon depletion of glycerol, a transition phase is initiated in which additional glycerol is fed to the culture at a growth-limiting rate.
- Finally, methanol, or a mixture of methanol and glycerol, is fed to the culture to induce expression and continue cell growth.

Potential advantages of the mixed feeding strategy are improved cell viability, shorter induction phase and higher protein production rate. However the glycerol has to be carefully monitored, as excess levels of this carbon source may repress the promoter, yielding lower product expression relative to induction on methanol alone. Glycerol metabolism can also trigger a build-up of ethanol and acetate, which also might result in repression of the promoter and hence lower product yield.

P. pastoris fermentations are based on inexpensive and defined medium and are therefore compatible with the production of vaccines and human pharmaceuticals. This organism can grow on a range of pH's, from 3-7. The ability to grow at a low pH is advantageous, as the culture is less likely to be contaminated by other microorganisms.

Problems related to precipitation of one or more of the salts present in the medium have been reported (Brady *et al.*, 2001), making it difficult to determine the actual concentration of dissolved minerals in the medium. In addition, the precipitates lead to turbidity and interfere with measurements of the optical density. This problem can be overcome by reducing the media salt concentration (Brady *et al.*, 2001), without interfering with growth rate, biomass yield or protein expression levels. Reduced salt concentration was reported to also solve a second problem, the formation of a lipid-like substance in the medium, interfering with purification processes downstream of fermentation.

As the *P. pastoris* cell density increases, so does the concentration of other cellular materials, such as proteases. Proteolysis generally is a more significant problem over time, as the number of viable cells decreases. Different strategies have been adopted in order to minimize the proteolytic instability of foreign proteins secreted into the *P. pastoris* culture medium. One is the addition of amino acid-rich supplements like peptone or casamino acids, which reduce product degradation by acting as excess substrates for proteases. Changing the pH of the culture medium is another strategy. *P. pastoris* is capable of growing at a broad pH range from 3 to 7, which makes it possible to adjust the pH to one that is not optimal for a problem protease. Jahic *et al.* (2003) reports an increase of full-length product, susceptible to serine proteases in the culture supernatant, from 40 to 90% due to decreasing the pH from 5.0 to 4.0. A third strategy is the use of protease-deficient *P. pastoris* host strains.

Heterologuous protein expression in *P. pastoris* is driven from the methanol-inducible alcohol oxidase I gene (*AOX1*). *AOX1* is a tightly regulated gene that is repressed in the absence of methanol. Monitoring the concentration of methanol used is important when optimising expression levels - the level of transcription initiated from the *AOX1* promoter has shown to be 3-5 times greater in cells fed methanol at

growth-limiting rates compared to cells grown in excess methanol (Cereghino and Cregg, 2000). Typically levels of 0.5-1.0% (v/v) methanol are used. Too high levels of methanol have negative effects on cell growth, and may inhibit protein expression. In order to maximise yields, it can be beneficial to reduce the induction period, this in order to reduce the extent of proteolysis occurring. The temperature during induction is also known to affect both the amount of proteolysis occurring as well as the amount of protein expressed (Jahic *et al.*, 2003).

Use of methanol in large-scale fermentations might be problematic, requiring special facilities and handling procedures, as well as regulatory approvals. Promoters that are induced by other sources rather than methanol are available. For example the GAP promoter has shown strong expression on glucose (Daly and Hearn, 2005).

1.4 Recovery of antibody fragments from fermentation broths

The following is a brief introduction to some of the main techniques applied in this project. More details and theoretical considerations will be provided in the following results chapters or in appendixes where appropriate.

1.4.1 Purpose of downstream processing

Following fermentation it is necessary to recover and purify the target product from the fermentation broth; the processes applied for this purpose are termed downstream processes. Efficient recovery of antibodies and antibody fragments from a cell culture is crucial for minimising manufacturing costs. Recovery processes consisting of few steps generally have lower capital and operating costs, and the overall yield is also expected to increase with a decreasing number of downstream processing steps.

Downstream processing is highly dependent on the characteristics of the fermentation broth. The most appropriate method for the initial stages of downstream processing also depends on the nature and the location of the target product. For

extracellular products, primary recovery usually involves removal of cells from the fermentation medium. This is often done by centrifugation or filtration. For products expressed in the periplasm, or as intracellular inclusion bodies, primary recovery involves harvesting of the cells by centrifugation or filtration, followed by release of the product by either mechanical cell disruption or permeabilisation of the membrane. Finally, cell debris is removed, again by centrifugation or filtration. Final purification of product is normally achieved by one or more chromatographic steps.

Integrated product recovery processes are also available, which combine solid-liquid separation with initial fractionation. Expanded bed adsorption (EBA) is an integrated method combining biomass removal, product concentration and partial protein purification in one method (Anspach *et al.*, 1999). Alternative options for integrated recovery include extraction using aqueous two-phase systems (ATPS) (Thömmes *et al.*, 2001) and suspended bed chromatography (SBC) (Ling *et al.*, 2003). The advantages of integrated product recovery processes include an increased efficiency of downstream processing, as the traditional time consuming solid-liquid separation and primary purification steps can be bypassed.

1.4.2 Separation of biomass

Primary recovery of proteins from fermentation broths mostly comprises removal of cells by conventional methods such as centrifugation or filtration.

1.4.2.1 Centrifugation

The application of centrifuges for separation of liquid and solid phases is widespread. In bioprocessing, centrifugation can be used for removal of whole cells, cell debris, spheroplasts and inclusion bodies from the liquid phase. It may therefore be used as an option for initial separation of cells from the fermentation medium as well as later on in the downstream processing sequence, for example for separation of cell debris resulting from homogenisation, or cell spheroplasts following periplasmic release of product.

Centrifugation takes advantage of the difference in density between the solid and liquid phases. The density gradient is amplified through the application of centrifugal force by rotating the solid-liquid suspension at high speeds. In the biotechnology industry, three different centrifuges are mainly used: disc-stack, multi-chamber bowl and tubular bowl centrifuges.

Disc-stack machines are typically used in bio-processing to separate and concentrate cells, cell-debris, inclusion bodies and precipitates (Boychyn *et al.*, 2004). The feed is introduced to the centrifuge bowl from the top and accelerated in a distributor before entering the disc-stack. Separation of liquid and solids takes place between the discs. Liquid moves through the disc-stack towards the centre of the bowl, from where it is pumped out under pressure, whereas solids are moved outwards to the solids holding space at the bowl periphery (Maybury *et al.*, 1998). Solids are discharged intermittently at a fixed time interval, or continuously through nozzles.

Multi-chamber bowls are solid bowl centrifuges, consisting of two or more chambers, applied for the recovery of fine biological material (Boychyn *et al.*, 2000). The feed enters the rotating bowl through an inlet at the top of the machine. It then flows through the individual chambers, from the inner chamber to the outer. The larger particles will be deposited in the inner chamber, whereas the lighter, smaller particles are deposited progressively in the outer chambers. The clarified liquid is discharged under pressure and the solids collected are removed manually when the bowl's solids capacity is reached.

An example of a tubular bowl centrifuge is the Carr Powerfuge™. Applications of the Powerfuges™ in the biotechnology industry include cell harvesting, cell debris clarification, and inclusion body recovery. In this device the feed is introduced at the top of the centrifuge when the bowl has reached its required speed. The clarified liquid exits from the bottom of the bowl, while solids are deposited at the bowl wall. In the Powerfuges™, solids are removed with the aid of a vibrating knife when the solids capacity of the centrifuge is reached. Due to the high centrifugal force of the Powerfuge (~20000g), clarification efficiency as well as solids compaction and dewatering are typically high (Boychyn *et al.*, 2004).

Disadvantages of centrifugation as an initial downstream processing step relate to the high shear environment, especially at the entrance of the machine, which may damage the product. Moreover, centrifugal operations are sometimes associated with incomplete biomass removal, and with high energy costs.

The application of centrifuges for the recovery of antibody fragments from high cell density feed-streams is discussed in more detail in Chapters 4 and 5.

1.4.2.2 Microfiltration

Microfiltration is a frequently used alternative to centrifugation when it comes to biomass separation. The process separates components according to their size, and is most efficient when the particles are within the range of 0.1–10 μm. Apart from membrane pore size, membrane composition is another important factor that must be considered, as components of the solute can interact with the membrane surface and cause fouling. Other factors to consider are solution conditions, such as pH and ionic strength, and operating conditions such as transmembrane pressure.

The simplest design of a microfiltration step is dead-end operation. Dead-end filtration implies that the feed-stream flow is perpendicular to the filter. Over time, cells or cell debris will build up on the surface of the filter and thereby foul the membrane and reduce the performance of the filtration operation. For industrial applications, crossflow operation is often preferred because of the lower tendency to membrane fouling relative to the dead-end mode. In crossflow operation, the feed flow is parallel to the filter surface and it is the continuous sweeping motion of the feed-stream across the membrane surface that results in reduced fouling.

Filtration has the advantage over centrifugation in that it can achieve 100% removal of solids, hence generating a cell free solution. Limitations to the technique include membrane fouling due to suspended solids, which results in a significant drop in the process efficiency.

1.4.3 Release of intracellular product

For products expressed intracellularly, cell disruption constitutes the next stage in the isolation of the target product. Cell-associated products can be released by either mechanical cell disruption, or by periplasmic release.

1.4.3.1 Homogenisation

High pressure homogenisation is one of the most widely used methods for cell disruption at industrial scale, and the process aims to break up cells in order to release intracellular proteins. During homogenisation the cell suspension is forced through a restricted orifice discharge valve at high pressure. The disruption is believed to occur due to a number of factors, such as high shear levels, and the level of cell breakage is affected by the nature of the organism, the culture medium, the specific growth rate of cells, cell concentration of feed etc (Sauer *et al.*, 1989).

Operation at high pressures is often desirable, as it increases the breakage efficiency for each pass. Operation at high pressure and increased number of passes can however generate very fine particles which may reduce the efficiency of subsequent centrifugal clarification or microfiltration steps. Another possible disadvantage of this disruption method is the concomitant release of cellular products and components other than the target product, such as proteases and nucleic acids. This may present problems during further downstream processing operations, for example due to product degradation.

1.4.3.2 Periplasmic release

The aim of periplasmic extraction (from Gram negative bacteria) is to release selectively periplasmic material whilst maintaining cell integrity in order to avoid contamination of the process stream with intracellular material. The presence of proteases, DNA or lipids is not desirable as these components may degrade the product or complicate subsequent purification stages. Another advantage with specific periplasmic release relative to homogenisation or other mechanisms

providing complete cell disruption is that the spheroplast is more or less intact after product release. The absence of fine particles increases the efficiency of subsequent centrifugal clarification.

Techniques for the specific release of periplasmic material include physical methods such as osmotic shock (Zimmermann *et al.*, 1991), freeze/thaw (Johnson and Hecht, 1994) and heat treatment (Tsuchido *et al.*, 1985); biological methods involving the use of enzymes (Neu and Heppel, 1964); chemical methods such as addition of triton X-100 and guanidine (Naglak and Wang, 1990), chloroform (Ames *et al.*, 1984) and EDTA (Ryan and Parulekar, 1991). Another method combines heat treatment with a chemical approach, and involves suspending the cells in a Tris-EDTA extraction buffer at a high temperature (Weir and Bailey, 1997).

1.4.4 One step recovery and initial purification by expanded bed adsorption

Expanded bed adsorption (EBA) combines the processes of clarification, concentration and initial purification in a one step unit operation (Barnfield-Frej *et al.*, 1994; Fenneteau *et al.*, 2003; Thömmes *et al.*, 1996) hence making it a very interesting alternative for initial product recovery from an unclarified feed-stream. The advantages of an integrated product recovery process like EBA are several fold, including an increased efficiency of downstream processing, as the traditional time consuming solid-liquid separation and primary purification steps can be bypassed. The reduction in number of process steps is advantageous with respect to both total processing time and overall yield. Moreover, a more time efficient process leads to less product degradation, as the time the product is exposed to for example proteolytic enzymes in the media, is shortened.

The principle of expanded bed adsorption is relatively simple. The liquid stream is upwards, through a bed of adsorbent beads that are constricted by a flow adapter. As a result of the upward flow and properties of the beads the bed expands as spaces open between the beads. The enlarged void fraction allows cells, cell debris and other particulates to pass through the bed while the target protein is captured by the

adsorbent (Anspach *et al.*, 1999). Capture of target product is by means of charge, hydrophobicity or ligand specificity.

Expanded bed adsorption is based on stable fluidization and uses specially designed adsorbent particles and columns in order to achieve this. The adsorbent particles are characterized by a well-defined size distribution and an increased density relative to conventional chromatography adsorbents. The higher density is usually due to a quartz or a steel core, which ensures sufficient particle density to achieve stable expansion at high flow rates. The column is equipped with a liquid distribution system that allows for the formation of a stable expanded bed with minimal back-mixing, and it has an adaptor which height can be adjusted during the process (Anspach *et al.*, 1999).

The applications of EBA are wide, and so far includes recovery of secreted product from *E. coli* (Brobjer, 1999) and yeast cells (Barnfield-Frej *et al.*, 1997; Calado *et al.*, 2002; Fernandez-Lahore *et al.*, 1999; Schiolach *et al.*, 2003), separation of proteins from of *E. coli* and yeast cell homogenates (Barnfield-Frej *et al.*, 1994; Chang *et al.*, 1995), *E. coli* lysate (Johansson *et al.*, 1996) and *E. coli* inclusion bodies, whole hybridoma fermentation broth (Thömmes *et al.*, 1996), whole mammalian cell culture broth (Feuser *et al.*, 1999b) and rapeseed extracts (Bay and Glatz, 2003).

Drawbacks of EBA relate to the biomass content of the feedstock and include reduced bed stability and sorption performance as a result of channelling and the formation of stagnant zones during loading, reduced static capacity as cell debris may penetrate into the pores and hence block the binding sites of the adsorbent, and modified fluidization behaviour. Moreover, the lifetime of the EBA adsorbent is limited by irreversible fouling and harsh CIP procedures (Feuser *et al.*, 1999a).

Theoretical considerations and applications of EBA of relevance to this work are described in more detail in Chapter 6.

1.5 Scale-down for prediction of industrial-scale performance

Scale-down is a concept that has been developed to mimic the operation of industrial-scale machinery using small amounts of process material, with typical working volumes in the order of 50-100 mL. Scale-down of industrial processes is a valuable tool for minimizing the time and cost required for bioprocess development. The ability to predict the performance of large-scale processes is important to ensure rapid process evaluation, and hence fast development of successful operations at the industrial scale. A major advantage using scale-down approaches to predict the performance of a large-scale process is the low requirement of process material, making it possible to evaluate several potential process options in early stages of process development. Time-consuming and expensive pilot-scale runs are avoided. The use of ultra scale-down (USD) techniques to investigate the clarification performance of industrial-scale centrifugation equipment handling dilute suspensions has been the subject of previous research (Boychyn *et al.*, 2000; 2001; 2004; Maybury *et al.*, 2000) and other work has applied scale-down techniques to depth filtration (Reynolds *et al.*, 2003), and to expanded bed adsorption (Willougby *et al.*, 2004).

1.5.1 Applications of scale-down in downstream processing

1.5.1.1 USD centrifugation

The scaling between centrifuges of different size and design is often done according to the Sigma theory (Ambler, 1961; Maybury *et al.*, 1998), which describes the solid–liquid separation performance of centrifuges. A brief introduction to the Sigma theory is given in section 4.1.1., and relevant equations and technical data are given in Appendix A2 and A3, respectively.

For scaling purposes it would be ideal to have access to equipment that was the exact small-scale replica of industrial-scale machines. The development of such miniaturised mimics would however be impractical to achieve. A more feasible

approach would be to modify existing equipment to allow reduced feed volumes to be processed. Mannweiler and Hoare (1992) modified an existing disc-stack machine by reducing the number of active discs – this resulted in a tenfold decrease in feed material requirement. Moreover, Maybury *et al.* (1998) showed that it was possible to lower the throughput requirement by a factor of four by reducing the solids holding space of the disc-stack.

The ultra scale-down approach (Boychyn *et al.*, 2000, 2001, 2004) involves the use of bench top equipment to mimic the performance of large-scale centrifuges. By utilising a laboratory centrifuge a reduction in process volume requirement to the millilitre-scale is achieved. A major challenge when scaling a centrifugation process from laboratory to industrial scale is related to the fragile nature of most biological materials. The laboratory centrifugation tube is of a discrete bottle design and hence the feed material is exposed to little or no shear forces relative to what it would experience in a large-scale machine. Until recently it has been difficult to quantify the impact of flow stresses in centrifuges on their performance. Work with a protein precipitate system (Mannweiler and Hoare, 1992) concluded that the majority of breakage occurred in the feed zone of disc-stack centrifuges. Similar results were observed in a multi-chamber bowl machine (Boychyn *et al.*, 2000). Such breakage of feed material in a centrifuge causes an increase in fines resulting in a reduction of clarification performance. The difficulties in characterising complex fluid flow patterns within centrifuges have been overcome, to some extent, by advances in computational fluid dynamics (CFD) software and have been well reported (Boychyn *et al.*, 2001, 2004; Levy *et al.*, 1999). These advances have enabled the feed zone of an industrial centrifuge to be mapped in terms of shear forces, and these forces reproduced in a small rotating disc device (Boychyn *et al.*, 2001, 2004). This, coupled with the Sigma theory (Ambler, 1961; Maybury *et al.*, 1998) mentioned above, has allowed an ultra scale-down centrifugation mimic to be developed and verified. The use of this approach for the prediction of industrial scale centrifugal clarification has been published (Boychyn *et al.*, 2000, 2001, 2004; Maybury *et al.*, 2000; Neal *et al.*, 2003) and forms the basis for the ultra scale-down centrifugation work presented in Chapter 4 of this thesis.

1.5.1.2 Scale-down of expanded bed adsorption

For EBA method scouting and development purposes, small-scale columns have proven very useful. The advantages of using such small columns are related to lower material usage and reduced cost compared to the large-scale columns used for commercial purposes. Even for a 5 cm column, the volume required for a typical separation run is no less than 12 L, whereas the corresponding volume for a 0.5 cm column would be 120 mL (Ghose and Chase, 2000a).

Chromatographic processes are usually scaled by keeping bed height and linear flow velocity constant whilst varying the column diameter and the volumetric flow rate. The sample product concentration should be the same, while the sample load is varied in order to keep the ratio of sample volume to adsorbent volume the same. To present a valid comparison between beds of different scales, they should demonstrate comparable performance in column hydrodynamics, adsorption kinetics, and separation performance.

Barnfield-Frej *et al.* (1997) studied the scale-down of the expanded bed adsorption of a model protein suspended in a culture of *Saccharomyces cerevisiae*. Columns ranging from 2.5 to 60 cm in inner diameter were applied, corresponding to feedstocks of 0.75 to 440 L. The outcome of the study suggested that the performance at the different scales were similar, and hence scale-down was successful.

Successful scale-down of expanded bed chromatography has also been reported by Ghose and Chase (2000a,b). Method development for the separation of two model proteins from yeast homogenate by hydrophobic interaction was performed using a 1 cm ID column, and the results verified in a 5 cm ID column – representing a 25-fold scale-down factor. Bed expansion, as well as recovery and outlet profiles of the two model proteins in the 5 cm bed showed good agreement with results obtained in the 1 cm bed.

Willoughby *et al.* (2004) achieved comparable performance between a specially developed 0.19 cm ID column (also applied in this work) and a 2.5 cm ID column.

This represents a 200-fold scale-down factor, and allowed predictions to be performed using sample volumes of ~5 mL. Expansion behaviour and hydrodynamics in buffer were tested and found to be very similar in the two beds. Breakthrough curves generated for adsorption of BSA on Streamline DEAE were also found to be comparable, as they varied with no more than ± 6% between the two beds at 50% breakthrough. Binding and elution behaviour of adsorption of a Fab antibody fragment from *E. coli* homogenate on Streamline rProteinA was generated and similar profiles were achieved for both columns on a column volume basis. Finally the purity of samples taken from the elution pools of the two columns were compared and found to be almost identical.

A not so successful scale-up was reported by Brobjer (1999), who experienced pressure build-up, binding of biomass to adsorbent and collapse of the small-scale expanded bed (Streamline 25) when processing an *E. coli* feedstock, resulting in lower recovery compared to the large-scale column (Streamline 200). This indicates that scale-down with complex feeds containing biomass may not be straightforward.

1.6 Visualisation of suitable operating conditions using Windows of Operation

Bioprocesses, and the operational stages which comprise them, have many interacting variables. This leads to a complex design task in which many variables must be considered simultaneously and in which the designer must select suitable values so as to obtain a desired level of performance. Without suitable computational tools this is a difficult task. Windows of Operation provide one such tool, which will help in design and also enable the rapid comparison of alternative operating strategies. A Window of Operation aims to visualise the available operating conditions for a given process or operation when constrained by limitations given by for example pre-set performance requirements as well as physical processing constraints. Previous work has demonstrated the use of Windows of Operation as a visualisation tool within bioprocessing. Zhou and Titchener-Hooker (1999) developed Windows examining the impact of fermentation conditions on the subsequent downstream processes of homogenisation and centrifugation. King *et al.*

(2004) extended the previously developed Windows of Operation to three dimensions. Windows of Operation have also recently been developed to assess integrated robotic systems for the measurement of bioprocess kinetics (Nealon *et al.*, 2005).

Generally, Windows of Operation have not only proved useful in the selection of suitable operating conditions for a given processing objective but also to indicate where a particular item of equipment is not suitable for the chosen process target.

Details regarding the construction of Windows of Operation for centrifugation and EBA processes are given in Chapters 5 and 7, respectively.

1.7 Project objectives

There is an increasing demand for antibodies and antibody derived therapeutics. In order to meet these demands, time- and cost efficient development of production and purification processes are necessary. This project focuses primarily on the primary recovery of antibody fragments expressed in high cell density cultures. Two systems are investigated; *P. pastoris* with extracellular expression of a scFv antibody fragment, and *E. coli* expressing a Fab antibody fragment directed to the periplasmic space.

The work addresses some of the challenges related to high cell density expression systems and aims to introduce a rapid method for evaluation of two different primary recovery processes for antibody fragments: centrifugation and expanded bed adsorption. This will be achieved by:

- Development and application of scale-down approaches for centrifugation and expanded bed adsorption in order to ensure rapid prediction of large-scale process performance.
- Visualisation of (predicted) large-scale process performance and determination of the most appropriate operating conditions for recovery of the high cell density cultures investigated using Windows of Operation.

1.8 Thesis layout

Chapter 2 provides details about the materials and methods used throughout this project. The results of the experimental studies are presented in Chapters 3-8. The results chapters are all structured in a similar fashion, each starting with an abstract briefly explaining the motivation for the chapter, as well as its objectives. The abstract is followed by an introduction section which includes theoretical considerations of relevance for the chapter, before the results are presented and discussed. At the end of each results chapter the main findings are summarised.

Chapter 3 describes the production of the two antibody fragments used in this study - Fab and scFv - in *E. coli* and *P. pastoris* fermentation cultures, respectively. It should be noted that the main purpose of these fermentations was to generate biomass for subsequent downstream processing studies, and no attempts to optimise growth and level of product expression were therefore made.

Chapter 4 describes the development of a USD centrifugation method aimed at dealing with high solids density feed-streams. The methodology is verified by comparison with pilot-scale data obtained for *E. coli* whole cells and periplasmically lysed *E. coli* cells. Furthermore, the novel USD technique is applied to predict the large-scale centrifugal clarification performance of *P. pastoris* and *E. coli* homogenate. For the two latter feed stocks, laboratory-scale predictions of dewatering and product yield are also presented.

Chapter 5 considers the selection of centrifuge type and operating conditions necessary for the efficient recovery of a product from a high cell density culture. This involves generation of Windows of Operation in order to visualise the available operating conditions for a number of industrial centrifuges. The use of centrifugation Windows of Operation is demonstrated by two case studies that examine centrifuge selection for the processing of *P. pastoris* cultures and *E. coli* homogenates of varying solids concentration, and are based on results obtained from the USD studies in Chapter 4.

Chapter 6 investigates the scalability of an EBA process when exposed to *E. coli* homogenates of varying solids concentration. The results obtained in the scale-down column are compared to data achieved in a Streamline 25 column for verification of the system. The comparison between the two columns is based on expansion behaviour, axial dispersion characteristics, Fab breakthrough curves, binding capacities and yield levels achieved.

Chapter 7 describes an alternative approach for prediction of the performance of an EBA process, and involves simulation of product breakthrough based on the general rate model. The model is solved numerically and data generated from the general rate model are used to develop a series of Windows of Operation, which visualise the most suitable operating conditions available for large-scale recovery of Fab from *E. coli* homogenate by EBA when the operation is restricted by predefined process performance criteria. To prove the validity of the general rate model, a verification is presented which involves a comparison of simulated breakthrough curves and experimental breakthrough curves generated in a Streamline 25 column.

Chapter 8 compares two different flowsheet options for the recovery of *E. coli* homogenate: 1) a conventional approach, comprising centrifugal separation, followed by filtration and packed bed chromatography and 2) expanded bed adsorption. The comparison is based on the calculation of total processing time, overall yield and throughput, and concentration factor for each flowsheet, and is based on operating conditions chosen from the Windows of Operation generated for centrifugation and EBA in Chapters 5 and 7, respectively. This chapter demonstrates the importance of scale-down technology, coupled with Windows of Operation, in relation to making flowsheet decisions in the bioprocessing industry.

Finally, Chapter 9 provides a summary of the main observations and conclusions of the project, and suggestions for future work are given in Chapter 10.

2 Materials and methods

This chapter provides details about the methods and protocols applied in this study.

All chemicals and reagents were purchased from Sigma-Aldrich, UK, unless otherwise stated, and were of the highest grade available.

2.1 Fermentation processes

2.1.1 *E. coli* fermentation

E. coli biomass for USD and pilot-scale centrifugation studies and EBA experiments was generated according to the protocol described below. The fermentations were carried out by fellow students at the Department of Biochemical Engineering, UCL.

2.1.1.1 *E. coli* strain and plasmid for expression of a Fab antibody fragment

The industrial *Escherichia coli* strain W3110 containing the plasmid pTTOD A33 IGS2 was kindly donated by Celltech Chiroscience Ltd (Slough, UK). A working cell bank was prepared as described elsewhere (Bowering *et al.*, 2002).

2.1.1.2 Culture media

All recipes given are per L of final media, unless otherwise stated.

Complex media for starter cultures: The complex media was used for starter cultures and contained 16 g Phytone (obtained from Becton-Dickinson Life Science Research Ltd, UK), 10 g yeast extract and 5 g NaCl.

SM6G$_c$ defined media: SM6G$_c$ was prepared as follows: 5.2 g $(NH_4)_2SO_4$, 4.4 g $NaH_2PO_4.H_2O$, 4.03 g KCl, 1.04 g $MgSO_4.7H_2O$, 4.16 g citric acid, 0.25 g

$CaCl_2.2H_2O$, 112 g glycerol, and 0.01% trace elements solution. pH was adjusted to 6.95 with 15% ammonia.

100 x trace element solution: 104 g citric acid, 5.22 g $CaCl_2.2H_2O$, 2.06 g $ZnSO_4.7H_2O$, 2.72 g $MnSO_4.4H_2O$, 0.81 g $CuSO_4.5H_2O$, 0.42 g $CoSO_4.7H_2O$, 10.06 g $FeCl_3.6H_2O$, 0.03 g H_3BO_3, 0.02 g $Na_2MoO_4.2H_2O$

2.1.1.3 20 L fermentation

Starter cultures were grown in 200 mL of complex media containing 10 μg mL^{-1} tetracycline for 4 h at 37°C. This culture was used as a 10% inoculum for $SM6G_c$ defined media shake flasks. These were incubated for 22 h at 30°C, 200 rpm, with 10 μg mL^{-1} tetracycline, until an OD_{600} of ~3-4 was achieved.

1 L of culture from the defined media shakes described above was used to inoculate 10 L of $SM6G_c$ media in a 20 L LH 2000 series fermenter (Ingeltech UK. Ltd., Berkshire, UK). pH was maintained at 6.95 using 15% (w/v) ammonia solution and 20% (v/v) H_2SO_4. Dissolved oxygen was maintained at 30%, using gas blending with 40:60 O_2:N_2 when necessary. The culture temperature was maintained at 30°C for ~32 h (OD_{600} ~ 42), after which it was reduced to 25°C for the remaining duration of the fermentation. Between OD_{600} of 42-88 multiple salt additions were given to maintain Mg^{2+} and PO_4^{2-} concentrations. When an OD_{600} of ~88 was achieved, DOT spiking and demand for acid indicated all the glycerol carbon source in the culture had been utilized and at this point Fab production was induced by addition of 25 mL of 15.3 g L^{-1} isopropyl β-D-thiogalactopyranoside (IPTG). After induction carbon was supplied to the culture for Fab synthesis and cell maintenance by a 16 mL h^{-1} glycerol feed. The culture was harvested 36 hours after addition of the IPTG.

2.1.2 *P. pastoris* fermentation

2.1.2.1 *P. pastoris* strain and plasmid for expression of a scFv antibody fragment

The plasmid pPICZαA-Fln-209 was constructed by inserting the gene encoding Fln-209 scFv into the expression vector pPICZαA (Invitrogen Ltd, UK). pPICZαA-Fln-209 was used to transform the *P. pastoris* strain X-33 for expression of the recombinant scFv protein. X-33 is a wild type *Pichia* strain that is useful for selection on Zeocin™ and large-scale growth. X-33 is Mut^+ and transformation of this strain with plasmid DNA will yield Mut^+ transformants, that is, they will retain their ability to metabolise methanol quickly (compared to Mut^S transformants in which methanol utilisation is slow).

2.1.2.2 Culture media

All recipes given are per L of media, unless otherwise stated.

10xD: 200 g D-glucose. The solution was filter-sterilised.

10xYNB: YNB consisted of 134 g Yeast nitrogen base (YNB) (with ammonium sulphate and without amino acids). The solution was filter-sterilised prior to use.

500xB: (per 0.1 L): 20 mg Biotin. The solution was filter-sterilised.

1M Potassium phosphate buffer, pH 6.0: Potassium phosphate buffer was made up of 23 g K_2HPO_4 and 118.4 g KH_2PO_4. pH was adjusted with KOH, and the buffer heat sterilized.

YPD: YPD contained 10 g yeast extract and 20 g peptone. 100 mL 10xD was added after heat sterilisation. 1 mL Zeocin™ was added to the medium where appropriate. For YPD agar plates, 20 g agar was added prior to heat sterilisation.

Complex glycerol containing medium, BMGY: Complex glycerol-containing medium was used to initiate shake-flask growth. BMGY was prepared by heat sterilising a mixture of 10 g yeast extract and 20 g peptone in 700 mL RO H_2O. The autoclaved solution was then added 100 mL 1M Potassium phosphate buffer pH 6.0, 100 mL 10xYNB, 2 mL 500xB and 100 mL autoclaved 10% (v/v) glycerol.

Complex methanol containing medium, BMMY: BMMY for shake-flask induction and further cell growth was prepared by adding 10 g yeast extract and 20 g peptone to 700 mL RO H_2O. The mixture was autoclaved, then added 100 mL 1M Potassium phosphate buffer, pH 6.0, 100 mL 10xYNB, 2 mL 500xB and 100 mL filter sterilised 5% (v/v) methanol.

MGY: MGY is a glycerol containing media used for preparing inoculum cultures for 5 L fermentations. It contained 100 mL 10xYNB, 2 mL 500xB and 100 mL autoclaved 10% (v/v) glycerol.

Defined medium: The defined medium for 5 L fermentations was prepared by autoclaving a solution consisting of 26.7 mL H_3PO_4 (85%), 0.93 g $CaSO_4$, 18.2 g K_2SO_4, 14.9 g $MgSO_4$, 4.13 g KOH. This was then added 40 g autoclaved glycerol (87%), 4.35 mL trace elements and 1 mL Zeocin™. pH was adjusted to 5 with 28% NH_4OH.

Trace elements: The trace elements consisted of 6 g $CuSO_4$-$5H_2O$, 0.08 g NaI, 3 g $MnSO_4$-H_2O, 0.2 g Na_2MoO_4-$2H_2O$, 0.02 g H_3BO_3, 0.5 g $CoCl_2$-$6H_2O$, 20 g $ZnCl_2$, 65 g $FeSO_4$-$7H_20$, 0.2 g Biotin and 5 mL H_2SO_4. The trace element solution was filter-sterilised prior to use.

2.1.2.3 Maintenance of X-33/pPICZαA-Fln-209

The strain was streaked for single colonies on YPD agar plates and incubated at 28°C for two days. A single colony was cultured overnight in 100 mL YPD medium containing 0.1 mg mL^{-1} Zeocin™. The culture was grown at 28°C and 200 rpm until an OD_{600} of 2-6 was reached. Cells are now in exponential phase. The cells were

harvested for 10 min at 5000 rpm in room temperature in a Beckman centrifuge (Beckman Coulter, Ltd, High Wycombe, UK), rotor JA10 and suspended in YPD containing 15% (v/v) glycerol to a final OD_{600} of approximately 75. The suspension was aliquoted into sterile 1.5 mL Eppendorf tubes and stored at –80°C.

2.1.2.4 Shake-flask cultivation of *P. pastoris*

To generate biomass for preliminary freeze-thaw and shear sensitivity studies, 100 mL BMGY was inoculated with 50 µL stock culture (see 2.1.2.3) in a 500 mL baffled shake-flask. The culture was incubated for 18-24 h at 28°C and 200 rpm until an OD_{600} of 2-6 was reached. The cells were harvested by centrifugation at room temperature for 10 min at 5000 rpm in a Beckman centrifuge (Beckman Coulter, Ltd, High Wycombe, UK), rotor JM10. The supernatant was discarded and the pellet re-dissolved in methanol-containing media (BMMY) for further cell growth and induced product expression in a 2 L shake flask to a final OD_{600} of approximately 1. Growth was continued at 28°C and 200 rpm until stationary phase was reached (about 96 h). To maintain the methanol concentration at the desirable level, 100% methanol was added to the culture to a final concentration of 0.5% (v/v) every 24 h.

Samples for OD_{600} measurements were collected to monitor the cell growth. In addition, samples for future analysis of product expression (section 2.3.1) were collected. These samples were spun in 1.5 ml Eppendorf tubes at room temperature for 3 min at 13000 rpm in the Eppendorf 5810R centrifuge. Both the supernatants and the pellets were frozen at –80°C.

2.1.2.5 5 L *P. pastoris* fermentation

Fed-batch fermentations were performed in order to generate biomass for scale-down experiments. Fermentations were carried out in a 5 L Chemap fermenter (Chemap, Alpha Laval Engineering Ltd., Middlesex, UK). A colony of *P. pastoris* from an YPD + Zeocin™ agar plate was used to inoculate a 500 mL baffled shake-flask containing 50 mL MGY medium. After about 26 h of growth at 28°C and 250 rpm, 5 mL of the 50 mL culture was used to inoculate a 2 L baffled shake-flask containing

300 mL MGY medium. After 24 hrs of growth at 28°C and 250 rpm the 300 mL culture was inoculated into the 5 L fermenter containing 3 L of sterilised defined medium.

P. pastoris was fermented in a three-stage process starting with batch and fed-batch growth on glycerol followed by fed-batch growth on methanol. Batch glycerol mode continued until depletion of glycerol (indicated by a rapid increase in the level of dissolved oxygen, DOT). Glycerol feed was then initiated and kept at 54.5 mL h^{-1} until the wet cell weight reached about 200 g L^{-1}. Glycerol feed phase was followed by methanol fed-batch to continue cell growth and induce product expression. Methanol was fed at a rate of 10.9 mL h^{-1} for 2.5 h, followed by 22.8 mL h^{-1} for 4.5 h and finally at 26 mL h^{-1} for the rest of the fermentation.

The fermentation was controlled at a temperature of 28°C and DOT > 20%. pH was adjusted by 28% NH_4OH and kept at 5. O_2 and CO_2 out levels were monitored and logged during the fermentation. Samples for measurement of OD_{600}, wet cell weight (section 2.2.1.2) and product expression were collected at regular intervals throughout the fermentation.

2.2 General analytical techniques

2.2.1 Determination of biomass

2.2.1.1 Optical density

Measurements of optical density were performed using a Genesys™ 10 series spectrophotometer (ThermoSpectronic, Cambridge, UK). The sample to be analysed was, if necessary, diluted in order to keep the absorbance reading (A) within the range of the spectrophotometer (A < 0.9). RO water was used as a blank.

2.2.1.2 Sample solids concentration

Solids concentration was determined by filling a pre-weighed 2.2 mL Eppendorf tube with a know volume of sample and spinning it for 30 min at 14000 rpm in an Eppendorf 5810R centrifuge, rotor T-60-11 (Eppendorf UK Ltd, Cambridge, UK). (See Appendix A1 for the relationship between applied rpm and corresponding RCF.) The supernatant was discarded and the solids concentration determined on a wet cell weight per volume (ww/v) basis by re-weighing the Eppendorf tube.

2.2.1.3 Determination of solids volume fraction

Solids volume fraction was determined by centrifuging the feed in a 15 mL graduated Falcon™ tube in an IEC Centra CL3R centrifuge, rotor 243 (IEC Engineering Ltd, West Sussex, UK) at 4600 rpm for 90 min. The ratio of resulting cell volume to initial feed volume (v/v) was determined on a packed volume basis.

2.2.1.4 Dry weight to wet weight ratio of cells

The dry weight to wet weight ratio of *E. coli* and Bakers' yeast is reported in literature to be 0.3 and 0.36, respectively (Ward, 1989). No literature value was available for *P. pastoris*.

In order to determine the cell dry to wet weight ratio for *P. pastoris* the cell suspension was filtered to remove the majority of the interstitial water. The resulting filter cake was dried at 100°C for 5 h and the ratio of dry to wet weight was calculated. The same protocol was applied to a suspension of Bakers' yeast, with a known cell dry to wet weight ratio (Ward, 1989). Based on the relationship between this ratio and the experimentally determined cell dry to wet weight ratio for Bakers' yeast a correction factor was developed to convert the experimental dry cell mass of *P. pastoris*. The dry weight to wet weight ratio for *P. pastoris* was found to be 0.6.

2.2.2 Viscosity measurements

Viscosity measurements were carried out in a concentric cylinder Rheomat 115 viscometer (Contraves Industrial Products, Middlesex, UK). 20 mL samples were exposed to shear rates in the range 24 to 877 s^{-1}. Resulting shear stresses were recorded and plotted against the corresponding shear rates, and the viscosities of the respective samples were determined from the gradient of the linear correlation. (This assumes Newtonian behaviour of the sample. For non-Newtonian suspensions, alternative ways of determining the viscosity will be discussed in the relevant results sections). All measurements were performed in duplicates with a reproducibility of ± $1.05x10^{-3}$ mPa.s in terms of viscosity. The temperature was maintained at 4°C by circulating cold water through the viscometer housing via a water bath.

2.2.3 Shear sensitivity

The following describes the preparation of samples for the analysis of the effect of shear forces. Using a 20 mL disposable syringe, a sample of cell culture was injected into the high speed rotating disc device described by Boychyn *et al.* (2001). All gaps were closed using disposable syringes and the sample was exposed to a shear rate of $1x10^{6}$ s^{-1} (corresponding to ~ 20000 rpm) for 20 s at 20°C in order to mimic the impact of high-shear regions at the inlet of centrifuges leading to potential cell disruption and carry over of solid contaminants. The device was emptied using a clean 20 mL syringe.

2.2.4 Bradford assay for determination of total protein concentration

In order to determine the total protein concentration of a sample, the Bradford assay (Bradford, 1976) was applied. Supernatant samples for analysis of total protein concentration were prepared by centrifugation of the culture for 30 min at 3500 rpm in room temperature in a Beckman centrifuge (Beckman Coulter, Ltd, High Wycombe, UK), rotor GS-6. Samples were diluted to give absorbance readings within the range of the spectrophotometer and 1.2 mL of each sample was mixed

with 0.3 mL Coomassie Brilliant Blue dye reagent concentrate (BioRad Laboratories GmbH, Germany). After incubation in room temperature for 5 min, OD_{595} was measured. The protein concentration of each sample was quantified using a standard curve prepared from known concentrations of bovine serum albumin (BSA).

2.3 Analysis of product expression

2.3.1 ELISA assay for detection of Fln-209 scFv

The following gives an overview of the protocol that was used to determine the concentration of Fln-209 scFv in samples from *P. pastoris* cultures.

1. Coat a Nunc MaxiSorp microtiterplate with 100 µL Streptavidin (Promega, Southampton, UK, dissolved to 5 mg mL^{-1} in water) per well, diluted to 10 µg mL^{-1} in phosphate buffered saline (PBS). Leave overnight at 4°C.
2. Wash 3x with 200 µL PBS.
3. Add 100 µL Fln-PEG-biotin, diluted to 1.3 µg mL^{-1} in PBS, to each well. Incubate for 30 min.
4. Wash 3x with 200 µL PBS with 0.05% (v/v) Tween-20 (PBST).
5. Add samples in 1:2 dilution series. Add first 100 µL PBST to each well. Then add 100 µL of the sample to one of the wells in the top row. Mix 10x and transfer 100 µL from this well to the next one down the microtiterplate etc. Leave for 1 h.
6. Wash 3x with 200 µL PBST.
7. Add 100 µL of Anti-c-myc (Invitrogen Ltd, UK) diluted 1:5000 in PBST, to each well. Incubate at room temperature for 1 h.
8. Wash 3x with PBST.
9. Add 100 µL Rabbit-anti-mouse-IgG-HRP (conjugate) (Dako, Glostrup, Denmark) diluted 1:1000 in PBST, to each well. Incubate at room temperature for 1 h.
10. Wash 3x with 200 µL PBST and 1x with 200 µL PBS.

11. Add 100 µL substrate ABTS (Calbiochem, Darmstadt, Germany) to each well and leave for 5-30 min.
12. Measure the absorbance at 405 nm in a Tecan Safire^2 plate reader (Tecan Austria GmbH, Salzburg, Austria).

2.3.2 Protein G assay for detection of Fab

In order to determine the concentration of Fab from samples of *E. coli*, *E. coli* lysate and *E. coli* homogenate, the Protein G assay was used.

A Protein G Hi-Trap column (GE Healthcare, Uppsala, Sweden) was connected to a modified Agilent 1100 series HPLC system (Agilent Technologies UK Ltd, West Lothian, UK). The sample to be analysed was spun for 15 min at 14000 rpm in an Eppendorf centrifuge. The resulting supernatant was filtered into vials using 0.2 µm sterile syringe filter units (VivaScience AG, Hannover, Germany). The column was equilibrated in buffer A (20 mM sodium phosphate, pH 7.4). 100 µL samples were collected from a vial tray using the auto-sampler and loaded onto the column. Elution was performed using buffer B (20 mM sodium phosphate, pH 2.5).

Peak integration was performed and the resulting Fab concentration determined from a standard curve generated from samples of Fab in known concentrations.

2.4 General downstream processing techniques

2.4.1 Harvesting of *E. coli* cells

E. coli cells for downstream processing studies were harvested from the fermentation broth by solid–liquid separation using a CSA-1 disc-stack centrifuge (Westfalia Separator, AG, Oelde, Germany) operated at 9810 rpm and at a flow rate of 50 L h^{-1}.

2.4.2 Release of periplasmic product

2.4.2.1 Periplasmic extraction

Periplasmic extraction was used in order to selectively release Fab from harvested *E. coli* cells. The *E. coli* cell culture was harvested as described in section 2.4.1. The harvested cells were then resuspended in periplasmic extraction buffer (100mM Tris, 10mM EDTA at pH 7.4) to an appropriate solids concentration and heated to 60^{O}C for 16 h in a 20 L Chemap stirred tank fermenter (Chemap, Alpha Laval Engineering Ltd., Middlesex, UK).

2.4.2.2 Homogenisation

Harvested *E. coli* cells were resuspended in PBS, pH 7, to an appropriate solids concentration. The cell culture was homogenised in order to disrupt the cells and consequently release the periplasmically expressed Fab antibody fragment. Cell disruption was achieved by passing the cell suspension through a Lab60 homogeniser (APV Ltd., Crawley, UK) at 550 bar for 4 passes. Glycol cooling was supplied to ensure a temperature of 4^{0}C.

2.5 Centrifugal separation performance

Section 2.5.1 provides the equations applied in order to analyse centrifugal performance in terms of levels of clarification, dewatering and yield. Section 2.5.2 describes the USD experimental procedure applied in order to predict the separation performance of a pilot-scale centrifuge. Section 2.5.3 gives the protocol for pilot-scale centrifugation for the purpose of clarification measurements. Typical characteristics and relevant dimensions for the centrifuges applied in the USD and pilot-scale studies are provided in Table 5.1 and Appendix A3, respectively.

2.5.1 Evaluation of centrifuge performance: clarification, dewatering and yield

Centrifuge performance was evaluated on the basis of the level of clarification, dewatering and yield achieved. Percentage clarification, $\%C$, was calculated using Equation 2.1:

$$\%C = \frac{OD_f - OD_s}{OD_f - OD_r} \times 100 \qquad 2.1$$

where OD_f, OD_s and OD_r are the optical density of the feed, the sample supernatant and the supernatant of a reference sample, respectively. The reference sample was a well-spun sample and OD_r was taken as the lowest OD achievable for the feed-stream under investigation.

For extracellular product expression, dewatering may be considered to be just as important as clarification, as any liquor in the sediment results in loss of product and hence a decrease in yield. For the determination of dewatering and yield, a mass balance over the process is necessary. Figure 2.1 presents a schematic of the laboratory-scale process used to develop a mass balance across the centrifuge step.

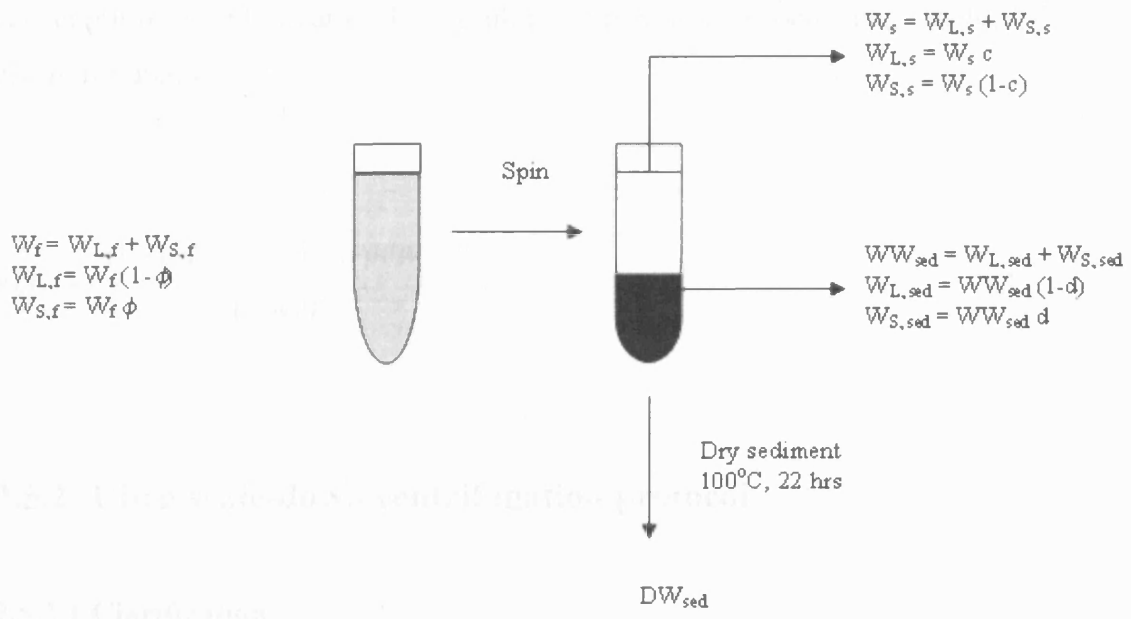

Figure 2.1. A mass balance over the laboratory centrifugation step. W_f is the total weight of the feed, W_s the total weight of supernatant and WW_{sed} and DW_{sed} the weight of wet sediment and the weight of dried sediment, respectively. The subscripts L and S denote liquid and solid phases, respectively. W_f, WW_{sed} and DW_{sed} are measurable parameters, as are solids fraction (ϕ), the fraction of %dewatering (d) and the fractional level of %clarification achieved (c).

Percentage dewatering, %*D*, was calculated by Equation 2.2:

$$\%D = 100 - \left[\frac{WW_{sed} - DW_{sed}/dw_r}{WW_{sed}} \times 100 \right] \qquad 2.2$$

where WW_{sed} is the weight of the wet sediment, DW_{sed} is the weight of the dried sediment and dw_r is the cell dry weight to wet weight ratio. This ratio is a measure of the amount of intracellular water in the cells, water that will be removed by drying but not by the dewatering process itself. Hence dw_r must be taken into account when considering the ratio of interstitial to intracellular water evaporated during oven drying. dw_r was determined according to section 2.2.1.4.

For an extracellular expression system the overall yield can be calculated by considering the ratio of recovered liquid to initial liquid, assuming a constant product

concentration in all streams. The resulting expression for percentage yield, %Y, is given in Equation 2.3:

$$\%Y = \frac{(1-\phi)W_f - (1-d)WW_{sed}}{(1-\phi)W_f} \times 100 \qquad 2.3$$

2.5.2 Ultra scale-down centrifugation protocol

2.5.2.1 Clarification

Clarification was measured by adding a known quantity of material to a 2.2 mL Eppendorf tube and spinning it in the Eppendorf 5810R centrifuge, rotor T-60-11. The spin conditions (speed and time) varied between the experiments, and the details are given in the relevant results sections. The supernatant was removed by pipetting and its OD_{600} measured (OD_s). A well-spun sample (14000 rpm, 30 min) was prepared for the purpose of a clarification reference sample, and the OD_{600} of the top 1 mL taken to be representative of 100% clarification (OD_r). Clarification efficiency was calculated according to Equation 2.1. All experimental points were carried out in triplicate, with the average standard deviation ranging from ±0.02 to ±0.9 in terms of % clarification, depending on the feed-stream of interest.

In order to compare clarification performances between centrifuges of different size and design, %C was plotted versus the equivalent flow rate per centrifuge settling area ($V_{lab}/c_{lab}t_{lab}\Sigma_{lab}$ or $Q_{PS}/c_{PS}\Sigma_{PS}$, PS indicating a pilot-scale centrifuge and c a Σ correction factor to account for non-ideal flow). Relevant equations and technical data for calculation of Σ factors are given in Appendix A2 and A3, respectively.

2.5.2.2 Dewatering

For the purpose of measuring dewatering, a known quantity of feed was placed in a 2.2 mL pre-weighed Eppendorf tube. The weight of the feed was recorded (W_f). The

samples were spun in an Eppendorf 5810R centrifuge. The spin conditions varied between the experiments, and the details are given in the relevant results sections. The supernatant was removed by pipetting and the remaining liquid on the wall of the tubes was removed by the aid of tissue. The weight of the wet sediment was recorded (WW_{sed}). The tube was dried at 100^0C to constant mass (~22 h) and the weight of the dried sediment was recorded (DW_{sed}). Level of dewatering was calculated using Equation 2.2. All experimental points were carried out in triplicate, with the average standard deviation ranging from ±0.3 to ±1.9 in terms of % dewatering, depending on the feed stock under investigation.

The yield levels predicted for the centrifugation process were calculated from Equation 2.3, and were based on the dewatering efficiencies determined as described above.

In order to compare dewatering and yield performances achieved for centrifuges of different size and design, %D and %Y was plotted against the equivalent flow rate per centrifuge settling area ($V_{lab}/c_{lab}t_{lab}\Sigma_{lab}$ or $Q_{PS}/c_{PS}\Sigma_{PS}$).

2.5.3 Pilot-scale centrifugation

Experimental pilot-scale clarification data was obtained by using a CSA-1 disc-stack centrifuge (Westfalia Separator, AG, Oelde, Germany) operated at 9810 rpm and at flow rates ranging from 3-80 L h^{-1}. Clarification levels were determined from Equation 2.1 by measuring the OD_{600} of the feed (OD_f), the supernatant sample (OD_s) and a well-spun sample (OD_r). OD_s was estimated by taking the average OD_{600} of supernatant samples after 1 L and 2 L of fluid had entered the centrifuge bowl.

2.6 Expanded bed adsorption

The following describes the equipment and the methods applied for processing of *E. coli* homogenate by EBA.

2.6.1 EBA columns and media

Two different expanded bed columns were applied in this work; a Streamline 25 column (GE Healthcare, Uppsala, Sweden) and a specially developed column intended for scale-down work (SD column).

The scale-down bed is custom-built and was constructed from a precision bore glass capillary with an internal diameter of 0.19 cm and length of 50 cm. The capillary was supplied by GPE (Leighton Buzzard, UK), and was fitted with a distributor at the base of the column in-house. It has a movable top adaptor. A more detailed description of the column can be found in Willoughby *et al.* (2004). The Streamline 25 column has an inner diameter of 2.5 cm, and a length of 100 cm. It is equipped with a unique liquid distributor at the base, which ensures the formation of a stable bed. The column has an adaptor which height can be altered during the process. The column dimensions, the settled bed height and the flow velocities applied to each of the columns are summarised in Table 2.1.

Table 2.1. Dimensions and operating conditions for the columns used for expanded bed adsorption.

	Dimensions (IDxL, cm)	**Initial settled bed height (cm)**	**Flow rate (cm h^{-1})**
SD column	0.19 x 50	8.5	100, 200 and 300
Streamline 25	2.5 x 100	8.5	200

Both columns were packed with the cation exchange adsorbent Streamline SP (GE Healthcare, Uppsala, Sweden). The matrix consists of cross-linked 6% agarose that has been modified by including an inert quartz core to achieve the high particle density that is required in order to get stable expansion at high flow rates. The typical

range of particle size is 100-300 μm, with an average particle size of 200 μm. The protein binding capacity is due to sulphonate ligands.

2.6.2 Sample conditioning

E. coli homogenate was prepared according to section 2.4.2.2 and clarified by centrifugation at 10000 rmp for 90 min in a Beckman J2-M1 centrifuge, rotor JA 10 (Beckman Coulter Ltd, High Wycombe, UK). The supernatant conductivity was reduced to a sufficiently low level (~4.5 mS cm^{-1}) (Jenway conductivity meter, Jenway, Essex, UK) by dilution with de-ionised water, and the pH adjusted to 5.5 with HCl.

For the preparation of solid-containing samples, the homogenate pellet was re-dissolved over night in the conditioned supernatant in order to generate feed-streams of appropriate solids concentrations. The conductivity and pH was maintained at the target levels.

In order to meet the desired levels of both ionic strength and Fab titre, it was sometimes necessary to concentrate the sample. Sample concentration was achieved by using a 10 kDa cut-off high flux Vivaflow 200 filter (VivaScience AG, Hannover, Germany) connected to a Masterflex console drive pump (Cole Parmer Instrument company, London, UK). Fab concentration in the conditioned sample was measured as described in section 2.3.2. The sample solids concentration was determined as outlined in section 2.2.1.2

2.6.3 Determining EBA buffer conditions

2.6.3.1 Determining buffer pH

A series of 2.2 mL Eppendorf tubes were prepared by adding 600 μL 50% Streamline SP slurry to each. The adsorbent was equilibrated by washing three times with 300 μL 0.5 M MES buffer adjusted to different pH. The pH range investigated was from 4-10, with 1 pH unit interval between tubes. The matrix in each tube was

then equilibrated to a lower ionic strength by washing three times with 300 µL 0.05 M MES buffer of the same pH. 1.5 mL of sample was added to each tube and mixed for 5 min. The slurry was allowed to settle and the liquid phase assayed for Fab as described in section 2.3.2. This procedure was performed for clarified homogenate samples with conductivities of 2.5, 10 and 21 mS cm^{-1}.

2.6.3.2 Determining buffer molarity

A series of 2.2 mL Eppendorf tubes were prepared and each tube was added 600 µL 50% Streamline SP slurry. The adsorbent was equilibrated with 0.5 M MES buffer at the starting pH (as determined in 2.6.3.1). The matrix in each tube was then equilibrated to different ionic strengths, at constant pH, by washing three times with 300 µL MES buffer ranging from 0.05 M to 0.5 M. 1.5 mL sample was added and the tubes mixed for 5 min. The liquid phase was assayed for Fab as described in section 2.3.2.

2.6.4 Column experiments

In order to study the breakthrough behaviour, bed expansion performance and the mixing effects in the bed, the columns were connected to and controlled by an AKTA-Explorer 100 system (GE Healthcare, Uppsala, Sweden). UV_{600} and UV_{280}, temperature, pH and conductivity were monitored and logged throughout the runs. Flow-through fractions were collected using a FRAC-100 fraction collector.
A method, consisting of column equilibration followed by sample load, wash-out of unbound sample, elution and re-equilibration of the adsorbent, was generated for each of the columns using the Unicorn software tool. A cleaning-in-place (CIP) step was performed after each run. Each step of the method is detailed below.

Equilibration: The settled bed was expanded in equilibrium buffer (0.2 mM MES, pH 5.5) at the desired flow velocity (100, 200 or 300 cm h^{-1} for the SD column, 200 cm h^{-1} for the Streamline 25 column) for 40 minutes to ensure a fully equilibrated and stable column.
Load: The conditioned feed (section 2.6.2) was loaded onto the column at the equilibration flow rate. For the SD column the sample was loaded from a 50 mL

superloop. Due to the considerably larger sample volumes, direct load was used in the case of the Streamline 25 column.

Wash: Any unbound sample was washed out from the column using equilibration buffer. For the SD column, the wash step consisted of 5 CV equilibration buffer. Due to the limited volume of flow-through that could be collected during the Streamline 25 run, wash was limited to 3 CV buffer.

Elution: Elution was, as column equilibration, load and wash, performed in upwards direction using elution buffer (20 mM MES, pH 5.5 + 1 M NaCl). The adapter position was not adjusted (this in order to ensure a comparable process. The adaptor was at 32 cm for the 25 mm column at all times, as that was as low as the SD adaptor went). All elutions were performed at 200 cm h^{-1} with 15 CV elution buffer.

Re-equilibration: The columns were re-equilibrated with 15 CV equilibration buffer.

CIP: Cleaning-in-place was performed after each run. The CIP step consisted of 10 CV NaOH and 10 CV equilibration buffer, both at 100 cm h^{-1}.

During load and wash, flow-through fractions of 1 mL and 50 mL were collected from the SD column and the Streamline 25 column, respectively, for generation of Fab breakthrough curves. Elution fractions of 3x5 mL and 3x800 mL for the SD column and the Streamline 25 column, respectively, were collected through different outlet valves. Bed height was monitored during the process in order to study the variation in bed expansion between the experiments.

3 Production of antibody fragments by fermentation

Abstract

This chapter describes the fermentation processes for the production of a Fab and a scFv antibody fragment in *E. coli* and *P. pastoris*, respectively. The purpose of these fermentations was to generate biomass for scale-down and pilot-scale downstream processing studies, and no attempts to optimise growth and level of product expression were made. Results are presented for a 20 L *E. coli* Fab fermentation, for shake-flask cultures of the *P. pastoris*–scFv system, and finally the characteristics of a 5 L *P. pastoris* fermentation are given. Factors affecting the performance of the respective fermentations will be discussed, and alterations to improve the outcome of the processes are suggested where appropriate.

E. coli was grown on glycerol to a final OD_{600} of 120, and following induction by IPTG a Fab concentration of 750 mg L^{-1} was achieved in the periplasmic space. A low concentration of Fab was detected in the supernatant, suggesting that only small amounts of the product had leaked into the fermentation medium. *P. pastoris* was grown on glycerol, followed by the addition of methanol for induction of product expression and further cell growth. An OD_{600} of 35 and 280 was achieved in the shake-flask culture and in the 5 L fermentation culture, respectively. Proteolysis has been reported to be a problem in previous *P. pastoris* scFv fermentations; hence in order to avoid loss of product, the 5 L fermentation was terminated at an earlier stage than estimated. The total protein concentration in the supernatant reached 350 mgL^{-1}.

3.1 Introduction

The production of antibody fragments from *E. coli* and *P. pastoris* was briefly discussed in Chapter 1, and Chapter 2 described the protocols applied for the generation of biomass and the expression of the antibody fragments of interest to this work.

It should be emphasised that the development of the fermentation processes described, and the optimisation of product expression, have not been the focus of this study. The purpose of the fermentations was to provide sufficient biomass for downstream processing studies. The aim of this chapter is to provide a brief description of the typical characteristics associated with the fermentation of *E. coli* and *P. pastoris*.

The fermentation procedure for the *E. coli*-Fab system is well established at UCL. Such fermentations are conducted on a regular basis, and biomass from these runs was provided for this project. Typical experimental results of a 20 L fermentation were kindly provided by EngD student Andrew Tustian. The *P. pastoris* shake-flask experiments and the 5 L *P. pastoris* fermentation described were performed within this PhD in collaboration with Biosentrum (Stavanger, Norway).

3.1.1 *E. coli* fermentation for the expression of a Fab antibody fragment

In section 1.3.2.1 a number of factors were discussed that need to be considered in order to achieve a successful *E. coli* fermentation and associated high levels of product expression. In order to achieve acceptable product titres, the rate of antibody production must be carefully controlled. If the antibody is expressed at too high a rate, the periplasmic folding pathway may become saturated and the product might accumulate as insoluble aggregates. In the current protocol the temperature was reduced from 30^0C to 25^0C prior to induction (Tustian *et al.*, manuscript under preparation) in order to limit the growth rate and thereby minimise the level of unsuccessful folding. The product yield can also be limited due to the formation of by-products such as acetate. This growth-inhibitory factor is produced in the

presence of excess glucose. For the *E. coli* expression system applied in this work, this has been addressed by replacing glucose with glycerol as the carbon source, as the latter is not associated with acetate formation. The use of a defined fermentation medium is advantageous in terms of controlling the concentration of various nutrients during the fermentation in order to optimise the cell growth. The addition of Mg^{2+} and PO_4^{2-} throughout the *E. coli* Fab fermentation also serves to strengthen the cell wall and hence reduce the amount of product leakage. Product leakage may also be limited to a certain extent by the before-mentioned reduction in temperature prior to induction.

3.1.2 *P. pastoris* fermentation for the production of a scFv antibody fragment

The level of product expressed during fermentation of *P. pastoris* is highly dependent on the induction-strategy chosen. As mentioned in section 1.3.2.2, the initial growth phase utilises glycerol as the carbon source, first in batch mode, followed by a short fed-batch glycerol phase. The final step is a fed-batch methanol (MeOH) period, which serves to induce product expression and continue cell growth. Alternatively a mixture of MeOH and glycerol may be used in this final step. If the latter alternative is applied, it is important to monitor carefully the level of glycerol in the medium, as too high a concentration will repress the *AOX1* promoter and reduce yields. In the current protocol MeOH served as the inducer and the sole carbon source during the induction period. The feed concentration of MeOH was carefully monitored in order to achieve optimal expression levels. In the presence of excess MeOH, the cell growth may be adversely affected, and protein expression may be inhibited. The level of transcription initiated from the promoter can be 3-5 times greater in cells fed MeOH at growth-limiting rates compared to cells grown in excess MeOH. The protocol applied for the *P. pastoris* scFv system ensures a MeOH concentration of 0.5-1% (v/v).

Proteolysis has been reported as a potential problem at the later stages of *P. pastoris* fermentations. Biosentrum has observed this on several occasions for the *P. pastoris*-scFv system, and it was therefore decided to shorten the induction period for the 5 L fermentation described in this chapter, so as to avoid a reduction in product yield.

3.2 Results and discussion

3.2.1 *E. coli* Fab fermentation

The following describes typical results observed during a 20 L *E. coli* Fab fermentation. The experimental results presented below have been provided by EngD student Andrew Tustian, Department of Biochemical Engineering, UCL.

3.2.1.1 *E. coli* fermentation characteristics

E. coli was fermented as described in section 2.1.1. During the fermentation the pH was controlled at 6.95, and the DOT was kept above 30% throughout the process. The temperature was maintained at 30^0C until an OD_{600} of ~42 was reached, and then lowered to 25^0C for the remaining fermentation time. Salts were added to the culture during the course of the fermentation in order to maintain the required level of Mg^{2+} and PO_4^{2-} in solution. When the entire glycerol carbon source in the culture had been utilized, as indicated by DOT spiking, Fab production was induced by addition of IPTG. After induction, carbon was supplied to the culture for Fab synthesis and further cell growth by a glycerol fed-batch feed. The culture was harvested 36 hours after addition of the IPTG.

Figure 3.1 shows a growth curve generated from a typical 20 L *E. coli* Fab fermentation. Glycerol depletion is indicated after ~32 h. At this stage Fab production was induced by the addition of IPTG. For the remaining time of the fermentation glycerol was added to the culture in a fed-batch mode for Fab production and further cell growth. The glycerol feed rate applied was optimised in order to control the Fab production rate and thereby minimise the amount of product leakage. Cell growth slowed down post-induction, as a consequence of the cells using the energy and the carbon supplied to express Fab rather than divide.

The variation in level of dissolved oxygen during the fermentation can be seen in Figure 3.2. Glycerol depletion is indicated by the spike in the DOT level at ~32 h. At this stage IPTG was added, followed by the addition of glycerol in a fed-batch

fashion. In response to the addition of fresh carbon the DOT decreased to a normal level. If necessary, stirrer speed or air flow was adjusted to keep the level of dissolved oxygen above the set point of 30%.

Figure 3.3 shows the expression levels of Fab measured during the course of the induction step (as determined according to section 2.3.2), and indicates in which compartment the product is found. It is evident that there is hardly any leakage of Fab into the fermentation medium. This was attributed to the temperature reduction prior to induction, and to careful control of the glycerol feed rate. In addition, the addition of Mg^{2+} and PO_4^{2-} salts during the fermentation serves to strengthen the cell wall and thereby reduces the level of leakage. The total concentration of Fab appears to be higher than the sum of the periplasmic and supernatant concentrations. This might be a result of an in-efficient periplasmic lysis step, preventing 100% release of Fab from the periplasm. The product that is not released might still be located in the cytoplasm.

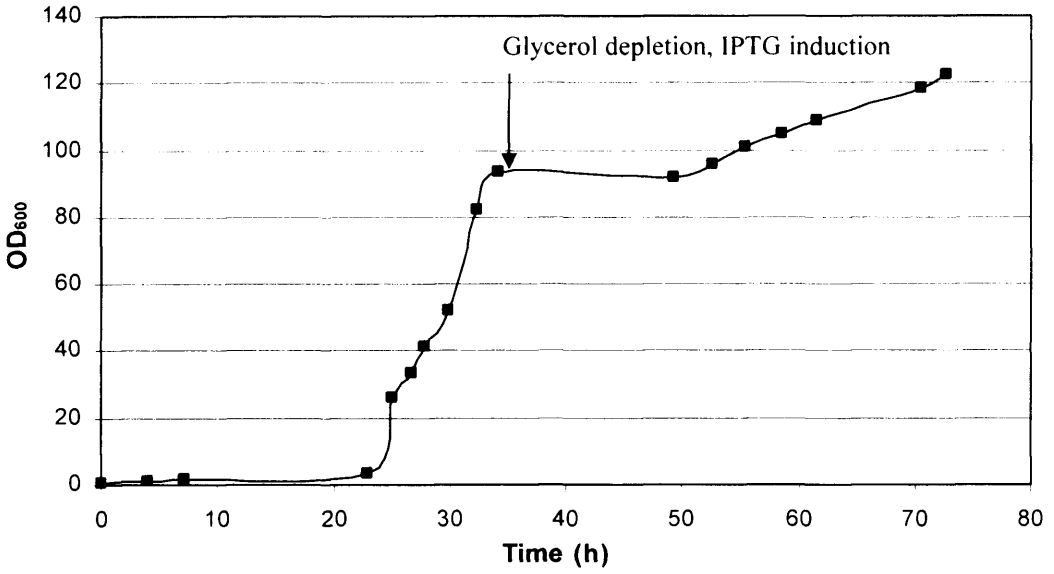

Figure 3.1. Growth curve generated from a typical 20 L *E. coli* Fab fermentation. Glycerol depletion is indicated by the second lag-phase at ~32 h. At this point Fab production was induced by the addition of IPTG.

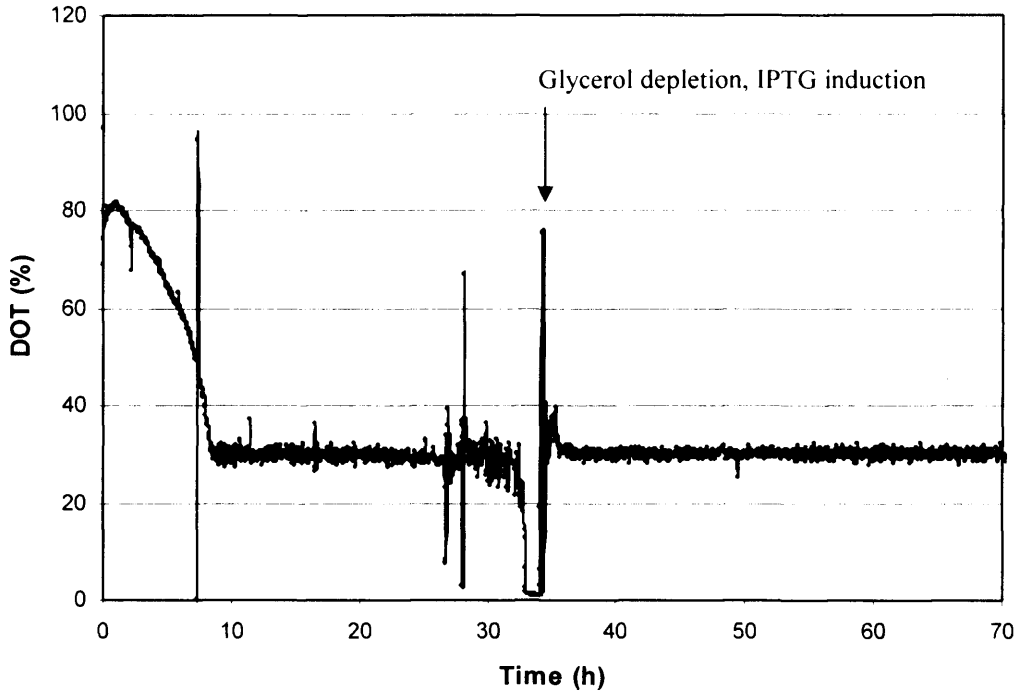

Figure 3.2. DOT over time in a 20 L *E. coli* fermentation. The spike seen at ~32 h indicates glycerol depletion. At this stage IPTG was added to induce Fab production.

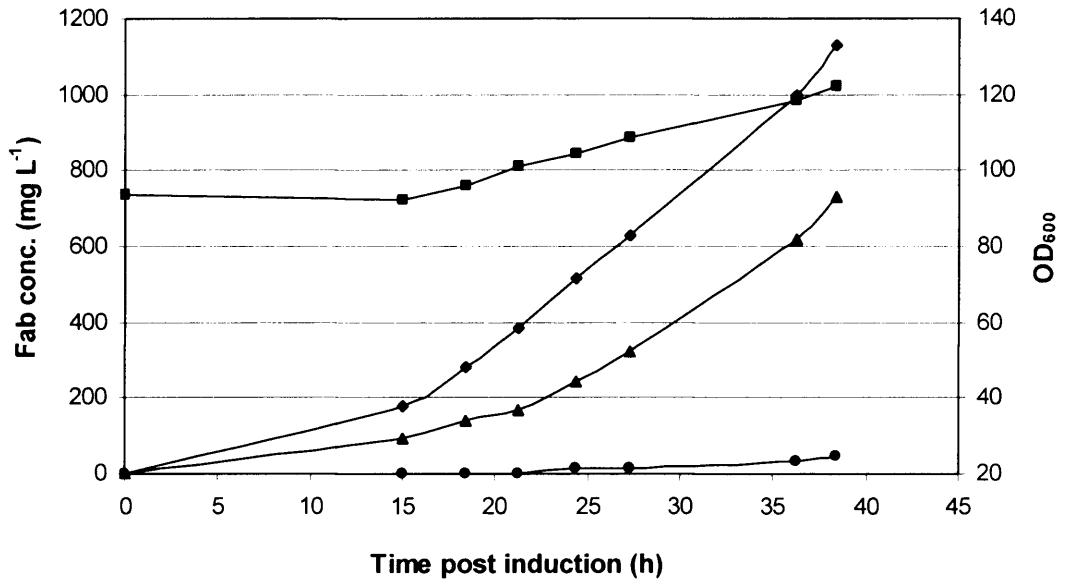

Figure 3.3. Fab production post IPTG induction. The graph indicates the concentrations of Fab measured in the periplasm (▲) and in the supernatant (●), as well as total Fab concentration (♦). OD_{600} post induction is also included (■).

3.2.2 *P. pastoris* scFv fermentation

A preliminary shake-flask study was performed in order to investigate the effect of freeze-thaw on the *P. pastoris* cells. The outcome of the study would indicate whether it is feasible to freeze the fermentation broth prior to further analysis or not. A test was also performed to get an indication of the susceptibility of *P. pastoris* cells to shear. The outcome of the shake-flask study is presented in section 3.2.2.1. Section 3.2.2.2 provides the characteristics of a typical 5 L *P. pastoris* scFv fermentation.

3.2.2.1 Shake-flask cultivations

P. pastoris shake-flask cultures were prepared and grown as detailed in section 2.1.2.4. A typical growth curve resulting from shake-flask cultivation of *P. pastoris* is shown in Figure 3.4.

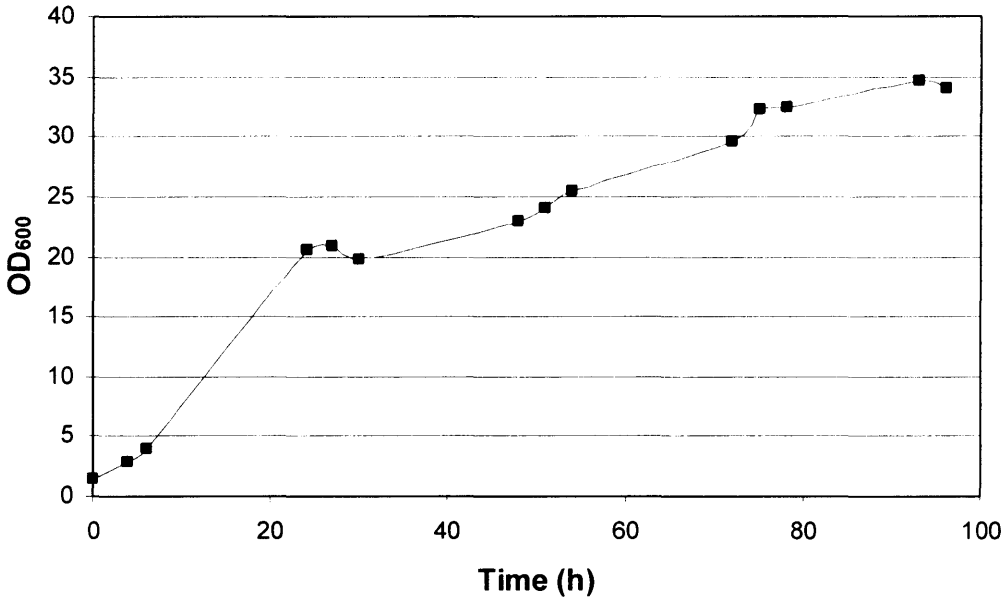

Figure 3.4. Typical growth curve for the cultivation of *P. pastoris* in shake-flasks.

The biomass generated from *P. pastoris* shake-flask cultures (OD_{600} ~35) were used to investigate the effect of storage conditions on the cells, and of particular interest was the establishment of any consequences of freeze-thaw treatment. The total protein concentration in the supernatant from fresh fermentation broth was measured using the Bradford assay (section 2.2.4) and compared to that of supernatant generated from samples stored at $+4^0$C and -80^0C. The results shown in Figure 3.5 suggest that freezing had no effect on the total protein content in the respective supernatants, suggesting that the cells do not permeabilise and release cell protein into the culture. The importance of this finding lies in the possibility of performing the fermentation at a different time, or even at a different location, than future downstream processing studies.

The shear sensitivity of the *P. pastoris* cells was investigated by measuring the total protein concentration in the supernatant of sheared and non-sheared fresh samples as well as of sheared and non-sheared samples stored at $+4^0$C and at -80^0C. The sheared samples were prepared according to the protocol described in section 2.2.3. The results are given in Figure 3.6 and indicate a minor effect of shear on the *P. pastoris* cells for all storage conditions tested.

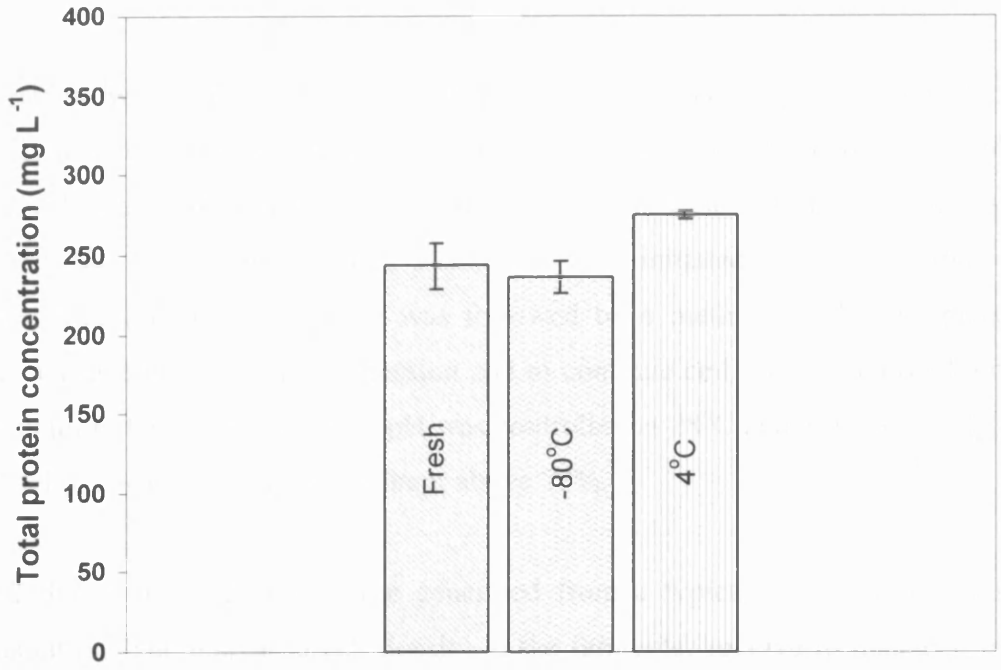

Figure 3.5. The effect of freeze-thaw on the *P. pastoris* cells. The level of total protein concentration is indicated for supernatant generated from fresh broth and from broths stored at -80^{0}C and +4^{0}C.

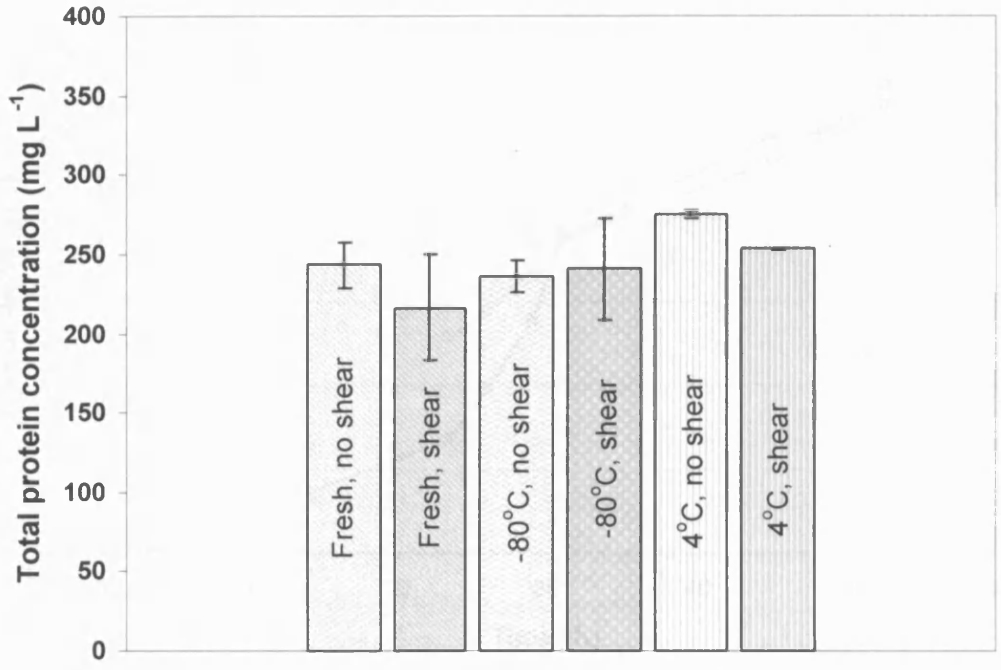

Figure 3.6. The effect of shear on *P. pastoris* cells subject to different storage conditions.

3.2.2.2 5 L fermentation

P. pastoris was fermented in a three-stage process according to section 2.1.2.5. Initially a batch glycerol phase was providing carbon for cell growth. This phase continued until depletion of glycerol occurred, as indicated by a rapid increase in DOT. A short glycerol fed-batch phase was then initiated to ensure further cell growth. The glycerol feed phase was followed by a methanol fed-batch phase to induce extracellular product expression and to continue cell growth. Throughout the fermentation the temperature and pH was controlled at 28°C and 5, respectively, and the level of dissolved oxygen was kept above 20%.

Figure 3.7 shows a growth curve generated from a typical 5 L *P. pastoris* scFv fermentation. The increased cell density in the fermenter relative to that seen in the shake-flask culture is due to the fact that the culture environment is much easier controlled in a fermenter compared to in a shake-flask. Two major advantages of fermenters are the possibility to monitor accurately and adjust oxygen levels, and the possibility to feed methanol at a growth limiting rate.

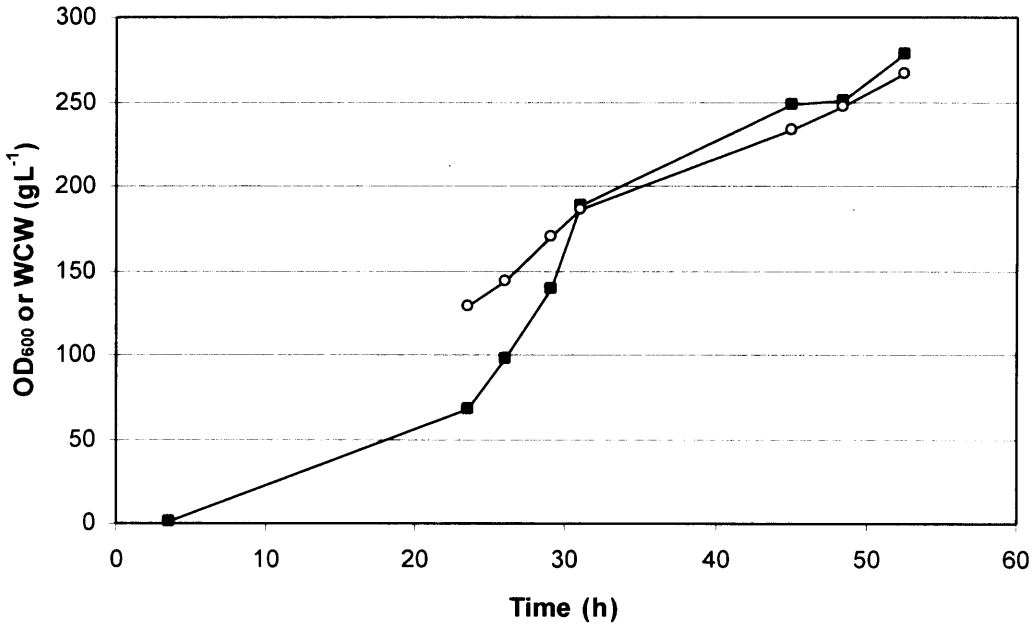

Figure 3.7. Cell growth (■) and wet cell weight (○) measured during the course of a 5 L *P. pastoris* fermentation.

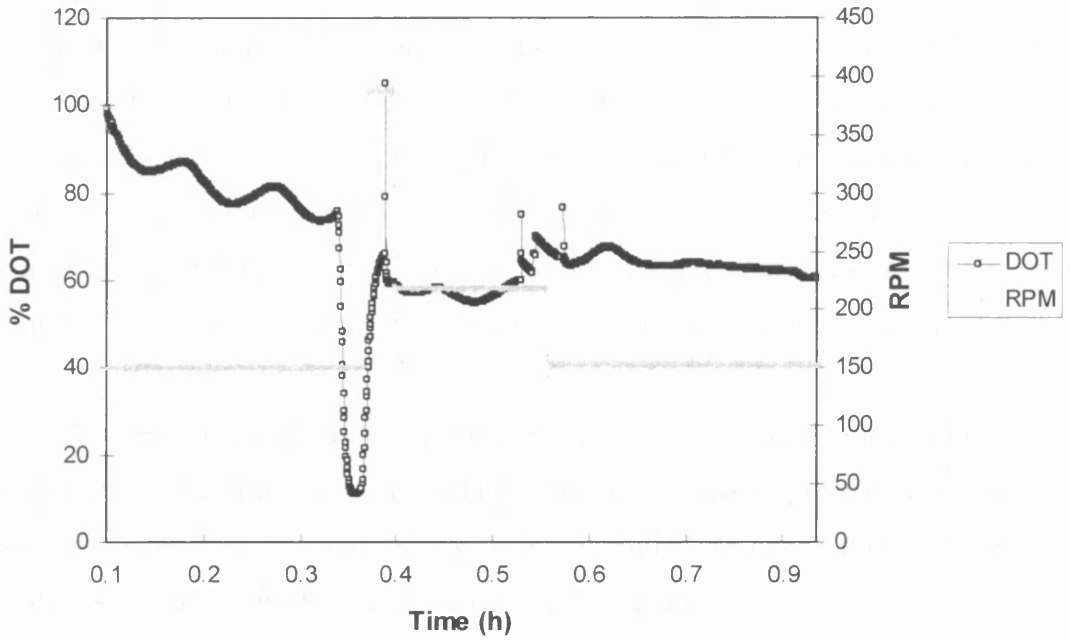

Figure 3.8. The level of dissolved oxygen and the effect of the stirrer speed on DOT during the *P. pastoris* inoculation phase.

Figure 3.8 illustrates the dependence of the level of dissolved oxygen on the stirrer speed applied during the very initial stage of the fermentation (up to 1 h). By increasing the speed, more oxygen is made available to the cells for further growth.

Figure 3.9 shows the concentration of total protein during the course of the *P. pastoris* fermentation. As expected, a minimal concentration of protein is detected before the onset of the induction (~31 h). This observation also suggests that the *Pichia* strain release very few of its own proteins during fermentation. Post-induction, the protein content of the culture increases steadily until the fermentation is terminated. Previous experience with this particular expression system has seen that the presence of proteases is a problem, and that the proteolytic activity increases during the course of the fermentation. In effect, the concentration of product has been seen to drop towards the end of the fermentation. In order to avoid loss of product, the duration of the induction period was reduced to 21 h for the fermentation discussed in this chapter.

In order to optimise the *P. pastoris* fermentation protocol applied, a number of strategies have been suggested to minimise the proteolytic activity, such as the

addition of amino acid supplements, which will act as substrates for the proteases. Fermentation at reduced pH is another option, which has been successfully applied by Jahic *et al.* (2003). Moreover, several protease deficient strains are available and are known to reduce effectively degradation of heterologous proteins. However, these strains have shown a lower viability, slower growth rate and are also more difficult to transform. Hence use of such protease deficient strains is only recommended if all other attempts to reduce the proteolytic activity have failed.

An established ELISA assay (described in section 2.3.1) was performed in order to monitor the concentration of scFv during the fermentation process. However, the assay failed repeatedly, possibly due to a contamination in the provided standard, and the assay did not provide sufficiently accurate results.

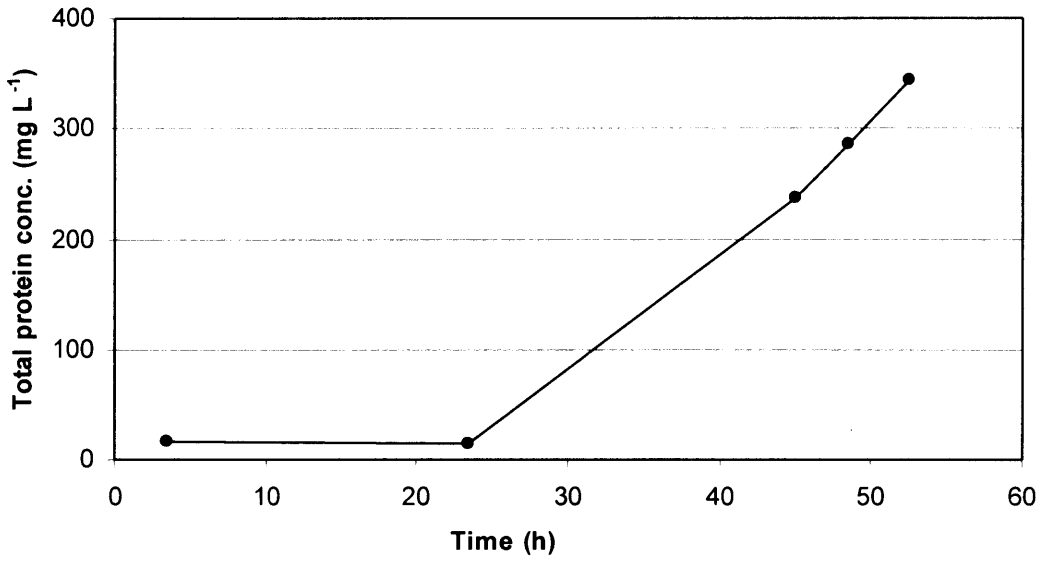

Figure 3.9. Total protein concentration in the *P. pastoris* supernatant measured during the 5 L fermentation.

3.3 Summary

This chapter has provided a brief introduction to the processes applied for the generation of biomass for the scale-down and pilot-scale downstream processing studies described in the following chapters.

An *E. coli* strain expressing a periplasmic Fab antibody fragment was induced by the addition of IPTG. A very low concentration of Fab in the supernatant indicated that little product had leaked into the fermentation medium during the process. This was attributed to the use of a temperature reduction prior to induction and to careful control of the glycerol feed rate, both serving to limit the growth rate, and also to the addition of Mg^{2+} and PO_4^{2-} salts during the fermentation to strengthen the cell wall.

Shake-flask cultivations of *P. pastoris* expressing an extracellular scFv antibody fragment were conducted in order to generate biomass for an initial study aimed at establishing the effect of freeze-thaw as well as shear on the yeast cells. It was found that the total protein concentration in the supernatant from sheared and non-sheared samples of fresh cultures and of cultures stored at -80^0C and $+4^0$C was relatively constant, and it was concluded that the cells were not susceptible to freeze-thaw treatment, or to shear.

The *P. pastoris* fermentation was scaled up to 5 L, with the result of a significant increase in cell density relative to the shake-flask cultures. This is not surprising, as the culture environment is much easier controlled in a fermenter compared to in a shake-flask, for example in terms of supplied oxygen and MeOH (inducer) feed rate. Due to previous experience with proteolytic degradation of the product, the fermentation was ended after only 21 h on MeOH.

The next chapters (4-8) will involve the use of the *E. coli* and *P. pastoris* biomass to investigate different options for the primary recovery of the antibody fragments expressed.

4 A novel ultra scale-down approach for predicting the centrifugal separation performance of high cell density cultures

Abstract

Current trends in bioprocessing are leading to higher cell densities as manufacturers strive for greater levels of product expression using recombinant systems. Solids concentrations of up to 30% are readily achievable (Persson *et al.*, 2005). This presents a unique challenge to the downstream processing engineer in terms of handling process streams with significant solids loads, especially in terms of selecting appropriate operating conditions for high speed centrifuges, which will be needed to harvest the cells from the fermentation liquors. Recent research at UCL has focused on the concept of ultra scale-down (USD) (Boychyn *et al.*, 2000, 2001, 2004; Maybury *et al.*, 2000; Neal *et al.*, 2003) and its ability to predict accurately the performance of industrial-scale centrifuges using small quantities (~50 mL) of process material in dedicated devices.

Previous work on USD centrifugation has focussed mainly on mammalian cell culture and protein precipitate systems (Boychyn *et al.*, 2000, 2001, 2004; Maybury *et al.*, 2000), which are characterised by fairly low solids density (< 2% ww/v) and high shear sensitivities. In recent studies investigating the validity of the existing USD centrifugation technology when applied to high cell density feeds it was found that the laboratory-scale mimic resulted in a substantial over-prediction of separation efficiency. This is probably due to cell-cell interactions, leading to various degrees of aggregation effects in the low shear environment of a laboratory centrifuge, which will not be apparent in the settling region of a continuous-flow industrial centrifuge.

In this chapter a novel USD clarification methodology is described, which is based upon the dilution of high solids feed material to ~2% (ww/v) solids, at which level cell-cell interactions are minimal, prior to the application of the clarification test.

Mathematical corrections are then applied to the resultant clarification curves in order to account for the effects of dilution in terms of i.e. reduced hindered settling and lower viscosity.

The methodology is demonstrated and verified using *E. coli* whole cell broth as well as *E. coli* cells that have been subject to a periplasmic lysis step. Following a successful validation of the novel USD approach, the method is applied to predict large-scale clarification performance of high cell density *P. pastoris* cultures and *E. coli* homogenates. For *P. pastoris* and *E. coli* homogenates, the performance parameters of dewatering and yield are also predicted on a laboratory-scale basis.

Note: The USD clarification, dewatering and yield results presented for *P. pastoris* in this chapter forms the basis for a paper that has been accepted for publication in Biotechnology and bioengineering (Salte *et al.*, 2006). The paper is attached in Appendix A5.

4.1 Introduction

The following describes the development of a new USD centrifugation approach developed to deal with high cell density feed-streams, and includes a brief introduction to Sigma theory (section 4.1.1), a derivation of the theoretical correlations forming the basis of the new USD clarification method (section 4.1.2), as well as a discussion regarding the motivation for the generation of this novel method (section 4.1.3).

4.1.1 Sigma theory

The scaling between centrifuges of different size and design is often done by means of the Sigma theory (Ambler, 1961; Maybury *et al.*, 1998). According to Sigma theory, each centrifuge is associated with a unique Sigma factor (Σ), defined as the surface area of a gravity settling tank required in order to give the equivalent separation performance to the particular centrifuge. The general equation for the Sigma factor is given by Equation 4.1 (Ambler, 1959):

$$\Sigma = \frac{V\omega^2 r_e}{g s_e} \qquad 4.1$$

where V is the volume of liquid in the bowl, $\omega = 2\pi N$, N is the rotational speed, g is acceleration due to gravity, r_e is the effective radius of the centrifuge and s_e is the effective settling distance. Specific expressions for the calculation of Σ values for laboratory batch centrifuges, disc-stack machines, multi-chamber bowls and tubular bowls are given in Appendix A2. Technical data required for the calculation of the Σ factor of each centrifuge of interest to this study is provided in Appendix A3.

The solid-liquid separation ability of a particular centrifuge is given by the ratio of the volumetric flow rate through the centrifuge to the equivalent settling area of the centrifuge. The separation performance of centrifuges of different size and design, operating on the same feed-stream, may be compared using Equation 4.2:

$$\frac{Q_{PS1}}{\Sigma_{PS1} c_{PS1}} = \frac{Q_{PS2}}{\Sigma_{PS2} c_{PS2}} = \frac{V_{lab}}{c_{lab} t_{lab} \Sigma_{lab}} \qquad 4.2$$

where Q is the volumetric flow rate, Σ is the equivalent settling area, V_{lab} is the volume of liquid in the laboratory spin tube, t_{lab} is residence time in laboratory centrifuge, and c_{PS1}, c_{PS2} and c_{lab} are correction factors to account for non-ideal fluid flow patterns. *PS1* and *PS2* refer to pilot-scale centrifuge 1 and 2, respectively. The value of c depends on centrifuge design; the correction factor is defined as 1.0 for the laboratory centrifuge, and the correction factors applied for disc-stacks (ds), multi-chamber bowls (mc) and tubular bowls (tb), are $c_{ds} = 0.4$, $c_{mc} = 0.88$ and $c_{tb} = 0.9$, respectively (Boychyn *et al.*, 2004).

4.1.2 Settling of high cell density cultures

The Sigma concept used for scaling of centrifugation processes is related to Stokes' Law for settling of particles in a centrifugal field via Equation 4.3 (Bowering, 2000; Clarkson *et al.*, 1996).

$$\frac{Q}{\Sigma} \propto V_{sg} = \frac{(\rho_p - \rho)}{18\mu} d_p^2 \omega^2 r \qquad 4.3$$

where V_{sg} is the centrifugal settling velocity, ρ_p is the density of the particles, ρ is the density of the suspending fluid, μ is the viscosity of the fluid, d_p is the particle diameter, ω is the angular velocity and r is the radial position of the particle. Stokes' Law assumes that the particles being processed are present as single, spherical particles in a very dilute suspension. As the solids concentration of the feed increases, the distance between the particles present decreases, resulting in a reduced settling rate of the particles. This phenomenon is known as hindered settling. To account for the effect of hindered settling during the sedimentation process, the Richardson-Zaki equation (Richardson and Zaki, 1954) may be applied:

$$\frac{V_{sg}^*}{V_{sg}} = (1-\phi)^{\sigma} \qquad 4.4$$

where V_{sg}^* is the hindered settling velocity in a centrifugal field, ϕ is the fraction of solids and σ a particle geometric factor. For spherical particles, $\sigma = 4.65$ (Richardson and Zaki, 1954).

For biological suspensions, another effect of higher solids concentration is that of increased viscosity, which will also result in reduced settling velocity (according to Stokes' Law). The Richardson-Zaki equation (Equation 4.4) assumes no change in any of the parameters on the right hand side of Equation 4.3 as solids concentration increases or decreases. Whilst it is reasonable to assume that ρ, ρ_p, d_p, ω and r remain constant in the case of the biological suspensions, μ varies. Consequently it is necessary to factor in a viscosity ratio to the Richardson-Zaki equation above, resulting in Equation 4.5:

$$\frac{V_{sg}^*}{V_{sg}} = \frac{\mu}{\mu^*}(1-\phi)^{\sigma} \qquad 4.5$$

where μ^* is the viscosity of a suspension of high solids concentration and μ is the viscosity of a dilute suspension (effectively zero solids concentration). The relationship between μ and μ^* can be described using a power-law relationship between viscosity and solids fraction, as given by Equation 4.6 (Leung, 1998).

$$\frac{\mu^*}{\mu} = \frac{1}{(1-\phi)^{\alpha}} \qquad 4.6$$

The exponent α is determined experimentally for the feed-stream of interest in the relevant results sections. Substituting Equation 4.6 into Equation 4.5 gives a modified Stokes' Law (Equation 4.7).

$$\frac{V_{sg}^*}{V_{sg}} = (1-\phi)^{\sigma}(1-\phi)^{\alpha} = (1-\phi)^{\sigma+\alpha} \qquad 4.7$$

Equation 4.7 allows settling velocity at a given solids concentration to be related back to the settling velocity in effectively zero solids concentration. In this work we dilute the suspensions for the USD experimentation not to zero solids, but to a solids concentration below the level at which hindered settling occurs (< 2% ww/v) (Rumpus, 1997). Equation 4.7 was modified to account for this:

$$\frac{\left(Q/c\Sigma\right)^{PS}}{\left(V/t\Sigma\right)^{USD}} = \frac{V_{sg}^{PS}}{V_{sg}^{USD}} = \frac{\left(1-\phi^{PS}\right)^{\sigma+\alpha}}{\left(1-\phi^{USD}\right)^{\sigma+\alpha}} \qquad 4.8$$

where *PS* and *USD* refer to the undiluted pilot-scale feed and the diluted USD feed, respectively.

4.1.3 The motivation for a USD centrifugation method adapted to deal with high cell density cultures

One of the central concepts behind the USD centrifugation mimic is to compensate for the effect of shear levels seen within the internal volume (particularly in the feed zone) of an industrial centrifuge. Laboratory centrifuges tend to be of a discrete, bottle design and hence expose the feed-stream to no (or at least minimal) shear forces. Work at UCL (Boychyn *et al.*, 2001, 2004) has demonstrated the validity of using a high speed rotating disc device prior to laboratory centrifugation to mimic the shear forces experienced in industrial machines. Following shearing (according to section 2.2.3), material is separated in the laboratory centrifuge using conditions based on sedimentation theory as described above (section 4.1.1 and 4.1.2). The combination of these elements provides the USD mimic.

Traditionally, USD centrifugation experiments have been performed using undiluted feed material as processed in the pilot-scale centrifuge. This has proven to work well for low cell density cultures (Boychyn *et al.*, 2000, 2001, 2004; Maybury *et al.*, 2000). However, initial trials using the previously developed USD methodology for predicting separation performance levels resulted in significant over-prediction of process-scale clarification of high solids density feed-streams. This implies that the high solids density material settles more quickly in the laboratory-scale centrifuge than it does at large-scale. The most likely explanation for this is that some form of temporary aggregation of the particles occurs in the non-turbulent flow environment of a spinning centrifuge tube, which is unlikely to prevail in a disc-stack centrifuge where the high shear environment would most likely break up any such aggregate structure.

The effects of different types of weak aggregation in low shear environments are illustrated schematically in Figure 4.1. In all cases, an indication of the relative downward settling velocity and the upflow velocity are given by the blue top left arrow and the red bottom right arrow, respectively. In case (a) the solids concentration is low, and due to a low level of liquid and particle upflow, the particles experience only minimal hindrance to settling. In case (b), the solids

concentration is higher, and the level of upflow consequently increases, resulting in a reduced particle settling rate relative to in (a). Case (c) illustrates the effect of solid-solid interactions with minimal entrainment of liquid. As a result of an increase in particle size and -density, the aggregates settle faster than individual particles, despite the level of upflow being approximately the same as in case (b). In case (d), the particles flocculate and more liquid is entrained between the particles compared to in case (c). The reduced density of the flocs, combined with a high level of hindered settling due to upflow, results in a slower rate of settling of the flocs relative to what would be expected for the aggregates in case (c). In case (e), the level of flocculation and liquid entrainment is so high that "blanket" settling occurs, where free small particles are "swept down" and entrained by the settling mass of linked particles, and upflow is limited to liquid only. This results in a higher rate of settling than occurs in case (d).

It is difficult to put the different settling conditions illustrated in Figure 4.1 into a complete order; however it is reasonable to believe that in cases (c) and (e) the overall settling rate will be higher than for case (b). In both cases it is believed that the resultant effect will be an over-prediction of the clarification performance by the traditional USD model compared to the actual performance achieved in a continuous-flow centrifuge.

While the different types of aggregates described above may be expected to form in both experimental cases (pilot-scale and USD), in the pilot-scale centrifuge they are broken up by the shear in the feed zone and the complex flow pattern in the bowl of the centrifuge does not permit them to reform. In the case of the USD method, although the use of the shear device will break up any aggregates, the lack of flow inside the laboratory centrifuge tubes allows them to reform. This effectively results in higher clarification levels for the laboratory-scale centrifuge than for the large-scale machine for the equivalent separation conditions.

The aim of the new USD procedure detailed in this chapter is therefore to use pre-dilution to prevent solid-solid interaction effects from occurring during USD experimentation, and then to apply mathematical correction (by means of Equation

4.8) of the settling data so obtained to yield a prediction of sedimentation behaviour of high solids load feeds.

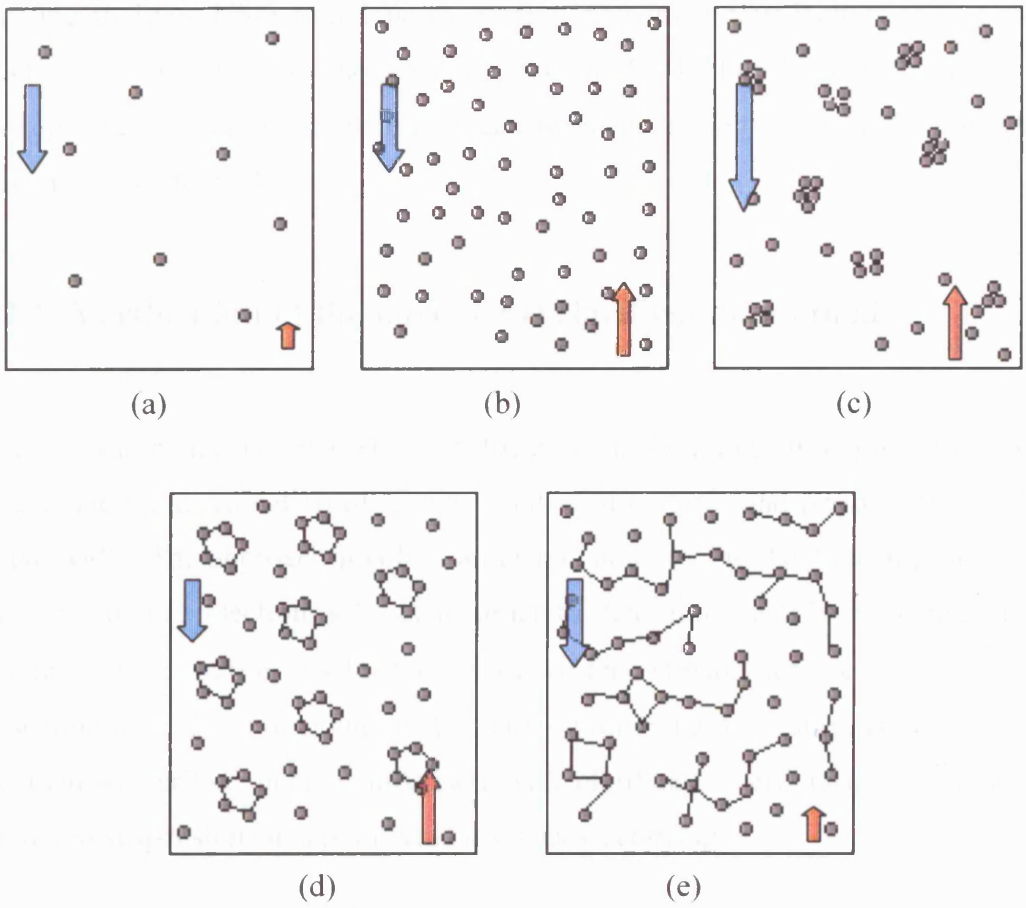

Figure 4.1. Illustration of various degrees of weak aggregation effects in low shear environments. In all cases, downward settling velocity is illustrated by the blue top left arrow, and upflow by the red bottom right arrow. Arrow sizes are indicative of relative flow velocities only. In (a) the solids concentration is low and the effect of hindered settling is minimal, whereas in (b), some hindrance to particle settling is observed due to an increase in solids concentration relative to (a). In case (c) aggregate formation results in increased settling velocity due to a higher particle density and -size. In (d), the particles flocculate, with the result of decreased density and hence decreased settling velocity, while (e) illustrates blanket settling as a result of extensive flocculation.

4.2 Results and discussion

This section demonstrates the use of the USD centrifugation methodology described above. Section 4.2.1 presents the verification of the novel USD clarification method by comparing the results of the USD study to those obtained in a pilot-scale disc-

stack centrifuge for the separation of *E. coli* whole cell cultures and periplasmically lysed *E. coli* cells. This is followed by a presentation of the results achieved when utilising the new USD technique to predict centrifugal clarification of *P. pastoris* (section 4.2.2) and *E. coli* homogenate (section 4.2.3). For *P. pastoris* and *E. coli* homogenate, the centrifugal performance parameters of dewatering and product yield were also investigated.

4.2.1 Verification of the novel USD clarification method

In this section, the novel USD centrifugation methodology is applied in order to investigate the clarification of *E. coli* whole cell cultures and periplasmically lysed *E. coli* cells. The approach involves an examination of the rheological properties of the feed-streams (section 4.2.1.1) in order to determine sample viscosities and to calculate the α-coefficients for the respective feed-streams for use in Equation 4.8. In section 4.2.1.2 the outcome of the clarification experimentation is presented and the method verified upon comparison with clarification efficiencies obtained for undiluted suspensions in a pilot-scale disc-stack centrifuge.

4.2.1.1 Rheological properties of *E. coli* whole cells and periplasmically lysed *E. coli* cells

The viscosity of suspensions of *E. coli* whole cells and periplasmically lysed *E. coli* cells at a range of solids concentrations was determined from the gradient obtained when plotting the relationship between shear stress and shear rate for each sample, as described in section 2.2.2 (results not shown). This method is however only valid when the viscosity is constant over the range of shear rates applied (Newtonian behaviour). In order to prove, or disprove, Newtonian characteristics of each sample, log-log plots of shear stress versus shear rate were generated. Figure 4.2 presents the resulting curves for *E. coli* whole cell samples of ~15% and ~2% (ww/v) solids and samples of periplasmically lysed *E. coli* cells containing ~9% and ~2% (ww/v) solids. The fitted lines were analysed as power-law curves of the form $\tau = k\gamma^n$, where k is the consistency index and n is the flow behaviour index (represented by the slope of the line). Generally, if the flow behaviour index is greater than 0.9,

Newtonian behaviour is assumed for the sample of interest. For *E. coli* periplasmic lysate, $n > 0.9$ over the whole range of solids concentrations tested (~2-9% ww/v), and hence this feed was considered as Newtonian. *E. coli* whole cell suspensions containing up to 10% solids (ww/v) were also characterised by Newtonian behaviour, whereas samples of *E. coli* whole cells of $\geq$ 10% (ww/v) solids were found to be non-Newtonian.

For non-Newtonian fluids it is difficult to determine the exact viscosity, as it will vary with the shear rate applied. However for high shear rates, such as the ones experienced in a large-scale centrifuge, it is assumed that the viscosity best approximates to that at the high end of the range of shear rates used (~1000 s^{-1}). Hence the viscosities of the non-Newtonian *E. coli* whole cell samples ($\geq$ 10% ww/v solids) were taken as the apparent viscosity at 1000 s^{-1} ($\mu_a = \gamma^{n-1}k$), whereas the viscosities of the Newtonian liquids were determined according to section 2.2.2 ($\mu=\tau/\gamma$).

By plotting the resulting viscosities versus $(1-\phi)$ on a log-log scale for the range of solids concentrations tested, straight lines resulted for both the *E. coli* whole cell suspension and the periplasmically lysed *E. coli* cells (Figure 4.3), the slopes of which correspond to the coefficient α in Equation 4.8. For *E. coli* whole cells α was found to be 6.6, and for the periplasmically lysed *E. coli* culture $\alpha = 5.0$.

Figure 4.3 illustrates that, as would be expected, increasing solids concentration results in a proportional increase in viscosity for both whole *E. coli* cell broth and periplasmically lysed *E. coli* cells. Lysed cells release their internal nucleic acids and proteins into free suspension, which serves to increase the liquid viscosity. However in this particular case the lysis step is also designed to break down these proteins by holding the lysis mixture at an elevated temperature for a prolonged period. The Fab of interest is heat-stable under these conditions (60^{O}C, 16h) but many contaminating proteins are degraded and precipitate (Weir and Bailey, 1997). Furthermore the periplasmic lysis utilised releases much less nucleic acid material from the cells than a complete cellular lysis would. The combination of these factors results in a lysate with a lower viscosity than the whole cell broth.

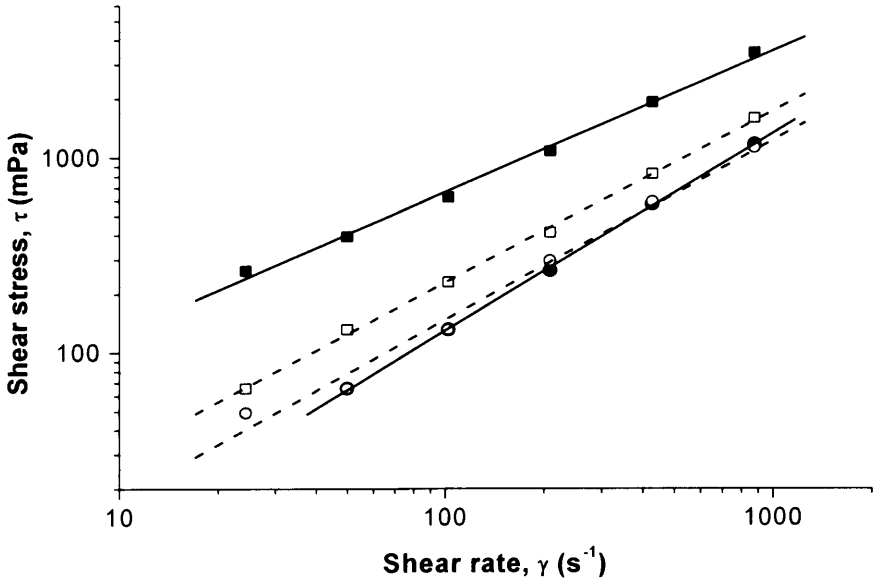

Figure 4.2. Shear stress - shear rate relationship for *E. coli* whole cells and periplasmically lysed *E. coli* cells at 25°C. The linear fits show power-law relationships ($\tau = k\gamma^n$), where for *E. coli* whole cells: 15% ww/v (■): n = 0.72, k = 24 mPa.s^n , μ_a = 3.49 mPa.s; 2% ww/v (●): n = 1.01, k = 1.25 mPa.s^n , μ = 1.35 mPa.s; for *E. coli* lysate: 9% ww/v (□): n = 0.88, k = 4.07 mPa.s^n , μ = 1.76 mPa.s; 2% ww/v (○): n = 0.92, k = 2.17 mPa.s^n , μ = 1.27 mPa.s.

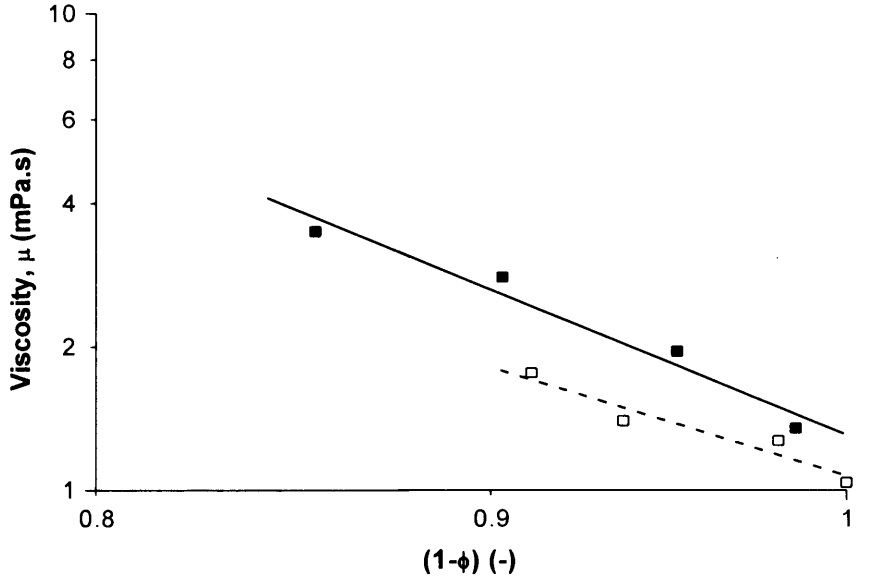

Figure 4.3. Relationship between viscosity and sample solids fraction for *E. coli* whole cells (■) and periplasmically lysed *E. coli* cells (□). The linear fits are power-law curves ($\mu^* = \mu\ (1-\phi)^{-\alpha}$) where for *E. coli* whole cells and *E. coli* lysate α was found to be 6.6 and 5.0, respectively.

4.2.1.2 USD and pilot-scale clarification of *E. coli* whole cells and periplasmically lysed *E. coli* cells

The application of the novel USD clarification method - including pre-dilution and subsequent mathematical correction of resulting clarification curves - is illustrated in Figures 4.4-4.6.

To start with, Figure 4.4 shows the clarification efficiencies achieved for samples of undiluted *E. coli* whole cell broth (~15% ww/v) and undiluted periplasmically lysed *E. coli* cells (~9% ww/v) using traditional USD methodology. USD centrifugation for the purpose of clarification was carried out in the Eppendorf 5810R centrifuge at spin speeds varying between 4000 and 6000 rpm and spin times in the range of 2–30 min, corresponding to Σ_{lab} values between 0.064 and 0.160 m^2 (refer to Appendix A2 and A3 for equations and relevant technical data for calculation of Σ factors). According to USD methodology, both feed-streams had been subject to shear in a high speed rotating disc device (section 2.2.3) prior to settling in the laboratory scale centrifuge. (The shear sensitivity of both feed stocks have previously been investigated and found to be negligible.)

Figure 4.5 shows the effect of diluting the feed material down to ~2% solids (ww/v) prior to shearing in the disc device. The diluted and sheared material was clarified in the Eppendorf 5810R centrifuge at conditions identical to the ones applied for the undiluted feed-streams in Figure 4.4. This experimental methodology prevents the formation of aggregates in the laboratory spin tube by diluting the material down to a level where cell-cell interactions are likely to be minimal. According to the novel USD clarification method described in the introduction to this chapter, the clarification curves obtained for the pre-diluted material were mathematically adjusted to compensate for the dilution by means of the modified Stokes' equation (Equation 4.8). The resulting predicted separation performances of an *E. coli* whole cell feed-stream of ~15% (ww/v) solids and a culture of *E. coli* lysate of ~9% (ww/v) solids are included in Figure 4.5.

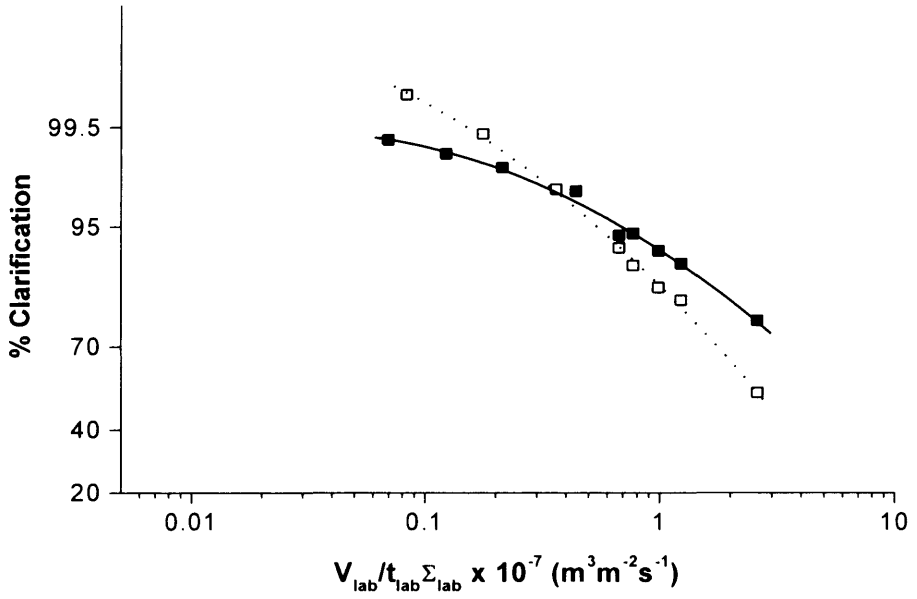

Figure 4.4. Clarification levels achieved for undiluted (~15% ww/v) *E. coli* cell broth (■) and undiluted (~9% ww/v) periplasmically lysed *E. coli* cells (□) using traditional USD methodology. Clarification was carried out in the laboratory Eppendorf 5810R centrifuge (N = 4000-6000 rpm, t_{lab} = 2-30 min, V_{lab} = 0.001-0.002 L, Σ_{lab} = 0.064-0.160 m^2). Data points represent the mean value of three measurements, with an average standard deviation of ± 0.9 and ± 0.7 in terms of % clarification for whole cells and periplasmically lysed cells, respectively. Correlation coefficients indicate that linear fits are probably not relevant in these cases, and hence the lines drawn are those of best polynomial fit.

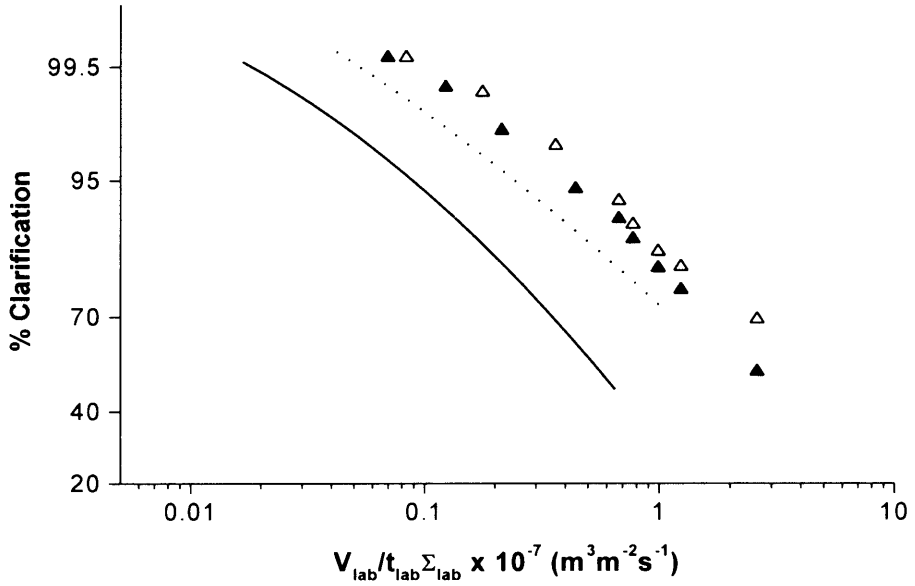

Figure 4.5. Clarification levels achieved for cultures of diluted (~2% ww/v) *E. coli* cell broth (▲) and diluted (~2% ww/v) periplasmically lysed *E. coli* cells (Δ). Clarification was carried out in the laboratory Eppendorf 5810R centrifuge (N = 4000-6000 rpm, t_{lab} = 2-30 min, V_{lab} = 0.001-0.002 L, Σ_{lab} = 0.064-0.160 m^2). Experimental data points represent the mean value of three measurements, with an average standard deviation of ± 0.2 and ± 0.4 in terms of % clarification for whole cells and periplasmic lysate, respectively. Centrifugal recovery performance of concentrated suspensions in a continuous-flow disc-stack centrifuge was predicted by means of the modified Stokes' equation (Equation 4.8) based on the ~2% (ww/v) experimental data presented. Predicted clarification levels for an *E. coli* whole cell feed of 15% (ww/v) solids are represented by —— and for a feed of 9% (ww/v) periplasmically lysed *E. coli* cells by ····· .

In Figure 4.6 the predicted clarification performances shown for undiluted *E. coli* whole cells (~15% ww/v solids) and *E. coli* periplasmic lysate (~9% ww/v solids) in Figure 4.5 are compared to the actual separation performance of the undiluted feed-streams as determined experimentally in the CSA-1 disc-stack centrifuge.

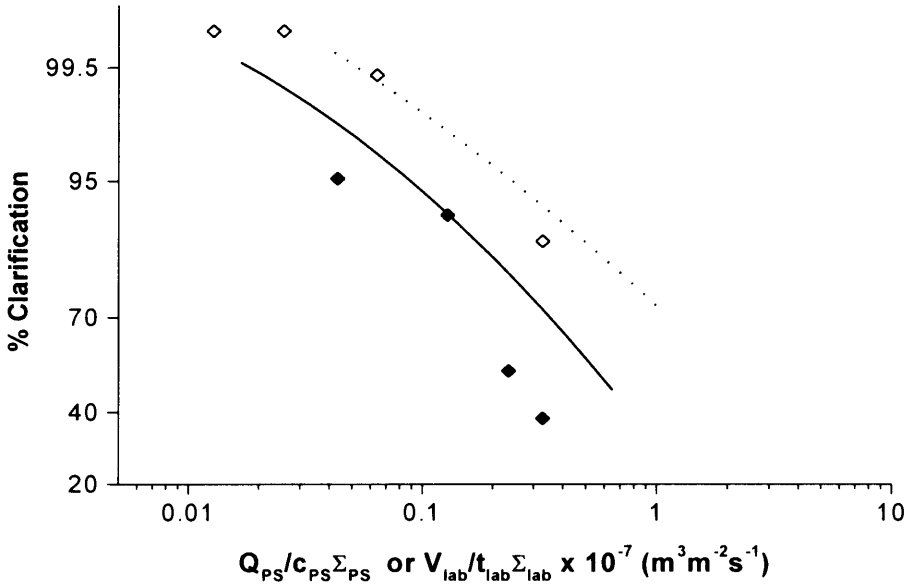

Figure 4.6. Comparison of actual and predicted clarification performances of *E. coli* cell broth and periplasmically lysed *E. coli* cells at pilot-scale. Whole *E. coli* cells (~15% ww/v): actual CSA-1 ◆ (N = 163.3 rps, Q = 10-80 L h^{-1}). Periplasmically lysed *E. coli* cells (~9% ww/v): actual CSA-1 ◊ (N = 163.3 rps, Q = 3-80 L h^{-1}). Corresponding USD predictions taken from Figure 4.5 are given for whole cell broth (——) and for periplasmic lysate (·····).

The ability of the modified method to predict accurately different behavioural changes at high cell density, as illustrated by the results shown in Figure 4.6, demonstrates the validity of the approach as a predictive process tool. To summarise this verification section, Table 4.1 shows the differences in predicted Q/cΣ values for two clarification levels using the different approaches. The error associated with the traditional USD clarification method upon comparison with actual pilot-scale

clarification data was found to be in the range 200-1000%. On the other hand, the modified USD clarification approach detailed in this chapter gave an average error of 30%.

Table 4.1. Comparison between the $Q/c\Sigma$ values required to achieve 95% and 99.5% clarification as identified by different USD methods for predicting large-scale clarification behaviour, and actual results achieved for *E. coli* whole cells and *E. coli* periplasmic lysate with the CSA-1 disc-stack centrifuge. Closest agreement is gained for the dilution and correction USD approach illustrated in this chapter (maximum error of 50%, average error of 30%). The conventional approach gives errors of ~200 to ~1000%.

	Level of clarification of material			
Method of study	95%		99.5%	
	Whole cells	Lysate	Whole cells	Lysate
USD, undiluted sample (Fig 4.4) Predicted $\frac{Q}{c\Sigma}$ x10^{-8} ($m^3m^{-2}s^{-1}$)	7.0	5.5	0.6	2.0
USD, diluted sample (Fig 4.5) Predicted $\frac{Q}{c\Sigma}$ x10^{-8} ($m^3m^{-2}s^{-1}$)	4.5	5.5	0.9	1.1
USD, diluted sample; corrected by means of Eq. 4.8. (Fig 4.5) Predicted $\frac{Q}{c\Sigma}$ x10^{-8} ($m^3m^{-2}s^{-1}$)	0.9	2.5	0.2	0.5
Disk-stack results (Fig 4.6) Actual $\frac{Q}{c\Sigma}$ x10^{-8} ($m^3m^{-2}s^{-1}$)	0.6	2.0	n/a	0.6

In the two following sections, the novel USD centrifugation methodology will be applied to predict clarification efficiencies of *P. pastoris* (section 4.2.2) and *E. coli* homogenates (section 4.2.3) of up to 15% (v/v for *P. pastoris* and ww/v for *E. coli* homogenate, respectively) solids concentration. In addition, the centrifugal performance parameters of dewatering and yield are introduced for these cultures.

4.2.2 USD predictions of *P. pastoris* centrifugal separation performance

The following section describes the use of USD methodologies to predict centrifugal separation behaviour of *P. pastoris* fermentation broths of varying solids concentration – in terms of clarification, dewatering and yield. First, the rheological properties of *P. pastoris* feed-streams of 2.5, 5, 10 and 15% (v/v) solids concentration were investigated in order to determine sample viscosities and to calculate the α-coefficient for *P. pastoris* (for use in Equation 4.8) (section 4.2.2.1). Following this, it is shown how experimental clarification data obtained for a 2.5% (v/v) solids feed can be utilised to predict the clarification levels of feeds of 5, 10 and 15% (v/v) solids concentration using the method described in section 4.2.1 (section 4.2.2.2). Finally, the dewatering and yield properties of the feed-streams of interest were determined in the laboratory-centrifuge (section 4.2.2.3).

4.2.2.1 Rheological properties of *P. pastoris*

In order to analyse the rheological properties of *P. pastoris* suspensions of 2.5, 5, 10 and 15% (v/v) solids concentration, log-log relationships between shear stress and shear rate for each sample were generated (Figure 4.7). The fitted lines were analysed as power-law curves of the form $\tau = k\gamma^n$, where k is the consistency index and n is the flow behaviour index (represented by the slope of the line). As the flow behaviour index was found to be greater than 0.9 in all cases, Newtonian behaviour (constant viscosity) was assumed as an acceptable approximation. The viscosity of each feed solution could therefore be determined from the best least-square gradient fit of the relationship between shear stress and shear rate (as described in section 2.2.2).

A log-log plot of viscosity versus $(1-\phi)$ yields a straight line (Figure 4.8), the slope of which corresponds to the coefficient α in Equation 4.8. α was found to be 2.9 for *P. pastoris*.

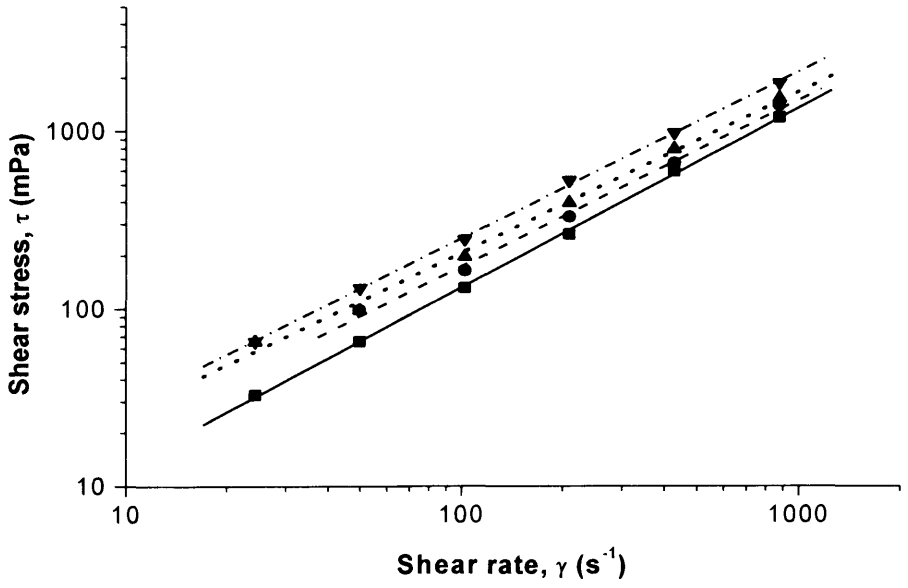

Figure 4.7. Shear stress - shear rate relationship for *P. pastoris* of 2.5 (■), 5 (●), 10 (▲) and 15 (▼) % (v/v) feed solids concentration at 25°C. The linear fits are power-law curves ($\tau = k\gamma^n$), where for 2.5%: n = 1.0, k = 1.29 mPa.s^n; 5%: n = 0.92, k = 2.40 mPa.s^n; 10%: n = 0.9, k = 3.26 mPa.s^n; 15%: n = 0.93, k = 3.39 mPa.s^n. Average viscosities over the shear rate range were for 2.5%: μ = 1.36 mPa.s; 5%: μ = 1.55 mPa.s; 10%: μ = 1.71 mPa.s; 15%: μ = 2.07 mPa.s

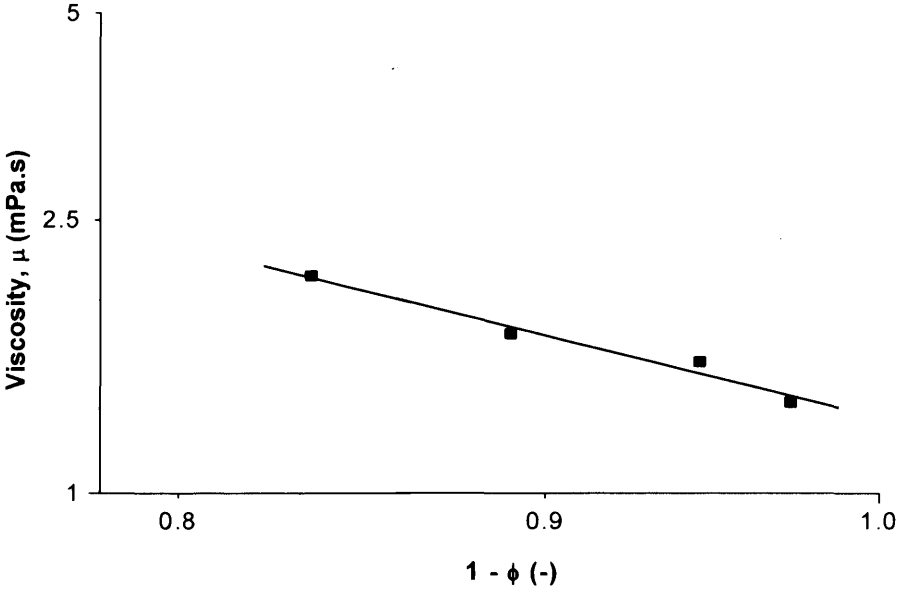

Figure 4.8. Relationship between average viscosity and feed solids fraction for *P. pastoris*. The linear fits are power-law curves ($\mu^* = \mu (1-\phi)^{-\alpha}$) where α was found to be 2.9.

4.2.2.2 USD clarification predictions for *P. pastoris*

Shear study

Chapter 3 examined the impact of *P. pastoris* cell damage resulting from the high shear regions at the inlet of centrifuges, as mimicked by a high speed rotating disc device (according to section 2.2.3), by measuring the total protein concentration in the supernatant of sheared and non-sheared samples. The total protein concentration was relatively constant between the samples and it was concluded that shearing has a minimal effect on the cells. In this section another study to investigate the effect of shear on *P. pastoris* cells was conducted, which was based on a comparison of clarification efficiencies between sheared and non-sheared samples. Figure 4.9 shows the effect on clarification of exposing the *P. pastoris* process material to a shear rate of 1×10^{6} s^{-1} for 20 s prior to lab scale centrifugation in the case of a 2.5% (v/v) feed solids concentration. Both the sheared and the non-sheared feed-streams were clarified in the Eppendorf 5810R centrifuge at 4000 rpm for times ranging between 4.5 and 257 min. This corresponds to Σ_{lab} values in the range 0.064–0.068 (refer to Appendix A2 and A3 for equations and relevant data for calculation of Σ factors). The result suggests that any differences in clarification efficiency when comparing sheared to non-sheared material are minor and within the range of experimental reproducibility, and is in accordance with the outcome of the shear study presented in Chapter 3. This result is as expected for whole cells with a tough outer cell wall and regular shape.

Clarification study

For the dilute feed-stream of 2.5% (v/v) solids presented in Figure 4.9, any high cell density effects were deemed sufficiently small as to be negligible. As mentioned in the previous section, the prediction of separation efficiencies for high solids density feed-streams using bench top centrifugation equipment has proven to be more problematic. As solids concentration increases so do the particle interaction effects in the test tube (according to Figure 4.1). For *P. pastoris*, increased solids concentration resulted in increased clarification levels (see Figure 4.10) at spin conditions identical to the ones described in the shear study above; this result is most likely due to the cells interacting and forming aggregates, or even due to blanket settling effects,

effectively leading to an increase in the overall settling velocity. This result is opposite to what would be expected in a large-scale centrifuge, where dilution effects and flow patterns in the bowl would break up any aggregates formed and separation would be expected to be more efficient for a dilute rather than a concentrated feed-stream. Therefore, in order to give a more accurate prediction of large-scale clarification behaviour, the predicted recovery efficiencies for 5, 10 and 15% (v/v) feed solids concentrations shown in Figure 4.11 were based on the 2.5% (v/v) USD experimental data (Figure 4.9) and subsequently corrected for any effects of high solids content by means of the modified Stokes' Law (Equation 4.8) as described previously in this chapter.

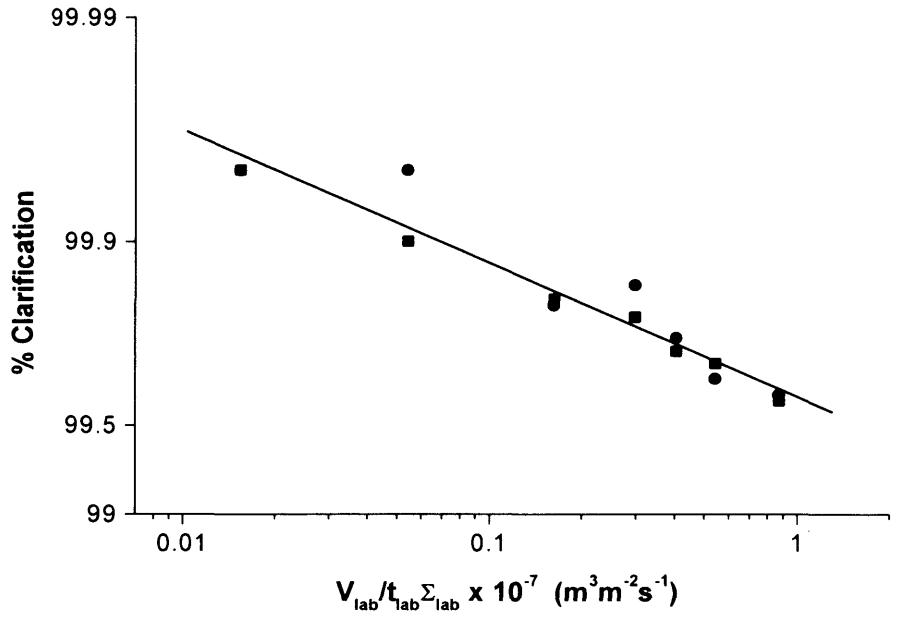

Figure 4.9. Comparison of clarification levels achieved for sheared (●) and non-sheared (■) *P. pastoris* feed-streams of 2.5% (v/v) solids. Centrifugation for the purpose of clarification measurements was carried out in an Eppendorf 5810R centrifuge (N = 4000 rpm, t_{lab} = 4.5–257 min, V_{lab} = 0.0015 L, Σ_{lab} = 0.064-0.068 m^2). The sheared suspension was exposed to a shear rate of 1×10^6 s^{-1} for 20 s prior to centrifugation. Data points represent the mean value of three measurements, with an average standard deviation of ± 0.02 in terms of % clarification. The fitted line represents both sheared and non-sheared data points.

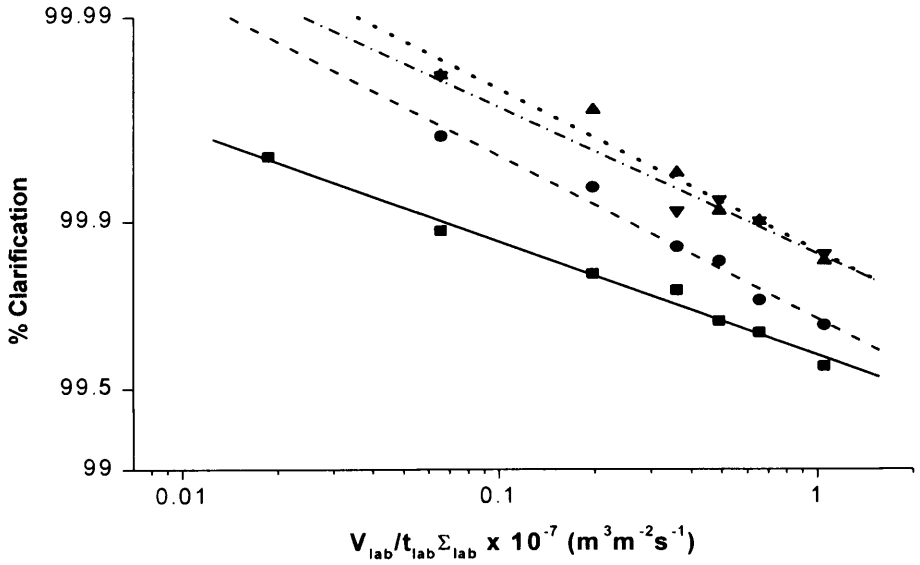

Figure 4.10. Experimental clarification efficiencies for *P. pastoris* cultures of 2.5 (■), 5 (●), 10 (▲) and 15 (▼) % (v/v) solids. Centrifugation was carried out in an Eppendorf 5810R centrifuge (N = 4000 rpm, t_{lab} = 4.5–257 min, V_{lab} = 0.0015 L, Σ_{lab} = 0.064-0.068 m^2). Data points represent the mean value of three measurements, the average standard deviation being ± 0.02, 0.03, 0.01 and 0.01 in terms of % clarification for feed-streams of 2.5, 5, 10 and 15% (v/v) solids, respectively. The lines represent linear fits of the data sets.

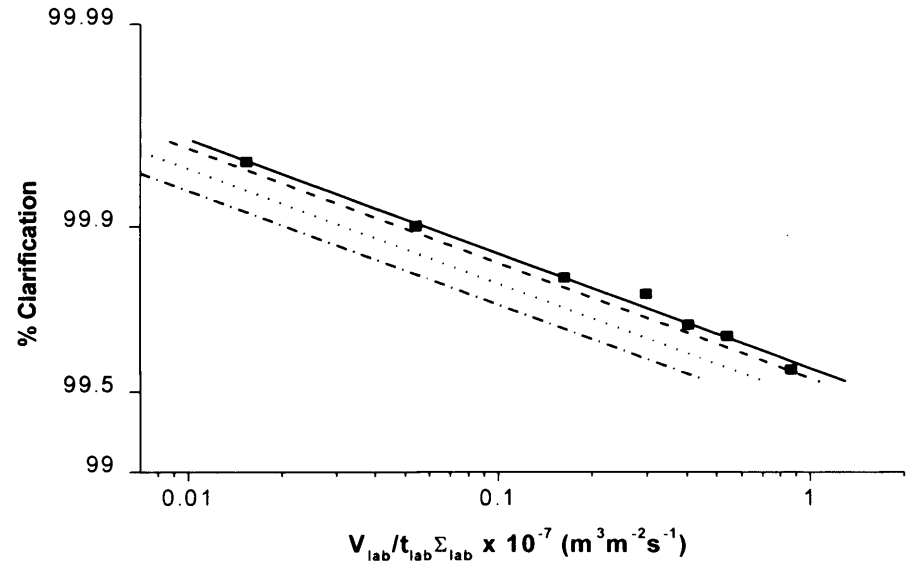

Figure 4.11. Predicted clarification efficiencies for *P. pastoris* cultures of 5, 10 and 15% (v/v) solids. Predictions were based on the 2.5% (v/v) experimental data (■) and corrected for the effects of increased viscosity and hindered settling by means of the modified Stokes' Law (Equation 4.8). Linear fits of recovery efficiencies are presented for 5 (·····), 10 (- - - - -) and 15% (- · - · - · -) (v/v) feed solids concentrations.

4.2.2.3 USD dewatering and yield predictions for *P. pastoris*

In addition to clarification, dewatering is another important parameter reflecting centrifugation performance. The level of dewatering is an indication of the amount of water trapped in the sediment following the centrifugal separation of liquid and solid phases. For extra-cellular products high dewatering is crucial for high product yields. Whereas centrifugal clarification is a property well-studied in literature, there is considerably less information regarding dewatering properties of biological feed-stocks separated by centrifugation. The level of dewatering was determined as described in section 2.5.2.2, and the protocol involves an investigation of how much water is removed from a known amount of sediment by oven drying, taking into consideration any cell internal water. The methodology involves centrifugation of the sample at an RCF identical to the forces experienced in industrial-scale machines, at spin times corresponding to industrially relevant flow rates; so as to produce a sufficiently accurate mimic of the dewatering properties of the feed materials investigated. The following presents dewatering and yield data obtained for *P. pastoris* in a laboratory-scale centrifuge, calculated according to Equations 2.2 and 2.3, respectively.

Figure 4.12 gives the percentage dewatering as a function of equivalent flow rate per centrifuge separation area for the solids concentrations tested. The dewatering experiments were carried out in the Eppendorf 5810R centrifuge at RCF values between 5500 and 16300, corresponding to the average RCF levels calculated for a range of industrially relevant centrifuges. The spin times varied between 0.3 and 60 min, and the corresponding Σ factor for the lab-scale centrifuge ranged from 0.198 to 1.005 m^2 (see Appendix A2 and A3 for equations and relevant data for calculation of Σ factors).

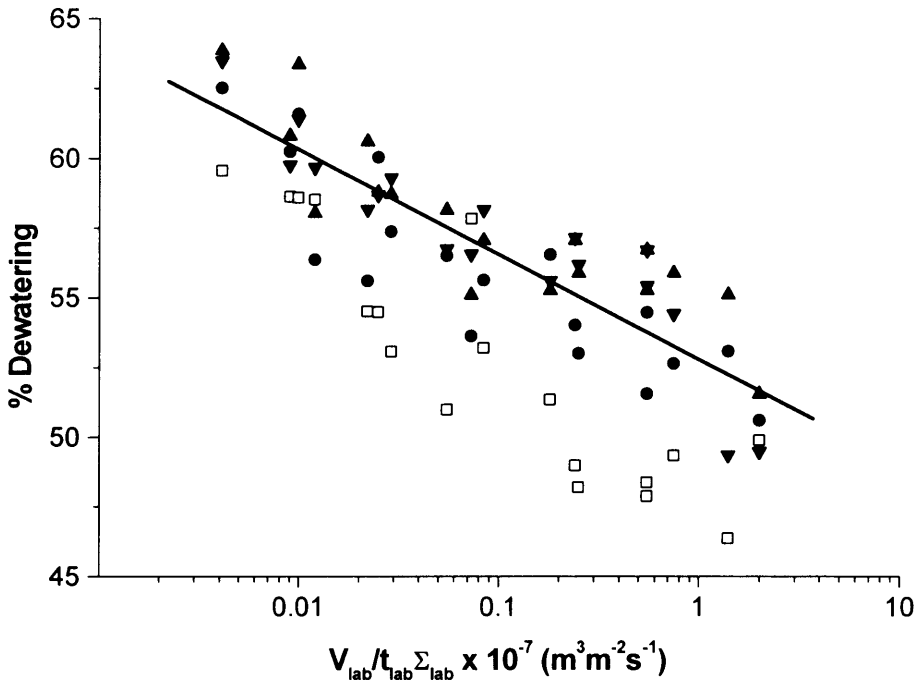

Figure 4.12. Level of dewatering achieved for *P. pastoris* cultures of 2.5 (□), 5 (●), 10 (▲) and 15 (▼) % (v/v) solids concentration. Centrifugation for the purpose of dewatering was carried out in an Eppendorf 5810R centrifuge (RCF = 5500–16300, V_{lab} = 0.0015 L, t_{lab} = 0.033–60 min, Σ_{lab} = 0.198–1.005 m^2). All data points represent the mean of three measurements, the average standard deviation being ± 1.9, 0.9, 0.8 and 0.8 in terms of % dewatering for feed-streams of 2.5, 5, 10 and 15% (v/v) solids, respectively. The fitted line is based on the dewatering levels for feeds of 5, 10 and 15% solids (v/v), as the 2.5% (v/v) solids suspension was found to be significantly different from the feed-streams of higher solids concentration (see main text).

In all cases, the level of dewatering was found to increase with increasing centrifuge separation area and/or decreasing equivalent flow rate with the 2.5% (v/v) solids feed giving a significantly lower level of dewatering compared to the higher concentrations. There is no significant difference between the dewatering levels achieved for 5, 10 and 15% (v/v) solids concentration. Evidently at higher solids concentrations the pressure applied to the sediment at the very bottom of the spin tube will increase, and hence the level of solids compression, and consequently the level of dewatering, of the sediment at the bottom zone of the tube will increase. Sediment recovered above this zone should be less dewatered, giving wetter sediments as solids concentration increases. This is in contradiction to the observed result, which may be due to the complicating fact that the solids will be elastic and

will tend to re-expand on de-acceleration of the centrifuge. This effect appears to be more significant for the reduced sediment volumes resulting from centrifugation of low solids concentration feeds. The dewatering calculations based on a feed of low solids concentration will also be more prone to the error arising from any remaining traces of supernatant at the sides of the test tubes than a feed of high solids concentration. The results indicate some of the difficulties in mimicking the dynamics of centrifugal dewatering at scale.

Figure 4.13 shows the percentage yield as calculated from Equation 2.3. Contrary to the dewatering results presented in Figure 4.12, there is a small difference in yield between the four solids concentrations investigated, with the highest yield achieved for the lowest solids concentration. It appears that the effect of dewatering on yield is offset by the increasing proportional amount of product-containing supernatant trapped in sediment as solids concentration increases.

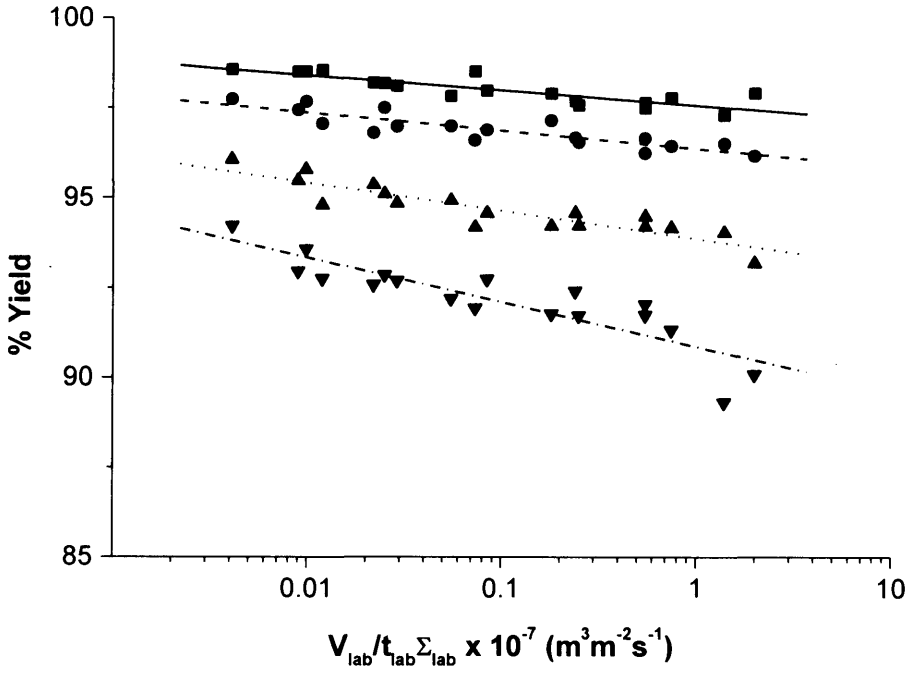

Figure 4.13. Level of yield achieved for *P. pastoris* feed-streams of 2.5 (■), 5 (●), 10 (▲) and 15 (▼) % (v/v) solids. Yield levels were calculated from Equation 2.3. The lines represent linear fits of the respective data sets.

4.2.3 USD predictions of *E. coli* homogenate centrifugal separation performance

In this section, USD methodology is applied to predict centrifugal clarification, dewatering and yield behaviour of *E. coli* homogenates of varying solids concentration. The rheological properties of homogenates of 0.9, 2.8 and 5.2% (ww/v) solids concentration were investigated in order to determine sample viscosities and to calculate the α-coefficient for *E. coli* homogenate (for use in Equation 4.8) (section 4.2.3.1). Clarification performance for feed-streams of 5, 10 and 15% (ww/v) solids were predicted by means of the novel USD approach described in 4.2.1, based on experimental 0.9% (ww/v) data (section 4.2.3.2). Finally, the dewatering and yield properties of the feed-streams of 0.9, 2.8 and 5.2% (ww/v) were determined (section 4.2.3.3).

4.2.3.1 Rheological properties of *E. coli* homogenate

Figure 4.14 shows the log-log relationship between shear stress, τ, and shear rate, γ, for *E. coli* homogenates of 0.9, 2.8 and 5.2 % (ww/v) solids concentration. The fitted lines were analysed as power-law curves on the form $\tau = k\gamma^n$, where k is the consistency index and n is the flow behaviour index (represented by the slope of the line). As the flow behaviour index was found to be greater than 0.9 in all cases, Newtonian behaviour was assumed as an acceptable approximation. The viscosity of each feed solution could therefore be determined from the best least-square gradient fit of the relationship between shear stress and shear rate, according to the method described in section 2.2.2.

A log-log plot of the resulting viscosities versus $(1-\phi)$ yielded a straight line (Figure 4.15), the slope of which corresponds to the coefficient α in Equation 4.8. α was found to be 8.5 for *E. coli* homogenate.

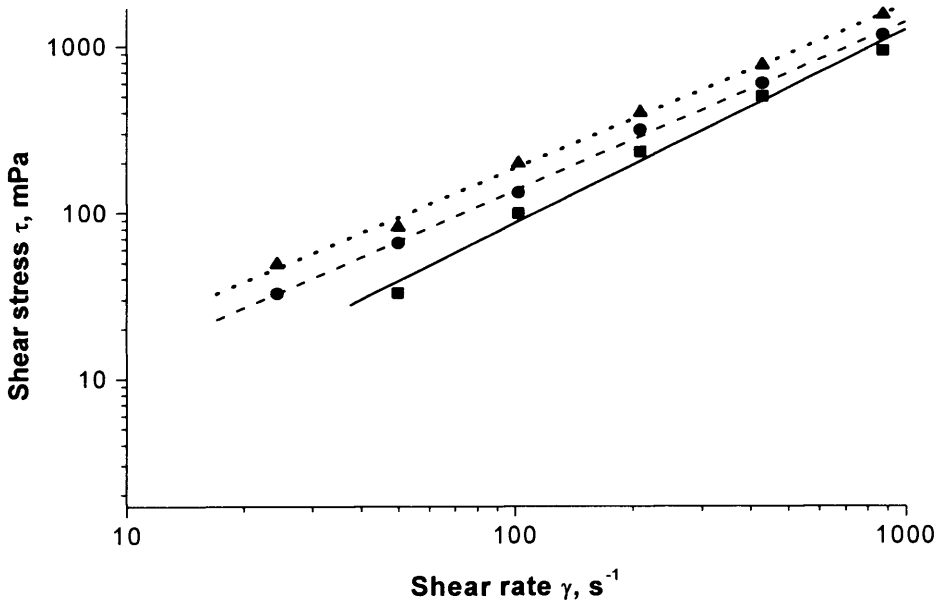

Figure 4.14. Shear stress - shear rate relationship for *E. coli* homogenates of 0.9 (■), 2.8 (●) and 5.2 (▲) % (ww/v) solids concentration at 25^{0}C. The linear fits are power-law curves ($\tau = k\gamma^n$), where for 0.9%: n = 1.15, k = 0.42 mPa.s^n; 2.8%: n =1.01, k = 1.32 mPa.s^n; 5.2%: n = 0.97, k = 2.57 mPa.s^n. Average viscosities over the shear rate range were for 0.9%: μ = 1.08 mPa.s; 2.8%: μ = 1.31 mPa.s; 5.2%: μ = 1.70 mPa.s.

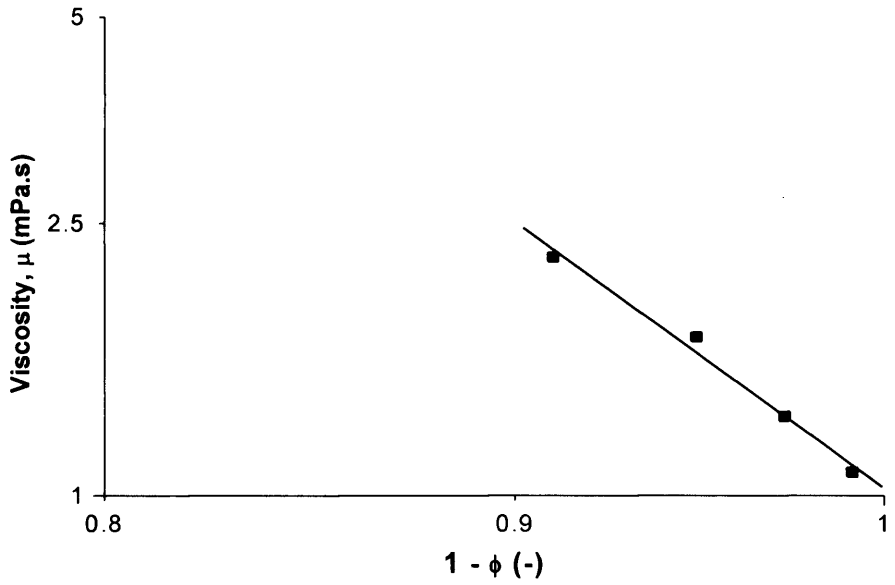

Figure 4.15. Relationship between average viscosity and feed solids fraction for *E. coli* homogenate. The linear fits are power-law curves ($\mu^* = \mu\,(1-\phi)^{-\alpha}$) where α was found to be 8.5.

4.2.3.2 USD clarification predictions for *E. coli* homogenate

Figure 4.16 presents clarification levels for *E. coli* homogenates of 5, 10 and 15% (ww/v) solids concentration, as calculated from Equation 4.8, based on experimental clarification levels determined for the dilute 0.9% (ww/v) feed-stream. Centrifugal clarification was carried out in the Eppendorf 5810R centrifuge at spin speeds between 4000 and 6000 rpm, and spin times ranging from 2 to 25 min, and the resulting Σ ranged between 0.064 and 0.160 m^2 (refer to Appendix A2 and A3 for equations and relevant data for calculation of Σ factors). The predicted curves show the expected trend of increasing clarification as solids concentration decreases.

The clarification levels achieved are significantly lower than what was seen for *P. pastoris* in Figure 4.10 and 4.11, as well as for *E. coli* whole cells and periplasmically lysed *E. coli* cells (section 4.2.1), and the dependency of clarification on the centrifugal settling conditions is much more pronounced. The reduction in separation performance is likely to be due to an increase in fine particles in the case of the *E. coli* homogenate relative to that for the other feed-streams investigated. These fines will settle with a reduced settling velocity, according to Stokes' Law. The total number of particles remaining in the supernatant following separation at a constant $V_{lab}/t_{lab}\Sigma_{lab}$ will therefore be higher for the homogenised *E. coli* cell cultures compared to for *E. coli* whole cells, periplasmically lysed *E. coli* cells and undisrupted *P. pastoris* cells.

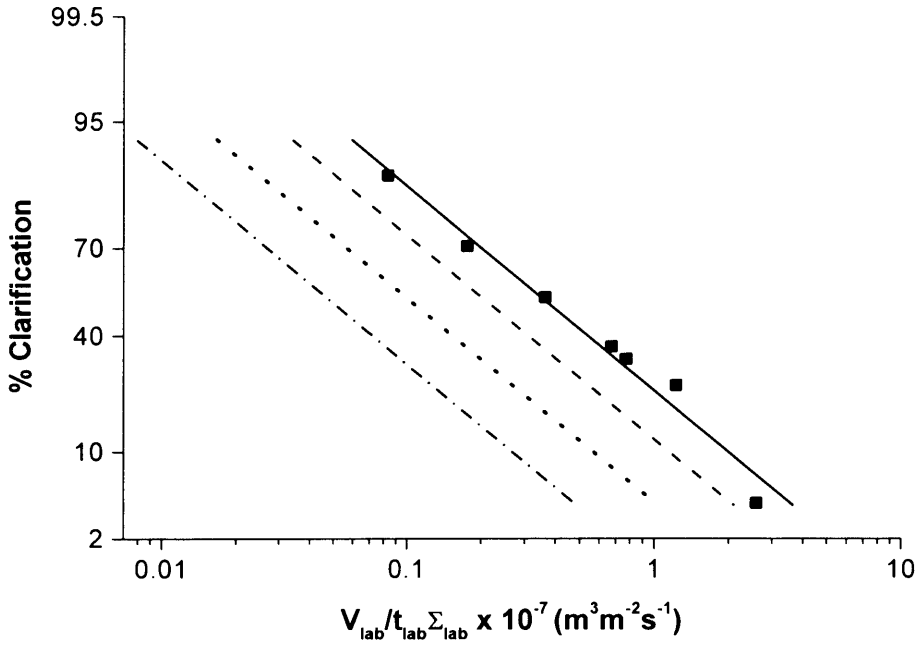

Figure 4.16. Predicted clarification efficiencies for *E. coli* homogenates of 5, 10 and 15% (ww/v) solids concentration. Predictions were based on the 0.9% (ww/v) experimental data (■) (N = 4000–6000 rpm, t_{lab} = 2–25 min, V_{lab} = 0.0015 L, Σ_{lab} = 0.064–0.160 m^2) and the resulting clarification curves corrected for the effect of increased viscosity and solids interactions by means of the modified Stokes' Law (Equation 4.8). All data points represent the mean of three measurements, the average standard deviation being ± 0.4 in terms of % clarification. Linear fits of recovery efficiencies for 5 (·····), 10 (- - - - -) and 15 (- · - · - · - · -) % (ww/v) feed solids concentrations are represented by the dashed, dotted and dashed-dotted lines, respectively.

4.2.3.3 USD dewatering and yield predictions for *E. coli* homogenate

Centrifugal dewatering experiments were carried out in the Eppendorf 5810R centrifuge at RCF values between 5500 and 16300, corresponding to the average RCF levels calculated for a range of industrially relevant centrifuges. Spin times varied from 0.2–30 min, and the resulting Σ_{lab} ranged between 0.154 and 0.995 m^2. As seen in Figure 4.17, the level of dewatering achieved for *E. coli* homogenate increases with increasing feed solids content. This was also observed for the *P. pastoris* cultures investigated in section 4.2.2.3. However the dewatering levels obtained for *P. pastoris* was significantly higher than for the *E. coli* homogenates at a similar solids concentration and same settling conditions. The homogenate has a

wider particle size distribution and the cell debris possess a more irregular shape relative to the spherical *Pichia* cells. It is believed that due to the amorphous characteristic of the homogenate feed material it does not drain very well. Moreover, the situation may also be complicated by the fact that the homogenate consists of intracellular material, which might possess hydrophilic properties. The result would be that the water in the homogenate is chemically bound to the cell debris and can not be removed by force.

The yield levels obtained for the *E. coli* homogenates (Figure 4.18) seems to be relatively constant over the range of conditions tested. The trend observed is similar to that obtained for *P. pastoris*; however the levels of yield achieved were higher for the yeast system. This difference in predicted yield is a consequence of the variation in dewatering levels seen between the two biological systems.

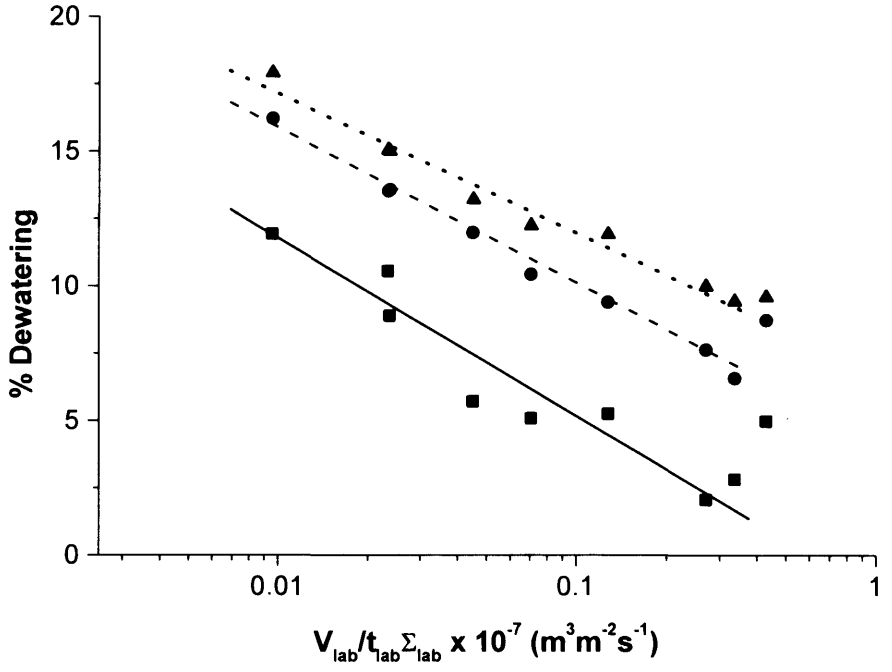

Figure 4.17. Level of dewatering achieved for *E. coli* homogenates of 0.9 (■), 2.8 (●) and 5.2 (▲) % (ww/v) solids concentration. Dewatering measurements were carried out in the Eppendorf 5810R centrifuge (RCF 5500–16300, V_{lab} = 0.0015 L, t_{lab} = 0.2–30 min, Σ_{lab} = 0.154-0.995 m^2). All data points represent the mean of three measurements, the average standard deviation being ± 1.3, 0.7 and 0.3 in terms of % dewatering for the feed stocks of 0.9, 2.8 and 5.2 % (ww/v) solids, respectively.

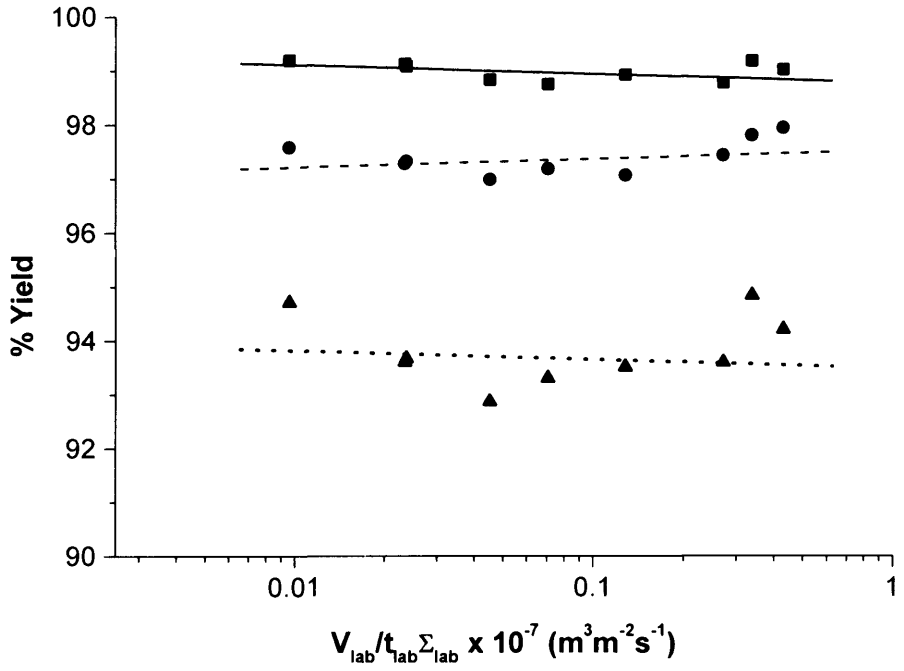

Figure 4.18. Level of yield achieved for *E. coli* homogenates of 0.9 (■), 2.8 (●) and 5.2 (▲) % (ww/v) solids concentration. Yield levels were calculated from Equation 2.3. The lines represent linear fits of the respective data sets.

4.3 Summary

The work presented in this chapter has described a new ultra scale-down methodology for predicting centrifugal clarification performance in the case of high cell density cultures. Existing USD approaches generated for dilute systems lead to an over-prediction of clarification performance when applied to such high cell density feeds. This difference in performance is attributed to cell-cell interactions, leading to effects such as aggregation, or even blanket sedimentation, occurring in the low shear environment of a laboratory centrifuge, which will not be apparent in the settling region of a continuous-flow industrial centrifuge. The novel USD methodology described here is based upon the dilution of high solids feed material down to ~2% (ww/v), at which level cell-cell interactions are minimal, prior to the application of the clarification test. Mathematical corrections were then applied to the resultant clarification curves in order to account for the effects of dilution in terms of i.e. reduced hindered settling and lower viscosity.

The methodology was successfully verified in a pilot-scale disc-stack centrifuge. Prediction of separation performance at high solids loads (up to 15% ww/v) was demonstrated using whole *E. coli* cells and *E. coli* cells that had been subject to a periplasmic lysis step. Corrected USD curves accurately predicted pilot-scale clarification performance of the high cell density broths investigated, with an average error of 30%. In comparison, the conventional USD clarification method was associated with errors up to 1000%.

The USD methodology developed was applied to predict the clarification efficiency of *P. pastoris* cultures and *E. coli* homogenates of varying solids concentration. Moreover, a USD tool to determine dewatering levels, and hence process yield, was described and applied to the *P. pastoris* and *E. coli* homogenate cultures. These performance parameters, together with that of clarification, will be utilised in relation to the development of a series of Windows of Operation for industrial-scale centrifugation, as presented in Chapter 5.

5 Visualisation of centrifugal separation performance using Windows of Operation

Abstract

Expression systems capable of growing to high cell densities are now readily available and are popular due to the benefits of increased product concentration. However, such high solids density cultures pose a major challenge for bioprocess engineers as choosing the right separation equipment and operating it at optimal conditions is crucial for efficient recovery.

Windows of Operation provide a tool, which will help in design and also enable the rapid comparison of alternative operating strategies. Previous work has demonstrated the use of Windows of Operation as a visualisation tool within bioprocessing (King *et al.*, 2004; Nealon *et al.*, 2005; Woodley and Titchener-Hooker, 1996; Zhou and Titchener-Hooker, 1999). Such Windows have not only been shown to be useful in the selection of suitable operating conditions for a given processing objective but also to indicate where a particular item of equipment is not suitable for the chosen process target.

The objective of this chapter is to consider the selection of centrifuge type and operating conditions necessary for the efficient recovery of products from high cell density cultures. Windows of Operation will be generated in order to visualise the available operating conditions for a number of centrifuge types, and to aid the decision on which centrifuge design is best suited for particular process tasks when subject to defined constraints.

Two case studies are presented that examine centrifuge selection for the processing of *P. pastoris* cultures and *E. coli* homogenates of varying solids concentration. The Windows of Operation generated will consider recovery and yield levels as determined by USD centrifugation technology in Chapter 4, but will also indicate operational constraints imposed by factors such as centrifuge solids holding capacity

and flow rate limitations and how these concert to restrict and define the operating space available to the design engineer when making flowsheet decisions. The insight gained from the case studies provides a useful indication of the utility of the methodology presented and illustrates the challenges of centrifuge selection for the demanding case of high solids concentration feed-streams.

Note: A modified version of this chapter has been accepted for publication as a paper in Biotechnology and bioengineering (Salte *et al.*, 2006). The paper is attached in Appendix A5.

5.1 Introduction

Chapter 4 described an ultra scale-down approach for the prediction of clarification, dewatering and yield levels achieved upon centrifugal recovery of high cell density cultures. In this chapter the outcome of the *P. pastoris* and *E. coli* homogenate USD studies (sections 4.2.2 and 4.2.3, respectively) will be combined with a visualisation tool, a Window of Operation, in order to provide a rapid evaluation of available operating conditions, as an aid in the selection of the centrifuge equipment most appropriate for the respective process duties. The chapter examines semi-continuous disc-stack centrifuges and batch-operated machines such as multi-chamber bowls and Carr Powerfuges^{TM}. Performance is assessed based on the variables of clarification and product yield. Inclusion of limits imposed by the centrifuge type and design, and operation itself, serve to constrain the process and to define the Windows of Operation.

Section 5.1.1 describes the construction of Windows of Operation and discusses the parameters that have to be considered when generating a Window of Operation for a centrifugation process. Section 5.1.2 provides the necessary specifications for the centrifuges examined in this chapter.

5.1.1 Windows of Operation for centrifugation

When constructing a Window of Operation it is necessary to consider which parameters affect the performance of the unit operation of interest. Factors of significance for centrifugation have been discussed previously (Boychyn *et al.*, 2000; Zhou *et al.*, 1997) and include properties related to centrifuge type and design – such as solids holding capacity, feed material properties - such as size and shape of particles and concentration of solids in the feed, and operating parameters - such as flow rate and processing time.

For the Windows of Operation presented in this chapter, the centrifuge type is pre-set, with a fixed spin speed and bowl size, and thus fixed Sigma value. For the purpose of direct comparisons it is assumed that the process material is obtained from a batch of fixed initial size and initial solids concentration. The solids concentration fed to the centrifuge can be altered by dilution, but this will be at the expense of an increased final batch volume to be processed. The variables of flow rate and solids concentration fed to the centrifuge were chosen to define the axis of the Windows of Operation developed in this chapter, as they are both parameters that can easily be varied by the designer and operator in order to optimise the step.

The Windows of Operation developed for centrifugation present information with regards to separation performance levels, and are constructed with a minimum acceptable solids recovery and yield level in mind. The performance parameters of clarification and dewatering are determined by ultra scale-down techniques, as described in Chapter 4. Based on the dewatering levels predicted, the product yield is calculated according to Equation 2.3. Clarification and yield are displayed as a function of feed solids concentration and flow rate in a 2-D contour plot using a function of the software program Origin^{TM} (Microcal Software Inc., Northampton, USA). The contour plots are generated from data matrices which correlate sets of either solids concentration, flow rate and clarification, or solids concentration, flow rate and yield, based on the experimental data relating clarification and yield to the operating parameters of solids concentration and flow rate.

The Windows of Operation also include operational constraints imposed by the centrifuge design of interest. For example, there are obvious equipment constraints relating to the range of flow rates that may be pumped through the centrifuge, giving rise to an upper flow rate limit. Above the upper limit it will not be possible to pump material through faster without flooding the machine.

In practice there will often be a processing time constraint, imposed by the operating company shift patterns. The impact of this constraint will be dependent upon whether the centrifuge is operated with batch or continuous solids removal. For batch operation the time constraint depends on the solids holding capacity of the bowl, the solids concentration of the process suspension, as well as the fixed time needed to dismantle, empty and refit the bowl, each time it becomes full. The time constraint may then be represented as a maximum processing time, $t_{proc.}$:

$$t_{proc.} = \frac{V_{total}}{Q} + \frac{V_{total}}{V_S} \phi \, t_{down} \qquad 5.1$$

where V_{total} is the total batch volume to be processed (i.e feed suspension volume plus volume of added diluent where appropriate), V_S the solids holding capacity of the bowl, Q the flow rate of feed through the centrifuge, ϕ the solids fraction entering the centrifuge and t_{down} the downtime for emptying, cleaning, and assembly, between each full bowl. This time constraint is also present for continuously operated equipment, but the second term in Equation 5.1 is no longer relevant ($t_{down} = 0$). For the case of a semi-continuous centrifuge operated with intermittent solids discharge, t_{down} exists, but is relatively insignificant compared to the downtime for machines operated with batch solids recovery. The downtime for a machine operated with intermittent discharge is related to the fact that feed flow may be stopped during discharge and also that there is a lag time taken to bring the centrifuge bowl back to full speed after discharge. No dismantling or cleaning of the bowl is necessary in this case.

For a disc-stack centrifuge operated with intermittent solids discharge a second time constraint, based on the minimum interval between solid discharges, exists. This is

set by the time needed for the machine motor to cope with changes in bowl speed associated with the discharge process. Too frequent a level of discharge will lead to an unacceptable rate of wear of the motor and gears. A typical minimum interval of about 120 s is usually recommended. This interval between discharges equates then to the time available for solids to accumulate in the bowl and for compaction of these to occur. The time for compaction can be expressed by Equation 5.2 (Boychyn *et al.*, 2000):

$$t_{comp.} = \frac{V_S}{2F\phi Q} \qquad 5.2$$

where $t_{comp.}$ is the average residence time of solids in the holding area of the centrifuge (V_S), Q is the flow rate, ϕ the feed solids fraction and F is the fractional recovery of solids.

Applying these operation-related constraints to the centrifuge performance data enables a Window of Operation to be constructed and for an examination of operational trade-offs to be made.

5.1.2 Centrifuge selection

Centrifugal separation performance was predicted for *P. pastoris* and *E. coli* homogenate by ultra scale-down methodologies in Chapter 4. The performance parameters of clarification and yield are in this chapter related to centrifuges of different design and size, representative of the range of machines used in the biotechnology industry. The performance data will be used to construct Windows of Operation for a semi-continuous disc-stack machine as well as for batch-operated centrifuges. Table 5.1 gives the characteristics of the centrifuges examined, including those of the laboratory centrifuge required for USD measurements. (The equations and the technical specifications required to calculate Σ for each of the centrifuges are given in Appendix A2 and A3, respectively. General information regarding the different types of centrifuges was provided in Chapter 1).

Table 5.1. Characteristics of the centrifuges studied.

Property	**Westfalia SC35 Disc-Stack**	**Westfalia KA6 Multi-chamber**	**Westfalia KB25 Multi-chamber**	**Carr P12 Powerfuge™**	**Carr P18 Powerfuge™**	**Eppendorf 5810R Lab**
Max bowl speed (rps)	120	142	110	181	148	233
RCF_{max}	7500	11400	9600	20000	20000	16400
Q_{max} (Lh^{-1})	25000	2800	8000	500	1700	-
Bowl volume (L)	18	10.7	30.5	9	36	$1.5x10^{-3}$
Solids holding volume (L)	7.5	7.5	22.5	8	32	<0.002
Solids recovery mechanism	Intermittent discharge	Batch	Batch	Batch	Batch	-
Downtime (h)	< 0.01	1.5 (1 bowl) 0.5 (2 bowls)	1.5 (1 bowl) 0.5 (2 bowls)	0.25	0.25	-
Settling area $c*\Sigma$ (m^2)*	10400	2100	3700	4500	10100	1.005 (max)

* Settling areas given are adjusted to take into account variations in flow patterns between the different centrifuge designs. c = 0.4 for disc stack centrifuges, 0.88 for multi-chamber bowls, 0.9 for Carr Powerfuges™ and 1.0 for laboratory scale centrifuges (Boychyn *et al.*, 2004).

For both Carr Powerfuges™ and multi-chamber centrifuges batch solids recovery is necessary. Hence when evaluating these centrifuges and comparing their performance to that of a semi-continuous disc-stack machine operated with intermittent solids discharge – for which downtime is considered to be significantly lower than for the batch operated centrifuges (see Table 5.1) - the number of bowl volumes of solids required to process a given feed volume and the downtime between the handling of each bowl volume must be considered, as these factors will affect the overall processing time (according to Equation 5.1). The effect of the downtime on the total process time will be especially prominent for feed-streams of very high solids content, since the bowl will be filled very rapidly. For the multi-chamber bowl, it was therefore assumed that the number of bowls available could be a design variable. Providing an additional empty bowl for replacement once the first bowl has become full will serve to minimise the downtime and hence maximise the utilisation of the equipment. Such a practice is used in industry in situations where bowl capacity is a constraint, and might be a more economically feasible solution than purchasing two separate multi-chamber machines and operating them simultaneously.

5.2 Results and discussion

The *P. pastoris* and *E. coli* homogenate centrifugation performance parameters of clarification, dewatering and yield were determined by USD techniques and presented in Chapter 4. A case study to evaluate the Windows of Operation corresponding to the operation of disc-stack, multi-chamber bowl and Carr Powerfuges™ for each of the feed stocks investigated was developed based on the results presented in sections 4.2.2 and 4.2.3 and using machine data as detailed in Table 5.1. Table 5.2 summarises the feed characteristics and operational constraints that were applied when generating the Windows of Operation displayed in sections 5.2.1 and 5.2.2.

Table 5.2. Feed characteristics and constraints applied when generating Windows of Operation for centrifugation.

Feed characteristics	**Value**	**Justification**
Initial fermenter batch volume (L)	1000	Pilot-scale/industrial-scale
Initial solids concentration (% v/v and % ww/v for *P. pastoris* and *E. coli* homog., respectively)	30	Typical level measured in high cell density pilot-scale fermentations
For *E. coli*: solids concentration post-homogenisation (% ww/v)	15	Solids concentration is reduced as a result of the release of cell internal water during homogenisation
Constraints		
Maximum processing time, $t_{proc.}$ (h)	8	Standard working shift (clean up in second shift)
Minimum time between discharges in disc-stack machines, $t_{comp.}$ (s)	120	Manufacturer's recommendation
Minimum yield (%)	94	Yield desired for a primary recovery step
Minimum clarification (%) *P. pastoris* *E. coli* homogenate	 99 50	Chosen based on the clarification performance data presented for the respective feed stocks in Chapter 4
Maximum flow rate	See Table 5.2	Fixed by hydrodynamic properties of machine

5.2.1 Case study I: Centrifugation of a high cell density *P. pastoris* culture

Figures 5.1a)-d) demonstrate the construction of the Window of Operation for a SC35 disc-stack centrifuge upon separation of *P. pastoris* of varying solids concentrations. In Figure 5.1a), only the 8 h processing time constraint is incorporated into the Window, leaving the process engineer with a large area of available operating conditions – represented by the shaded region to the right of and above the blue line i). The area to the left of and below line i) corresponds to a processing time of more than 8 h. In Figure 5.1b), the 120 s discharge constraint is included and is represented by the purple line ii). To the right of and above the constraint line ii), solids discharge would have to be carried out at intervals shorter

than 120 s, and operation in this area is therefore not possible. The region where lines i) and ii) overlap would represent the available operating conditions for the SC35, if only the two pre-set requirements related to time were to be met. In 5.1c), the operational area is further constricted by the integration of the yield performance parameter into the Window of Operation, represented by the green line iii). Operation below line iii) is predicted to give a yield of 94% or above. In the case of *P. pastoris*, the level of clarification were high (>99%) for all circumstances investigated and this parameter therefore will not put any restriction on the Windows of Operation in this case study. Finally, in Figure 5.1d), the maximum flow rate for the SC35 is included in the Window of Operation, represented by the vertical red line iv). To the right of this line, the flow rate exceeds the maximum hydrodynamic capacity of this machine.

In order to process the given material within the desired time limit whilst maintaining the required level of separation performance and yield, the engineer should operate the SC35 disc-stack machine anywhere within the shaded region in Figure 5.1d). The shaded area indicates where the constraints (given by lines i)-iv)) overlap to form the Window of Operation for this machine.

The Window of Operation for the SC35 disc-stack in Figure 5.1d) shows that when processing a feed of low solids concentration, a higher flow rate is required compared to when processing a feed-stream of moderate solids concentration. This is a consequence of diluting the original feed, which increases the volume to be processed to the point where, at the lower flow rates, the final volume cannot be processed within the time constraint imposed by the 8 h shift. The SC35 Window also indicates that the highest possible solids concentration one can process in this machine, and still achieve a minimum yield of 94% is ~10% (v/v).

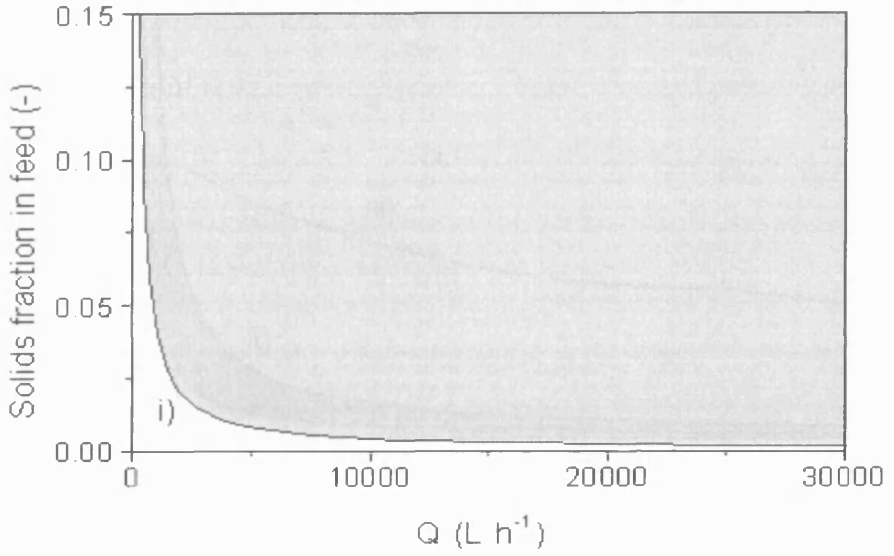

Figure 5.1a). Construction of the Window of Operation for separation of *P. pastoris* in the SC35 disc-stack – step 1. Only the 8 h processing constraint is defining the Window at this stage. The constraint is represented by the blue line labelled i). The available operating conditions are represented by the shaded region to the right of and above line i). To the left of and below the line, operation is predicted to exceed 8 h.

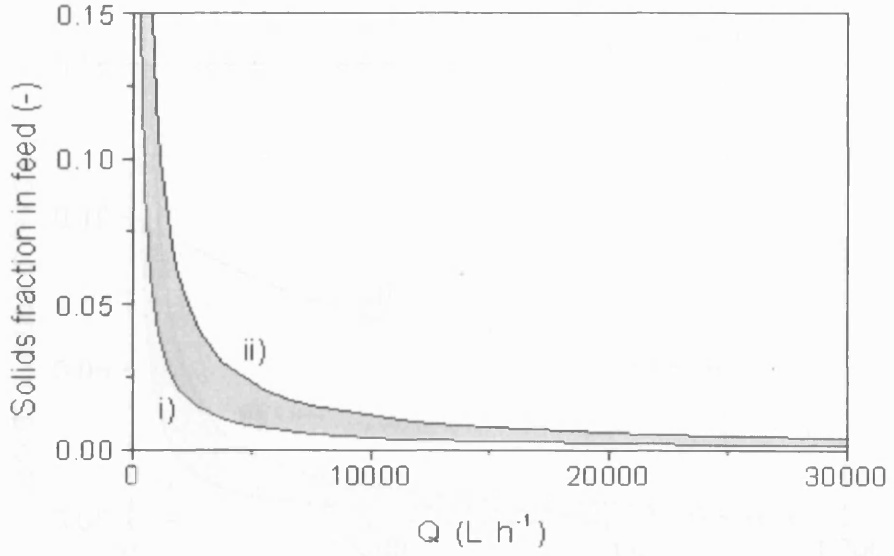

Figure 5.1b). Construction of the Window of Operation for separation of *P. pastoris* in the SC35– step 2. An additional time-constraint, the minimum time between discharges, is included in the Window – represented by the purple line labelled ii). To the right of and above line ii) discharge would have to be carried out too frequently (< 120 s between each discharge) and operation in this area is therefore not feasible. The shaded region represents the overlap between lines i) and ii), and operation in this area will ensure that the given duty is processed within 8 h and with a time interval between discharges that is greater than 120 s.

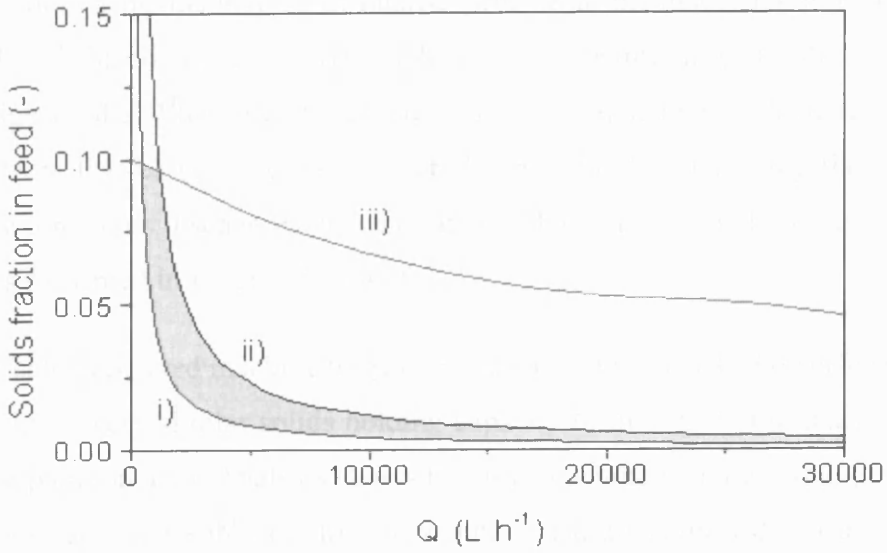

Figure 5.1c). Construction of the Window of Operation for separation of *P. pastoris* in the SC35– step 3. The performance parameter of product yield is included in the Window of Operation. The yield is represented by the green line labelled iii), and below this line the yield is predicted to be 94% or above. The other performance parameter considered, level of clarification, was high (>99%) under all circumstances investigated and will not put any constraint on the Window of Operation in the case of centrifugation of *P. pastoris.*

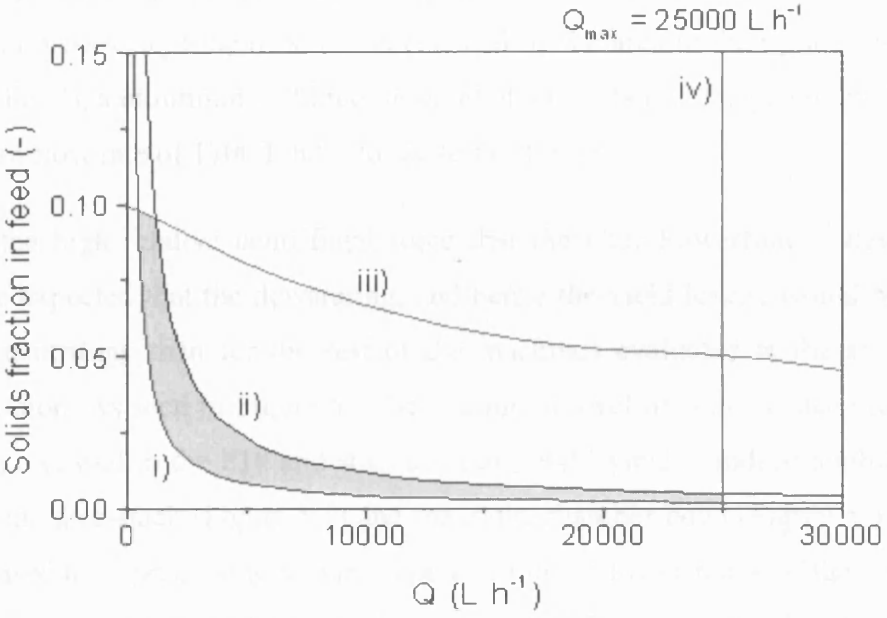

Figure 5.1d). Completed Window of Operation for separation of *P. pastoris* in the SC35 disc-stack machine. The available operating conditions are represented by the shaded area. The operating region is constructed by considering the maximum processing time of 8 h – given by the region to the right of and above blue line i), a minimum time between solid discharges of 120 s – left of and below the purple line ii), the minimum acceptable level of yield of 94% - below the green line iii) and finally, by the last constraint added to the Window, the maximum hydrodynamic flow rate for the machine (25, 000 L h^{-1}) – left of the red line iv).

The remaining centrifuges to be evaluated differ from the disc-stack in that they are operated with batch solids recovery rather than with intermittent solids discharge. The design of the Windows of Operation for these machines will therefore differ slightly from that of the disc-stack, since the constraint representing the minimum time between solids discharges does not apply. Hence line ii) will not appear in the Windows presented in Figures 5.2 and 5.3.

The first batch operated machine to be considered is the Carr P12 Powerfuge™. This machine has a very similar solids holding capacity to the SC35 disc-stack, but only half the separation area. Analysis shows that this machine is not capable of handling the given process task subject to the processing constraints outlined in Table 5.2. The reason why an operating region is not achieved is a relatively low upper flow rate of 500 L h^{-1}, which fails to overlap with the operating area defined by the 8 h processing time constraint (no overlap between lines i) and iv)). An alternative to the P12 is the P18, with twice the separation area and four times the solids capacity of the P12. Figure 5.2 shows the Window of Operation for this machine. The shaded region represents the available operating area when operation is constrained by a maximum processing time of 8 h – represented by the area to the right of and above the blue line i), a minimum yield requirement of 94% - below the green line iii) and a maximum flow rate of 1700 L h^{-1} – to the left of line iv).

Due to the high relative centrifugal force that the Carr Powerfuge™ develops, it might be expected that the dewatering, and hence the yield levels, would be greater for this centrifuge than for the rest of the machines evaluated at the same solids concentration. As seen in Figure 5.2 the maximum level of solids concentration that may be processed in the P18 and still result in $\geq$ 94% yield is indeed slightly higher than for the disc-stack (Figure 5.1) and the multi-chamber bowl (Figure 5.3). Due to an increased total processing volume, operation in the lower range of the feed solids concentrations investigated (solids fraction $<$ 0.025) is not feasible for the P18 machine. Operation in this area would correspond to a processing time $>$ 8 h.

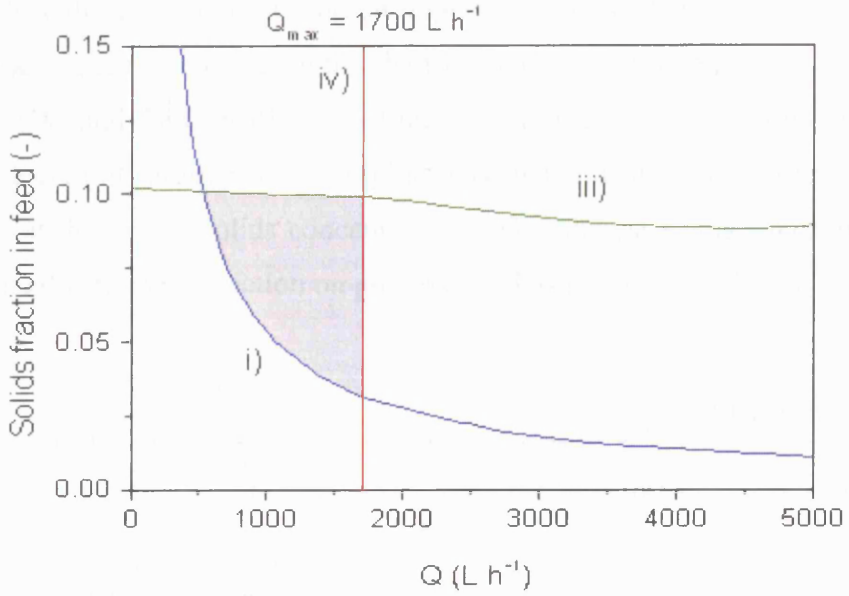

Figure 5.2. Window of Operation for separation of *P. pastoris* in the batch operated Carr P18 Powerfuge™. The shaded area represents the available operating conditions for this centrifuge. Operation is constrained by the 8 h shift constraint – to the right of and above the blue line i), as well as by a minimum yield of 94% - below the green line iii), and the maximum hydrodynamic flow rate of 1700 L h^{-1} – to the left of the red line iv).

Finally we analyse the Windows of Operation for the multi-chamber bowl centrifuges. Analysis of the capability of the KA6 multi-chamber machine to cope with the stated process task and feed characteristics subject to the processing constraints given in Table 5.2 showed that no operating Window was possible. This is due to the processing time constraint defined by Equation 5.1. The equation describes the processing time in terms of flow rate and feed characteristics. The second term in Equation 5.1, representing the downtime, becomes so large that no feasible flow rates exist which comply with the 8 h time constraint. The widely used alternative industrial configuration is to have a spare (second) bowl. Having two bowls available minimises the downtime due to solids recovery and cleaning etc between cycles. However, in the case of the KA6 a second bowl is still not enough to give a Window of Operation.

The larger multi-chamber alternative KB25 is however able to deal with the given process duty, provided that two bowls are available (Figure 5.3). The operating region that results when the process is constrained by the maximum processing time of 8 h - to the right of and above the blue line i), a minimum yield requirement of

94% - below the green line iii) and an upper flow rate of 8000 L h^{-1} - to the left of the red line iv), is represented by the shaded region in Figure 5.3. Again, as seen for both the SC35 and the Carr P18 centrifuges, due to the increase in volume caused by the high degree of dilution of the original feed material it is not feasible to operate the KB25 at the lowest solids concentrations. The highest solids concentrations are unavailable due to the restriction on process yield as stated in Table 5.3.

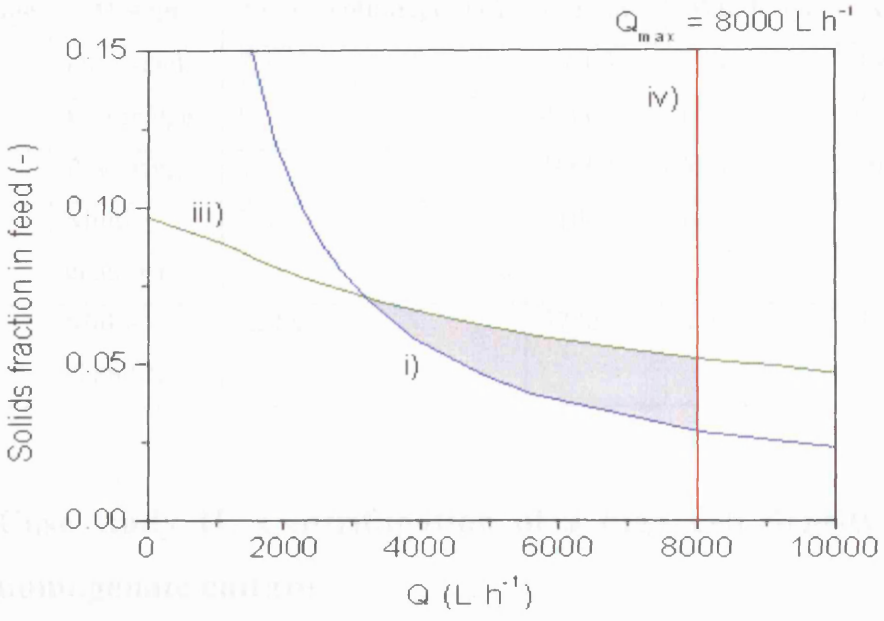

Figure 5.3. Window of Operation for separation of *P. pastoris* in the KB25 multi-chamber batch centrifuge, assuming two bowls are available. Operation is restricted by a maximum processing time of 8 h – given by the area to the right of and above the blue line i) and a minimum yield requirement of 94% - below the green line iii), in addition to an upper flow rate of 8000 L h^{-1} – to the left of the red line iv).

Table 5.3 summarises the results of the *P. pastoris* case study. The table allows for direct comparison between centrifuges on the basis of centrifuge separation area and/or solids holding capacity. As seen, the SC35 disc-stack, the P12 Powerfuge™ and the KA6 multi-chamber all have comparable solids holding capacities, whereas the SC35 disc-stack, the P18 Powerfuge™ and the KB25 multi-chamber bowl (assuming 2 bowls are available) are similar in size when it comes to corrected Sigma area (cΣ). Of the machines with similar solids capacity, only the SC35 disc-stack was able to handle the given process task subject to the constraints outlined in Table 5.2. When comparing the centrifuges with similar separation area, they were

all able to deal with the process duty of interest, with the SC35 giving the largest operational area (based on size estimates from the respective Windows of Operation) when assuming the process was limited by the constraints outlined in Table 5.2.

Table 5.3. Summary of the outcome of the *P. pastoris* case study. The table indicates which of the centrifuges are able to cope with the given process duty subject to the set constraints and limitations, and which are not. The operational areas suggested are based on size estimates calculated directly from the respective Windows of Operation.

Centrifuge	Design	Solids volume, V_S (L)	$c^*\Sigma$ (m^2)	Window ?	Area (L h^{-1})
SC35	Disc-stack	7.5	10400	Yes	300
P12	Powerfuge	8	4500	No	N/A
P18	Powerfuge	32	10000	Yes	50
KA6	Multi-chamber	7.5	2100	No	N/A
2xKB25	Multi-chamber	22.5x2	3700x2	Yes	75

5.2.2 Case study II: Centrifugation of a high cell density *E. coli* homogenate culture

This section considers the visualisation of available operating conditions for centrifugal recovery of *E. coli* homogenates of various solids concentrations when the process is restricted by limitations and constraints as given in Table 5.2. Note that the minimum acceptable level of clarification in this case is set to 50%, which is considerably lower than the clarification constraint applied for *P. pastoris* (99%). This is a necessity resulting from the significantly poorer clarification performance of the homogenate relative to *P. pastoris*, as discussed in Chapter 4. In addition, even if the original *E. coli* fermentation broth was characterised by the same batch volume (1000 L) and initial feed solids concentration (30% ww/v) as *P. pastoris*, the homogenisation process reduces the solids concentration of the broth to about half due to the release of cell internal water. Hence whereas an *E. coli* homogenate feed of 15% (ww/v) solids concentration corresponds to a volume of 1000 L, in order to obtain a *P. pastoris* feed of the same solids concentration a 1:2 dilution of the initial

feed material is required, giving a total volume of 2000 L. The remaining constraints listed in Table 5.2 are constant between the two case studies.

Figure 5.4 shows the Window of Operation for the SC35 disc-stack centrifuge upon separation of *E. coli* homogenates of varying solids concentration. The Window is defined by an 8 h shift constraint - represented by the area to the right of and above the blue line i), the minimum time interval of 120 s between solid discharges - to the left of and below the purple line ii), a minimum yield requirement of 94% - below the green line iii), a minimum clarification level of 50% - to the left of the orange line v) and finally, a maximum hydrodynamic flow rate - to the left of the red line iv). In order to process the given material within the desired time limit and at the same time maintain the required level of separation performance the engineer should operate this disc-stack machine anywhere within the shaded region in Figure 5.4. This region indicates where the constraints (given by lines i)-v)) overlap to form the Window of Operation for this machine.

Due to the smaller volume to be processed for the homogenate relative to the *P. pastoris* feed, as discussed above, the blue 8 h constraint line i) is shifted to the left and downwards – expanding the area available for operation in these directions. However, due to the reduced separation efficiency compared to *P. pastoris*, and hence the inclusion of a clarification restriction in the Window of Operation, the overall effect is a smaller operating region for processing of *E. coli* homogenate in the SC35 disc-stack than for separation of *P. pastoris* in the same centrifuge (displayed in Figure 5.1d)). In addition to a reduced level of clarification, the maximum solids concentration one can apply during operation at a low flow rate and still achieve a yield of 94% or above, is reduced from ~10% (v/v) for *P. pastoris* to ~ 5% (ww/v) for *E. coli* homogenate. This also contributes towards the reduction in available operating conditions seen in the case of the latter feed stock upon separation in the SC35 disc-stack.

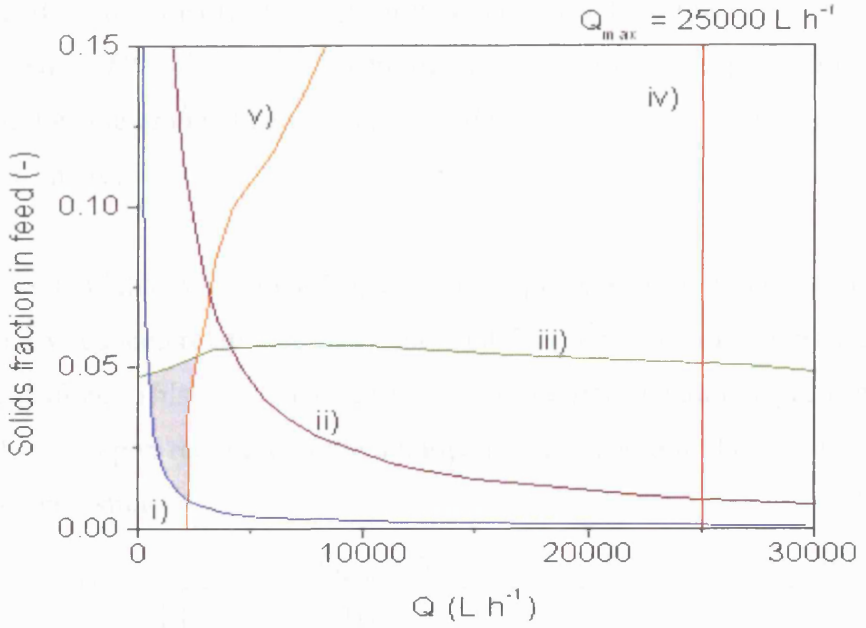

Figure 5.4. Window of Operation for centrifugation of *E. coli* homogenate in the SC35 disc-stack machine. The available operating conditions are represented by the shaded area. The operating region is constructed by considering the maximum processing time of 8 h – given by the region to the right of and above the blue line i), a minimum time between solid discharges of 120 s – to the left of and below the purple line ii), the minimum acceptable level of yield of 94% - below the green line iii), the minimum clarification requirement of 50% - to the left of the orange line v) and the maximum hydrodynamic flow rate for the machine (25,000 L h^{-1}) – left of the red line iv).

In section 5.2.1, the separation of *P. pastoris* by the Carr P12 Powerfuge™ was found to be restricted by a low upper flow rate (500 L h^{-1}) to such an extent that no available operating conditions existed when the process was subject to the constraints outlined in Table 5.2. This was a result of a lack of overlap between the line defining the upper flow rate constraint of 500 L h^{-1} and the operating area defined by the 8 h processing time constraint (no overlap between lines i) and iv)). For the case of the homogenate investigated in this section, the lines i) and iv) do overlap. However, the area generated from this overlap does not enclose either of the lines iii) or v), hence due to the constraints related to yield and clarification, the P12 will not be able to meet all pre-set requirements in the case of *E. coli* homogenate either.

The other Carr Powerfuge™ considered is the P18. Figure 5.5 shows the Window of Operation for this machine. The shaded region represents the available operating area when operation is constrained by a maximum processing time of 8 h –

represented by the area to the right of and above the blue line i), a minimum yield requirement of 94% - below the green line iii), a minimum clarification level of 50% - to the left of the orange line v), and a maximum flow rate of 1700 L h^{-1} – to the left of the red line iv).

Again, the available Window of Operation for processing of *E. coli* homogenate is significantly reduced relative to that generated for processing of *P. pastoris* using the same centrifuge. This is a direct result of the poorer separation performance and yield achieved upon recovery of the homogenate compared to the results achieved in the *P. pastoris* study.

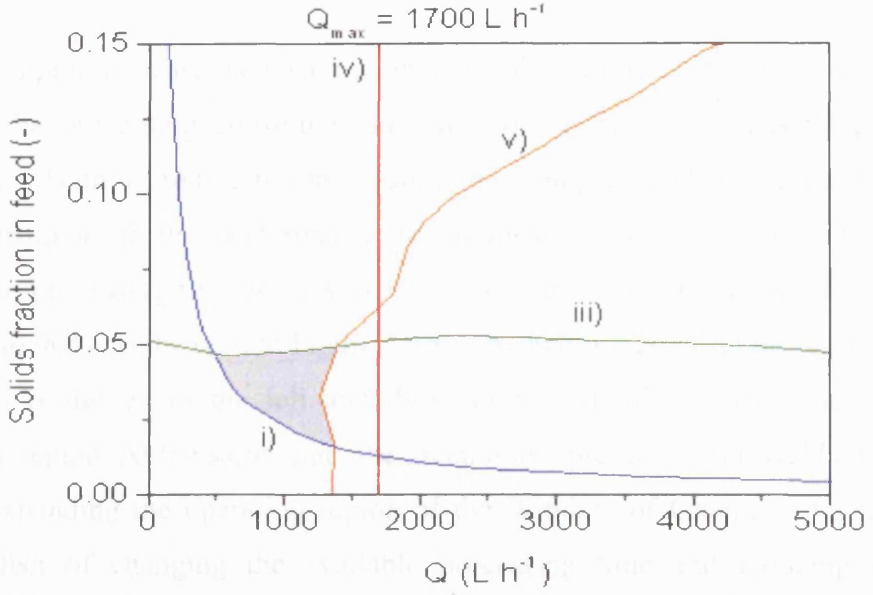

Figure 5.5. Window of Operation for separation of *E. coli* homogenate in the batch operated Carr P18 Powerfuge™. The shaded area represents the available operating conditions for this centrifuge. Operation is constrained by the 8 h shift constraint – to the right of and above the blue line i), a minimum yield of 94% - below the green line iii), a minimum clarification requirement of 50% - to the left of the orange line v) and the maximum hydrodynamic flow rate of 1700 L h^{-1} – to the left of the red line iv).

Moving on to the Windows of Operation for the multi-chamber bowl centrifuges, analysis once again showed that the KA6 was not capable of processing the given duty subject to the constraints and limitations stated in Table 5.2. As discussed for *P. pastors* in section 5.2.1, the lack of an operating region for this machine is a result of the total downtime between the batches, which becomes so large that no feasible flow rates exists which comply with the 8 h time constraint (see Equation 5.1). As for *P. pastoris*, exploiting the option of a second bowl still does not give a Window

of Operation for the separation of *E. coli* homogenates of various solids concentration in the KA6.

The larger multi-chamber alternative KB25 was however seen to be able to deal with the given process duty, provided that two bowls are available. The operating region that results when the process is constrained by the maximum processing time of 8 h – represented by the area to the right of and above the blue line i), a minimum yield requirement of 94% - below the green line iii), a minimum level of clarification of 50% - to the left of the orange line v), and an upper flowrate of 8000 L h^{-1} - to the left of the red line iv), is represented by the shaded region in Figure 5.6a).

In an attempt to increase the resulting operational area further, the designer may seek to alter the processing constraints in order to identify more feasible processing conditions. Within limits this can be done for example by changing the processing time constraint or the performance requirements. The effect of increasing the maximum processing time from 8 to 12 h whilst lowering the minimum yield limit from 94 to 90% can be seen in Figure 5.6b). The line representing the shift constraint (line i)) is moved to the left and downwards and this results in an expanded operating region. At the same time, the green line representing the yield constraint is raised, expanding the operating region of the Window of Operation upwards. The same effect of changing the available processing time and reducing the yield requirement would be seen for the other centrifuges evaluated and illustrates the flexibility of using a Window of Operation approach to visualise rapidly the alternative processing conditions.

Table 5.4 summarises the results of the *E. coli* homogenate case study. A comparison with Table 5.3, which provides the outcome of the *P. pastoris* case study, shows that the suitable options identified correspond to the same centrifuges in both studies. However, due to the reduced level of separation performance and yield achieved in the case of the homogenate, the available Window of Operation generated for each machine is considerably smaller than was the case for *P. pastoris*. As discussed, this is mainly due to the low level of clarification achieved in the case of *E. coli* homogenate, which is acknowledged as a difficult separation problem.

a)

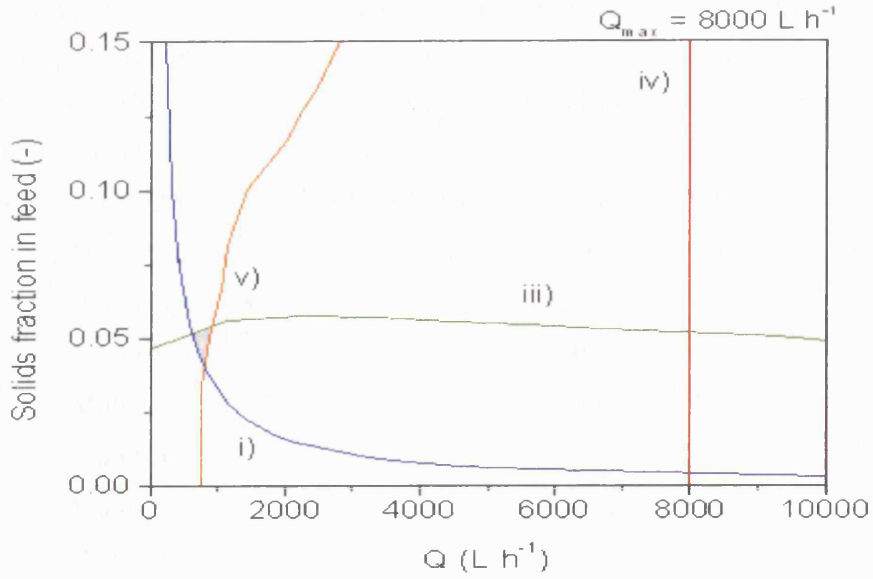

b)

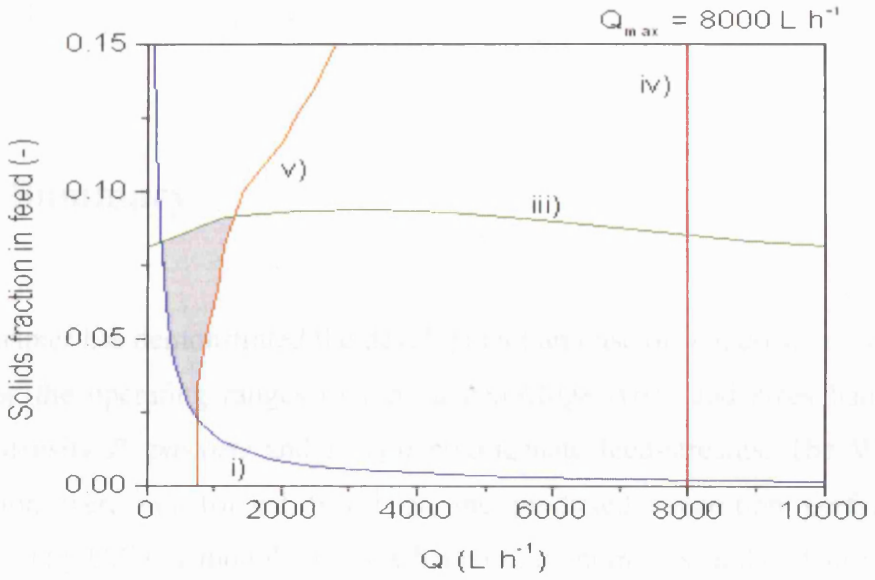

Figure 5.6 Window of Operation for separation of *E. coli* homogenate in the KB25 multi-chamber batch centrifuge, assuming two bowls are available. a) Operation is restricted by a maximum processing time of 8 h – given by the area to the right of and above the blue line i) and a minimum yield requirement of 94% - below the green line iii), in addition to an upper flow-rate of 8000 L h^{-1} – to the left of the red line iv). b) Window of Operation for the KB25 showing the impact of increasing the processing time from 8 to 12 h and reducing the yield requirement from 94 to 90%, on the available operating area for this centrifuge.

Table 5.4. Summary of the outcome of the *E. coli* homogenate case study. The table indicates which of the centrifuges are able to cope with the given process duty subject to the set constraints and limitations, and which are not. The operational areas suggested are based on size estimates calculated directly from the respective Windows of Operation.

Centrifuge	Design	Solids volume, V_S (L)	$c^*\Sigma$ (m^2)	Window?	Area (L h^{-1})
SC35	Disc-stack	7.5	10400	Yes	50
P12	Powerfuge	8	4500	No	N/A
P18	Powerfuge	32	10000	Yes	15
KA6	Multi-chamber	7.5	2100	No	N/A
2xKB25	Multi-chamber	22.5x2	3700x2	Yes	<1
2xKB25 (12 h shift, 90% yield)	Multi-chamber	22.5x2	3700x2	Yes	25

5.3 Summary

This chapter has demonstrated the development and use of Windows of Operation to describe the operating ranges of typical centrifuge types and sizes handling high solids density *P. pastoris* and *E. coli* homogenate feed-streams. The Windows of Operation were constructed based on the predicted separation performance as generated by USD methodologies in Chapter 4, combined with the identification and application of key constraints, which restrict the operation of each centrifuge type, such as maximum processing time and maximum flow rate. For semi-continuous disc-stack centrifuges operated with intermittent discharge, an additional time constraint applies; the minimum interval between discharges. The Windows of Operation presented provide for the identification of satisfactory operating conditions for the range of centrifuges evaluated; disc-stack, multi-chamber and Carr Powerfuges^{TM}. The method can also be used for identification of separation equipment which is not capable of dealing with the given process duty subject to the particular processing constraints applied. By further examination using the

methodology it is possible to demonstrate whether alternative operating strategies are capable of producing a more feasible solution, for example by altering the operational constraints, such as shift time, or the performance parameters, i.e clarification and yield, or by the supply of additional equipment such as spare centrifuge bowl.

The Windows of Operation presented demonstrate a difference in available operating conditions between *P. pastoris* and *E. coli* homogenate of varying solids concentration. The significantly lower clarification levels obtained for the latter feed stock results in a great reduction in available operating conditions when compared to the area of feasible processing conditions achieved for *P. pastoris* upon separation in the same centrifuge.

Having examined the utility of traditional methods for the processing of high solids density feeds the next two chapters will focus on the recovery of Fab from high cell density *E. coli* homogenate by expanded bed adsorption as a more recent alternative to centrifugal methods. Chapter 6 describes the scaling of an EBA process and how column performance and scalability is affected by increasing solids concentration. In Chapter 7 EBA performance is predicted by simulation and Windows of Operation are generated for an industrial-scale EBA process. In Chapter 8 the unit operations of EBA and centrifugation are compared on the basis of operating conditions identified using Windows of Operation.

6 A scale-down approach for the recovery of Fab from *E. coli* homogenate by expanded bed adsorption

Abstract

Having established the ability to mimic the centrifugal separation performance for a range of high cell density materials, this chapter investigates the scalability of an expanded bed adsorption process when dealing with *E. coli* homogenates of varying solids concentration.

Several successful attempts to scale down expanded bed adsorption processes have been reported in the literature (Barnfield-Frej *et al.*, 1997; Ghose and Chase, 2000a,b; Willoughby *et al.*, 2004). However, many of these studies are based on the use of model systems containing only a few proteins and no cell contaminants. Potential challenges related to the processing of samples of high biomass concentration by EBA are summarised by Feuser *et al.* (1999a) and include a reduction in bed stability and adsorption performance due to the formation of channels and stagnant zones during loading, a reduction in static capacity as small cells or cell debris penetrate into porous adsorbents, and modified fluidisation behaviour as a result of increased particle radius and lowered density of cell-associated matrix particles.

In this chapter, the results obtained upon processing of *E. coli* homogenates of varying solids concentration in a 1.9 mm ID scale-down (SD) column are compared to data achieved in a column of 25 mm inner diameter, which currently represents the smallest column accepted for EBA scale-down studies. The process performance is investigated and measured in terms of bed expansion, mixing effects in the bed (the latter by means of residence time distribution (RTD) traces and axial dispersion coefficients), breakthrough behaviour, binding capacity and yield levels achieved. In addition to direct comparison between the columns, evaluation of bed expansion data

is performed by comparison with theoretical data achieved from established correlations.

The main challenge related to the processing of *E. coli* homogenates of varying solids content was identified and found to be interactions between nucleic acids and/or cell debris from the homogenate, and the adsorbent, which consequently lead to disrupted expansion behaviour in the scale-down bed. It is believed that due to a high particle to column diameter ratio, the effect of these interactions was more prominent in the SD bed than in the 25 mm column, consequently resulting in a variation in binding capacity and yield data obtained between the scale-down bed and the 25 mm column. Increasing the feed solids concentration reduced the total binding capacity in both columns, whereas the effect of solids concentration on yield was mainly evident in the scale-down column.

6.1 Introduction

An introduction to EBA and the scaling of such processes was given in Chapter 1. In this chapter the performance of the two EBA systems investigated are assessed by direct comparison with one another, and by comparison with predictions based on established theoretical correlations. The correlations include equations describing expected expansion behaviour (section 6.1.1), as well as correlations used to determine the bed structure in the form of the number of theoretical plates (section 6.1.2) and degree of mixing (section 6.1.3). Section 6.1.4 discusses and exemplifies the potential challenges of processing solids-containing feed-streams by EBA. Finally, section 6.1.5 provides the equations used to determine column performance in terms of binding capacity and product yield.

6.1.1 Expansion characteristics

In order to fluidise a bed, the liquid velocity has to be greater than the minimum fluidisation velocity, U_{mf} (De Felice, 1995). U_{mf} is controlled by the size and density of the adsorbent particles, the linear flow velocity and the viscosity of the fluid. As

the fluid velocity is increased from U_{mf} to the particle free-fall velocity, U_t, the fluidised bed is characterised by stable and smooth expansion. At this stage there is theoretically no movement of particles, a situation achieved due to the particle free-fall velocity and the upward superficial flow velocity being equal and opposite.

The particle free-fall velocity U_t can be expressed by Stokes' Law:

$$U_t = \frac{d_p^2(\rho_p - \rho)g}{18\mu} \qquad 6.1$$

where d_p is particle diameter, ρ_p and ρ are the particle and liquid density, respectively, μ is the liquid viscosity and g is the acceleration due to gravity.

The Richardson-Zaki equation[1] (Richardson and Zaki, 1954) describes the relationship between the particle free-fall velocity, U_t, the superficial liquid velocity in a fluidised bed, U, and the bed voidage, ε:

$$\frac{U}{U_t} = \varepsilon^n \qquad 6.2$$

where the Richardson-Zaki parameter n is a function of the particle to column diameter (d_p/D_c) and of the dimensionless Reynolds number under terminal free-fall conditions, Re_t. The following equations allow for the determination of the parameter n for given values of Re_t:

$$n = 4.65 + 20\frac{d_p}{D_c} \qquad (Re_t < 0.2) \qquad 6.3$$

$$n = \left(4.4 + 18\frac{d_p}{D_c}\right)Re_t^{-0.03} \qquad (0.2 < Re_t < 1) \qquad 6.4$$

[1] The R-Z equation was previously applied in relation to sedimentation theory in Chapter 4. In the current chapter the R-Z equation is given on the form normally used when considering EBA processes.

The Reynolds number under terminal free-fall conditions is given in Equation 6.5:

$$\mathrm{Re}_t = \frac{U_t d_p \rho}{\mu} \qquad 6.5$$

Based on the Richardson-Zaki relationship given in Equation 6.2, it is possible to predict the bed expansion. The Richardson-Zaki parameter n can be determined from either Equation 6.3 or 6.4, whereas the particle free-fall velocity can be calculated from Stokes' Law. Alternatively, if experimental data is available, both U_t and n can be derived from a plot of ln (U) against ln (ε), where the intercept of the plot on the y-axis represents ln (U_t) and the gradient of the line is n.

The voidage of an expanded bed can be estimated by a mass balance:

$$H = \frac{H_0(1 - \varepsilon_0)}{(1 - \varepsilon)} \qquad 6.6$$

where H and H_0 is the expanded and the settled bed height, respectively, and a value of 0.4 for ε_0, the voidage of a settled bed, is commonly used.

By combining Equations 6.2 and 6.6, the expanded bed height can be predicted from Equation 6.7:

$$H = \frac{H_0(1 - \varepsilon_0)}{(1 - (\frac{U}{U_t})^{\frac{1}{n}})} \qquad 6.7$$

6.1.2 Residence time distributions

Residence time distributions (RTD) are used for assessing the degree of longitudinal (axial) mixing in the expanded bed, and the method involves determining from an RTD response an equivalent number of theoretical plates in the bed. A common way

in which an RTD curve is generated is by introducing a step, or a pulse, of a non-retained tracer at the column inlet, and monitoring the outlet signal (positive input signal). In this work a step method was employed. Once the outlet signal is stable, the solution is changed back to the original composition and the UV-trace allowed to reach a stable baseline level (negative input signal). The tracer applied should have similar physical properties to the fluid stream of interest, but has to be different in some non-flow property that can be easily detected. Acetone and dextrane blue are often used tracers; for the work presented in this thesis the conductivity traces resulting from a high-molarity buffer were applied. Figure 6.1 presents a typical residence time distribution curve.

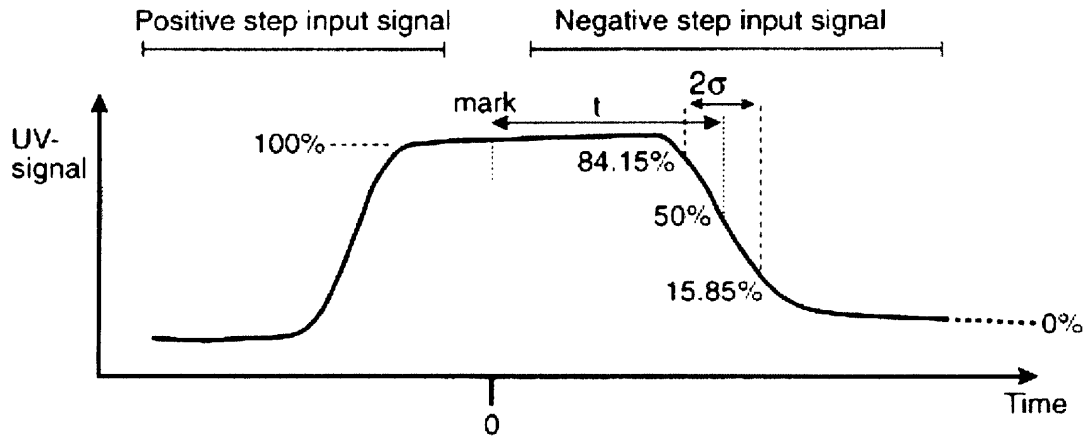

Figure 6.1. Schematic of a RTD curve for determination of the number of theoretical plates. t_r is defined as the distance from the "mark" (end of sample load) to 50% of the maximum UV-signal, whereas 2σ is the distance between 15.85% and 84.15% of maximum absorbance. (Figure adapted from Barnfield-Frej *et al.*, 1997)

The number of theoretical plates, N_T, is calculated from the mean residence time of the tracer in the column (t_r) and the variance of the tracer output signal (σ) using Equation 6.8.

$$N_T = \frac{t_r^2}{\sigma^2} \qquad 6.8$$

where t_r is defined as the distance from the start (positive input signal), or end (negative input signal), of the step, to 50% of maximum absorbance. σ represents the

standard deviation of the response, and is half the distance between 15.85% and 84.15% of maximum absorbance. The number of theoretical plates can be calculated from either the positive or the negative input UV-signal, however the negative step is recommended, as it is associated with greater reproducibility (Barnfield-Frej *et al.*, 1997).

The method described above gives the number of theoretical plates for the whole system, including column, pumps, valves and tubing. Large dead volumes in a system may result in low number of theoretical plates (EBA handbook, GE Healthcare) and as such the plate number data must be treated with some degree of caution.

6.1.3 Axial dispersion

Axial dispersion is another measure of the degree of mixing occurring within the column, and gives an indication of the flow characteristics of the bed. The degree of mixing within the expanded bed can be evaluated using residence time distribution experiments to calculate the axial dispersion coefficient, D_{ax}. An axial dispersion coefficient approaching infinity suggests turbulent flow, whereas a D_{ax} approaching zero indicates plug flow, which is desirable for achieving high column efficiency and sharp breakthrough curves.

Several models have been developed that describe dispersion and non-ideal flow in a system. An often-used model is the dispersion model (Levenspiel, 1999). Dispersion models describing mixing in expanded beds often regard the column as a closed boundary system (Fenneteau *et al.*, 2003; Thömmes *et al.*, 1996; Willoughby *et al.*, 2004). This implies that the bed is considered a series of sections where no transfer between the sections occur, and no back mixing of fluid into a section once it has left that section takes place. The flow pattern outside the tanks boundaries is characterised by plug flow (Levenspiel, 1999).

According to the dispersion model, mixing can be described by the means of the dimensionless dispersion number N_D:

$$\sigma_\theta^2 = 2[N_D] - 2[N_D]^2(1 - e^{-\frac{1}{N_D}}) \qquad 6.9$$

where σ_θ^2 is the dimensionless variance determined from the RTD curve ($\sigma_\theta^2 = \frac{\sigma^2}{t_r^2}$). The equation was solved for N_D by using Microsoft Excel solver, and D_{ax} calculated by means of Equation 6.10.

$$N_D = \frac{1}{Pe} = \frac{D_{ax}}{UH} \qquad 6.10$$

where *Pe* is the dimensionless Peclet number (=UH/D_{ax}), *U* is the liquid velocity and *H* is the expanded bed height.

6.1.4 The effect of biomass concentration on EBA

Despite the numerous applications of EBA, and the fact that the main feature of this process is to handle unclarified feedstocks, there is relatively limited information available from the literature when it comes to the impact of solids load on expanded bed adsorption.

Feuser *et al.* (1999a) summarised potential problems due to high biomass concentration that may occur during an expanded bed adsorption process. They include reduced bed stability and sorption performance due to the formation of channels and stagnant zones during loading, reduced static capacity as small cells or cell debris may penetrate into porous adsorbents, modified fluidization behaviour due to increased particle radius and lowered density of cell-associated adsorbent, biomass-contaminated eluate and reduced life time of the adsorbent due to irreversible fouling effects and harsh regeneration conditions.

The effect of *E. coli* homogenate solids concentration on an expanded bed adsorption process capturing annexin V to an anion exchange matrix was investigated by Barnfield-Frej *et al.* (1994). It was found that the feed solids concentration influenced the process, both in terms of expansion and bed stability. A solids concentration of about 7-8% dry weight lead to excessive expansion, and the adsorbent was elutriated out of the column – a typical result of increased viscosity. In addition, flow channels were observed in the bed. It was thought that these effects were due to cell-adsorbent interactions.

Feuser *et al.* (1999a) studied interactions between different cell types and a range of adsorbents, and identified that yeast and yeast homogenate interacted strongly with the anion exchanger Streamline DEAE, under the operating conditions tested (pH 7). Hybridoma cells caused the bed to collapse upon injection onto Streamline Phenyl and Streamline DEAE at a pH of 7, but did not interfere with either Streamline rProteinA or Streamline SP at the same pH. A reduction of pH upon loading onto the Streamline SP adsorbent did however result in an increase in cell adsorption. This can be explained by an increasing number of positive charges on the cell surface as the pH is reduced, which leaves the cells more likely to bind to the negatively charged ligands on the cation exchanger. *E. coli* whole cell broth did not interact significantly with any of the adsorbents tested. It is emphasised that most products expressed in *E. coli* are either periplasmic or located in the cytosol, hence cell disruption is required in order to release these products. Together with the target protein one would then also release nucleic acids, which could potentially be an issue in terms of bed stability and process efficiency.

Thömmes *et al.* (2001) investigated the interactions between *P. pastoris* cells and Streamline SP XL. It was found that pH was a critical parameter for cell-adsorbent interaction. At pH 4.5 the interactions between cells and adsorbent were minimal, whereas below pH 4.5 the cells interact strongly with the cation exchanger. Once again this indicates that the cell surface is positively charged as pH is lowered, favouring binding to the negatively charged exchanger. Moreover, by increasing the conductivity from 5 mS cm^{-1} to 9.5 mS cm^{-1} (at pH 4.5) Thömmes *et al.* (2001) demonstrated improved cell transmission upon separation of product expressed in *P. pastoris* on Streamline SP.

Upon Fab recovery from *E. coli* homogenate using the affinity adsorbent rProteinA in a SD column identical to the one used in this work, Willoughby *et al.* (2004) did not experience any cell-adsorbent interactions. Thömmes *et al.* (1996) reported no sign of cell-adsorbent interactions during expanded bed adsorption of IgG2a from a hybridoma cell culture on a rProteinA modified matrix at a neutral pH. The same was observed by Feuser *et al.* (1999b) upon recovery of IgG1 on Streamline rProteinA adsorbent. However the same cells did interact with the cation exchanger Streamline SP at pH 5.5, as demonstrated by reduced transmission of hybridoma cells.

From what has been described above, a major mechanism responsible for binding of cells to ion exchangers appears to be electrostatic interactions of oppositely charged particles. In addition to pH variations, adjusting the sample conductivity is one way of reducing these unwanted interactions.

6.1.5 Separation behaviour

The separation performance of the expanded bed in terms of capacity and yield was calculated using the following equations:

$$Binding\ capacity\ (mg\ mL^{-1}) = \frac{Fab\ bound}{Volume\ of\ matrix} \qquad 6.15$$

$$Fab\ bound = Fab\ loaded - Fab\ lost\ in\ breakthrough \qquad 6.16$$

$$\%\ Fab\ yield = 100 \times \frac{Fab\ eluted}{Fab\ loaded} \qquad 6.17$$

6.2 Results and discussion

The results of the EBA studies performed in the scale-down and Streamline 25 columns are presented and discussed in the following sections. Section 6.2.1 presents the results of the method scouting study performed in order to determine the appropriate buffer pH and molarity for the adsorption of Fab onto Streamline SP. Section 6.2.2 compares bed expansion behaviour for the SD and 25 mm beds and relates the experimental results to the results predicted from theoretical correlations. Section 6.2.3 contains bed mixing data in the form of number of theoretical plates and axial dispersion coefficients for the two systems under investigation. Section 6.2.4 provides experimental Fab breakthrough curves as obtained in the scale-down and Streamline 25 beds. Finally, in section 6.2.5 the performance of the two columns is compared on the basis of dynamic and total binding capacities, and overall yield achieved.

6.2.1 Method optimisation

A study of the optimum buffer conditions in terms of pH and molarity was performed as described in section 2.6.3. The aim was to determine which buffer conditions would favour binding of Fab to the Streamline SP adsorbent the most. The binding of contaminants was not evaluated in this case.

6.2.1.1 Buffer pH

The binding of Fab to Streamline SP equilibrated at constant buffer molarity but at different pH values, was investigated using samples of clarified *E. coli* homogenate with conductivities varying from 2.5 mS cm^{-1} to 21 mS cm^{-1}. As seen in Figure 6.2, the amount of Fab bound to the adsorbent is significantly affected by sample conductivity. Binding appears to be most favourable at 2.5 mS cm^{-1} and pH 4.

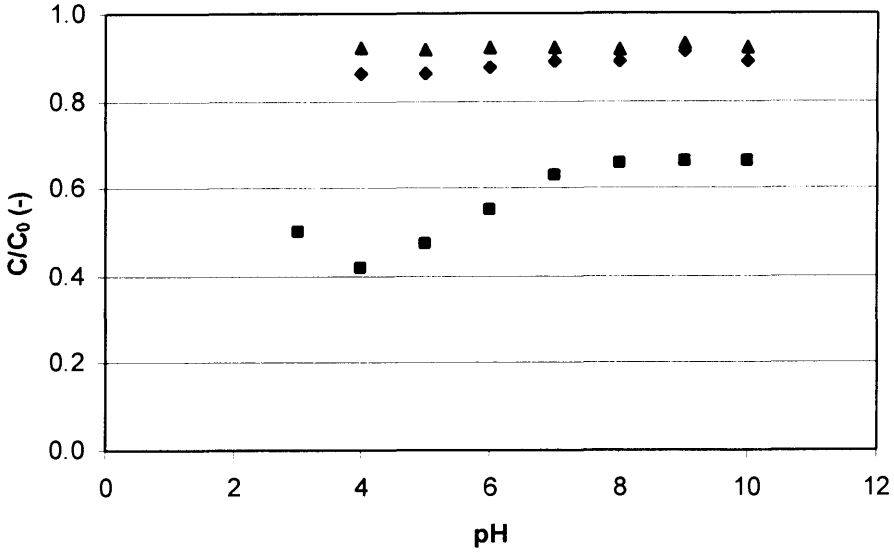

Figure 6.2. Batch binding of Fab to adsorbent (Streamline SP) equilibrated with MES buffer of different pH values. Sample conductivities tested were 21 mS cm^{-1} (▲) 10 mS cm^{-1} (♦) and 2.5 mS cm^{-1} (■).

6.2.1.2 Buffer molarity

Figure 6.3 shows binding of Fab from clarified *E. coli* homogenate at 2.5 mS cm^{-1} to adsorbent equilibrated at constant buffer pH (4) but with different molarities. The most favourable binding seems to occur at low buffer molarity. From 10-20 mM there is a steady decrease in Fab bound to adsorbent as molarity increases. The level of binding reaches a steady value at about 150 mM.

Based on the results presented in Figures 6.2 and 6.3, the initial buffer conditions were selected as pH 4 and 20 mM. The extensive dilution required in order to bring sample conductivity down to as low as 2.5 mS cm^{-1} necessitates a sample concentration step in order to obtain an acceptable Fab titre. This would in a sense defeat the purpose of EBA (processing crude material directly on column). By diluting the samples to only 4.5 mS cm^{-1}, the need for a concentration step was avoided; hence this sample conductivity was used throughout the expanded bed work presented here.

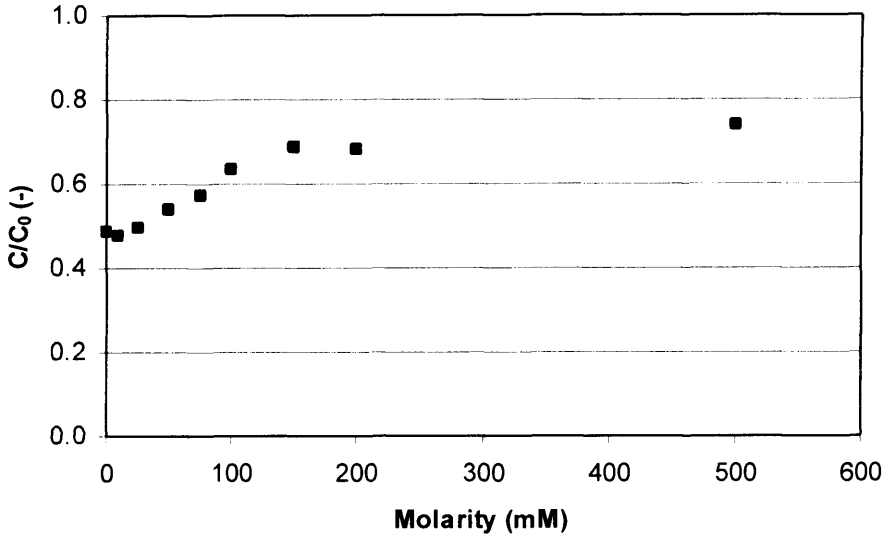

Figure 6.3. Batch binding of Fab to adsorbent (Streamline SP) equilibrated with MES buffer at pH 4, and different molarities. Sample conductivity was 2.5 mS cm^{-1}.

6.2.1.3 Re-evaluation of initial buffer conditions

Initial experiments applying the optimised buffer conditions as determined from Figures 6.2 and 6.3 (pH 4, 20 mM), resulted in very poor bed performance upon loading of a solids-containing feed-stream onto the SD bed. This could have been due to cell-cell interactions resulting in blockage of the lower adaptor net, or a result of interactions between cell debris and/or nucleic acids (from the homogenate) and adsorbent in the column. It was thought that these effects might have been induced by the relatively low pH, as some *E. coli* strains tend to aggregate around pH 4 and below (Barnfield-Frej *et al.*, 1994). Moreover, for cation exchangers like Streamline SP, cell-adsorbent interactions are more likely to occur at low pH. This is because the cell surface is more positively charged at reduced pH, and hence the cells are more susceptible of binding to the negatively charged adsorbent (Feuser *et al.*, 1999a). Figure 6.4 is a schematic of the non-ideal bed expansion seen upon loading a solids containing feed-stream (~3% ww/v) onto the SD column using the initial buffer conditions (pH 4, 20 mM).

A general recommendation is that pH should be kept at least one unit below the isoelectric point of the target protein when using cation exchangers. If the pH gets too close to the protein pI, this might lead to dissociation of product from adsorbent. The pI for the Fab used in this study is 8.6. In an attempt to avoid any cell-cell and/or cell-adsorbent interactions, the buffer pH was increased to 5.5, a pH that should still favour binding to the Streamline SP exchanger. This pH value was used in the experimental studies presented in the following sections.

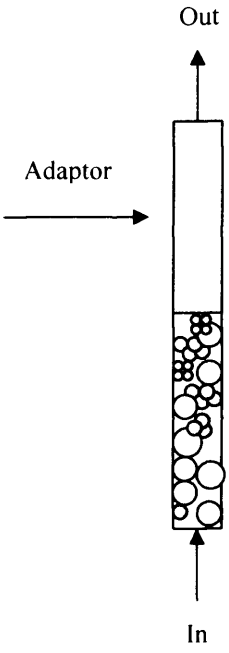

Figure 6.4. Illustration of non-ideal bed expansion, as experienced upon loading a solids-containing *E. coli* homogenate onto the SD column at pH 4. The white circles represent the matrix particles, whereas the shaded particles represent cell debris. Cell debris particles were found to interact with one another, and to a certain extent also with the adsorbent particles.

6.2.2 Bed expansion

The characteristics of the columns and the adsorbent applied for the EBA experiments were given in section 2.6.1. All samples were prepared according to section 2.6.2. Expanded bed adsorption in the scale-down and Streamline 25 columns was performed as outlined in section 2.6.4. The initial settled bed height was 8.5 cm for both columns. For the SD system, the flow rate during equilibration, load and wash was varied (see Table 6.1), whereas all experiments performed in the Streamline 25 column were run at 200 cm h^{-1}. Elution was performed in expanded

mode with an upward flow of 200 cm h^{-1} in both columns. Elution in EBA processes is often done in packed bed mode using a downward flow in order to keep the volume of the eluted fraction as low as possible. In the case of the specially developed SD column applied in this work, the upper adaptor could not be lowered to more than 32 cm from the bottom of the column, far above the level of the settled bed. No reduction in elution volume relative to operation in expanded bed mode would therefore be achieved, and it was decided that elution was to take place in expanded bed mode. The Streamline 25 column adaptor height was also kept at 32 cm throughout the experiment, in order to ensure a comparable process.

The scale-down study was performed using three different feed solids concentrations, each at three different flow rates. For the Streamline 25 column, feed-streams in the range of ~0-14% (ww/v) were processed, all at 200 cm h^{-1}. Table 6.1 summarises all the experiments conducted in the scale-down column, and those performed in the 25 mm column that are of relevance to this comparison study.

Table 6.1. Overview of experiments performed in the SD and the 25 mm columns. For the SD system, three different levels of solids concentration were used, each applied at flow rates of 100, 200 and 300 cm h^{-1}. For the 25 mm ID column, three levels of solids concentration were used, each processed at 200 cm h^{-1}.

Flow rate (cm h^{-1}) / **Bed - %solids (ww/v)**	**100**	**200**	**300**
SD - Clarified (~0)	✓	✓	✓
SD – 3	✓	✓	✓
SD – 5	✓	✓	✓
25mm - Clarified (~0)	×	✓	×
25mm – 3	×	✓	×
25mm – 5	×	✓	×

6.2.2.1 SD column: Experimental vs. theoretical bed expansion

Tables 6.2-6.4 provide experimental versus theoretical values for degree of bed expansion and bed voidage for the clarified (~0%), 3% and 5% (ww/v) SD systems, respectively. The theoretical bed heights were predicted using Equation 6.7, assuming $\varepsilon_0 = 0.4$ and based on theoretically determined particle free-fall velocities (Equation 6.1) and values for n (determined as a function of Reynolds number by Equation 6.3 or 6.4). $\varepsilon_{theor.}$ was estimated using the Richardson-Zaki equation (Equation 6.2) for each flow velocity applied, based on the same assumptions as above. The experimental voidage, $\varepsilon_{exp.}$, was determined from Equation 6.6.

The experimental data generally matches the theoretical values for degree of bed expansion and voidage relatively well, with an average error of 23% for the bed height data, and 5.2% for the voidage data. At the higher flow rates applied, the deviation was in some cases more significant.

A possible explanation for any deviation between experimental and theoretical expansion values lies in the presence of interactions between nucleic acids and/or cell debris present in the homogenate, and the adsorbent particles, as discussed by several authors (Barnfield-Frej *et al.*, 1994; Brobjer, 1999; Feuser *et al.*, 1999a). A build up of a layer of cell debris on the surface of the adsorbent would lead to a reduced density of the particle (according to Stokes' Law), and in effect result in an increased level of expansion. As mentioned in section 6.2.1.3, the initial buffer pH applied (pH 4) resulted in significant cell-cell and/or cell-adsorbent interactions. These interactions lead to aggregate formation and non-ideal bed expansion, as illustrated in Figure 6.4. Based on the observed deviations between theoretical and experimental values for degrees of expansion in the current section, altering the buffer pH (from 4 to 5.5) seems to have reduced, although apparently not completely removed, these interactions. It is likely that the high d_p/D_c ratio of the scale-down column serves to enhance the effect of such interactions and to promote aggregation behaviour.

6.2.2.2 Streamline 25 column: Experimental vs. theoretical bed expansion

Table 6.5 provides a comparison between experimental and theoretically determined bed expansions and average bed voidages for the solids concentrations investigated in the Streamline 25 column. The data presented in Table 6.5 suggest that the Streamline 25 column is behaving in a manner very close to what is predicted from the theoretical correlations, even at the highest solids concentrations tested. The average error for bed height measurements were 10.7%, and for voidage the average error was 4.9%.

6.2.2.3 Bed expansion: SD column vs. Streamline 25 column

Figure 6.5 relates experimental and theoretical expansion data achieved for the two columns in a parity plot. As seen, the scale-down bed expands more than the 25 mm bed over the whole range of solids concentrations tested (~0-5% ww/v). This observation is however consistent with the theoretical values presented in Tables 6.2-6.5. The higher degree of expansion estimated for the SD column is due to the large particle to column diameter ratio (d_p/D_c), which results in a higher Richardson-Zaki parameter n (Equation 6.3 and 6.4) compared to for the Streamline 25 column. This in effect leads to a higher average bed voidage in the SD system and hence increased expansion, in accordance with Equation 6.6.

Table 6.2. Experimental versus theoretical values for bed expansion (H/H_0) and bed voidage (ε) for a clarified feed-stream processed in the SD column at pH 5.5 and 20mM MES.

U (cm h^{-1})	$H_{exp.}/H_0$	$H_{theor.}/H_0$	$\varepsilon_{exp.}$	$\varepsilon_{theor.}$
100	1.87	1.73	0.67	0.65
200	2.53	2.18	0.76	0.72
300	4.65	2.56	0.87	0.77

Table 6.3. Experimental versus theoretical values for bed expansion (H/H_0) and bed voidage (ε) for a feed-stream of 3% (ww/v) solids processed in the SD column at pH 5.5 and 20 mM MES.

U (cm h^{-1})	$H_{exp.}/H_0$	$H_{theor.}/H_0$	$\varepsilon_{exp.}$	$\varepsilon_{theor.}$
100	1.88	1.88	0.69	0.68
200	3.03	2.42	0.80	0.76
300	4.06	3.13	0.85	0.81

Table 6.4. Experimental versus theoretical values for bed expansion (H/H_0) and bed voidage (ε) for a feed-stream of 5% (ww/v) solids processed in the SD column at pH 5.5 and 20 mM MES.

U (cm h^{-1})	$H_{exp.}/H_0$	$H_{theor.}/H_0$	$\varepsilon_{exp.}$	$\varepsilon_{theor.}$
100	2.34	2.03	0.74	0.70
200	3.00	2.83	0.80	0.78
300	4.60	3.60	0.87	0.83

Table 6.5. Experimental versus theoretical values for bed expansion (H/H_0) and bed voidage (ε) for experiments conducted in the Streamline 25 column. All experiments were performed at 200 cm h^{-1}, at pH 5.5 and 20 mM.

Feed	$H_{exp.}/H_0$	$H_{theor.}/H_0$	$\varepsilon_{exp.}$	$\varepsilon_{theor.}$
Clarified	1.88	1.65	0.67	0.64
3% (ww/v)	2.00	1.88	0.71	0.68
5% (ww/v)	2.40	2.13	0.75	0.71

The plot indicates, as also seen in Tables 6.2-6.5, that both the SD and the Streamline 25 experimental expansion levels are somewhat high compared to the predicted degrees of expansion. The deviation between the theoretical and experimental data appears, on average, to be slightly larger for the SD column than for the 25 mm column. The deviation between experimental and theoretical bed expansion performance in the SD bed were discussed in section 6.2.1.2 and were attributed to cell-cell and/or cell-adsorbent interactions.

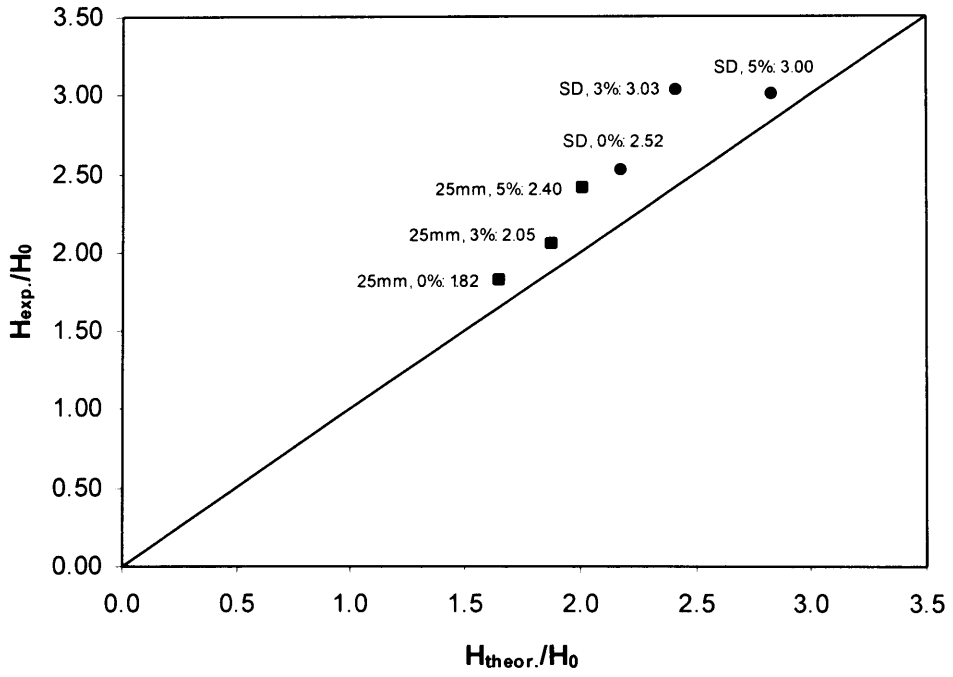

Figure 6.5. Predicted and experimental levels of expansion (H/H_0) for the SD (●) and Streamline 25 (■) columns for processing of *E. coli* homogenates of different solids concentrations at a flow rate of 200 cm h^{-1}. The labels indicate column, %solids (ww/v) and experimental H/H_0.

6.2.3 Axial dispersion

The mixing characteristics of both columns were assessed using the dispersion coefficient, which was calculated using the approach described in section 6.1.3. This method is based on the number of theoretical plates in a column, which was obtained from residence time distribution curves in the form of the conductivity trace obtained during elution in the expanded bed column.

6.2.3.1 SD column: Experimental vs. literature dispersion data

The number of theoretical plates per meter expanded bed height for each SD experiment is presented in Table 6.6. A plate number of 170-200 N_T m^{-1}, based on a sedimented bed height of 15 cm and a flow rate of 300 cm h^{-1}, is considered good (EBA Handbook, GE Healthcare). Although the number of plates per meter presented in Table 6.6 are generally lower than this, the corresponding axial dispersion coefficients range between 3-19 x 10^{-6} m^2 s^{-1} and are comparable to D_{ax} values reported in literature. Willoughby *et al.* (2004) reports a D_{ax} value for a column identical to the scale-down bed used in this work (1.9 mm ID) of 3.4 x 10^{-6} m^2 s^{-1}. An axial dispersion coefficient of 3.3 x 10^{-6} m^2 s^{-1} for Streamline SP was reported by Thömmes *et al.* (1996), and D_{ax} values of 2 x 10^{-6} m^2 s^{-1} and 8-9 x 10^{-6} m^2 s^{-1} was reported by Batt *et al.* (1995) and Lindgren *et al.* (1993), respectively.

Table 6.6. Number of theoretical plates and axial dispersion coefficients achieved in the experiments performed in the scale-down bed.

	Clarified			**3% solids**			**5% solids**		
Flow rate (cm h^{-1})	100	200	300	100	200	300	100	200	300
N_T per meter	39	28	24	50	42	39	49	44	51
D_{ax} x 10^{-6} (m^2 s^{-1})	4.0	10.8	19.0	3.0	7.1	13.0	3.0	4.4	8.5

The axial dispersion coefficients presented in Table 6.6 indicate increased deviation from plug flow as liquid velocity is increased. Several groups (Chang and Chase, 1996; Chung and Wen, 1968; Dasari *et al.*, 1993; Fenneteau *et al.*, 2003; Goto *et al.*, 1995) have reported a similar trend. Thömmes *et al.* (1995), however, observed the opposite, that increasing liquid velocity resulted in decreased axial mixing.

At constant flow velocity, Chang and Chase (1996) observed increased mixing in the liquid phase with increasing liquid viscosity or bed voidage; D_{ax} ranging from 6.4 x 10^{-6} m^2 s^{-1} for expansion in buffer with an average bed voidage of 0.7, to 31.7 x 10^{-6} m^2 s^{-1} for a solution of 32% (v/v) glycerol and an average bed voidage of 0.9. The data presented in Table 6.5 show an opposite trend of reducing D_{ax} with increasing viscosity (as a result of increased solids concentration). This may be an artefact of

the SD column but is constant across all of the conditions tested. (It is worth noting that conflicting data such as this is not unique, as indicated by the contradicting studies on the impact of liquid velocity noted above.)

6.2.3.2 Streamline 25 column: Experimental vs. literature dispersion data

The number of theoretical plates for the Streamline 25 system ranged from 16 to 22 plates per meter expanded bed. As mentioned earlier, the number of plates calculated using the RTD curve gives the number of theoretical plates in the whole system, not only in the expanded bed section. The low numbers of theoretical plates in the Streamline 25 column is probably related to the relatively large dead-volume in the column set-up, which again is a result of the fixed position of the top adaptor (~ 23 cm above the settled bed).

The low number of theoretical plates corresponds to increased values for the axial dispersion coefficient. The D_{ax} values achieved for solids concentrations between ~ 0% and 5% (ww/v) in the Streamline 25 column were in the range $20 \times 10^{-6} \pm 5 \times 10^{-6}$ $m^2 s^{-1}$, which are in the upper range of values reported in literature (as discussed in 6.2.3.1).

6.2.3.3 Axial dispersion: SD column vs. Streamline 25 column

Table 6.6 and section 6.2.3.2 provided the derived numbers of theoretical plates and the axial dispersion coefficients for the SD column and the Streamline 25 column, respectively. For the SD bed, the number of plates per meter expanded bed height varied from 24 to 51 $N_T m^{-1}$, whereas the plate numbers ranged from 16-22 $N_T m^{-1}$ in the Streamline 25 bed. As discussed in previous sections care must be taken when comparing the plate numbers and levels of axial dispersion between to systems with different set-ups, since these characteristics relate to the complete system.

Evidence from the literature (Ghose and Chase, 2000a) suggest that the axial dispersion is not significantly affected by changing the particle to column diameter ratio between experiments. However, the average particle to column diameter ratio

in the SD bed used in this study is 0.1, which is significantly higher than that of the 25 mm bed (0.008). The variation in particle to column diameter ratio between the two columns investigated in this study is larger than what has been reported from scaling studies elsewhere (Barnfield-Frej *et al.*, 1997; Brobjer, 1999; Ghose and Chase, 2000a,b), and therefore the difference in level of axial dispersion between the two EBA columns may be expected to be more apparent.

6.2.4 Breakthrough curves

Full breakthrough curves were achieved for all the experiments summarised in Table 6.1. Section 6.2.4.1 discusses the effect of flow rate and solids concentration on breakthrough of Fab in the scale-down column, whereas section 6.2.4.2 provides a comparison between the breakthrough profiles obtained in the SD and the Streamline 25 columns, on the basis of similar solids concentration and flow rate.

6.2.4.1 Fab breakthrough curves in the scale-down column

Figure 6.6 shows the effect of operating flow rate on the breakthrough of Fab from a 5% (ww/v) *E. coli* homogenate feed-stream processed in the SD column. As expected, breakthrough occurs more quickly as flow rate is increased.

Figure 6.7 presents breakthrough curves obtained at 200 cm h^{-1} for each level of solids concentration tested in the SD bed. Initial breakthrough occurs almost simultaneously for all the solids concentrations investigated. From about 30-40% breakthrough the effect of solids content becomes more evident, and the breakthrough curve is seen to get steeper as the level of solids increases. It is likely that this reduction in level of adsorption is a result of the cell debris blocking the binding sites on the adsorbent, and/or competing with the adsorbent for the product.

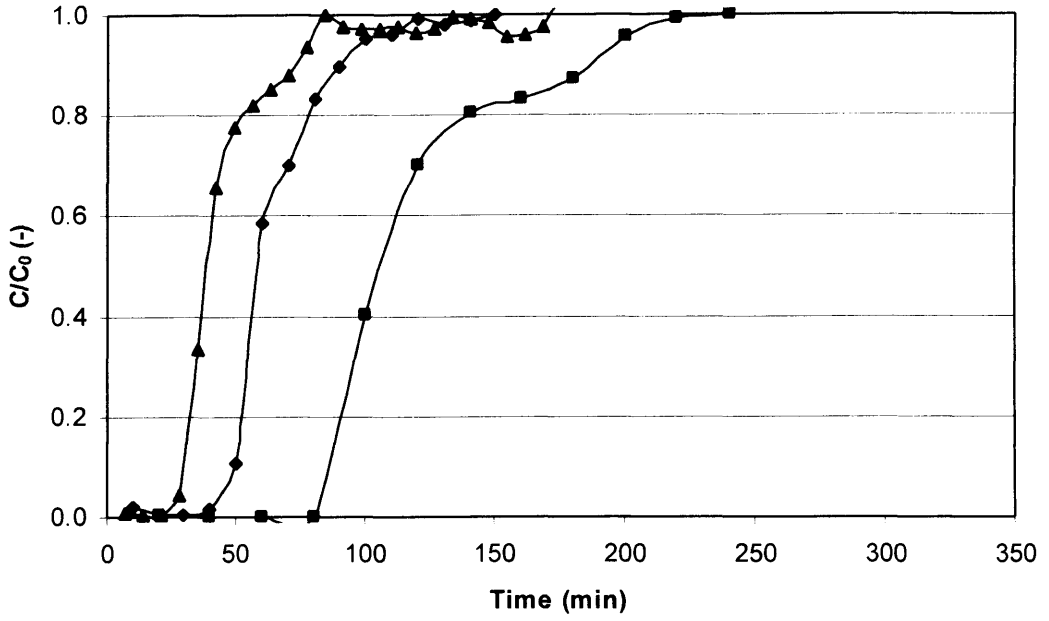

Figure 6.6. Adsorption of Fab from 5% (ww/v) *E. coli* homogenate to Streamline SP in the SD column at flow rates of 100 (■), 200 (♦) and 300 (▲) cm h^{-1}.

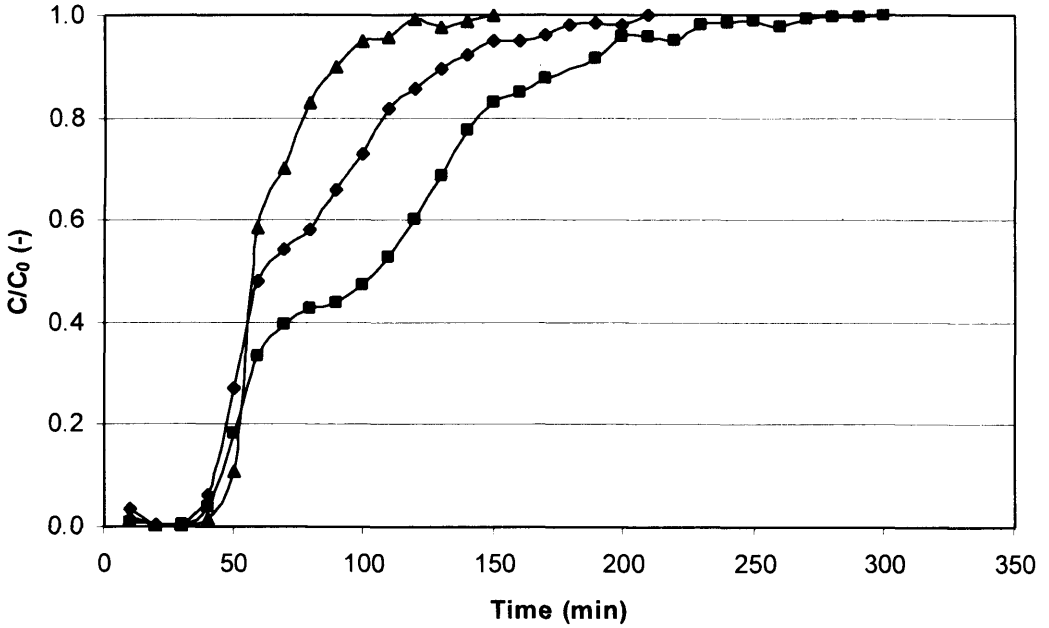

Figure 6.7. Impact of feed solids concentration on Fab breakthrough in the SD column. Breakthrough curves for clarified (■), 3 (♦) and 5 (▲) % (ww/v) solids were all obtained at 200 cm h^{-1}.

6.2.4.2 Fab breakthrough curves: SD column vs. Streamline 25 column

Figures 6.8-6.10 present comparisons of breakthrough curves in the two columns on the basis of similar solids concentration and the same flow rate. The breakthrough data is a function of the overall system volume and not just the volume of the column itself (Gardner *et al.*, 2005). This should be taken into consideration when comparing two systems, especially when of such different scale as in this work. In order to compensate for this effect, which will artificially displace the breakthrough curves, the dead volume of each system was determined. The feed volume consumed from initiation of load to the point at which an increase in UV_{280} was detected (due to breakthrough of proteins) was taken as the system volume during the loading step. For the SD system breakthrough was delayed approximately 20 min due to the low ratio of column volume to total system volume. The SD data presented in Figures 6.8-6.10 have been shifted 20 min to the left on the time axis to account for this. The time axis is referred to as "Corrected time" to reflect the shifting.

The breakthrough comparisons show that whereas the shape of the breakthrough curves between the two systems at the same flow rate and similar solids concentration is comparable, the SD bed appears to provide a better contact efficiency between Fab and Streamline SP than the Streamline 25 bed. This is reflected by a later breakthrough of Fab in the scale-down system.

The apparent increase in breakthrough capacity might be a result of a higher degree of expansion in the SD bed relative to the Streamline 25 column, with the effect of an increased residence time for Fab in the scale-down column and hence more time available for binding to the adsorbent. In section 6.2.2.3 it was established that due to the high d_p/D_c ratio of the scale-down bed, the degree of expansion is expected to be higher in this column relative to in the 25 mm column. On top of this, the SD bed was found to over-expand relative to the predicted level of expansion, resulting in an even larger difference in the degree of expansion between the two columns. The over-prediction was attributed to cell-cell and/or cell-adsorbent interactions in the scale-down bed (section 6.2.2.1).

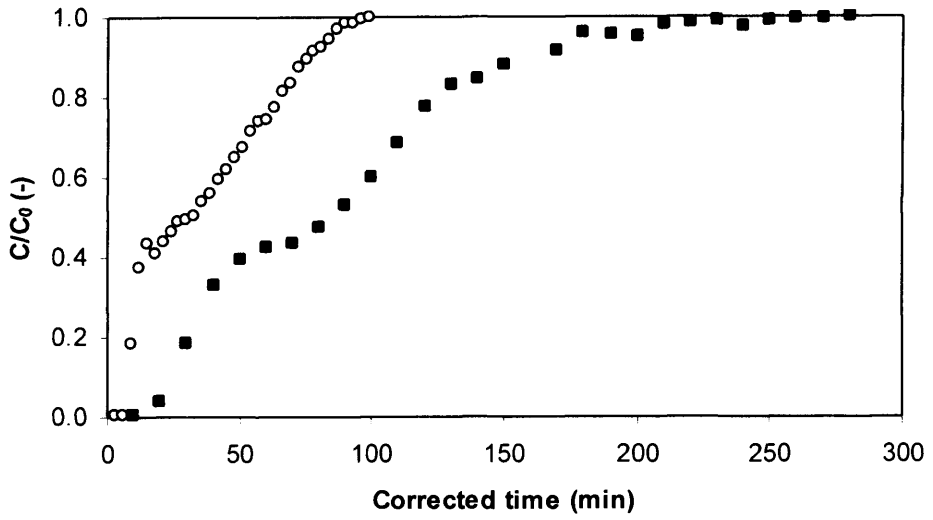

Figure 6.8. Breakthrough curves for adsorption of Fab from a clarified homogenate onto Streamline SP in the SD (■) and Streamline 25 (○) columns. The curves were generated at 200 cm h^{-1}.

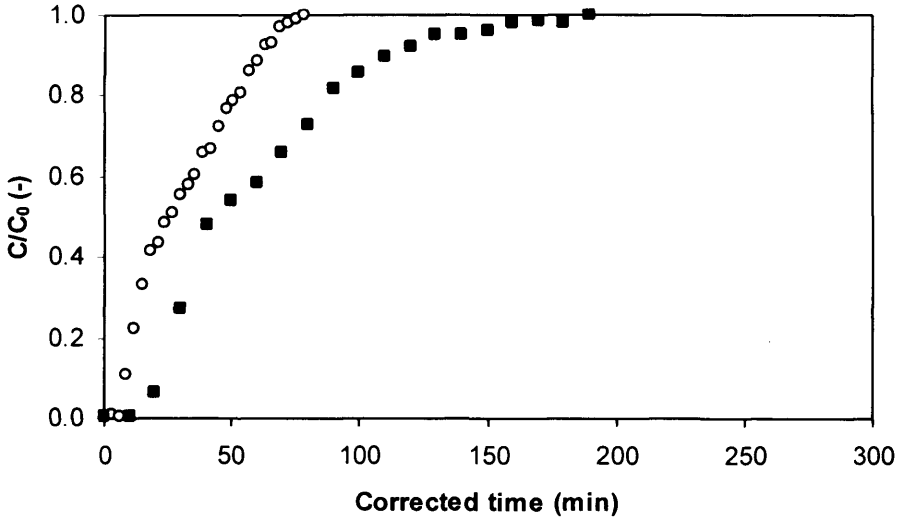

Figure 6.9. Breakthrough curves for adsorption of Fab from a 3% (ww/v) homogenate onto Streamline SP in the SD (■) and Streamline 25 (○) columns. The curves were generated at 200 cm h^{-1}.

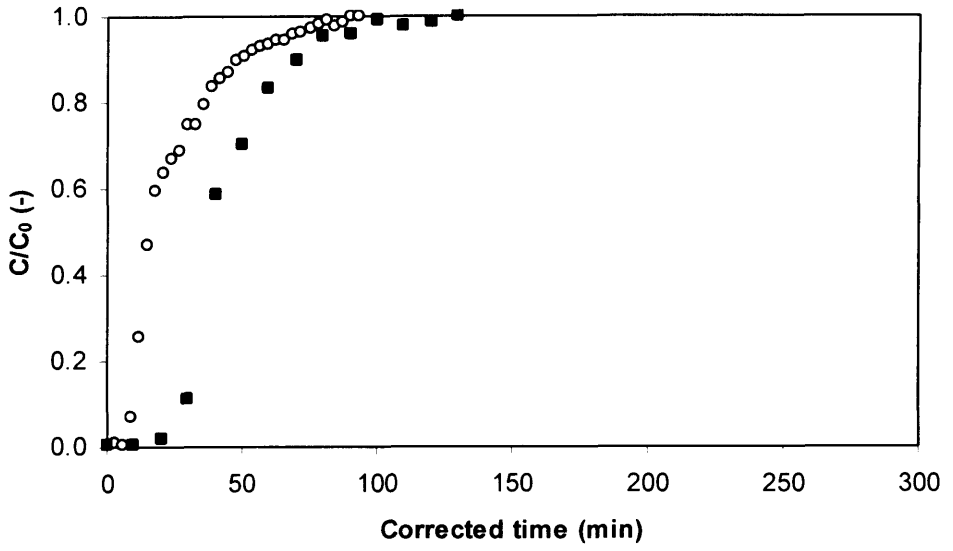

Figure 6.10. Breakthrough curves for adsorption of Fab from a 5% (ww/v) homogenate onto Streamline SP in the SD (■) and Streamline 25 (○) columns. The curves were generated at 200 cm h^{-1}.

6.2.5 Capacity and yield

The behaviour of the SD column is here compared to that of the Streamline 25 column on the basis of binding capacity and yield.

6.2.5.1 Capacity in the SD and Streamline 25 columns

Table 6.7 provides a comparison between the binding capacities achieved in the scale-down and Streamline 25 columns at 10, 25 and 100% product breakthrough. The SD column is seen to over-predict the capacity of the 25 mm system. This observation corresponds to the later Fab breakthrough in the SD column relative to the Streamline 25 column as seen in Figures 6.8–6.10. Possible explanations for the difference in breakthrough behaviour between the two columns were discussed in section 6.2.4.2.

The dynamic binding capacity at 10 and 25% breakthrough is not significantly affected by solids concentration. For the SD system, this corresponds well with Figure 6.4, which indicates that up to about 30-40% breakthrough there is little difference in the breakthrough curves between feed-streams of ~0, 3 and 5% (ww/v)

solids concentration upon loading at 200 cm h^{-1}. Above 30-40% breakthrough it was seen that feed-streams of increased solids concentration resulted in more rapid Fab breakthrough, suggesting reduced binding capacity with higher solids density.

From Table 6.7 it appears that the total capacity (capacity at 100% breakthrough) decreases with increasing solids content in the Streamline 25 column as well as in the SD column. This suggests that the presence of solids also affects the binding capacity in this larger-scale column to a certain extent. As seen throughout this study, the effects of solids concentration on bed performance in the Streamline 25 column are not as pronounced as in the SD bed. As discussed in previous sections, the high particle to column diameter ratio of the SD bed is believed to be causing the difference in response to cell-adsorbent interactions observed between the two expanded bed systems investigated.

Table 6.7. Binding capacity (mg mL^{-1}) as determined at different levels of Fab breakthrough for the SD column and the Streamline 25 column for clarified, 3%, and 5% (ww/v) homogenate. All runs were conducted at 200 cm h^{-1}.

	Clarified		**3% solids**		**5% solids**	
% Breakthrough	SD	Streamline 25	SD	Streamline 25	SD	Streamline 25
10	1.61	0.64	1.71	0.54	2.28	0.61
25	2.18	0.81	2.18	0.74	2.64	0.74
100	5.76	3.06	4.66	1.94	3.71	1.54

6.2.5.2 Yield in the SD and Streamline 25 columns

When studying the yield (Table 6.8) achieved for clarified homogenate, there seems to be good agreement between the two columns investigated. This confirms the basic scale-down philosophy explained by Willoughby *et al.* (2004). When solids are introduced, the yields for the SD column are greatly reduced relative to the 25 mm column data. It seems likely that the aggregation behaviour discussed throughout this chapter is the cause of these deviations.

Table 6.8. Fab yields achieved in the SD and the Streamline 25 columns for clarified, 3% and 5% (ww/v) homogenate. All experiments were performed at 200 cm h^{-1}.

	Clarified		**3% solids**		**5% solids**	
	SD	Streamline 25	SD	Streamline 25	SD	Streamline 25
% Yield	32.0	38.5	16.8	49.3	9.5	48.6*

*Due to experimental difficulties experienced in relation to the determination of the yield from the 5% (ww/v) data, the level of yield stated is that achieved upon processing of a 7.5% (ww/v) solids feed-stream in the Streamline 25 column.

6.3 Summary

This chapter has identified limitations to the existing system used for scale-down of EBA. Upon challenging the SD bed with an industrially relevant feedstock of varying solids concentration, the performance of the scale-down system was found to differ from that of the currently-accepted smallest column for scale-down studies (25 mm ID).

The main challenge identified in this scaling study was that of interactions between nucleic acids and/or cell debris from the homogenate, and the adsorbent particles. These interactions were mainly observed in the narrow SD column, where they occasionally lead to aggregate formation. As a result, the expansion behaviour observed for the scale-down column was different from the level of bed expansion estimated from established theoretical correlations. Moreover, this aggregation behaviour, combined with a high adsorbent particle diameter to column diameter ratio for the SD bed, may explain the deviation in degree of bed expansion seen between the scale-down column and the 25 mm column when operated under the same conditions.

The cell-cell and/or cell-adsorbent interactions seen in the scale-down bed are believed to have enhanced the binding efficiency of the SD system, as evidenced by a later Fab breakthrough compared to in the Streamline 25 column and an over-prediction of the dynamic and total binding capacities in the Streamline 25 system by the scale-down bed. Increasing the feed solids concentration resulted in a reduction

of the total binding capacity for both systems investigated, whereas the effect of solids concentration on the yield was mainly evident in the scale-down column.

The following chapter (Chapter 7) investigates an approach for predicting breakthrough curves via the general rate model. This model will be used to predict large-scale EBA behaviour, and the resulting relationship between operating parameters and performance parameters then visualised by Windows of Operation to illustrate the likely trade-offs that will need to be sought under realistic conditions of large-scale operation.

7 Simulation of EBA breakthrough by the general rate model and visualisation of process performance using Windows of Operation

Abstract

Scale-down is a powerful tool for predicting large-scale process performance. By providing essential information regarding expected performance parameters and corresponding process variables, scale-down technology aims to speed up process development, reducing both time and cost related to the design of a process. Chapters 4 and 5 demonstrated how ultra scale-down centrifugation predictions, coupled with Windows of Operation, provide a tool for the rapid evaluation of separation performance and determination of the most suitable operating conditions for large-scale centrifugal recovery of *P. pastoris* cultures and *E. coli* homogenates.

The attempt to scale down the expanded bed adsorption process for recovery of Fab from *E. coli* homogenate, presented in Chapter 6, was complicated by cell-adsorbent interactions that occurred mainly in the SD bed. Comparison with the results achieved in the larger Streamline 25 column demonstrated that the SD bed did not provide the necessary confidence in the data that would be required if the results were to be used for large-scale predictions.

This chapter describes an alternative approach to enable the rapid evaluation of the effect of various operating parameters on the performance of the EBA process, and involves simulation of product breakthrough based on the general rate model (GRM) (Gu *et al.*, 1993; Gu, 1995). The model was solved numerically and data generated from the general rate model was used to develop a series of Windows of Operation, which visualise the most suitable operating conditions available for large-scale recovery of Fab from *E. coli* homogenate by EBA, when the operation is restricted by predefined process performance criteria.

To prove the validity of the general rate model, a verification of the GRM is presented, which involves a comparison of simulated and experimental breakthrough behaviour as obtained for the Streamline 25 column.

7.1 Introduction

The general rate model simulates a chromatographic process by considering the influences of axial liquid phase dispersion and external and intra-particle mass transfer on the breakthrough profile for defined components. Section 7.1.1 provides an introduction to the general rate model, and section 7.1.2 considers the generation of Windows of Operation for an EBA process.

7.1.1 General rate model for prediction of expanded bed adsorption performance

In this section the assumptions related to the model are discussed (section 7.1.1.1), as are the isotherm equation (section 7.1.1.2) and mass transfer equations (section 7.1.1.3) involved in the model.

7.1.1.1 General rate model assumptions

The following assumptions are built in to the general rate model (Gu *et al.*, 1993, Gu, 1995; Kaczmarski *et al.*, 2001):

1. The chromatographic process is isothermal
2. The column is packed with porous particles which are spherical and uniform in size
3. Radial concentration gradients in the bed are negligible
4. There exists a local equilibrium for each component between the adsorbent pore surface and the stagnant fluid inside the macropores
5. The interfacial mass transfer between the bulk fluid and the particle phase can be described by the film mass transfer mechanism

6. Diffusion and mass transfer coefficients are assumed constant and independent of mixing effects.

The general rate model can handle multi-component separations. However as the focus of this work is purely on Fab recovery, the GRM will here be treated as a single component model.

Once the assumptions above are established, the mass balances of a component in the bulk-fluid phase and in the particle phase can be described by the set of differential equations (Gu *et al.*, 1993, Gu, 1995; Kaczmarski *et al.*, 2001) given in Appendix A4.

It should be noted that the general rate model in the form described here – and which was applied in this work - is developed for non-fluidised chromatographic systems. Several successful simulations of EBA breakthrough performance based on modified general rate models have been reported (Chen *et al.*, 2003; Tong *et al.*, 2002; Wright and Glasser, 2001). In addition to liquid phase axial dispersion and external and intra-particle mass transfer resistances, these models take into account the axial dispersion of the mobile solid phase. Moreover, recent papers have investigated the dependency of particle size distribution (Kaczmarski and Bellot, 2005; Tong *et al.*, 2003) and axial bed porosity distribution (Kaczmarski and Bellot, 2004) on the EBA models. Hence upon application of the general rate model as described in Appendix A4 to an expanded bed adsorption process, some additional assumptions to the ones listed above should be considered:

7. Axial solid phase dispersion is negligible
8. Expanded bed voidage is constant through the column

When considering observations reported in literature, the above assumptions 7. and 8. are not unreasonable. Kaczmarski and Bellot (2004, 2005) and Thömmes (1997) have reported that the dispersion of the mobile solid phase is negligible, and Kaczmarski and Bellot (2004) also found that the bed porosity distribution had an insignificant effect on the simulated breakthrough curves.

Finally, as assumption 2. has already stated, the adsorbent particles are assumed to be uniform in size. This is not true for the purpose-built EBA matrixes, as they are developed so as to have a particle size distribution that allows for fluidisation with an increased voidage relative to a packed bed, resulting in stable expansion upon loading of a solids-containing feed. The particle diameter has been reported to be one of the parameters having the greatest effect on modelled breakthrough behaviour (Kaczmarski and Bellot, 2004; Tong *et al.*, 2003; Wright and Glasser, 2001). However due to lack of any other available model, it was assumed that overall, the general rate model for non-fluidised systems was sufficiently accurate for the purpose of this work.

7.1.1.2 Isotherm equation

Adsorption of protein to the matrix was assumed to follow a single component Langmuir isotherm, described by Equation 7.1.

$$C_p^* = \frac{aC}{1 + bC} \qquad 7.1$$

where C_p^* is the concentration of product on the adsorbent particles, C is the equilibrium concentration of product in the fluid, $a = bC_p^{max}$ where C_p^{max} is the maximum concentration of product on the matrix surface and b is the binding equilibrium constant. The Langmuir parameters a and b are both required to simulate breakthrough by the general rate model.

A more realistic approach for the adsorption of Fab from homogenate would be to use a competitive Langmuir isotherm, which considers the adsorption of several components on the matrix particles. This would however be a very complex and impractical approach, and would in some ways defeat the purpose of this model as a tool for rapid evaluation of adsorption performance.

7.1.1.3 Mass transfer parameters

The general rate model predicts breakthrough behaviour for the product of interest based on several parameters characteristic of the current system. Some of these parameters are related to product, column size and type of adsorbent, and others to flow rate and expansion behaviour. These parameters are either known, or can be estimated to a reasonable degree of accuracy.

Another parameter required in the model is that of axial dispersion, which was covered in detail in Chapter 6. The axial dispersion coefficient can be determined based on RTD traces and the axial dispersion model as discussed in the previous chapter.

Other transfer parameters, such as the film mass transfer coefficient (k_f) and the intra-particle diffusivity (D_P) are often not available from literature for the specific system under investigation, and may be difficult to determine experimentally. These parameters are therefore often estimated using established correlations. The Wilson-Geankopolis correlation (Wilson and Geankopolis, 1966) may be used to estimate the film mass transfer coefficient:

$$Sh = \frac{1.09}{\varepsilon} Sc^{1/3} \mathrm{Re}^{1/3} \qquad 7.2$$

where Sh is the Sherwood number (= $2k_fR_p/D_m$), Sc is the Schmidt number (= $\mu/\rho D_m$) and Re is the Reynolds number (= $2R_p\rho U/\mu$). The resulting expression for k_f is given in Equation 7.3:

$$k_f = 0.687 v^{1/3} \left(\frac{\varepsilon R_p}{D_m} \right)^{-2/3} \qquad 7.3$$

where v is the interstitial velocity, ε is the bed void fraction, R_p is the adsorbent particle radius and D_m is the molecular diffusivity. The molecular diffusivity can be

calculated from the molecular weight (MW) of the product by the following equation (Marshall, 1978):

$$D_m = 2.74 \times 10^{-5} MW^{-1/3} \qquad 7.4$$

Finally, the intra-particle diffusivity D_P is determined from the correlation below (Yau *et al.*, 1979):

$$D_p = \frac{D_m}{\tau_{tor}}(1 - 2.104\lambda + 2.09\lambda^3 - 0.95\lambda^5) \qquad 7.5$$

where τ_{tor} is the particle tortuosity factor and λ is the ratio of the molecular diameter of the component to the pore diameter of the adsorbent.

7.1.1.4 Numerical solution of the GRM

The partial differential equations constituting the general rate model (see Appendix A4) were solved using a numerical method developed by Gu *et al.* (1993). The method involves discretization of the mobile phase using a finite element method (five elements) and discretization of the particle phase using orthogonal collocation (2 collocation points). The resulting set of first order ordinary differential equations (ODE's) was solved using a variable order MATLAB (The MathWorks, Inc., Natick, MA, USA) Ordinary Differential Equation solver (ODE15s) based on the numerical differentiation formulas. The output of the model is a breakthrough curve defined by C/C_0 versus time. Further information regarding the solution to the general rate model can be found in Gu *et al.* (1993) and Gu (1995).

7.1.2 Windows of Operation for EBA

As demonstrated in Chapter 5 for the case of centrifugation processes, Windows of Operation are useful for the visualisation of suitable operating conditions for a process when restricted by predefined performance criteria. For centrifugation, the effect of feed solids concentration and flow rate on performance parameters, such as

yield and clarification, was investigated. Additional constraints identified included a maximum processing time and an upper flow rate constraint.

The performance parameters characterising a chromatographic process are usually yield, productivity and purity. High yield and productivity are important as both parameters will contribute towards the overall yield and total processing time for the whole purification process, respectively. For EBA, purity is frequently less of a concern, as the product eluted from the expanded bed column will usually be further purified and polished in subsequent chromatographic steps. The Windows of Operation for expanded bed adsorption presented in this chapter will examine the effect of flow rate and load volume on the yield and productivity performance parameters. Parameters related to column hydrodynamics, such as the degree of expansion, must also be considered, especially when processing a high solids density feed-stream. A restriction on the maximum level of expansion is therefore included in the Windows of Operation where appropriate.

The Windows of Operations for EBA are constructed by displaying productivity and yield as a function of feed solids concentration and flow rate in a 2-D contour plot using a function of the software program Origin™ (Microcal Software Inc., Northampton, USA). The contour plots are generated from data matrices which correlate sets of either solids concentration, flow rate and productivity, or solids concentration, flow rate and yield, based on the simulated data relating productivity and yield to the operating parameters of solids concentration and flow rate.

7.2 Results and discussion

In the following sections the choice of input parameters for the simulation of a large-scale EBA process is discussed (section 7.2.1), followed by a presentation of typical breakthrough curves generated by the model (section 7.2.2). The general rate model is then verified by comparing experimental and simulated breakthrough curves for a Streamline 25 column (section 7.2.3). Finally Windows of Operation for the large-scale process are presented for each of the feed-streams investigated (section 7.2.4).

7.2.1 Input parameters for simulation of large-scale EBA performance

7.2.1.1 Feed properties

As for the Windows of Operation generated for centrifugation of *E. coli* homogenate in Chapter 5, the load volume for each EBA simulation was derived from the assumption of an initial batch of 1000 L fermentation broth with a solids concentration of 30% (ww/v). Cells are harvested by centrifugation and re-suspended to 1000 L in buffer prior to homogenisation. Due to cell disruption and subsequent release of cell internal liquid in the homogeniser, this will result in 1000 L homogenate of approximately 15% (ww/v) solids concentration. The 15% homogenate is assumed to form the basis for the generation of feed-streams of various solids content to be processed by EBA, with the total processing volume increasing with the degree of dilution. Table 7.1 summarises the properties of the feed-streams investigated.

Table 7.1. Feed solids concentrations and corresponding volumes for the simulation of EBA breakthrough behaviour by the general rate model.

Solids concentration (% ww/v)	**Total feed volume, V_{load} (L)**
1	15000
5	3000
10	1500
15	1000

7.2.1.2 Column and adsorbent characteristics

The Windows of Operation presented in the following text aim to present available operating conditions and trade-offs for an industrial-scale expanded bed adsorption process performed in a 1 m ID column. The column is assumed to be packed with ~120 L of the cation exchanger Streamline SP, which has a reported average particle diameter of 200 μm (Expanded bed adsorption handbook, GE Healthcare, Sweden).

Information regarding Streamline SP pore porosity (ε_p) was not available. Various values for particle porosity have been reported for different matrixes in literature, ranging from 0.62 for DEAE Spherodex M (Chen *et al.*, 2003), to 0.75 for a 4% agarose gel (Gutenwik *et al.*, 2004), and 0.84 for Sepharose FF (Chang and Lenhoff, 1998). The effective particle porosity is dependent not only on the matrix applied, but also on the size of the protein to be captured, and the effective porosity decreases as more product is adsorbed. The sensitivity of the model to the value of ε_p was investigated by varying the pore porosity parameter while keeping all other model parameters constant. The shape of the breakthrough curve was found to be affected by the assumed pore porosity – the lower the value of ε_p, the shallower the breakthrough curve became. A value of 0.8 for pore porosity was assumed in this work since when compared to the experimental breakthrough curves generated from the Streamline 25 column data (section 7.2.4), this was found to give a good curve fit.

The pore diameter is another unknown characteristic of the adsorbent. When varying the pore diameter input value between 100 and 500 Å while keeping all other parameters constant, hardly any difference was detected in the breakthrough curve. A mid-range value of 275 Å was applied in this work.

Particle tortuosity is related to the structure of the adsorbent pores, and is a difficult parameter to measure experimentally. In this work a tortuosity value of 0.1 was used, as this value has been successfully applied for prediction of EBA breakthrough curves in the past (personal communication, Dr. Nik Willoughby). Upon comparison with experimental Streamline 25 breakthrough curves, simulations based on this value were found to produce good mimics of Fab breakthrough. Applying a higher value for tortuosity (0.5 and above) resulted in a poor mimic with premature breakthrough being predicted.

7.2.1.3 Bed hydrodynamics

The settled bed height assumed in the simulations was 15 cm. The expanded bed height and column void fraction was determined from the Richardson-Zaki equation as described in Chapter 6, and takes into account the increased viscosity as feed solids concentration increases. The expansion estimates are based on the settling velocity of an average-size particle, however for this purpose this simplification was believed to give a sufficiently accurate prediction of the expansion behaviour. The flow rates applied were 100, 200 and 300 cm h^{-1}, corresponding to 785, 1571 and 2356 L h^{-1}, respectively.

7.2.1.4 Isotherm parameters

The values of the Langmuir isotherm parameters a and b were determined after investigating the effect of changing parameter a between 100 and 200 in intervals of 25, and b between 5 and 15 in intervals of 5, on the breakthrough curve. Parameter a was found to affect the shape of the breakthrough curve the most, whereas changing parameter b had no effect on the curve. Based on a comparison with the experimental Streamline 25 breakthrough data, it was found that the value of parameter a resulting in the best curve fit was dependent on the solids concentration of the feed. This effect is believed to be a result of the solids reducing the maximum level of adsorption achievable, either by blocking the binding sites on the adsorbent, or by competing with the adsorbent for the product. It appeared that for solids concentrations below 7.5% (ww/v), a value of 150 for a resulted in the best curve fit. For 10% and 15% (ww/v) solids the a values producing the best match between the simulated and experimental curves were 125 and 100, respectively. Hence for the simulations performed for prediction of the large-scale EBA breakthrough curves, parameter a was varied from 150 for the 1% and 5% solids feeds, to 125 for 10% and 100 for 15% solids concentration. Parameter b was kept constant at a value of 10.

7.2.1.5 Axial liquid phase dispersion

The axial liquid dispersion coefficient was discussed in Chapter 6, where both experimental and literature values were presented. As discussed in 6.2.3.1, there are

opposite trends reported in literature when it comes to the dependence on D_{ax} of both liquid velocity and solids content. After performing a sensitivity analysis where D_{ax} was varied while all other parameters were kept constant, it was evident that the model was not particularly sensitive to variation in liquid axial dispersion and it was therefore decided to keep the axial dispersion coefficient constant between the simulations. A typical value of 5×10^{-6} m^2 s^{-1} was applied.

7.2.1.6 Transport parameters

The molecular diffusivity for Fab was calculated as 7.6×10^{-11} m^2 s^{-1} from Equation 7.4. This value compares well to the molecular diffusivity of 7.1×10^{-11} m^2 s^{-1} for BSA (a similar sized molecule to Fab) reported by Gutenwick *et al.* (2004).

The film mass transfer coefficient (k_f) was estimated according to Equation 7.3 for each condition tested and was found be within the range 5.3-7.8×10^{-6} m s^{-1}, which corresponds well with literature values (Tong *et al.*, 2002; Wright and Glasser, 2001).

Intra-particle diffusivity (D_p) was calculated from Equation 7.5 and relates to molecular diffusivity, particle tortuosity and the ratio of molecular diameter of product to adsorbent pore diameter. Based on values given in previous sections, D_P was calculated at 4.7×10^{-10} m^2 s^{-1}. This value is almost an order of magnitude larger than what has been reported in literature (Chen *et al.*, 2003; Kaczmarski and Bellot, 2004; Tong *et al.*, 2003; Wright and Glasser, 2001), and is most likely a direct result of the low particle tortuosity factor used (see section 7.2.1.2). Reduced tortuosity reflects an easier diffusion path for the compound within the matrix, resulting in increased pore diffusivity. It is believed that this observation reflects the structure of the matrix particles applied, combined with the size of the product of interest.

A summary of the parameter values used for simulation of the large-scale EBA process is provided in Table 7.2.

Table 7.2. Summary of the model parameters applied in the general rate model and their values.

Model input parameter	**Value**
Solids concentration (% ww/v)	1, 5, 10, 15
V_{load} (L), sample volume	Table 7.1
C_0 (mg mL^{-1}), Fab inlet concentration	0.03 - 0.5
MW (Da), Fab molecular weight	47000
D_c (m), column diameter	1
R_p (μm), (average) particle radius	100
U (cm h^{-1}), flow rate	100, 200, 300
H_0 (m), settled bed height	0.15
H (m), expanded bed height	Equation 6.7
ε (-), bed void fraction	Equation 6.2
ε_p (-), particle porosity	0.8
Pore diameter (Å)	275
τ_{tor} (-), particle tortuosity factor	0.1
D_{ax} (m^2 s^{-1}), axial dispersion	5×10^{-6}
Langmuir parameter a (-)	1%, 5%: 150 10%: 125 15%: 100
Langmuir parameter b (mL mg^{-1})	10
k_f (m s^{-1}), film mass transfer coefficient	Equation 7.5
D_m (m^2 s^{-1}) (from Equation 7.6)	7.6×10^{-11}
D_p (m^2 s^{-1}) (from Equation 7.7)	4.7×10^{-10}

7.2.2 Simulated breakthrough curves

Modelling of breakthrough of Fab from a 1 m ID column was based on the parameter values provided in Table 7.2. The resulting breakthrough curves for feed-streams of 1, 5, 10 and 15% (ww/v) solids processed at 200 cm h^{-1} are presented in Figure 7.1. Figure 7.2 shows the dependence of flow rate on the shape of the breakthrough curve of a 10% (ww/v) feed-stream.

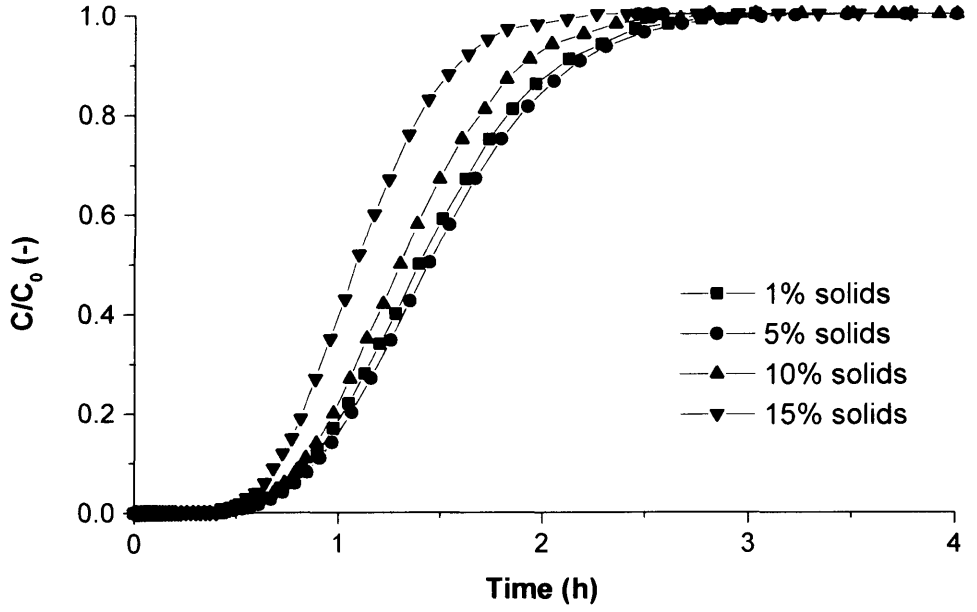

Figure 7.1. Simulated breakthrough curves for *E. coli* homogenate feed-streams of 1, 5, 10 and 15% (ww/v) solids concentration processed at 200 cm h^{-1} in a 1 m ID column.

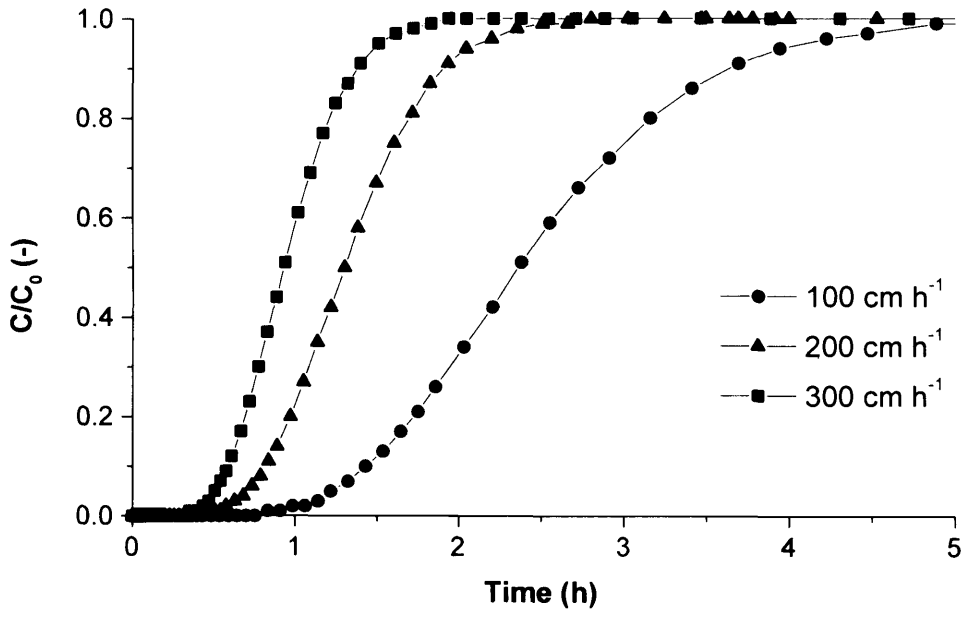

Figure 7.2. Simulated breakthrough curves for processing of a 10% (ww/v) solids *E. coli* homogenate feed-stream in a 1 m ID column at 100, 200 and 300 cm h^{-1}.

7.2.3 Verification of the general rate model for simulation of expanded bed adsorption breakthrough

In order to verify the model used to predict the breakthrough curves for the large-scale expanded bed adsorption process in section 7.2.2, experimental breakthrough curves for the Streamline 25 column was compared to breakthrough curves generated from the model. The simulations were in these cases carried out with experimental parameters where possible; otherwise the estimates obtained from literature correlations were applied (according to Table 7.2). Available experimental parameters include C_0, load volume, bed height and -voidage, and axial liquid dispersion.

Figures 7.3-7.5 show simulated versus experimental breakthrough curves obtained in the Streamline 25 column for feed-streams of 3, 10 and 14% (ww/v) solids, all experiments performed at 200 cm h^{-1}. It is assumed that the Langmuir parameter a is a function of feed solids concentration (as discussed in 7.2.1.4), and the values for a applied when simulating breakthrough for the 3, 10 and 14% (ww/v) feed-streams were 150, 125 and 100, respectively.

The simulated breakthrough curves are seen to fit the experimental curves very well and give confidence in the ability of the general rate model to predict accurately expanded bed adsorption behaviour. The simulations generated for the large-scale process (section 7.2.2) were therefore used as the basis for the generation of a series of Windows of Operation which will be detailed in section 7.2.4.

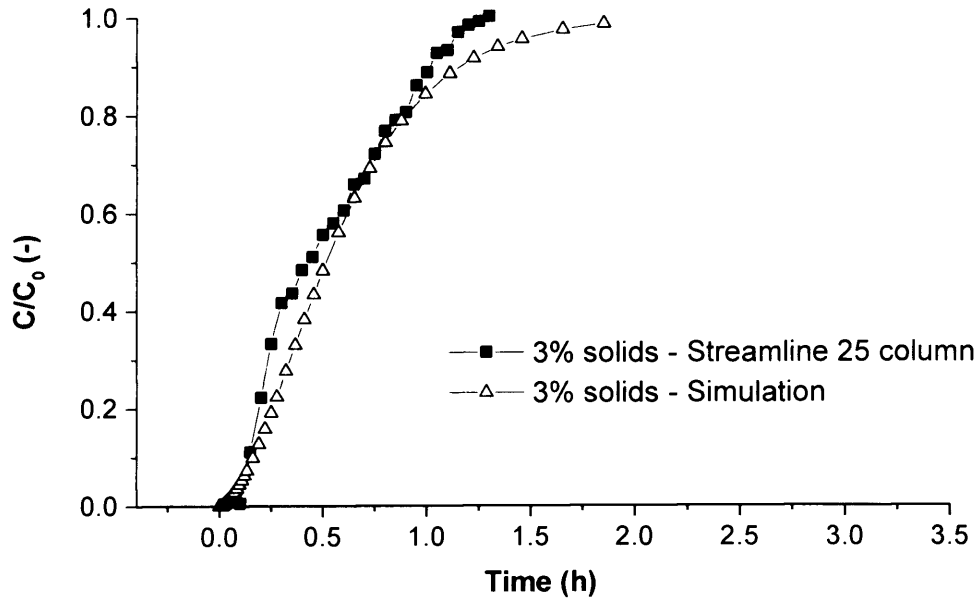

Figure 7.3. Experimental and simulated breakthrough curves for an *E. coli* homogenate feed-stream of 3% (ww/v) solids concentration processed at 200 cm h^{-1} in the Streamline 25 column.

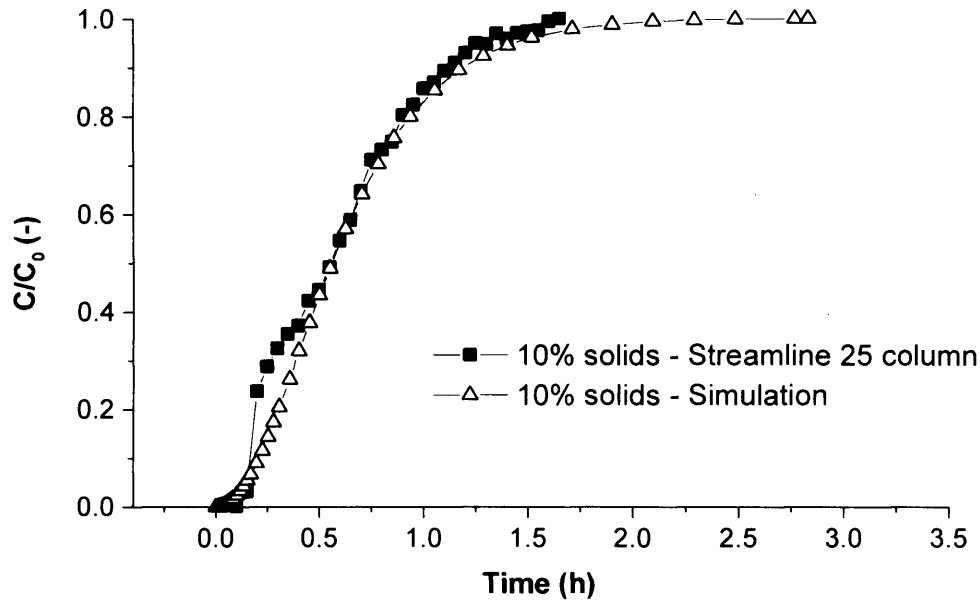

Figure 7.4. Experimental and simulated breakthrough curves for an *E. coli* homogenate feed-stream of 10% (ww/v) solids concentration processed at 200 cm h^{-1} in the Streamline 25 column.

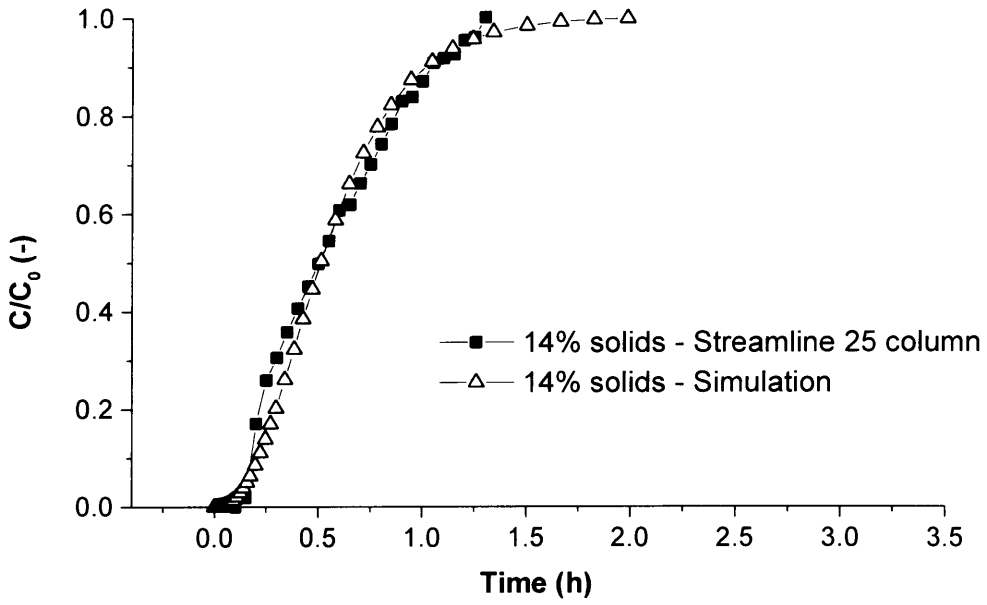

Figure 7.5. Experimental and simulated breakthrough curves for an *E. coli* homogenate feed-stream of 14% (ww/v) solids concentration processed at 200 cm h^{-1} in the Streamline 25 column.

7.2.4 Windows of Operation

The breakthrough curves simulated using the general rate model provided information for the generation of a series of Windows of Operation for a range of *E. coli* homogenate solids concentrations processed at different flow rates. From the breakthrough curves, yield and productivity was calculated from the following equations:

$$\%\ Fab\ yield\ =\ 100 \times \frac{Fab\ eluted}{Fab\ loaded} \qquad 7.6$$

$$Productivity\ =\ \frac{Fab\ eluted}{Processing\ time \times Matrix\ volume} \qquad 7.7$$

where it is assumed that all Fab bound is recovered during the elution step (Fab eluted = Fab bound). The processing time in Equation 7.7 includes column equilibration, sample loading, wash, elution and cleaning-in-place (CIP). For each

process, either a constant number of column volumes (CV) or a constant time was used (Table 7.3). The time for loading depends on the total feed volume to be processed (V_{load}) and the flow rate applied (U).

Table 7.3. The individual processes contributing towards the overall processing time for expanded bed adsorption in a 1 m ID column. For each process, either a constant CV or a constant time was applied. Time for wash-out was based on experimental values (Streamline 25 column), whereas times for equilibration, elution and CIP were based on values suggested in the literature (Barnfield-Frej *et al.*, 1994; Hjort, 1997).

Process step	**Number of CV (-)***	**Time (h)**
Column equilibration	-	0.67
Loading		V_{load}/U
Wash out unbound sample	5	-
Elution	3	-
CIP	-	6

*on a sedimented bed basis

The Windows of Operation presented express the operating conditions which fulfil predefined process performance criteria - in terms of yield, productivity and bed expansion - for each feed solids concentration as a function of flow rate applied. Table 7.1 provided information regarding the feed-streams to be processed, and Table 7.4 summarises the operational constraints that were applied when generating the Windows of Operation displayed in Figures 7.6-7.9.

Table 7.4. Operational constraints applied when generating Windows of Operation for the EBA process.

Constraints	**Value**
Minimum productivity (g L^{-1} h^{-1})	0.1
Minimum yield (%)	95
Maximum degree of expansion, H/H_0 (-)	3

Figures 7.6 a)-d) demonstrate the step-by-step development of the Window of Operation for a 15% (ww/v) solids feed-stream. In Figure 7.6 a) the shaded region defined by the blue lines labelled I) represents the available operating conditions if the process was constrained only by a minimum productivity of 0.1 g L^{-1} h^{-1}. Figure 7.6 b) displays the operating area corresponding to a yield of 95% and above - represented by the shaded area below the green line labelled II). The shaded region in Figure 7.6 c) corresponds to the operating conditions which are predicted to result in a productivity of 0.1 g L^{-1} h^{-1} and above *and* yield greater than 95%. This Window of Operation is generated by overlapping the regions presented in Figures 7.6 a) and 7.6 b). The final constraint to be considered is the maximum degree of expansion, represented by H/H_0. In this work the limit is defined by $H_{max} = 3H_0$, and the effect of incorporating this restriction in the Window of Operation for the processing of a 15% (ww/v) solids feed-stream is shown in Figure 7.6 d). The expansion constraint translates into an upper flow rate constraint - represented by the vertical red line labelled III) - above which one would expect H to exceed $3H_0$. This reduces the processing conditions available to the operating engineer, an effect that will be more significant the higher the viscosity of the feed stock applied.

Figure 7.7 presents the Window of Operation for processing of a 10% (ww/v) solids feed-stream when operation is constrained by a minimum productivity of 0.1 g L^{-1} h^{-1} – corresponding to the area between the blue lines I), a minimum yield requirement of 95% - below the green line II), and a maximum degree of expansion of $3H_0$ – to the left of the red line III). Due to the lower viscosity of the 10% (ww/v) feed relative to the 15% (ww/v) feed, the maximum flow rate at which one can operate the bed at and still be within the acceptable H/H_0 limit, is higher for the former. Hence the operating region for the 10% (ww/v) solids feed-stream is slightly larger than what was seen in Figure 7.6 for the 15% (ww/v) feed.

As seen in Figure 7.8, representing the Window of Operation for the feed-stream of 5% (ww/v) solids, there is no overlap between the regions defined by the productivity and the yield constraints at the lowest flow rates. This is due to the increase in total processing volume as feed solids concentration decreases, consequently leading to an increased processing time. At the lower level of flow rates the total processing time exceeds that which is acceptable if the pre-defined

level of productivity is to be met. Because of the reduced viscosity of this low solids concentration feed, the degree of expansion is predicted to be below $3H_0$ for all conditions investigated, hence line III) is not present in this Window of Operation.

For the 1% (ww/v) solids feed, the productivity requirement of 0.1 g L^{-1} h^{-1} could not be met. This is due to an extensive dilution of the assumed initial feed material (see section 7.2.2.1), resulting in a total processing volume of 15000 L and consequently a large increase in processing time. Figure 7.9 shows the Window of Operation for the 1% (ww/v) feed when operation is restricted by a minimum productivity of 0.01 g L^{-1} h^{-1} – between the blue lines I), and a minimum yield of 95% - below the green line II). As for the 5% (ww/v) feed-stream, the bed expansion is expected to be within the acceptable limit for all conditions investigated, hence the expansion constraint is not present in this Window of Operation.

Figures 7.6–7.9 demonstrate the trade-offs between load volume and flow rate that one has to consider when designing an expanded bed adsorption process. In the Windows of Operation presented, there is a relatively small margin between meeting the pre-defined performance criteria, and falling outside the defined limits. By manipulating the yield requirement, for example by aiming for a 90% yield instead of 95% - greater operating regions will be achieved as the limit is shifted upwards. This is demonstrated in Figure 7.10 for the case of the 10% (ww/v) feed-stream. If greater productivity is required, it will be on the expense of combinations of flow rate and load volume available, and the modified Window of Operation would indicate that the lowest flow rates are not feasible. This is illustrated in Figure 7.11 for the 10% (ww/v) homogenate feed-stream.

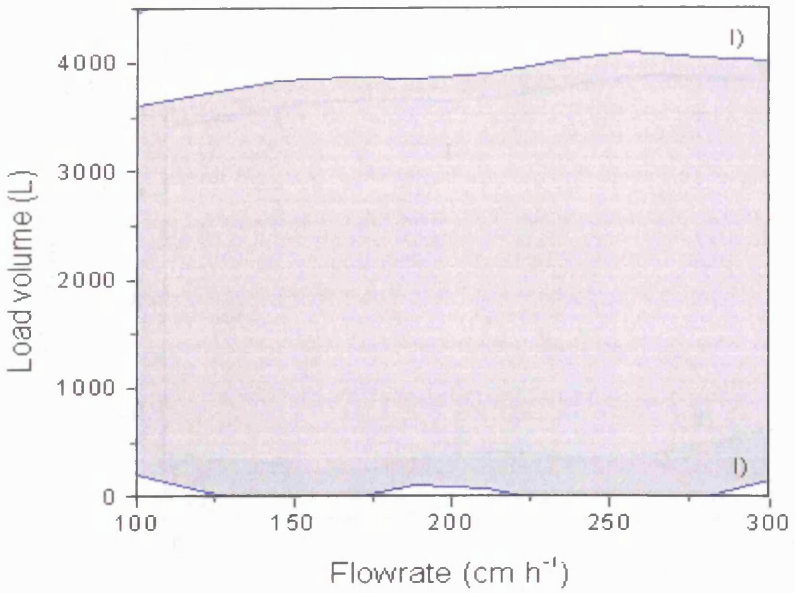

Figure 7.6 a). Window of Operation for a 15% (ww/v) solids *E. coli* homogenate feed-stream as it would appear if the process is limited only by the minimum productivity requirement of 0.1 g L^{-1} h^{-1}, represented by the shaded region constrained by the blue lines labelled I).

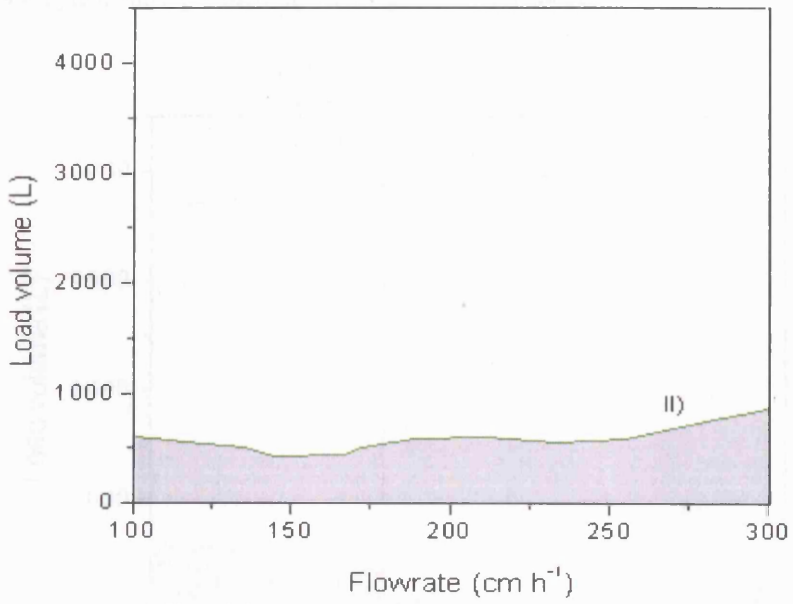

Figure 7.6 b). Window of Operation for a 15% (ww/v) solids *E. coli* homogenate feed-stream when assuming that the process is limited only by the minimum yield requirement of 95%, represented by the shaded area below the green line II).

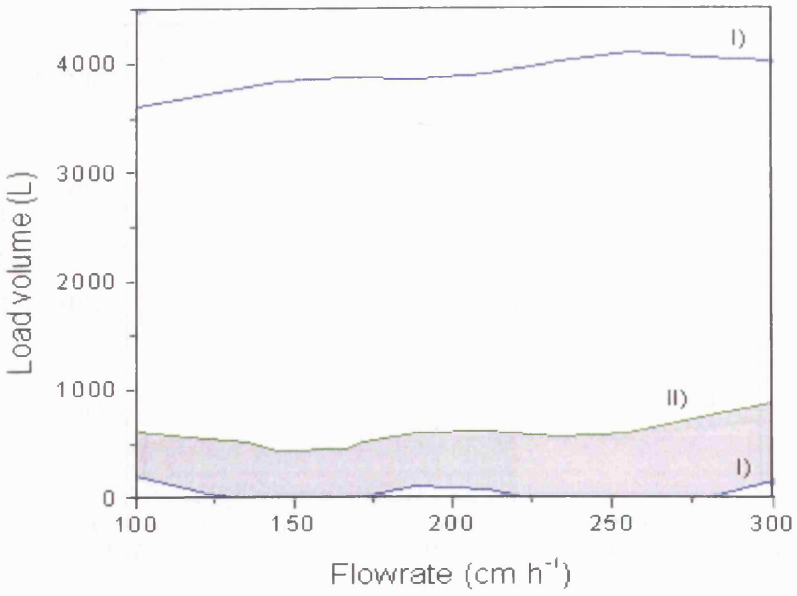

Figure 7.6 c). The Window of Operation for processing of a 15% (ww/v) solids *E. coli* homogenate feed-stream when operation is constrained by a minimum yield and a minimum productivity requirement. The shaded area represents operating conditions that meets the requirements of minimum 95% yield and a productivity of 0.1 g L^{-1} h^{-1} and above.

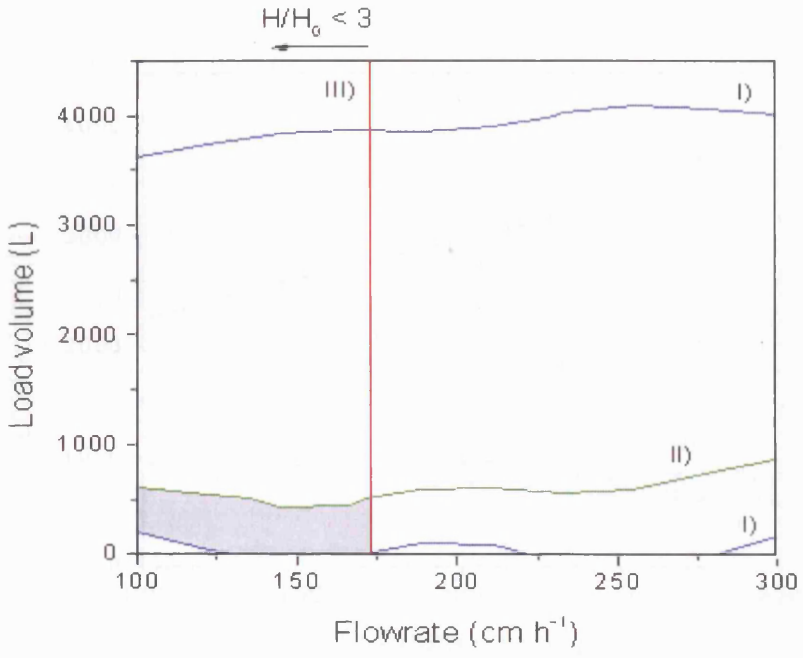

Figure 7.6 d). Window of Operation for a 15% (ww/v) solids *E. coli* homogenate feed-stream when the process is constrained by a minimum yield requirement, a minimum acceptable level of productivity and a maximum degree of expansion. The shaded region represents conditions predicted to give a yield > 95%, a productivity > 0.1 g L^{-1} h^{-1} and a bed expansion of maximum $3H_0$.

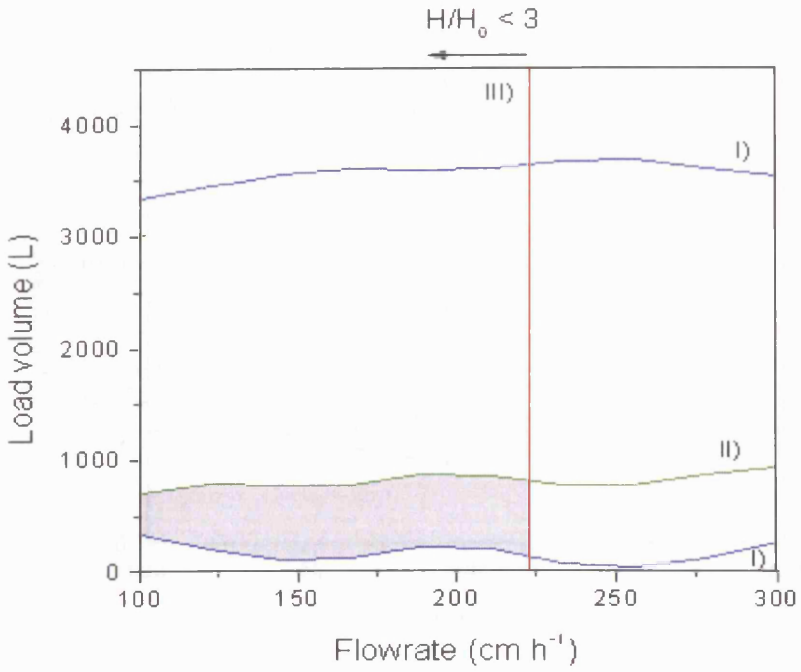

Figure 7.7. Window of Operation for a 10% (ww/v) solids *E. coli* homogenate feed-stream processed in a 1 m ID column. The shaded region represent the available operating conditions when the process is constrained by a minimum yield requirement of 95%, a minimum productivity of 0.1 g L^{-1} h^{-1} and a maximum expansion of $3H_0$.

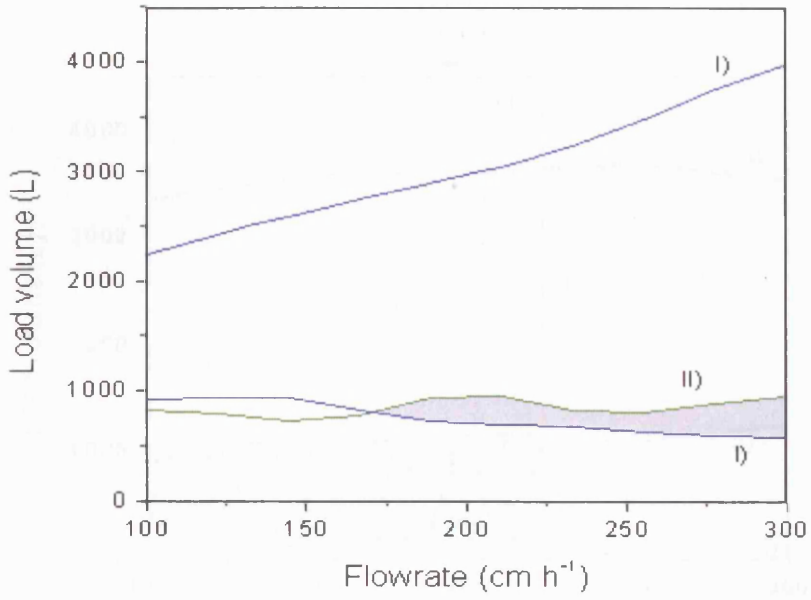

Figure 7.8. Window of Operation for an *E. coli* homogenate feed of 5% (ww/v) solids concentration processed in a 1 m ID column. The shaded region represents feasible operating conditions when the EBA process is restricted by a yield demand of greater than 95% and productivity higher than 0.1 g L^{-1} h^{-1}. Due to a low feed viscosity the bed expansion is expected to be within the acceptable limit for all conditions investigated.

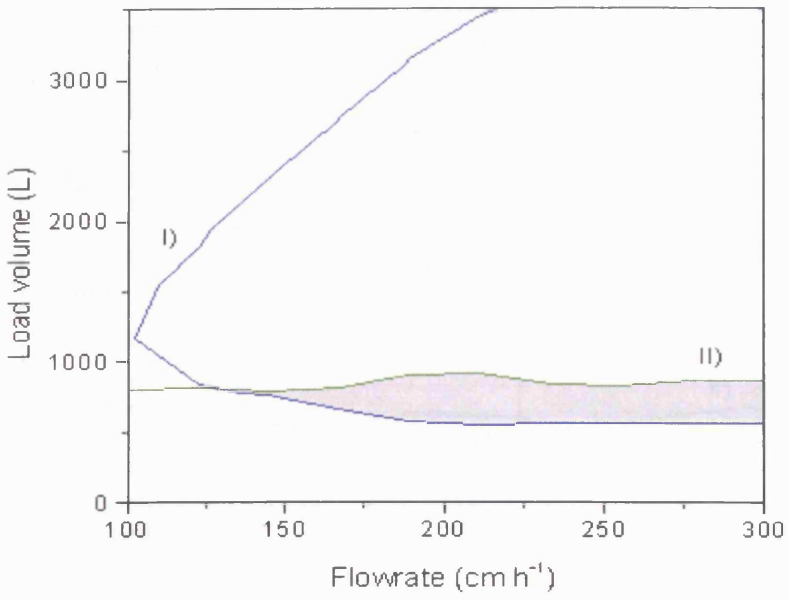

Figure 7.9. Window of Operation for an *E. coli* homogenate feed-stream of 1% (ww/v) solids concentration processed in a 1 m ID column. The productivity requirement of 0.1 g L^{-1} h^{-1} was not achievable for this dilute feed. Therefore the shaded region in this case represents available operating conditions when the process is restricted by a minimum yield of 95% and a minimum productivity of 0.01 g L^{-1} h^{-1}. Due to a low feed viscosity the bed expansion is expected to be within the acceptable limit for all conditions investigated.

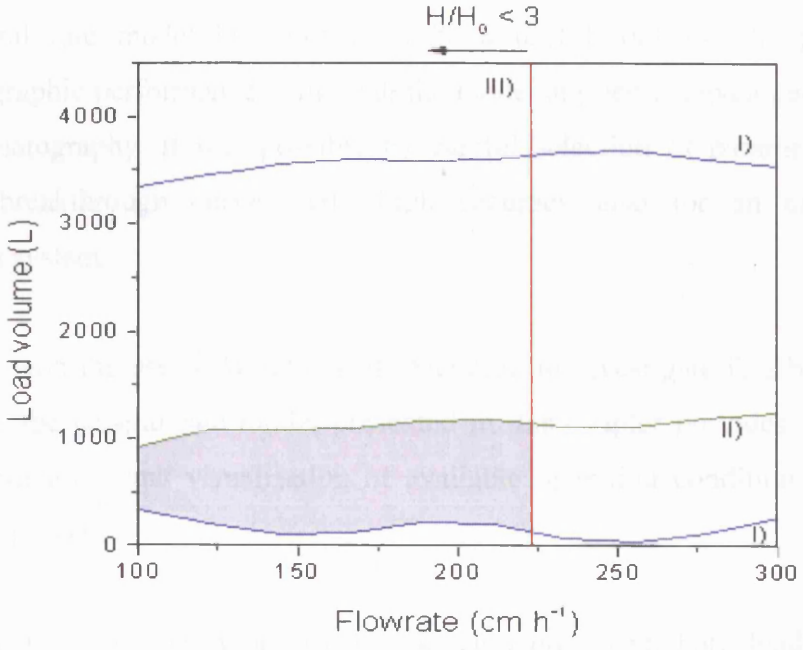

Figure 7.10. Window of Operation for the 10% (ww/v) solids *E. coli* homogenate feed-stream when the minimum yield requirement is reduced from 95% to 90%. The productivity is $\geq$ 0.1 g L^{-1} h^{-1}

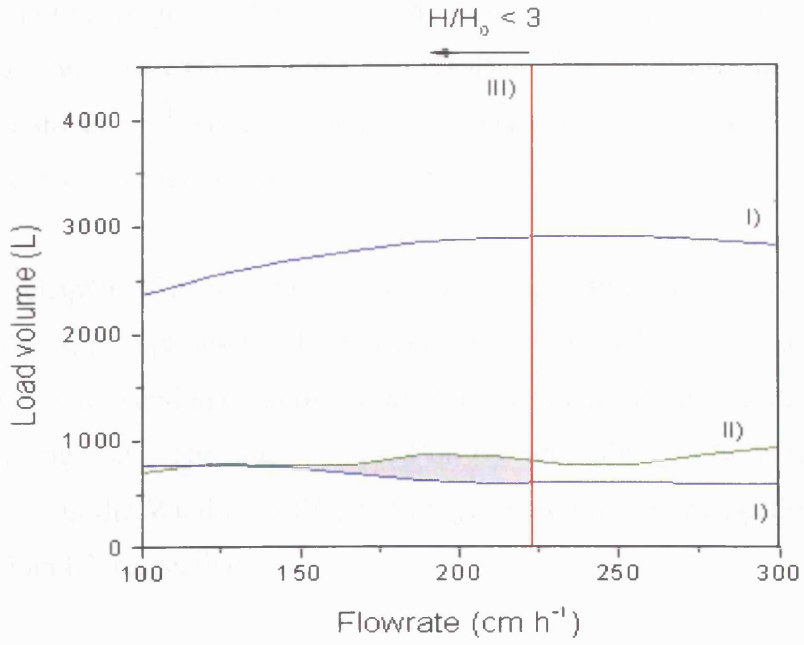

Figure 7.11. Window of Operation for the 10% (ww/v) solids *E. coli* homogenate feed-stream when the productivity requirement is increased from 0.1 to 0.2 g L^{-1} h^{-1}. The yield level is minimum 95%.

7.3 Summary

The general rate model has proved to be a useful tool for the prediction of chromatographic performance. Although the model applied is developed for packed-bed chromatography, it was possible by careful selection of parameter values to simulate breakthrough curves with high accuracy also for an expanded bed adsorption system.

Combined with the use of Windows of Operation to investigate feasible processing conditions, the general rate model presented in this chapter provides a tool for the rapid investigation and visualisation of available operating conditions for a large-scale EBA process.

As demonstrated by the Windows of Operation presented, both load volume and flow rate are important operating parameters when considering an expanded bed adsorption process. A relatively low load volume appears to be necessary in order to achieve the highest yields possible. Moreover, it was seen that the productivity

depended more strongly on flow rate as the feed solids concentration decreased. This is due to a larger processing volume as a result of dilution of the initial 15% (ww/v) solids feed-stream – consequently requiring increased flow rates in order to meet the pre-defined productivity criteria.

The next chapter (Chapter 8) presents a comparative study investigating two different flowsheet options for the recovery of Fab from *E. coli* homogenates: EBA versus a more conventional approach involving centrifugation, filtration and packed bed chromatography. The study is based on the identification of suitable operating conditions from the Windows of Operation generated for centrifugation and EBA in Chapters 5 and 7, respectively.

8 A comparison of two process flowsheet options for recovery and initial purification of Fab from *E. coli* homogenate

Abstract

The demands for antibodies and antibody derived therapeutics are high and as a consequence there is an increasing call for accelerated process development and optimisation. This thesis has focussed on methods for the rapid determination of suitable operating conditions for the recovery of antibody fragments from high cell density cultures. Windows of Operation have been presented for the unit operations of centrifugation (Chapter 5) and EBA (Chapter 7), based on the rapid assessment of process performance by scale-down predictions and by simulations, respectively. This chapter demonstrates how the information extracted from these Windows of Operation may be used to compare two different flowsheet options for the primary recovery of a Fab antibody fragment from *E. coli* homogenate. The process options investigated are expanded bed adsorption and a more conventional route, consisting of centrifugation, filtration and packed bed chromatography. It was found that EBA provided reduced processing times, higher yields and higher throughputs than the conventional process. The flowsheet based on centrifugation provided the greatest level of concentration.

8.1 Introduction

As a result of pressures on the pharmaceutical industry to increase the products' speed to market whilst keeping the costs at a minimum, the demand for tools aimed at evaluation of process options at an early stage in the development is increasing. Amongst decisions that have to be made are flowsheet selections, that is, which process route should one adopt for a given process duty.

This chapter considers two alternative processing routes for the primary recovery and initial purification of Fab from *E. coli* homogenate. EBA and a more conventional method, involving centrifugation, filtration and packed bed (PB) chromatography, will be explored. These flowsheet options are illustrated in Figure 8.1.

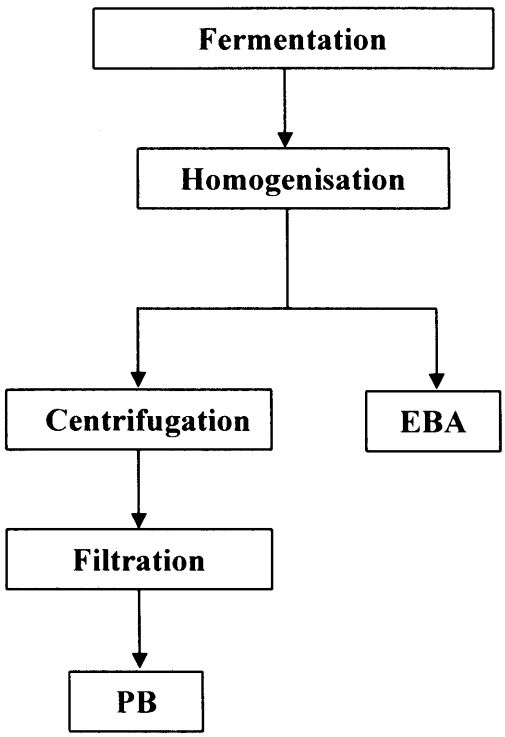

Figure 8.1. Flowsheet options for the primary recovery and initial purification of a Fab antibody fragment from *E. coli* homogenate. The conventional method involves solid-liquid separation by centrifugation. Further clarification is achieved by filtration and initial purification by packed bed chromatography. The EBA route offers solid-liquid separation, clarification and primary purification in one step.

A number of examples exist in literature that describe cell harvesting by centrifugation (Bentham *et al.*, 1990; Bracewell *et al.*, 2004; Clarkson *et al.*, 1996; Higgins *et al.*, 1978; Mosqueira *et al.*, 1981) and by EBA (Barnfield-Frej *et al.*, 1994; Brixius *et al.*, 2006; Brobjer, 1999; Chang *et al.*, 1995; Thömmes *et al.*, 1995), however only a few attempts are made to compare directly the two processes.

Johansson *et al.* (1996) compared an expanded bed approach to that of a conventional process for the recovery of a periplasmically expressed exotoxin A from *E. coli*. The conventional process comprised centrifugation, microfiltration and packed bed chromatography. The authors found that the EBA process was three times faster than the conventional route. In addition, the product volume was three times lower and the yield slightly higher in the EBA process.

When investigating the purification of a monoclonal antibody from a CHO culture by EBA and comparing the outcome to that of an approach based on clarification followed by packed bed chromatography, Fahrner *et al.* (1999) found that the expanded bed route compared well to that of the conventional method in terms of yield and purity. However, the authors expressed concern about the lifetime of an EBA column exposed to unclarified feeds, and the effect this may have on process economics.

Curbelo *et al.* (2003) performed a cost-comparative study and found that the superiority of EBA over a conventional centrifugation - filtration - packed bed approach depended greatly on factors such as the matrix lifetime and the capacity of the adsorbent. This work included the effects of cell-adsorbent interactions in the expanded bed. Such interactions were found to reduce the external mass transfer rate and result in a decreased matrix lifetime due to harsh CIP procedures.

Mustafa *et al.* (2004) applied a simulation tool for evaluating two flowsheet options for the recovery of a protein from a yeast culture, one based on EBA, the other using conventional solid-liquid separation followed by packed bed chromatography. The authors evaluated the different options from both a process and a business perspective. The expanded bed route was associated with lower cost of goods, and offered greater robustness than the conventional option.

8.2 Results and discussion

Section 8.2.1 provides a brief discussion of the basis for the comparison study performed in this chapter. Section 8.2.2 reproduces the Windows of Operation for the industrial centrifuges and the large-scale EBA column presented in Chapters 5 and 7, respectively. The route by which suitable operating conditions can be extracted from these Windows of Operation, and how this information may be used to produce process flowsheets and mass balances for the conventional process route as well as for EBA, is illustrated.

8.2.1 Basis for comparison

The previously developed Windows of Operation for processing of *E. coli* homogenate by centrifugation and EBA are based on ultra scale-down predictions and simulations, respectively. A detailed description of centrifugation scale-down methodology was provided in Chapter 4, whereas Chapter 5 presented the resulting Windows of Operation for a range of industrial centrifuges. These Windows of Operation visualised suitable operating conditions in terms of level of feed dilution (feed solids concentration) and flow rate, when the process was subject to certain pre-defined constraints. For the purpose of process comparisons, one set of operating conditions will be chosen for each centrifuge investigated. The operating conditions chosen from the Windows of Operation will determine the processing time for the centrifugation unit operation as well as the characteristics of the feed material to be processed in subsequent steps in the flowsheet. Due to the relatively poor centrifugal clarification performance predicted for *E. coli* homogenate (~50%) for relevant flow rates, a filtration step is necessary to provide further clarification of the feed. It is assumed that the filtration step is 100% efficient in the removal of solids from the feed-stream (Yavorsky *et al.*, 2003), and the processing time used for the filtration step is adapted from Johansson *et al.* (1996). For the final step in the conventional process flowsheet, packed bed (PB) chromatography, it is assumed that two cycles are necessary to process the filtered material in order to meet the required level of yield. Theoretical estimates of PB processing time were applied which for each cycle are based on load volume and flow rate, and time for equilibration, wash and elution.

For the final cycle CIP was also included. The required number of column volumes or duration for each of these processes is as given for EBA in Chapter 7, Table 7.3.

Chapter 7 discussed the use of the general rate model for simulation of the performance of an industrial-scale EBA process, and provided Windows of Operation for this unit operation. The EBA Windows of Operation illustrated available operating conditions in terms of load volume and flow rate, when the process was subject to certain constraints. For the purpose of generating EBA process flowsheets, one set of conditions will be chosen for each of the feed-streams of interest (5, 10 and 15% (ww/v) solids). As seen in Chapter 7, the feasible load volumes identified by the Windows of Operation were generally lower than the total volume to be processed. In order to process all the given feed material it was therefore necessary to perform the operation in several cycles. For the purpose of this comparison study, it was assumed that the processing time for each individual EBA cycle is based on time for equilibration, load, wash and elution, except for the final step, which also includes time for CIP.

Table 8.1 summarises the main parameter values applied when generating the process flowsheets and mass balances in the following section.

Table 8.1. The parameter values forming the basis for the process flowsheets presented.

	Centrifugation	**Filtration**	**PB/EBA**
Processing time	Equation 5.1	3 h (Johansson *et al.*, 1996)	Table 7.3
Yield	94% (90% for KB25)	90%	95%
Clarification	50% (Chapter 5)	100%	100%

For both processes, the basis for the generation of the Windows of Operation was a volume of 1000 L *E. coli* homogenate containing 15% solids (ww/v), with an initial Fab concentration of 0.5 mg mL^{-1}, as described in Chapters 5 and 7.

In this chapter the focus is the process perspective, and the analysis does not account for economical differences, or for any deterioration of the EBA matrix and the effect that would have on the comparison study.

8.2.2 Development of flowsheets and mass balances

Figures 8.2-8.4 illustrate the process flowsheets that are based on the conventional route, comprising centrifugation, filtration and packed bed chromatography. Three different processing alternatives are presented, based on initial solid-liquid separation by the SC35 disc-stack (Figure 8.2), the P18 Powerfuge™ (Figure 8.3) and the KB25 multi-chamber bowl centrifuge (Figure 8.4). The figures show how the centrifugal operating conditions in each case are chosen directly from the corresponding Window of Operation, and how these conditions serve to define the volume and the solids content of the feed to be processed further downstream in the flowsheet.

In the case of the SC35 disc-stack centrifuge (Figure 8.2), dilution of the initial homogenate feed-stream to 4% (ww/v) solids, combined with operation at 1500 Lh^{-1}, was regarded most feasible. This corresponds to an initial processing volume of 3750 L (based on a 1000 L homogenate batch of 15% (ww/v) solids, see above and Chapter 5) and a processing time of 2.5 h (according to Equation 5.1). The predicted clarification performance for the centrifugal separation of *E. coli* homogenate was determined in Chapter 5 and an average value of 50% clarification was used here. Based on this data it was calculated that ~75 L of solids would be removed from the initial process feed-stream by centrifugation. The difference between the initial feed volume and the solids removed gave the volume of suspension to be processed by the subsequent filtration step (3675 L). Assuming that the filtration step removes the remaining solids from the feed (75 L), the volume of clarified feed-stream applied onto the packed bed column could be determined (3600 L). It was assumed that two PB cycles were necessary to process this volume in order to achieve the required yield. The processing time for the packed bed unit operation was calculated as a function of load volume and flow rate (200 cm h^{-1}), and time for equilibration, wash and elution. For the second and final cycle CIP was also included in the processing time calculation. The final volume presented was based on elution using 3 CV buffer per cycle (see Table 7.3) and with basis in the initial volume (1000 L homogenate) this corresponds to a concentration factor of 1.4.

The approach described for the generation of the SC35 disc-stack flowsheet and mass balance was applied when analysing the processing options based on centrifugation by the P18 Powerfuge™ and the KB25 multi-chamber bowl machine in Figures 8.3 and 8.4, respectively.

Figures 8.5-8.7 present the flowsheets and mass balances for processing of feed-streams of 15% (Figure 8.5), 10% (Figure 8.6) and 5% (Figure 8.7) (ww/v) solids by EBA. A suitable combination of load volume and flow rate was chosen from the respective Windows of Operation. The load volume chosen determines the number of cycles needed to process the total volume of material, and combined with the corresponding flow rate this determines the processing time of the operation. For the case of the 15% (ww/v) feed-stream, the conditions chosen correspond to processing of the total volume of 1000 L in three cycles, each of 333 L. For a flow rate of 150 cm h^{-1} this results in a total processing time of 11.3 h. The processing time per cycle was calculated based on time for equilibration, load, wash and elution. For the last cycle the CIP was also included. The final liquid volume indicated in the figure was a result of elution using 3 CV buffer per cycle.

The above approach was also applied when analysing the flowsheets and mass balances for processing of feeds of 10% and 5% (ww/v) solids by EBA.

The information provided by the flowsheets may be used to assess parameters such as overall yield and processing time, throughput (the amount of Fab processed per hour) and the concentration factor of the process (initial volume/final volume). The outcome of the comparison study is presented in Table 8.2.

Table 8.2. Result of the flowsheet comparison study. Three conventional flowsheets, based on centrifugation by either the SC35 disc-stack, the P18 Powerfuge™ or the KB25 multi-chamber bowl, followed by filtration and packed bed chromatography, were assessed. In addition, three flowsheets based on processing of feed-streams of 5, 10 and 15% (ww/v) solids by EBA were investigated. The different processing options were compared in terms of processing time, overall yield, throughput and concentration factor.

	Conventional flowsheet			**EBA flowsheet**		
	SC35	**P18**	**KB25**	**15% feed**	**10% feed**	**5% feed**
Total processing time (h)	18.6	20.1	19.9	11.3	10.8	11.8
Overall yield (%)	80.4	80.4	77	95	95	95
Throughput (g h^{-1})	21.6	20.0	19.3	42.0	44.0	40.3
Concentration factor	1.4	1.4	1.4	0.9	0.9	0.7

The increased total processing time of the conventional flowsheets relative to the EBA processing routes reflects the relatively high level of dilution required to meet the pre-defined processing constraints in the former case, as visualised by the centrifugation Windows of Operation. The large volume to be processed has the most impact on the time taken to complete the packed bed chromatography step. The reduced yields achieved when applying the conventional flowsheet is a reflection of the fact that the overall yield decreases when the number of unit operations in the flowsheet increases, and the lower throughput is a direct result of the increased processing time and the reduced yield in the conventional route relative to the EBA flowsheet.

When comparing the three conventional flowsheets, the one based on centrifugation by the SC35 disc-stack appears to be the favourable choice both in terms of processing time, overall yield and throughput. This is a result of the higher flow rate chosen for this machine (see Figure 8.2), but is also related to its semi-continuous operation. Due to operation with intermittent discharge, the total downtime of this centrifuge is reduced compared to the semi-batch operated P18 Powerfuge™ and the batch KB25 multi-chamber centrifuge, as discussed in Chapter 4.

The EBA flowsheet for the feed-stream of 10% (ww/v) solids results in a lower processing time and a higher throughput compared to the EBA flowsheets for the 5%

and the 15% (ww/v) feeds. This observation demonstrates well the trade-offs between level of solids concentration and processing volume. A high solids concentration corresponds to a low level of dilution and hence a reduced volume to be processed. However, due to the increased feed viscosity as the solids content increases, the bed expansion is expected to be higher and the maximum flow rate at which one can operate, and still be within the upper limit of $3H_0$, is reduced. For a highly diluted feed material the total volume increases, but as seen in Figure 7.5 and reproduced in Figure 8.7, no expansion-constraint exists. As a result, operation at high flow rates is possible.

The sensitivity of the comparison approach described was investigated by relating the efficiency of the loading step (here defined as Fab produced per matrix volume and loading time) of the EBA process under the conditions selected, to the loading efficiency achieved when allowing for an increase in the total processing time of the EBA route to match that of the conventional process. The loading efficiency was calculated as a function of Fab bound to the adsorbent, the volume of adsorbent and the time for loading. The time for loading was calculated by subtracting the total times for equilibration, wash, elution and CIP from the overall processing time available. For the 10% (ww/v) EBA route the conditions selected in Figure 8.6 correspond to a loading efficiency of 4.1 g L^{-1} h^{-1}. When allowing for a total processing time identical to that of the conventional approach based on centrifugation by the SC35 disc-stack, the calculated loading efficiency is 0.46 g L^{-1} h^{-1}. In other words, up to a ten-fold reduction in loading efficiency can be accepted if the EBA flowsheet is to remain the favourable choice in terms of processing time and throughput in this case.

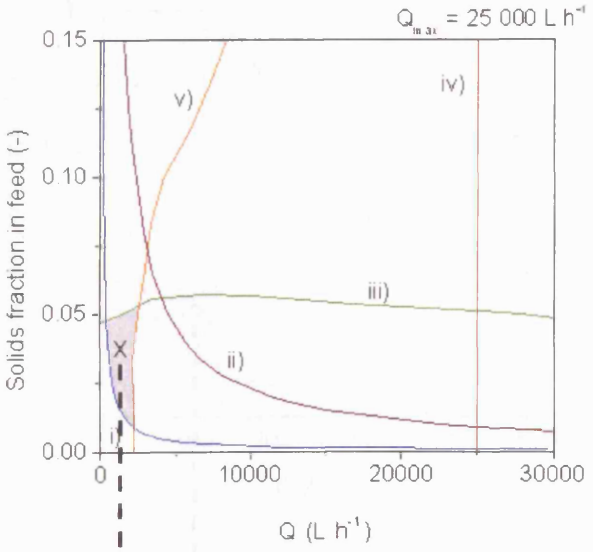

Figure 8.2. Processing of *E. coli* homogenate via the conventional route using the SC35 disc-stack centrifuge. Centrifuge operating conditions are chosen from the Window of Operation to the left (for details, see Chapter 5). Centrifugation is followed by filtration and packed bed chromatography. The mass balance for each step is indicated in the schematic below. Total processing time is estimated to 18.6 h and the overall yield ~80%. This corresponds to a throughput of 21.6 g Fab h^{-1}. The concentration factor is 1.4.

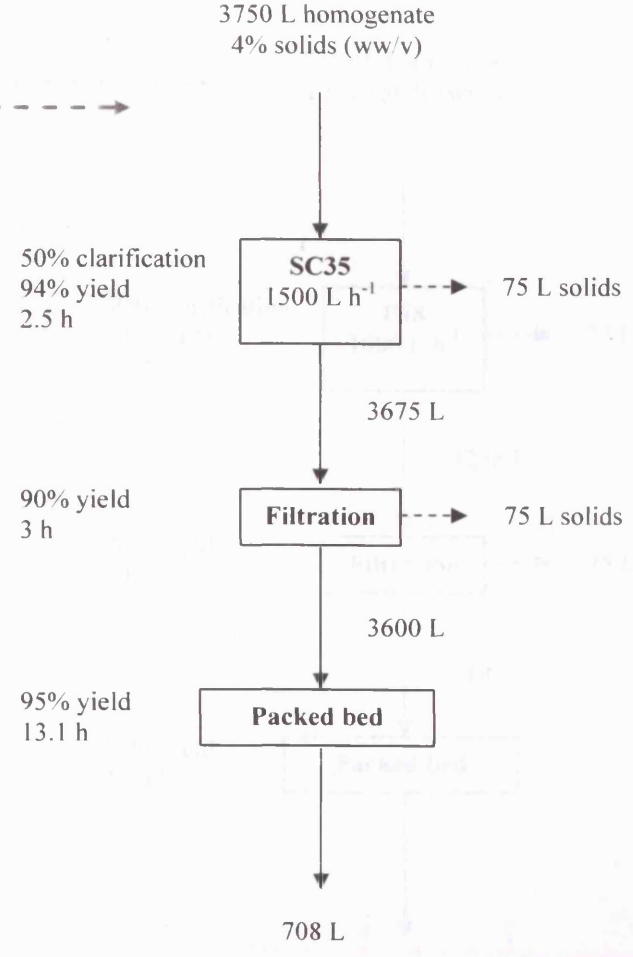

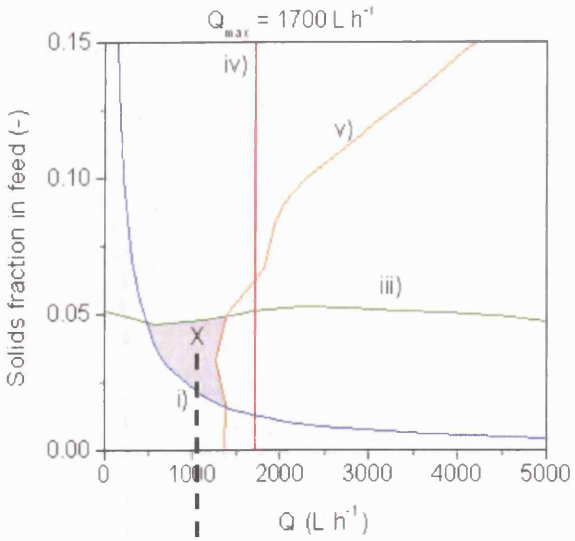

Figure 8.3. Processing of *E. coli* homogenate via the conventional route using the P18 Powerfuge™. Centrifuge operating conditions are chosen from the Window of Operation to the left (for details, see Chapter 5). Centrifugation is followed by filtration and packed bed chromatography. The mass balance for each step is indicated in the schematic below. Total processing time is estimated to 20.1 h and the overall yield ~80%, corresponding to a throughput of 20.0 g Fab h^{-1}. The concentration factor is 1.4.

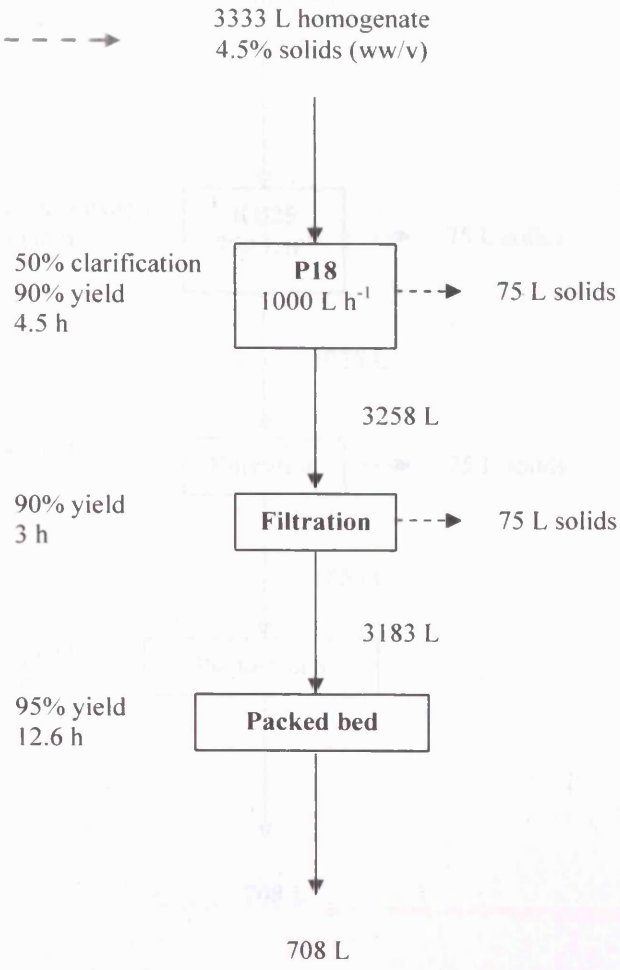

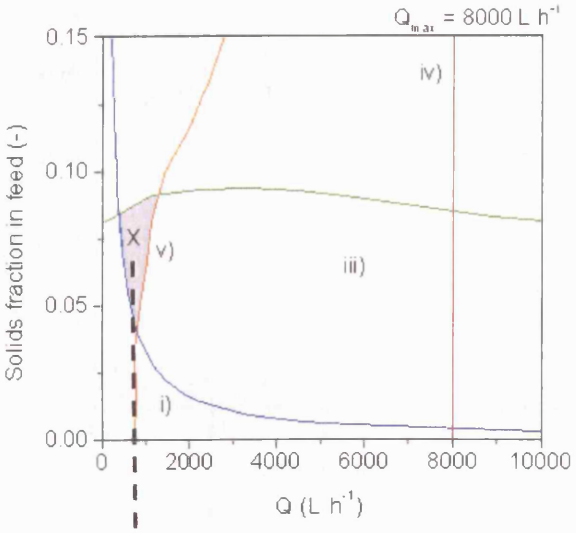

Figure 8.4. Processing of *E. coli* homogenate via the conventional route using the KB25 multi-chamber bowl, provided 2 bowls are available. Centrifuge operating conditions are chosen from the Window of Operation to the left (for details, see Chapter 5). Centrifugation is followed by filtration and packed bed chromatography. The mass balance for each step is indicated in the schematic below. Total processing time is estimated to 19.9 h and the overall yield 77%, corresponding to a throughput of 19.3 g Fab h^{-1}. The concentration factor is 1.4.

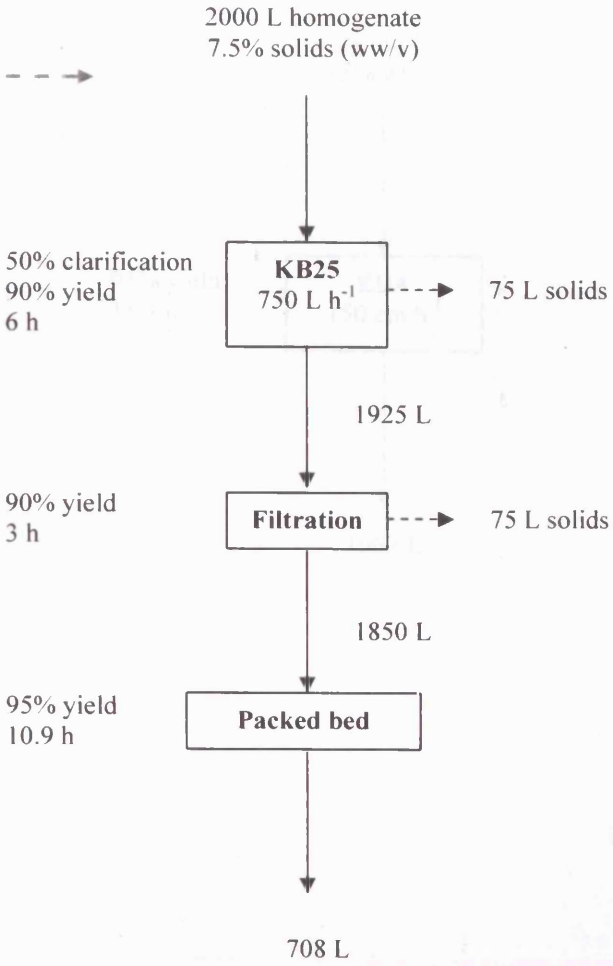

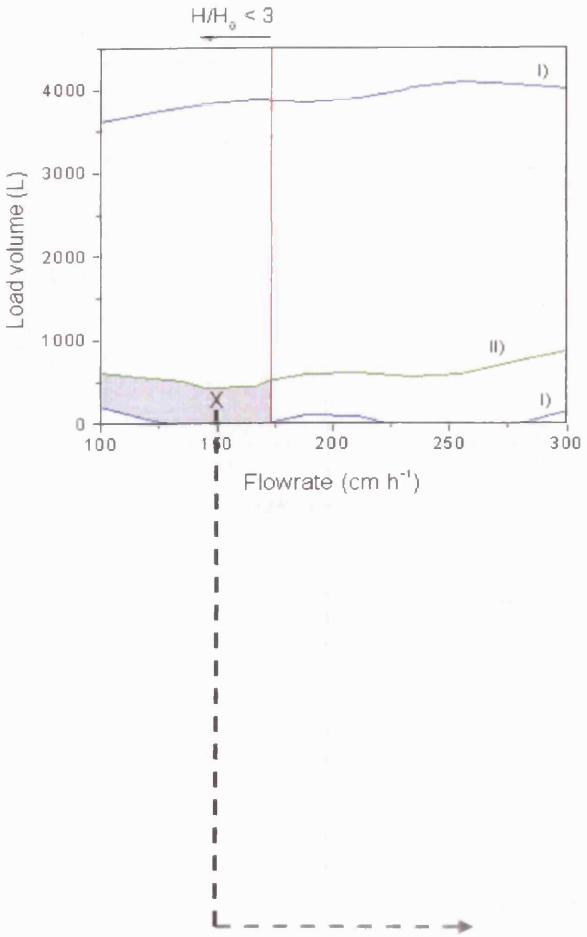

Figure 8.5. Flowsheet for the processing of *E. coli* homogenate containing 15% (ww/v) solids by EBA. Operating conditions in the form of load volume and flow rate are chosen from the Window of Operation to the left (for more information, see Chapter 7). In the case of the 15% (ww/v) feed, 3 cycles, each of 333 L, were necessary to process the total volume of homogenate. The flowsheet below shows the total mass balance. Total processing time was 11.3 h, the overall yield 95% and throughput was 42 g Fab h^{-1}. The concentration factor was 0.9.

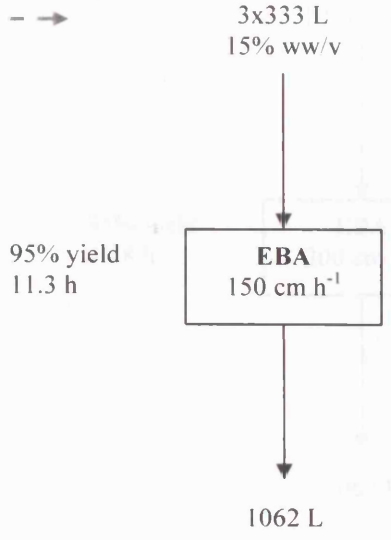

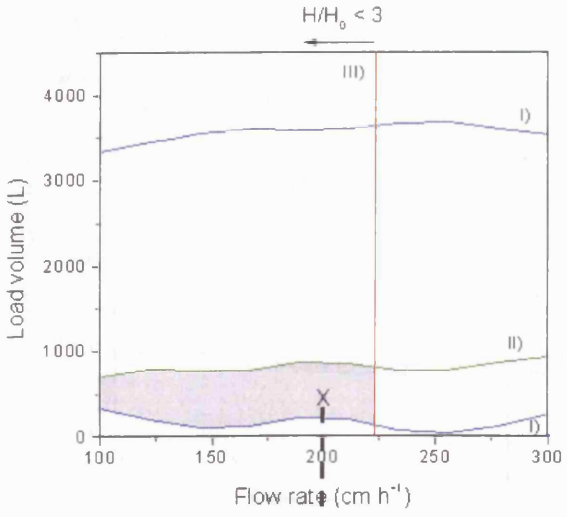

Figure 8.6. Flowsheet for the processing of *E. coli* homogenate containing 10% (ww/v) solids by EBA. Operating conditions in the form of load volume and flow rate are chosen from the Window of Operation to the left (for more information, see Chapter 7). In the case of the 10% (ww/v) feed, 3 cycles were necessary, each of 500 L, to process the total volume of homogenate. The flowsheet below shows the total mass balance. Total processing time was 10.8 h, the overall yield 95% and throughput was 44 g Fab h^{-1}. The concentration factor was 0.9.

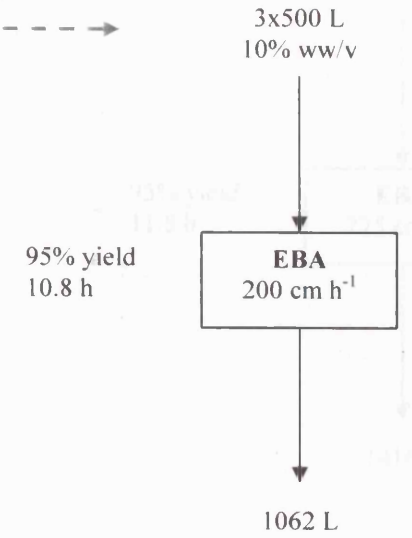

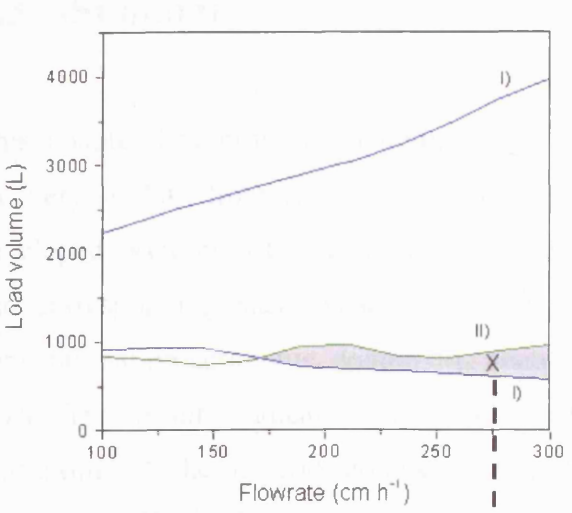

Figure 8.7. Flowsheet for the processing of *E. coli* homogenate containing 5% (ww/v) solids by EBA. Operating conditions in the form of load volume and flow rate are chosen from the Window of Operation to the left (for details, see Chapter 7). In the case of the 5% (ww/v) feed, 4 cycles were necessary, each of 750 L, to process the total volume of homogenate. The flowsheet below shows the total mass balance. Total processing time was 11.8 h, the overall yield 95% and throughput was ~40 g Fab h^{-1}. The concentration factor was 0.7.

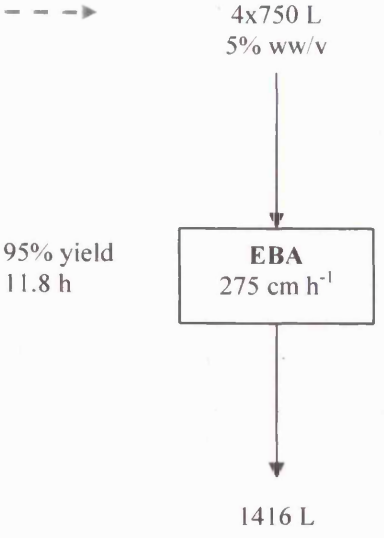

8.3 Summary

This chapter has provided a comparison of different flowsheet options for the recovery of Fab from *E. coli* homogenate. It was demonstrated how previously developed Windows of Operation may be used to produce such process flowsheets and corresponding mass balances for the process options under investigation: a conventional process route, comprising centrifugation, filtration and packed bed, and EBA. The results indicated that EBA is the favourable flowsheet option for processing of the *E. coli* homogenate in terms of processing time, yield and throughput. This reflects the fact that with a decrease in the number of processing steps the total processing time is reduced and higher overall yields are achieved. The higher throughput follows as a result of these observations.

Chapter 9 summarises the findings and conclusions of this thesis, and finally, Chapter 10 discusses ideas for future work.

9 Conclusions

This thesis has addressed the increasing demands for fast development of processes for the recovery of therapeutic antibody fragments from fermentation cultures. Predictive tools, such as scale-down techniques and process simulations, have been applied in order to enable the rapid assessment of alternative processing options and operating conditions. The work has identified and addresses some of the challenges related to the recovery of antibody fragments from high cell density expression systems by centrifugation and expanded bed adsorption.

Existing USD centrifugation approaches generated for dilute systems were found to over-predict the pilot-scale clarification performance when challenged with high cell density feed-streams. This was attributed to cell-cell interactions occurring in the low shear environment of the laboratory centrifuge tube, which consequently lead to aggregation, flocculation and blanket sedimentation. Such effects would not be apparent to the same extent in the settling region of a continuous-flow industrial centrifuge due to shear forces and irregular flow patterns. The work presented in this thesis describes a new ultra scale-down methodology for predicting centrifugal clarification performance in the case of high cell density cultures. The novel USD methodology described is based upon the dilution of high solids feed material down to ~2% (ww/v) solids, at which level cell-cell interactions are minimal, prior to the application of the clarification test. Mathematical corrections are applied to the resulting clarification curves in order to account for the effects of dilution in terms of i.e. reduced hindered settling and lower viscosity. The novel method was successfully verified in a CSA-1 pilot-scale disc-stack centrifuge. Prediction of separation performance of feeds containing up to 15% (ww/v) solids was demonstrated using whole *E. coli* cells and *E. coli* cells that had been subject to a periplasmic lysis step. Corrected USD curves accurately predicted pilot-scale clarification performance of the high cell density broths investigated, with an average error of 30%. In comparison, the conventional USD clarification method was associated with errors up to 1000%.

The novel USD methodology developed was applied to predict the clarification efficiency of *P. pastoris* cultures and *E. coli* homogenates of varying solids concentration. In addition, a USD tool to determine dewatering levels, and hence process yield, was described and applied to these feed stocks.

A series of Windows of Operation were generated for a range of industrially relevant centrifuges, based on the predicted centrifugal separation performance as generated by USD methodologies, combined with the identification and application of key constraints, which restrict the operation of each centrifuge type. The Windows of Operation generated provided for the identification of feasible operating conditions for the separation of *P. pastoris* and *E. coli* homogenate in disc-stack, multi-chamber and Carr Powerfuges^{TM}.

The centrifugation Windows of Operation developed revealed a significant difference in available operating conditions between *P. pastoris* and *E. coli* homogenate feeds of varying solids concentration. The significantly lower clarification and dewatering levels obtained for the latter feed stock resulted in a great reduction in available operating conditions when compared to the area of feasible processing conditions achieved for *P. pastoris* upon separation in the same centrifuge. However, for both systems, when subject to the same pre-defined constraints and limitations, the most appropriate centrifuge appeared to be the SC35 disc-stack. This machine provided the largest processing area for both systems. The estimated area of available operating conditions when using this disc-stack was ~300 L h^{-1} for the *P. pastoris* feed stock, and ~50 L h^{-1} for *E. coli* homogenate.

This project has also identified limitations to the existing system used for scale-down of EBA processes. The main challenge identified upon processing of *E. coli* homogenate by EBA was associated with interactions between nucleic acids and/or cell debris in the homogenate, and the adsorbent. The effects of these interactions were much more prominent in the scale-down bed compared to in the larger Streamline 25 column (the currently-accepted smallest column for scale-down studies), probably due to the high adsorbent particle diameter to column diameter ratio for the former bed. As a result, the level of expansion in the scale-down column

differed both from that estimated by theoretical correlations, and from the bed expansion observed in the Streamline 25 column when operated at the same flow rate and solids concentration. As a consequence of the increased level of expansion, the target protein experienced a longer residence time in the scale-down column than in the larger column. This could explain the enhanced the binding efficiency of the scale-down system relative to the Streamline 25 system, as indicated by a later Fab breakthrough and an over-prediction of the dynamic and total binding capacities of the Streamline 25 system by the scale-down bed. The total binding capacities of the Streamline 25 system were over-predicted by the scale-down bed by a factor of 2-2.5 (depending on level of solids concentration). Increasing the feed solids concentration resulted in a reduction of total capacity for both systems investigated, whereas the effect of solids concentration on the yield was mainly evident in the scale-down column.

As an adjunct to EBA scale-down, industrial-scale process performance was investigated using the general rate model. The general rate model proved to be a useful tool for the prediction of the performance of an EBA process handling *E. coli* homogenates at varying solids concentrations. Although the model applied was developed for packed-bed chromatography, it was possible by appropriate selection of parameter values to simulate breakthrough curves with high accuracy also for an expanded bed adsorption system. The results achieved formed the basis for the generation of a series of Windows of Operation, displaying the most suitable combinations of EBA load volume and flow rate needed to achieve defined levels of yield and productivity when processing *E. coli* homogenates at a range of solids concentrations. These Windows of Operation demonstrated that both load volume and flow rate are important operating parameters to consider when designing an expanded bed adsorption process. Another factor to consider is the expected degree of expansion. For all feed-streams investigated a relatively low load volume appears to be necessary in order to achieve the highest yields possible. Moreover, it was seen that the productivity achieved depended more strongly on flow rate as the feed solids concentration decreased. This is due to a larger processing volume as a result of dilution of the initial 15% (ww/v) solids feed-stream – which in turn requires increased flow rates in order to meet the pre-defined levels of productivity. For the

feed-streams of 10 and 15% (ww/v) solids, the highest flow rates were unavailable due to excessive expansion.

A comparative study was performed, evaluating different flowsheet options for the recovery of Fab from *E. coli* homogenate. Based on the identification of suitable operating conditions from the previously developed Windows of Operation, process flowsheets and corresponding mass balances were generated for the process options under investigation: a conventional process route, comprising centrifugation, filtration and packed bed chromatography, and one employing EBA. The results suggest that for this system, an EBA-based route provides higher yields, shorter processing times and greater throughput relative to more conventional processing routes.

From the main findings and conclusions of this work, it is evident that the ability to predict, and to visualise, the performance of large-scale unit operations on the basis of small-scale mimics and/or simulations is a major factor contributing towards the rapid and successful development of individual process steps as well as process flowsheets. This thesis has examined some key aspects of the recovery of recombinant products where issues of high initial cell densities must be dealt with. A series of techniques have been developed and then verified at scale to confirm their utility.

10 Future work

This final chapter will consider areas that would be of interest for future work which have been identified during the course of this project.

10.1 USD centrifugation

The new USD clarification approach developed in Chapter 4 was verified at pilot-scale for *E. coli* whole cells and for periplasmically lysed *E. coli* cells for solids concentrations of up to 14% and 9% (ww/v) respectively. Although this is believed to provide a sufficient validation of the methodology, for further confidence it would be of interest to 1) validate the USD clarification results presented for *P. pastoris* and *E. coli* homogenate in Chapter 4, and 2) challenge the methodology with bacterial or yeast cultures of even higher solids concentration.

When it comes to future USD centrifugation work, emphasis should now turn to developing a robust and reproducible ultra scale-down dewatering methodology, and to validate the approach at large-scale. Work is currently being done at UCL to improve further the method for the determination of the centrifugal dewatering of bacterial and yeast systems. Like the method described in this thesis, the new approach involves a careful consideration of the relative centrifugal force and spin time applied at lab-scale in order to mimic as accurately as possible the conditions in the pilot centrifuge. In addition, cake compressibility has been identified and found to be of great importance to the success of dewatering scale-down mimics. Cake compressibility is dependent on sediment height, and it has been found that by mimicking at the lab-scale the actual sediment height in a Carr Powerfuge^{TM}, the dewatering can be predicted to an accuracy of ±0.5%. (Tustian *et al.*, 2006, manuscript in preparation).

10.2 EBA scale-down

As discussed in Chapter 6, the effects of cell-cell and/or cell-adsorbent interactions were much more prominent in the scale-down column compared to in the Streamline 25 column, and the scaling between the two beds was therefore not as successful as hoped for. When analysed as an isolated system, key performance characteristics of the scale-down bed were as expected, following the usual trends of, for example, increased expansion upon loading a more viscous sample, and the results revealed the expected variation in breakthrough with flow rate and solids concentration. This suggests that the SD system can be used to predict the performance of larger beds, but that this will require a more careful monitoring of cell-adsorbent interactions. For future experimentation it is recommended to perform a more extensive method optimisation study, not only focusing on the optimal conditions for product binding and elution, but also including a study of the effects of pH and conductivity on cell-cell and cell-adsorbent interactions. This could for example be done according to the pulse/response method described by Feuser *et al.* (1999). The method involves the injection of a pulse of cells onto the column and measurement of the optical density at 600 nm before and after passage through the expanded bed. The ratio of pulse area before and after column is a measure of the degree of cell transmission, with a high level of transmission corresponding to a low level of cell-adsorbent interactions.

In the case of the SD column, the aggregation effect is believed to have been enhanced due to the high d_p/D_c ratio. The high ratio of particle to column diameter is potentially a limitation of the current SD bed, and increasing D_c would probably reduce the risk of formation of aggregate clumps, though clearly at the expense of requiring more material for the studies. This result perhaps indicates a limitation of the current SD approach.

10.3 Windows of Operation

In order to validate the Windows of Operation generated for centrifugation and EBA, it would be of interest to run the processes under conditions identified as feasible by

the Windows of Operation presented in Chapters 5 and 7, respectively. By comparing the actual outcome, in terms of clarification performance and yield for centrifugation, and yield and productivity for EBA, to that predicted by the respective Windows of Operation, one would get an idea of the accuracy and the reliability of the Windows of Operation.

10.4 Flowsheet decisions

The flowsheet study presented in Chapter 8 was based on USD predictions and simulations for the centrifugation and EBA unit operations, respectively, whereas the filtration and packed bed steps were based on theoretical estimates. For the purpose of this thesis this approach provided sufficient accuracy, as the aim was merely to suggest how the information generated throughout this thesis could be used to investigate rapidly alternative flowsheet options for product recovery. Should a more thorough investigation be required, the study might include experimental results for the filtration and packed bed steps, as determined for example by scale-down mimics. It would also be of interest to include process economics in the study, including the EBA adsorbent lifetime. This would yield a more industrially representative insight as to the relative merits of the different approaches.

References

Ambler, C.M. (1959) The theory of scaling up laboratory data for the sedimentation type centrifuge. Journal of biochemical and microbiological technology and engineering, **1**: 185-205

Ambler, C.M. (1961) The fundamentals of separation, including Sharple's "Sigma value" for predicting equipment performance. Industrial and engineering chemistry, **53** (6): 430-433

Ames, G.F-L., Prody, C., Kustu, S. (1984) Simple, rapid and quantitative release of periplasmic proteins by chloroform. Journal of bacteriology, **160**: 1181-1183

Anspach, F.B., Curbelo, D., Hartmann, R., Garke, G. and Deckwer, W.D. (1999) Review: Expanded-bed chromatography in primary protein purification. Journal of Chromatography A, **865**: 129-144

Baj, Y., Glatz, C.E. (2003) Capture of a recombinant protein from unclarified canola extract using Streamline expanded bed anion exchange. Biotechnology and bioengineering, **81**: 855-864

Baneyx, F. (1999) Recombinant protein expression in *Escherichia coli*. Current opinion in biotechnology, **10**: 411-421

Barnfield-Frej, A.-K., Hjort, R., Hammarstrom, Å. (1994) Pilot-scale recovery of recombinant annexin V from unclarified *Escherichia coli* homogenate using expanded bed adsorption. Biotechnology and bioengineering, **44**: 922-929

Barnfield-Frej, A.-K., Johansson, H.J., Johansson, S., Leijon, P. (1997) Expanded bed adsorption at production scale: scale-up verification, process expamle and sanitization of column and adsorbent. Bioprocess engineering, **16**: 57-63

Batt, B.C., Yabannavar, V.M., Singh, V. (1995) Expanded bed adsorption process for protein recovery from whole mammalian cell culture broth. Bioseparation, **5** (1): 41-52

Bentham, A.C., Bonnerjea, J., Orsborn, C.B., Ward, P.N., Hoare, M. (1990) The separation of affinity flocculated yeast cell debris using a pilot-plant scroll decanter centrifuge. Biotechnology and bioengineering, **36**: 398-401

Bird, R.E., Hardman, K.D., Jacobson, J.W., Johnson, S., Kaufman, B.M., Lee, S.M., Lee, T., Pope, S.H., Riordan, G.S. and Whitlow, M. (1988) Single-chain antigen-binding proteins. Science, **242**: 423-426

Boychyn, M., Doyle, W., Bulmer, M., More, J., Hoare, M. (2000) Laboratory scaledown of protein purification processes involving fractional precipitation and centrifugal recovery. Biotechnology and bioengineering, **69** (1): 1-10

Boychyn, M., Yim, S.S.S., Ayazi Shamlou, P., Bulmer, M., More, J., Hoare, M. (2001) Characterisation of flow intensity in continuous centrifuges for the development of laboratory mimics. Chemical engineering science, **56:** 4758-4770.

Boychyn, M., Yim, S.S.S., Bulmer, M., More, J., Bracewell, D.G., Hoare, M. (2004) Performance prediction of industrial centrifuges using scale-down models. Bioprocess and biosystems engineering, **26**: 385-391

Bowering, L.C. (2002) An engineering study of the design, integration and control of antibody fragment production processes, PhD Thesis, University of London

Bracewell, D.G., Brown, R.A., Hoare, M. (2004) Addressing a whole bioprocess in real-time using an optical biosensor-formation, recovery and purification of antibody fragments from a recombinant *E. coli* host. Bioprocess and biosystems engineering, **26**: 271-282

Bradford, M. (1976) A rapid and sensitive method for quantification of microgram quantities of protein using the principle of protein-dye binding. Analytical biochemistry, **72**: 248-254

Brady, C.P., Shimp, R.L., Miles, A.P., Whitmore, M., Stowers, W. (2001) High-level production and purification of P30P2MSP1$_{19}$, an important vaccine antigen for malaria, expressed in the methylotropic yeast *Pichia pastoris*. Protein expression and purification, **23**: 468-475

Brinkmannn, U., Di Carlo, A., Vasmatzis, G., Kurochkina, N., Beers, R., Lee, B., Pastan, I. (1997) Stabilization of a recombinant Fv fragment by base-loop interconnection and V_H-V_L permutation. Journal of molecular biology, **268**: 107-117

Brixius, P., Mollerup, I., Jensen, O.E., Halfar, M., Thömmes, J., Kula, M-R. (2006) Expanded bed adsorption as a primary recovery step for the isolation of the insulin precursor MI3 process development and scale-up. Biotechnology and bioengineering, **93**: 14-20

Brobjer, M. (1999) Development and scale up of a capture step (expanded bed chromatography) for a fusion protein expressed intracellularly in *Escherichia coli*. Bioseparation, **8**: 219-228

Calado, C.R.C., Cabral, J.M.S., Fonseca, L.P. (2002) Effect of Saccharomyces cerevisiae fermentation conditions on expanded bed adsorption of heterologous cutinase. Journal of chemical technology and biotechnology, **77**: 1231-1237

Carter, P., Kelley, R.F., Rodrigues, M.L., Snedcor, B., Covarrubias, M., Velligan, M.D., Wong, W.L.T., Rowland, A.M., Kotts, C.E., Carver, M.E., Yang, M., Bourell, J.H., Shepare, H.M., Henner, D. (1992) High level *Escherichia coli* expression and production of a bivalent humanised antibody fragment. Bio/Technology, **10**: 163-167

Cereghino, J.L. and Cregg, J.M. (2000) Heterologous protein expression in the methylotrophic yeast *Pichia pastoris*. FEMS Microbiology Reviews, **24**: 45-66

Chang, Y.K., McCreath, G.E., Chase, H.A. (1995) Development of an expanded bed technique for an affinity purification of G6PDH from unclarified yeast cell homogenates. Biotechnology and bioengineering, **48**: 355-366

Chang, Y.K., Chase, H.A. (1996) Development of operating conditions for protein purification using expanded bed techniques: the effect of the degree of bed expansion on adsorption performance. Biotechnology and bioengineering, **49**: 512-526

Chang, C., Lenhoff, A.M. (1998) Comparison of protein adsorption isotherms and uptake rates in preparative cation-exchange materials. Journal of chromatography A, **827**: 281-293

Chen, W-D., Dong, X-Y., Sun, Y. (2003) Modeling of the whole expanded-bed protein adsorption process with yeast cell suspensions as feedstock. Journal of chromatography A, **1012**: 1-10

Chung, S.F., Wen, C.Y. (1968) Longitudinal dispersion of liquid flowing through fixed and fluidized beds. AIChE Journal, **14**: 857-866

Clarkson, A.I., Bulmer, M., Titchener-Hooker, N.J. (1996) Pilot-scale verification of a computer-based simulation for centrifugual recovery of biological particles. Bioprocess Engineering, **14**: 81-89.

Cregg, J.M., Cereghino, J.L., Shi, J. and Higgins, D.R. (2000) Review: Recombinant protein expression in *Pichia pastoris*. Molecular Biotechnology, **16**: 23-52

Curbelo, D.R., Garke, G., Guilarte, R.C., Anspach, F.B., Deckwer, W-D. (2003) Cost comparison of protein capture from cultivation broths by expanded and packed bed adsorption. Engineering and life science, **3** (10): 406-415

Daly, R., Hearn, M.T.W. (2005) Review: Expression of heterologous proteins in *Pichia pastoris*: a useful experimental tool in protein engineering and production. Journal of molecular recognition, **18**: 119-138

Dasari, G., Prince, I., Hearn, M.T.W. (1993) High performance liquid chromatography for amino acids, peptides and proteins: CXXIV. Physical characterization of fluidized bed behaviour of chromatographic packing materials. Journal of chromatography, **631**: 115-124

Di Felice, R., (1995) Hydrodynamics of liquid fluidisation. Chemical engineering science, **50** (8): 1213-1245

Donovan, R.S., Robinson, C.W., Glick, B.R. (1996) Review: optimizing inducer and culture conditions for expression of foreign proteins under the control of the lac promoter. Journal of industrial microbiology and biotechnology, **16**: 145-154

Eldin, P., Pauza, M.E., Hieda, Y., Lin, G., Murtaugh, M.P., Pentel, P.R and Pennell, C.A. (1997) High-level secretion of two antibody single chain Fv fragments by *Pichia* pastoris. Journal of immunological methods, **201**: 67-75

Expanded bed adsorption handbook – Principles and methods, GE Healthcare, Sweden

Fahrner, R.L., Blank, G.S., Zapata, G.A. (1999) Expanded bed protein A affinity chromatography of a recombinant humanized monoclonal antibody: process development, operation, and comparison with a packed bed method. Journal of biotechnology, **75**: 273-280

Fenneteau, F., Aomari, H., Chahal, P., Legros, R. (2003) Modeling of scale-down effects on the hydrodynamics of expanded bed adsorption columns. Biotechnology and bioengineering, **81**: 790-799

Fernandez-Lahore, H.M., Kleef, R., Kula, M.-R., Thömmes, J. (1999) The influence of complex biological feedstock on the fluidisation and bed stability in expanded bed adsorption. Biotechnology and bioengineering, **64**: 484-496

Feuser, J., Walter, J., Kula, M-R., Thömmes, J. (1999a) Cell/adsorbent interactions in expanded bed adsorption of proteins. Bioseparation, **8**: 99-109

Feuser, J., Halfar, M., Lutkemeyer, D., Ameskamp, N., Kula, M.-R., Thömmes, J. (1999b) Interaction of mammalian cell culture broth with adsorbents in expanded bed adsorption of monoclonal antibodies. Process biochemistry, **34**: 159-165

Fisher, R., Drossard, J., Emans, N., Commandeur, U., Hellwig, S. (1999) Review: Towards molecular farming in the future: *Pichia pastoris*-based production of single-chain antibody fragments. Biotechnology and applied biochemistry, **30**: 117-120

Frenken, L.G.J., Hessing, J.G.M., Van den Hondel, C.A.M.J.J., Verrips, C.T. (1998) Recent advances in the large-scale production of antibody fragments using lower eukaryotic microorganisms. Research in immunology, **149**: 589-599

Gardner, P.J., Willoughby, N., Hjorth, R., Lacki, K., Titchener-Hooker, N.J. (2004) Use of dimensionless residence time to study variations in breakthrough behaviour in expanded beds formed from varied particle size distributions. Biotechnology and bioengineering, **87** (3): 347-353

Ghose, S., Chase, H. (2000a) Expanded bed chromatography of proteins in small diameter columns. I. Scale down and validation. Bioseparation, **9**: 21-28

Ghose, S., Chase, H. (2000b) Expanded bed chromatography of proteins in small diameter columns. II. Methods development and scale up. Bioseparation, **9**: 29-36

Glennie, M.J. and Johnson, P.W.M. (2000) Review: Clinical trials of antibody therapy. Immunology today, **21** (8): 403-410

Glockshuber, R., Malia, M., Pfitzinger, I. and Plückthun, A. (1990) A comparison of strategies to stabilize immunoglobulin F_v-fragments. Biochemistry, **29**: 1362-1367

Glockshuber, R., Schmidt, T. and Plückthun, A. (1992) The disulfide bonds in antibody variable domains: Effects on stability, folding in vitro, and functional expression in *Escherichia coli*. Biochemistry, **31**: 1270-1279

Goto, M., Imamura, T., Hirose, T. (1995) Axial dispersion in liquid magnetically stabilized fluidized beds. Journal of chromatography A, **690**: 1-8

Gu, T., Tsai, G.J., Tsao, G.T. (1993) Modeling of nonlinear multicomponent chromatography. Advances in biochemical engineering/Biotechnology, **49**: 45-71

Gu, T. (1995) Mathematical modelling and scale-up of liquid chromatography. Springer Verlag, Berlin

Gutenwik, J., Nilsson, B., Axelsson, A. (2004) Effect of hindered diffusion on the adsorption of proteins in agarose gels using a pore model. Journal of chromatography A, **1048**: 161-172

Harrison, J.S., Kesharvarz-Moore, E., Dunnill, P., Berry, M.J., Fellinger, A., Frenken, L. (1997) Factors affecting the fermentative production of a lyzosyme-binding antibody fragment in *Escherichia coli*. Biotechnology and bioengineering, **53**: 611-622

Higgins, J.J., Lewis, D.J., Daly, W.H., Mosqueira, F.G., Dunnill, P., Lilly, M.D. (1978) Investigation of the unit operations involved in the continuous flow isolation of β-galactosidase from *Escherichia coli*. Biotechnology and bioengineering, **20**: 183-202

Hjort, R. (1997) Expanded-bed adsorption in industrial processing: recent developments. Tibtech, **15**: 230-235

Jahic, M., Gustavsson, M., Jansen, A.K., Martinelle, M. and Enfors, S-O. (2003) Analysis and control of proteolysis of a fusion protein in *Pichia pastoris* fed-batch processes. Journal of Biotechnology, **00**: 1-9

Johansson, H.J., Jagersten, C., Shiolach, J. (1996) Large scale recovery and purification of Periplasmic recombinant protein from *E. coli* using expanded bed adsorption chromatography followed by new ion exchange media. Journal of biotechnology, **48**: 9-14

Johnson, B.H., Hecht, M.H. (1994) Recombinant proteins can be isolated from *E. coli* by repeated cycles of freezing and thawing. Bio/Technology, **12**: 1357-1360

Joosten, V., Lokman C., van den Hondel, C. and Punt, P.J. (2003) The production of antibody fragments and antibody fusion proteins by yeasts and filamentous fungi. Microbial Cell Factories, **2**:1-15

Kaczmarski, K., Antos, D., Sajonz, H., Sajonz, P., Guiochon, G. (2001) Comparative modeling of breakthrough curves of bovine serum albumin in anion-exchange chromatography. Journal of chromatography A, **925**: 1-17

Kaczmarski, K., Bellot, J-C. (2004) Theoretical investigation of axial and local particle size distribution on expanded bed adsorption process. Biotechnology progress, **20**: 786-792

Kaczmarski, K., Bellot, J-C. (2005) Influence of particle diameter distribution on protein recovery in the expanded bed adsorption process. Journal of chromatography A, **1069**: 91-97

King, J.M.P., Griffiths, P., Zhou, Y., Titchener-Hooker, N.J. (2004) Visualising bioprocesses using '3D-Windows of Operation'. Journal of chemical technology and biotechnology **79**: 518–525.

Korz, D.J., Rinas, U., Hellmuth, K., Sanders, E.A., Deckwer, W.D. (1995). Simple fed-batch technique for high cell density cultivation of *Escherichia coli*. Journal of biotechnology, **39**: 59-65

Leung, W. W-F. (1998) Industrial centrifugation technology. McGraw Hill, New York

Levy, S., Collins, I.J., Yim, S.S., Titchener-Hooker, N.J., Shamlou, P.A., Dunnill, P. (1999) Effect of shear on plasmid DNA in solution. Bioprocess and biosystems engineering, **20** (1): 7-13

Levenspiel, O. (1999) Chemical reaction engineering, 3rd edition. John Wiley & sons, New Jersey

Lindgren, A., Johansson, S., Nyström, L-E. (1993) Scale-up of expanded bed adsorption. In: Henon, B., editor. BED-the seventh bioprocess engineering symposium. American society of mechanical engineering, **27**: 27-30

Ling, T.C., Lyddiatt, A., Carmichael, I., Purdom, G., Hathi, P. and Levison, P.R. (2003) Direct enzyme adsorption from an unclarified microbial feedstock using suspended bed chromatography. Journal of Chromatography A, **989**: 109-118

Madigan, M.T, Martinko, J.M. and Parker, J. (2000) Biology of Microorganisms, 9th edition. Prentice-Hall Inc., New Jersey

Mannweiler, K., Hoare, M. (1992) The scale-down of an industrial disc-stack centrifuge. Bioprocess engineering, **8**: 18-25

Maybury, J.P., Mannweiler, K., Titchener-Hooker, N.J., Hoare, M., Dunnill, P. (1998) The performance of a scaled-down industrial disc-stack centrifuge with a reduced feed material requirement. Bioprocess and biosystems engineering, **18** (3): 191-199

Maybury, J.P., Hoare, M. and Dunnill, P. (2000) The use of laboratory centrifugation studies to predict performance of industrial machines: studies of shear-insensitive and shear-sensitive material. Biotechnology and bioengineering, **67** (3):256-273

Marshall, A.G. (1978) Biophysical chemistry: principles, techniques and applications. John Wiley & Sons, New York

Mosqueira, F.G., Higgins, J.J., Dunnill, P., Lilly, M.D. (1981) Characteristics of mechanically disrupted Bakers' yeast in relation to its separation in industrial centrifuges. Biotechnology and bioengineering, **23**: 335-343

Mustafa, A.M., Washbrook, J., Lim, A.C., Zhou, Y., Titchener-Hooker, N.J., Morton, P., Berezenko, S., Farid, S.S. (2004) A software tool to assist business-process decision-making in the biopharmaceutical industry. Biotechnology progress, **20**: 1096-1102

Naglak, T.J., Wang, H.Y. (1990) Recovery of a foreign protein from the periplasm of Escherichia coli by chemical permeabilisation. Enzyme and microbial technology, **12**: 603-611

Nealon, A.J., Willson, K.E., Pickering, S.C.R., Clayton, T.M., O'Kennedy, R., Titchener-Hooker, N.J., Lye, G.J. (2005) Use of operating windows in the assessment of integrated robotic systems for the measurement of bioprocess kinetics. Biotechnology progress, **21**: 283-291.

Neu, H.C., Heppel, L.A. (1964) The release of ribonuclease into the medium when *Escherichia coli* cells are converted to spheroplasts. Journal of biological chemistry, **239**: 3893-3900

Neal G., Christie, J., Keshavarz-Moore, E., Shamlou, P.A. (2003) Ultra scale-down approach for the prediction of full-scale recovery of ovine polycolonal immunoglobulins used in the manufacture of snake venom-specific Fab fragment. Biotechnology and bioengineering, **81** (2): 149-157

Pennel, C.A. and Eldin, P. (1998) *In vitro* production of recombinant antibody fragments in *Pichia pastoris*. Research in immunology. **149**: 599-603

Persson, J., Andersen, D.C., Lester, P.M. (2005) Evaluation of different primary recovery methods for *E. coli*-derived recombinant human growth hormone and compatibility with further down-stream purification. Biotechnology and bioengineering, **90** (4): 442 - 451

Reynolds, T., Boychyn, M., Sanderson, T., Bulmer, M., More, J., Hoare, M. (2003) Scale-down of continuous filtration for rapid bioprocess design: Recovery and dewatering of protein precipitate suspensions. Biotechnology and bioengineering, **83** (4): 454-464

Richardson, J.F., Zaki, W.N. (1954) Sedimentation and Fluidisation: Part I. Transactions of the institution of chemical engineers, **32**: 35-53

Roque, A.C.A., Lowe, C.R., Taipa, M.A. (2004) Review: Antibodies and genetically engineered related molecules: production and purification. Biotechnology progress, **20**: 639-654

Rumpus, J. (1997) Dewatering and scale-down of solids recovery in industrial centrifuges, PhD thesis, University of London

Ryan, W., Parulekar, S.J. (1991) Recombinant protein synthesis and plasmid instability in continuous cultures of *Escherichia coli* JM103 harbouring a high copy number plasmid. Biotechnology and bioengineering, **37**: 415-429

Salte, H., King, J., Baganz, F., Hoare, H., Titchener-Hooker, N.J. (2006) A methodology for centrifuge selection for the separation of high solids density cell broths by visualisation of performance using Windows of Operation. Biotechnology and bioengineering, available online July 2006

Sauer, T., Robinson, C.W., Glick, B.R. (1989) Disruption of native and recombinant *Escherichia coli* in a high-pressure homogeniser. Biotechnology and bioengineering **33**: 1330-1342

Schiolach, J., Santambien, P., Trinh, L., Schapman, A., Boschetti, E. (2003) Endostatin capture from *P. pastoris* culture in a fluidized bed from on-chip process optimization to application. Journal of chromatography B, **790**: 327-336

Skerra, A., Pluckthun, A. (1988) Assembly of a functional immunoglobin Fv fragment in *Escherichia coli*. Science, **240**: 1038-1041

Sommerville, Jr. J.E., Goshorn, S.C., Fell, H.P., Darveau, R.P. (1994) Bacterial aspects associated with the expression of a single-chain antibody fragment in *Escherichia coli*. Applied microbiology and biotechnology, **42**: 595-603.

Thömmes, J., Halfar, M., Lenz, S., Kula, M-R. (1995) Purification of monoclonal antibodies from whole hybridoma fermentation broth by fluidised bed adsorption. Biotechnology and bioengineering, **45**: 205-211

Thömmes, J., Bader, A., Halfar, M., Karau, A., Kula, M-R. (1996). Isolation of monoclonal antibodies from cell containing hybridoma broth using a protein A coated adsorbent in expanded beds. Journal of chromatography A, **752**: 111-122

Thömmes, J. (1997) Fluidized bed adsorption as a primary recovery step in protein purification. Advanced biochemical engineering, **58**: 185-230

Thömmes, J., Halfar, M., Gieren, H., Curvers, S., Takors, R., Brunschier, R. and Kula, M-R. (2001) Human chymotrypsinogen B production from *Pichia pastoris* by integrated development of fermentation and downstream processing. Part 2. Protein recovery. Biotechnology progress, **17** (3): 503-512

Tong, X-D., Dong, X-Y., Sun, Y. (2002) Lysozyme adsorption and purification by expanded bed chromatography with a small-sized dense adsorbent. Biochemical engineering journal, **12**: 117-124

Tong, X-D., Xue, B., Sun, Y. (2003) Modeling of expanded-bed protein adsorption by taking into account the axial particle size distribution. Biochemical engineering journal, **16**: 265-272

Tsuchido, T., Katsui, N., Takeuchi, A., Takano, M., Shibaski, I. (1985) Destruction of the outer membrane permeability barrier of *Escherichia coli* by heat treatment. Applied environmental microbiology, **50**: 298-303

Tustian, A.D., Salte, H., Hoare, M., Baganz, F., Titchener-Hooker, N.J. (2006) Rapid ultra scale-down approach for predicting the dewatering of cellular sediments in industrial centrifuges. Manuscript under preparation.

Verma, R., Boleti, E., George, A.J.T. (1998) Antibody engineering: Comparison of bacterial, yeast, insect and mammalian expression systems. Journal of immunological methods, **216**: 165-181

Ward, P.N. (1989) The characterisation of biological suspensions with a view to selecting and optimising dewatering processes, PhD thesis, University of London

Weir, A.N.C., Bailey, N.A., (1997) Process for obtaining antibodies using heat treatment. Unites States Patent 5,665,866

Willoughby, N., Martin, P., Titchener-Hooker, N.J. (2004) Extreme scale-down of expanded bed adsorption: Purification of an antibody fragment directly from recombinant *E. coli* culture. Biotechnology and bioengineering, **87** (5): 641-7

Wilson, E.J., Geankopolis, C.J. (1966) Liquid mass transfer at very low Reynolds numbers in packed beds. Industrial and engineering chemistry: fundamentals, **5**: 9-14

Woodley, J.M., Titchener-Hooker, N.J. (1996) The use of windows of operation as a bioprocess design tool. Bioprocess engineering, **14**: 263-268.

Wright, P.R., Glasser, B.J. (2001) Modeling mass transfer and hydrodynamics in fluidized-bed adsorption of proteins. Bioengineering, food and natural products, **47** (2): 474-488

Yau, W.W., Kirkland, J.J., Bly, D.D. (1979) Modern size exclusion liquid chromatography. John Wiley & Sons, New York

Yavorski, D., Blanck, R., Lambalot, C., Brunkow, R. (2003) The clarification of bioreactor cell cultures for biopharmaceuticals. Pharmaceutical technology, 62-76

Zhou, Y., Holwill, I.L.J., Titchener-Hooker, N.J. (1997) A study of the use of computer simulations for the design of integrated downstream processes. Bioprocess engineering **16**: 367-374

Zhou, Y., Titchener-Hooker, N.J. (1999) Visualizing integrated bioprocess designs through 'Windows of Operation'. Biotechnology and bioengineering, **65**: 550-557.

Zimmermann, J.J.F., Oddie, K., Langer, R., Cooney, C.L. (1991) The release of heparinase from the Periplasmic space of *Flavobacterium heparinum* by three step osmotic shock. Applied biochemistry and biotechnology, **30**: 137-148

Appendix A1: Centrifuge spin conditions: relating rpm to RCF

The spin speed (N) and the corresponding RCF value at which a centrifuge is operated, are related by the following equations:

$$RCF = \frac{r_{ln}\,\omega^2}{g} \qquad \text{A1.1}$$

$$r_{ln} = \frac{r_o - r_i}{\ln \frac{r_o}{r_i}} \qquad \text{A1.2}$$

$$\omega = 2\pi N \qquad \text{A1.3}$$

Example: the RCF value of the Eppendorf 5810R lab centrifuge operated at 14000 rpm (2 mL test volume, see Table A3.1) can be calculated from the following characteristics:

$r_i = 0.042$ m

$r_o = 0.075$ m

$\omega = 1466$ rad s^{-1}

→ RCF = 12469

Appendix A2: Σ equations for centrifuges of different design

Unique expressions for the Σ factor exist for each centrifuge design. Of interest for this research are the expressions used to calculate the Σ of a swing-out laboratory (lab) centrifuge, a disc-stack (ds) centrifuge, and of a tubular-bowl (tb) machine. For the purpose of Σ calculations the Powerfuge™ is considered a tubular bowl and multi-chamber bowls are treated as a series of tubular bowls; $\Sigma_{mc} = \Sigma_{tb,\,1} + \ldots . \Sigma_{tb,\,n}$, where n is the total number of chambers.

A2.1 The laboratory batch centrifuge

For the laboratory centrifuge, the expression for Σ_{lab} is given in Equation A2.1.

$$\Sigma_{lab} = \frac{V_{lab}\omega^2(3-2x-2y)}{6g\ln(\frac{2r_o}{r_o+r_i})} \qquad \text{A2.1}$$

where V_{lab} is the volume of process material in laboratory tube, $\omega = 2\pi N$, N is the rotational speed, r_i is the inner radius (the distance between the centre of rotation and the top of the liquid), r_o is the outer radius (the distance between the centre of rotation and the bottom of the tube), g is the acceleration due to gravity, and x and y are the fractional times required for acceleration and deceleration, respectively (Maybury *et al.*, 1998).

A2.2 The disc-stack centrifuge

For a disc-stack centrifuge, the value for Σ is given by Equation A2.2.

$$\Sigma_{ds} = \frac{2\pi N_{AD}\omega^2(r_2^3 - r_1^3)}{3g\tan\theta} f_1 \qquad \text{A2.2}$$

where N_{AD} is the number of active discs, r_1 and r_2 are the inner and outer disc radius, respectively, θ is the half disc angle and f_l is the correction factor for spacer caulks (assume $f_l = 1$).

A2.3 The tubular bowl centrifuge

For a tubular bowl centrifuge:

$$\Sigma_{tb} = \left(\frac{\omega^2}{g}\right)\Pi L\left[\frac{r_o^{\,2} - r_i^{\,2}}{\ln\left(\frac{2r_o^{\,2}}{r_o^{\,2} + r_i^{\,2}}\right)}\right] \qquad \text{A2.3}$$

where L is the length of the chamber, and r_i and r_o are the inner and outer bowl radius, respectively.

Appendix A3: Technical data for the centrifuges investigated

Table A3.1 specifies the technical data required to calculate the Σ factor for each of the centrifuges investigated in this study.

Table A3.1: Technical data required for calculating the Σ area of the centrifuges investigated in this thesis.

Centrifuge	**Dimensions**
Westfalia CSA-1 disc-stack	r_1: 0.0261 m; r_2: 0.053 m; N_{AD}: 45; θ: 40°; N_{max}: 163.3 rps
Westfalia SC35 disc-stack	r_1: 0.0.66 m; r_2: 0.13 m; N_{AD}: 135; θ: 50°;N_{max}: 120 rps
Westfalia KA6 multi-chamber	$r_{i,1}$: 0.044 m; $r_{o,1}$: 0.109 m; L_1: 0.17 m $r_{i,2}$: 0.12 m; $r_{o,2}$: 0.141 m; L_2: 0.17 m; N_{max}: 142 rps
Westfalia KB25 multi-chamber	$r_{i,1}$: 0.03 m; $r_{o,1}$: 0.163 m; L_1: 0.25 m $r_{i,2}$: 0.17 m; $r_{o,2}$: 0.195 m; L_2: 0.25 m; N_{max}: 110 rps
Carr P12 Powerfuge™	r_i: 0.102 m; r_o: 0.152 m; L: 0.305 m; N_{max}:180.6 rps
Carr P18 Powerfuge™	r_i: 0.152 m; r_o: 0.229 m; L: 0.457 m; N_{max}: 147.7 rps
Eppendorf 5810R lab	$r_{i,\ 1\ mL}$: 0.056 m; $r_{i,\ 1.5\ mL}$: 0.048 m; $r_{i,\ 2\ mL}$: 0.042 m; r_o: 0.075 m; N_{max}: 233.3 rps

Appendix A4: Mass balance equations for the general rate model

The following presents the mass balance equations applied in the general rate model, as described by Gu *et al.* (1993), Gu, (1995) and Kaczmarski *et al.* (2001).

Equation A4.1 gives the mass balance for the component in the mobile fluid phase:

$$-D_{ax}\frac{\partial^2 C_L}{\partial Z^2}+v\frac{\partial C_L}{\partial Z}+\frac{\partial C_L}{\partial t}+\frac{3k_f(1-\varepsilon)}{\varepsilon R_p}(C_L-C_{P,R=R_p})=0 \qquad \text{A4.1}$$

where D_{ax} is the axial liquid dispersion coefficient, C_L is the bulk phase concentration of the component, Z is the axial coordinate, v is the interstitial velocity, t is the time, k_f is the film mass transfer coefficient, ε is the bed void volume fraction, R_p is the particle radius, R is the radial coordinate for the particle and C_P is the concentration of the component in the stagnant fluid phase inside the pore.

In Equation A4.1, the first term represents transport of the component by axial liquid dispersion, the second term convective transport of the mobile phase; the third term is accumulation in the mobile phase, and the last term represents accumulation of the component in the stationary (solid) phase.

Equation A4.2 gives the mass balance for the component in the solid particle phase:

$$(1-\varepsilon_p)\frac{\partial C_P^*}{\partial t}+\varepsilon_p\frac{\partial C_P}{\partial t}-\varepsilon_p D_P\left[\frac{1}{R^2}\frac{\partial}{\partial R}\left(R^2\frac{\partial C_P}{\partial R}\right)\right]=0 \qquad \text{A4.2}$$

where ε_p is the particle porosity, C^*_P is the concentration of the component on the adsorbent, C_P is the concentration of the component in the stagnant fluid inside the pore, D_P is intra-particle (pore) diffusivity and R is the radial coordinate of the particle.

In Equation A4.2 the first term describes accumulation of the component in the particle phase, the second term relates to accumulation of the protein in the stagnant fluid phase inside the pores, and the final term represents radial diffusion inside the porous particle.

For each of the mass balance equations we have initial and boundary conditions. Initial conditions:

For t = 0:

$$C_L = C_L\,(0,\ Z) \qquad \text{A4.1a}$$

$$C_P = C_P\,(0,\ R,\ Z) \qquad \text{A4.2a}$$

The two boundary conditions for the bulk fluid phase describe the column inlet and the column exit.

For t > 0 and Z = 0:

$$\frac{\partial C_L}{\partial Z} = \frac{v}{D_{ax}}(C_L - C_f(t)) \qquad \text{A4.1b}$$

where $C_f(t)$ is feed concentration profile of the component, a time dependent variable.

For t > 0 and Z = L:

$$\frac{\partial C_L}{\partial Z} = 0 \qquad \text{A4.1c}$$

The boundary conditions for the solid phase mass balance, expressed by Equation A4.2, relates to the particle phase radial position.

For t > 0 and R = 0:

$$\frac{\partial C_P}{\partial R} = 0 \qquad \text{A4.2b}$$

For $t > 0$ and $R = R_p$:

$$\frac{\partial C_P}{\partial R} = \frac{k_f}{\varepsilon_p D_P}(C_L - C_{P,R=R_p}) \qquad \text{A4.2c}$$

Appendix A5: Publication

The paper "A methodology for centrifuge selection for the separation of high solids density cell broths by visualisation of performance using Windows of Operation" by Salte *et al.* (2006) is printed overleaf. This paper has been accepted for publication by Biotechnology and Bioengineering and is available online as of July 2006.

A Methodology for Centrifuge Selection for the Separation of High Solids Density Cell Broths by Visualisation of Performance Using Windows of Operation

Heidi Salte,[1,2] Josh M.P. King,[1] Frank Baganz,[1] Mike Hoare,[1] Nigel J. Titchener-Hooker[1]

Biotechnology and Bioengineering. DOI 10.1002/bit

DOI 10.1002/bit

Biotechnology and Bioengineering. DOI 10.1002/bit

DOI 10.1002/bit

Biotechnology and Bioengineering. DOI 10.1002/bit

DOI 10.1002/bit

Biotechnology and Bioengineering. DOI 10.1002/bit

DOI 10.1002/bit

Biotechnology and Bioengineering. DOI 10.1002/bit